12-2011

Determining CO2 Storage Potential: Characterization of Seal Integrity and Reservoir Failure in Exposed Analogs

Daniel Corey Barton
Utah State University

DETERMINING CO_2 STORAGE POTENTIAL: CHARACTERIZATION OF SEAL INTEGRITY AND RESERVOIR FAILURE IN EXPOSED ANALOGS

by

D. Corey Barton

A thesis submitted in partial fulfillment
of the requirements for the degree

of

MASTER OF SCIENCE

in

Geology

Approved:

_____	_____
Dr. James P. Evans Major Professor	Dr. Susanne U. Janecke Committee Member
_____	_____
Dr. Carol M. Dehler Committee Member	Dr. Mark R. McLellan Vice President for Research and Dean of the School of Graduate Studies

UTAH STATE UNIVERSITY
Logan, Utah

2011

ABSTRACT

Determining CO_2 Storage Potential: Characterization of Seal Integrity and Reservoir Failure in Exposed Analogs

by

D. Corey Barton, Master of Science

Utah State University, 2011

Major Professor: Dr. James P. Evans
Department: Geology

Sequestration of carbon dioxide (CO_2) into subsurface porous sandstone is proposed as a method for reducing accumulation of anthropogenic emissions of CO_2 into the atmosphere. Natural exposures of reservoir and top-seal pairs in central and southeastern Utah are identified as analogs to proposed CO_2 injection targets. Reservoir and top-seal pairs in natural analog exposures are analyzed in tandem to evaluate evidence for paleo-migration of fluids and/or hydrocarbons from the reservoir through the top seal. The San Rafael Swell and Monument Uplift exhibit similar structure and exposures of Jurassic units yet differ in amount and type of host rock alteration due to variable amounts and types of fluids and/or hydrocarbons that migrated along faults and fractures.

Macroscopic scale analysis of each monocline included processing of satellite imagery, and creation of depth contour maps. At the mesoscopic scale, fracture spacing acquired from scanline station measurements identified increased fracture frequency in proximity to major fault zones. At the microscopic scale, percentage of degradation and type of mineralization in pore space were used to verify increased fluid flow in proximity to major fault zones.

Faults with possible intersections with multiple antithetic faults at depth have an increased probability of allowing for upward migration of fluids and/or hydrocarbons along the fault plane and damage zone, effectively bypassing the top sealing formations. Fault leakage potential maps identified areas where seal bypass along major faults would likely occur during sequestration of CO_2. The method was validated by identifying potential migration pathways for oil seeps on the Little Grand Wash fault in central Utah. The San Rafael Swell was geometrically modeled through restoration of eroded formation tops along the fold axis to quantify the interaction between an outward migrating CO_2 plume and varying degrees of faulting and fracturing. Analysis of the migration of a CO_2 plume front through time exhibits an increasing probability of the outward migrating plume intersecting a leaking feature, with the highest probability of the advancing plume intersecting a potentially leaking feature achieved when faults with 1+ km trace length and mean fracture spacing of 17 cm are taken into consideration.

(177 pages)

PUBLIC ABSTRACT

Determining CO_2 Storage Potential: Characterization of Seal Integrity and Reservoir Failure in Exposed Analogs

by

D. Corey Barton, Master of Science

Utah State University, 2011

Major Professor: Dr. James P. Evans
Department: Geology

Storage of human generated carbon dioxide (CO_2) into geologic layers of sandstone in the subsurface, is proposed as a method for reducing the accumulation of CO_2 emissions in the atmosphere. Sandstone is identified as a reservoir for the ability to store fluid and gas between the rock particle matrix, and the shale and mudstone layers are identified as a seal due to the inability of fluid or gas to migrate through the very fine rock particle matrix. Sandstone layers identified as storage targets are bounded by thinly bedded mudstone and shale that act as natural boundaries that trap the CO_2 within the layer. Jurassic age layers of sandstone and shale extend laterally through the subsurface and can be exposed at the surface through structural processes such as faulting and folding. Exposed layers of sandstone and shale in central and southeastern Utah are analogous to the layers in the subsurface identified as CO_2 injection targets. The analog exposures of reservoir and seal rocks are analyzed to identify areas that exhibit features consistent with leakage of fluids and/or hydrocarbons through the above lying seal. The San Rafael Swell and Monument Uplift are similar asymmetric folds in which the sandstone and shale have been folded and uplifted through geologic time. Even though the folds are similar in structure and age

of Jurassic layers exposed at the surface, alteration of the rock exposures is dependent on the amount and type of fluids and/or hydrocarbons that migrated along faults and fractures.

Analysis of each asymmetric fold included processing of satellite imagery and creation of depth contour maps allowing for three-dimensional visualization of faults in the subsurface. Additionally, fracture spacing measurements identified increased fracturing in proximity to major fault zones. At the microscopic scale, evaluation of the amount of mineral infill in the open space of the rock matrix verified increased fluid flow in proximity to major fault zones.

Migration of fluid along a fault plane is possibly increased when multiple fault planes intersect. Faults that dip in opposite directions potentially intersect at depth, increasing probability of upward migration of fluids along the fault plane and through fractures, effectively bypassing the fine rock particle seal. Fault leakage potential maps based on fracture analysis, identified areas where migration of fluid along major faults would likely occur during injection of CO_2 into the subsurface reservoir. The fault leakage potential maps are validated by the presence of oil seeps at the surface in central Utah, revealing the migration potential along the Little Grand Wash fault plane. As the volume of fluid increases in a reservoir, the edges of the fluid will increase surface area by migrating outward. Restoration of the eroded Jurassic layers, exposed at the San Rafael Swell fold. aided in quantifying the outward migrating CO_2 plume and varying degrees of faulting and fracturing. Analysis of hypothetical CO_2 plume migrating outward through time, exhibits an increasing probability of intersecting a leaking feature such as faults or fractures, with the highest probability of the advancing plume intersecting a potentially leaking feature achieved, when faults with 1+ km trace length and average fracture spacing of 17 cm are taken into consideration.

(177 pages)

ACKNOWLEDGMENTS

This thesis was funded by the U.S. Department of Energy, Grant # DE-FC26-0xNT4 FE0001786 awarded to Dr. James P. Evans. Limited access satellite imagery was used by permission from the National Aeronautics and Space Administration. Data from drilling in central and southeastern Utah were provided by the Utah Division of Oil, Gas, and Mining. Geologic maps used in this study were provided by the Utah Geological Survey. Shapefiles used for the development and modification of geologic maps in this study were provided by the Utah Automated Geographic Reference Center.

I would like to thank my thesis advisor, Dr. James P. Evans, for his help, guidance, and support on this project. Additionally, I would like to thank Dr. Evans for imparting his vision and passion for geology to me as an undergraduate at Utah State University. I would also like to thank my committee members, Drs. Susanne U. Janecke and Carol M. Dehler, for their time and support, helping me to achieve my goals.

I would like to thank my colleagues that assisted and supported me through development of this project, including Elizabeth Petrie, Kelly K. Bradbury, Ryan Sonntag, Mitch Prante, and Dave Richey.

Last, but not least, I would like to thank my wife, Kayleen, for her enduring support and encouragement through the difficult times, and my son Landon for being the best field assistant that anyone could ever ask for. My completion of this thesis was made possible with support from all of you.

D. Corey Barton

CONTENTS

Page

Page

LIST OF TABLES

LIST OF FIGURES

Figure Page

Figure Page

Figure Page

Figure Page

INTRODUCTION

Injection of carbon dioxide (CO_2) into stacked saline aquifers separated by low-permeability shale units and depleted oil and gas reservoirs has been proposed as a method for reducing the amount of anthropogenic CO_2 in the atmosphere (Halloway, 2001). Large anticlines in central Utah are hydrostratigraphic reservoirs with trapping mechanisms that may be capable of storing large volumes of injected CO_2 in proximity to large point-sources of anthropogenic CO_2 emissions such as coal-fired powered plants (Allis et al., 2001). The Southwest Regional Partnership on Carbon Sequestration (SWP) has identified the Gordon Creek field in Carbon County, Utah to be a preliminary test injection site for future large scale commercial sequestration of CO_2 (McPherson and Grigg, 2010). The Navajo Sandstone is the target injection unit in the Gordon Creek field with the Carmel Formation identified as the caprock intended to mitigate upward migration of the injected CO_2. The nearby Hunter and Huntington power plants in central Utah have been identified as possible candidates for point-source injection of anthropogenic CO_2 into the underlying Jurassic strata (Allis et al., 2003) following the injection test at Gordon Creek. The migration of CO_2 to the surface may be inhibited by the presence of a low-permeability seal allowing for an estimated 99% of injected CO_2 to remain in place for 1000 years (Benson and Cook, 2005), but previous work has shown the integrity of the seal can be compromised by fractures and faults (Shipton et al, 2004; Cartwright et al., 2007). Additionally, stratigraphic and structural heterogeneities present in a reservoir can affect the migration of CO_2 by acting as conduits or barriers (Caine et al., 1996). This study analyzes exposures of the low-permeability caprock and porous sandstone reservoir in greater detail by correlating reservoir properties and alteration features observed in the caprock, in an effort to accurately determine the storage potential of the same caprock and reservoir pairs in a subsurface environment. Understanding how fractures and faults affect a potential CO_2 reservoir and overlying caprock is

vital to our understanding of the mechanics of fluid flow along major faults, and sub-seismic migration pathways.

Seal bypass is interpreted to result from a variety of processes, and may be associated with faulting, piping, and intrusion (Cartwright et al., 2007). The term seal bypass refers to any process or sequence that allows fluid to flow vertically or sub-vertically through a low-permeability caprock. The primary focus of this study is to analyze the occurrence of paleo-fracture- and fault-related seal bypass that allowed for the upward migration of fluids and/or hydrocarbons through a low-permeability seal preserved in exposed formations whose subsurface extents, nearby, are targets of sequestration.

Three factors are necessary considerations when attempting to analyze the sealing integrity of a caprock; time, thickness, and permeability (Deming, 1994). Factors of thickness and permeability may not be sufficient alone in determining the sealing capacity of a caprock, if enough time has passed to allow slow migration rates to bypass both thickness and permeability (Deming, 1994).

The integrity of the caprock is difficult to determine at depth due to anisotropy of the formation, sub-seismic nature of fractures that increase the connectivity of flow paths within the top seal, and limited resolution of wellbore-scale observations of subsurface processes.

Springs and geysers formed by CO_2 - charged water in central Utah are interpreted to be due to CO_2 migration through caprocks along faults, and abandoned oil wells (e.g., Heath et al., 2009). Evidence of paleo-migration of CO_2 charged fluid along fractures and faults is preserved in many formations throughout Utah in the form of bleached host rock (Hawley et al., 1968; Parry et al., 2004; Beitler et al., 2005), and secondary mineralization within pore space (Chan et al., 2000). The volume of CO_2 migrating to the surface is also potentially increased due to penetration of the top seal unit by drill holes. Many wells in the area are abandoned and

unmonitored, creating the potential for increased connectivity of migration pathways through low-permeability top sealing layers (Celia et al., 2004; Heath et al., 2009).

One such case is the CO_2 discharge at Crystal Geyser erupting from the abandoned Glen Ruby #1-X exploration well drilled in 1934 (Baer and Rigby, 1978), where modern travertine develops over the top of fossil travertine (Heath et al., 2009; Burnside, 2010; Dockrill and Shipton, 2010). In places, the fossil travertine deposits lie ~50 m above the current level of active travertine deposits (Doelling, 1994), indicating long-term leakage along the Little Grand Wash fault zone. The long-term leakage along the Little Grand Wash fault zone has occurred for more than 10^5 years (Baer and Rigby, 1978; Burnside, 2010), indicating that a CO_2 reservoir may continue to leak even if mineralization develops along faults and fractures (Heath et al., 2009; Burnside, 2010; Dockrill and Shipton, 2010). The ability to detect faults at depth with throws <10-15 m can be difficult, if not impossible with current seismic methods. The detectable resolution limit to detect offset in sub-vertical faults using current two- and three-dimensional methods is approximately 10 m (Behrens and Tran, 1999). Many of the faults and fractures exhibiting evidence for paleo-migration of fluid and/or hydrocarbons in exposed natural analogs would not be visible on 2-D or 3-D seismic profiles, making it difficult to predict potential migration pathways for a plume of injected CO_2 through formations at depth by seismic monitoring alone.

Utilizing geophysical data obtained from well logs is one method of analyzing subsurface geology, but the integrity of the caprock in many reservoir systems is difficult to characterize using geophysical well logs alone. One of the ways to characterize caprock integrity is through correlation of naturally exposed analogs to the data from geophysical well logs in order to quantify the mechanical response of the fine-grained matrix to local and regional stresses (Curtis, 2002). In addition to understanding the mechanical response of the seal and reservoir pair, the nature of the fractures in the formation can be determined, namely if the fractures are open or

closed (Laubach, 2003), as well as the presence and type of mineralization associated with the upward migration of fluid (Beitler et al., 2005). Characterization of fractures also involves an accurate determination of fracture spacing in formations at depth through analysis of core samples acquired from drilling (Narr, 1996; Laubach et al., 2009), and scanline analysis of exposures in natural analogs.

The feasibility of injecting human-produced CO_2 into geologic formations at depth is the focus of many research projects sponsored by the Department of Energy, relating to the reduction of anthropogenic CO_2 released into the atmosphere. Many projects are currently underway with the migration and potential leakage of CO_2 monitored through seismic methods (http://fossil.energy.gov/sequestration/partnerships/index.html). This Department of Energy initiative was launched in 2003, in an effort to develop large scale sequestration projects that demonstrate long-term, effective, and safe storage of CO_2 in major geologic formations throughout the United States and parts of Canada.

Analysis of the San Rafael Swell in central Utah, and the Monument Uplift in southeastern Utah, provide an opportunity to compare and contrast between two monoclinal folds in which the same Jurassic units have been exposed through uplift and erosion. The formations of interest in this study are the Jurassic Navajo Sandstone, Page Sandstone, Carmel Formation, Entrada Sandstone, and Curtis Formation. Each of the formations were analyzed for presence of alteration due to fluid and/or hydrocarbon migration, fractures that are constrained to the individual formation, fractures that extend into the overlying formations, and faults that cross stratigraphic boundaries between formations. The analysis of data sets and geometric reconstruction models that comprise this study provide an opportunity to correlate observations from exposed analogs to potential sub-seismic features at depth, to better predict the potential migration pathways of injected CO_2. Additionally, findings from this study can be correlated to

the test injection at the Gordon Creek field and future developments of point-source injection of anthropogenic CO_2 at the Hunter and Huntington power plants located west of the study area. Field analyses of exhumed analogs are used to quantify key parameters of caprocks and porous sandstone reservoirs (e.g., bed thickness, fracture density, fracture orientation). Geometric modeling of correlative data from well logs (e.g. formation top depth) is used to show that the sealing integrity of the caprock is largely dependent on spacing and orientation of fractures and faults that influence upward migration of fluid through caprocks.

Objectives and Justification

This study is part of a larger effort to determine the ability of a caprock to efficiently seal against upward migration of injected CO_2 for kya-time scales that was funded by the Department of Energy (Grant # DE-FC26-0xNT4 FE0001786 to Dr. James P. Evans). The geometric modeling associated in this study will add to other work being accomplished on both the mesoscopic and microscopic scale, including mineralized fractures, color alteration in eolian sandstones due to iron depletion or oxidation (Hawley et al., 1968; Parry et al., 2004; Loope et al., 2010), and secondary mineralization within pore space (Chan et al., 2000). This study utilizes recent progress that has been accomplished in analysis of seismic surveys (LaBarre and Davis, 2008), correlation of natural analogs to geophysical well logs, fracture modeling based on geochemistry and core analysis (Berg and Gangi, 1999), quantification of fracture connectivity (Zhang et al., 2009), and analyses of mineralized veins and fractures (Sibson, 1994).

The Jurassic Glen Canyon and San Rafael Groups near the San Rafael Swell focus area (Figure 1a), are potential targets for geologic storage of CO_2 at Gordon Creek, located northwest of the San Rafael Swell (White et al., 2001; Allis et al., 2001; Esser et al., 2010). Additional point-source sequestration projects are proposed at the Hunter and Huntington power plants located west of the San Rafael Swell in the same Jurassic units (Allis et al., 2003). The target

depth for sequestration would be as shallow as 900 m in the Jurassic Navajo Sandstone, allowing for a greater chance of surface leakage along faults and fractures (Allis et al., 2001). The Jurassic Glen Canyon and San Rafael groups not only provide reservoir and seal pairs with adequate permeability contrasts suitable for geologic sequestration of CO_2 at depth, but also provide exposed structural and stratigraphic analogs of the same Jurassic groups at the surface within reasonable proximity to proposed sequestration sites. Additionally the Jurassic groups are popular hydrocarbon drilling targets throughout central and southeastern Utah, making geophysical data from wellbores throughout the region accessible for analysis by the Utah Geological Survey, and Utah Division of Oil, Gas, and Mining.

Geologic and Structural Setting

The Cambrian through Cretaceous sedimentary rocks in the San Rafael Swell and Monument Uplift focus areas (Figure 1) uncomformably overlie Proterozoic metamorphic and metasedimentary basement (Nuccio and Condon, 1996) (Figure 2). Prior to the late Devonian Antler orogeny, sedimentation in the region was on a stable shelf in shallow marine conditions (Poole and Sandberg, 1991; Poole et al., 1992). Sediments in the late Devonian and Mississippian were deposited in shallow-marine conditions on the cratonic shelf (Baars and Stevenson, 1982; Poole et al., 1992), recording transgressive and regressive sequences in the carbonate rocks (Nuccio and Condon, 1996) (Figure 2). Collision of the Laurentia and Gondwana super-continents resulted in Pennsylvanian and Permian resulted in rapid uplift along the Uncompahgre Plateau and deposition of sediment in subsidence basins (Nuccio and Condon, 1996). Approximately 1200 meters of sediment accumulated during the Pennsylvanian and Permian and consist of marine limestone, dolostone, shale, anhydrite, halite, sandstone, and mudstone (Figure 2). Phosphate formation in warm shallow water with salinity stratification during the Permian (Stephens and Carroll, 1999; Hiatt and Budd, 2001) occurred during

deposition of organic-rich mudstones (Maughan, 1983). The Permian phosphorite is a natural source of petroleum in the Uinta Basin due to maturation of the organic-rich deposits and presence of phosphorite (Maughan, 1983).

Sedimentation in the region during the Triassic and Jurassic was influenced by the development of magmatic arcs that provided sedimentation through periodic uplift of source rocks (Dickinson, 1989, 2004). Triassic sediments are interpreted to have been deposited in fluvial, lacustrine, sabkha, and eolian environments (Stewart et al., 1972), with an unconformity separating the Triassic and Jurassic units (Pipiringos and O'Sullivan, 1978) (Figure 2). Jurassic units record regionally extensive eolian and marine depositional systems (Verlander, 1995; Kocurek, 2003) (Figure 2). The alternating transgressive and regressive sequences are recorded respectively by the marine and eolian units. During the Early Jurassic, an expansive eolian sand sheet covered all of eastern Utah, and extended over much of the western United States producing the cross-bedded eolian deposits of the Glen Canyon Group (Verlander, 1995; Kocurek, 2003), separated by gradational fluvial contacts (Nuccio and Condon, 1996). The Jurassic San Rafael Group was deposited within the margins of an inland sea and uncomformably overlie the Jurassic Glen Canyon Group (Nuccio and Condon, 1996) in the focus areas. By Middle Jurassic time, a shallow seaway extended from the present day location of Canada to Carmel Junction, Utah, producing the thick fossil-bearing limestone, shale, and mudstone of the Carmel Formation. As the seaway retreated to the north, the environment was dominated by tidal mudflats and eolian dune deposits comprising the Earthy and Slickrock Members of the Entrada Sandstone (Hintze, 1993). The fossil-bearing Curtis Formation records an additional marine advancement that is present in the San Rafael Swell focus area (Figure 1a) where the Curtis Formation is observed to inter-finger with marine shales and mudstones of the Jurassic Summerville Formation. Salt diapirs tectonically affected the area during the Triassic and Jurassic as sedimentation above the

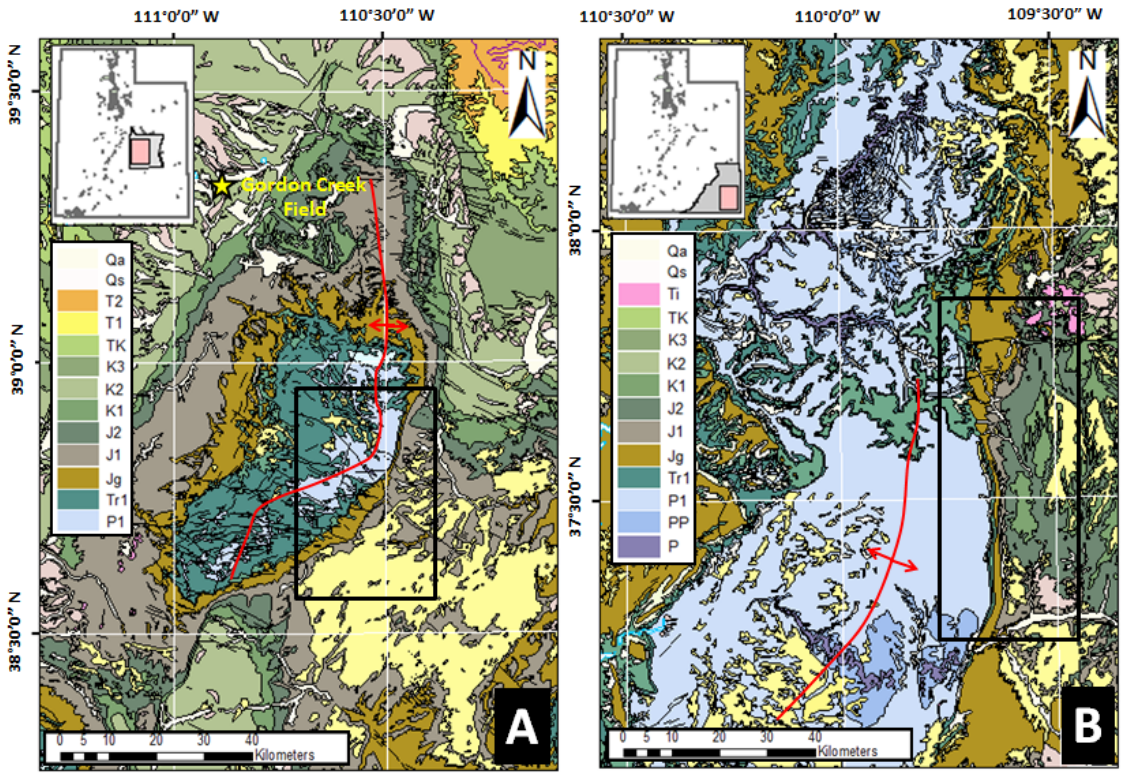

Figure 1. Location map of San Rafael Swell with Gordon Creek field location (A) and Monument Uplift focus areas (B). Fold axis in red, focus areas outlined by black line. (Geologic maps adapted from Hintze et al., 2000). Index map of Utah in upper left corner with county boundary shaded gray, and map boundary shaded red.

Pennsylvanian Paradox Formation led to the rise of salt into anticlines in the Paradox fold and fault belt (Nuccio and Condon, 1996).

The San Rafael Swell and Monument Uplift are broad, north-northeast trending monoclinal folds that resulted from the late Mesozoic to early Cenozoic eastward migration of the Laramide orogenic thrust belt (Dickinson et al., 1988; Bird, 1998; Bump, 2003). The San Rafael Swell is an asymmetric doubly plunging monocline in central Utah (Kelley, 1955; Davis, 1999), and the Monument Uplift is a monocline (Woodward, 1973; Bump, 2003) in southeastern Utah. Exposures of Jurassic formations exist on the eastern and western flanks of each of these exposed structures, with Permian formations exposed along the axis of both folds (Figure 1). The contrast in slope between the gently dipping western flank and the steeply dipping eastern flank of the San

Period	Formation / Members		Thick-ness	Rock Type
QUAT	Alluvium & surficial dep		0-100	
TERT	Alkalic diabase dikes & sills		NULL	
CRET	Mancos Shale	Blue Gate Shale Mbr	1500 +	
		Ferron Ss Member	150-400	
		Tununk Shale Mbr	400-700	
	Dakota Sandstone		0-50	
	Cedar Mountain Formation	Main Body	100-420	
		Buckhorn Cg Mbr	0-30	
JURASSIC	Morrison Fm	Brushy Basin Member	250-400	
		Salt Wash Mbr	200-300	
		Tidwell Member	60	
	San Rafael Group	Summerville Fm	200	
		Curtis Fm	100-250	
		Entrada Fm (earthy facies)	300-400	
		Carmel Fm	250-300	
		Page Sandstone	100	
		Navajo Ss	450-550	
	Glen Canyon Gp	Kayenta Fm	50-250	
		Wingate Ss	350-400	
		Chinle Fm	150-250	
TRIASSIC	Church Rock M		80-120	
	Moss Back Ss M		0-100	
	Moenkopi Fm	Temple Mtn Nl	400	
		Moody Canyon Member	250-300	
		Torrey Mbr	50-150	
		Sinbad Ls Mbr	140-200	

Period	Formation / Members		Thick-ness	Rock Type
PERMIAN	Black Box Dolomite	Black Dragon M	100-200	
	White Rim Sandstone		600-800	
	Pakoon Dolomite (Elephant Canyon)		500-700	
PENN	Honaker Trail Fm ?		200-500	
	Paradox Fm ?		300-500	
	Pinkerton Trail Fm ?		100-200	
MISS	Redwall Ls		600-1000	
DEV	Ouray Limestone		100-200	
	Elbert Fm		200-400	
CAMB	Lynch Dolomite & Maxfield Limestone undivided		1000-1300	
	Ophir Fm		200	
	Tintic Quartzite		150-300	
pC (PROT)	schist		NULL	

Figure 2. Generalized stratigraphic column of the San Rafael Swell and Monument Uplift focus areas. (Modified from Hintze and Kowalis, 2009).

Rafael Swell suggest that deformation may be due to a major reverse fault beneath the surface (Maerten et al., 2001)., or warming of heterogeneous lithosphere (Roy et al., 2009). However, a seismic transect across the San Rafael Swell by The Consortium for Continental Reflection Profiling did not clearly reveal a reverse fault associated with the fold (Allimendinger et al., 1986). The Chimney Rock fault system in the northern part of the San Rafael Swell has been identified as an orthorhombic system with multiple fault sets developed in a three-dimensional strain field (Krantz, 1988). The orthorhombic fault system was produced by vertical contractional strain, north-south oriented maximum extensional strain, and an east-west oriented minimum extensional strain (Krantz, 1988). Normal faults in the Chimney Rock area dip steeply (70-80°) (Shipton and Cowie, 2001), and are interpreted to have formed in response to the

Laramide age (~50 Ma) uplift of the San Rafael Swell (Shipton, 1999) with damage zones approximately two and half times the throw of the fault (Shipton and Cowie, 2003). The normal faults are identified forming when 1 to 2 km of overburden was present (Maerten, 2000). Davatzes et al. (2003) defined two distinct mechanisms of fault formation in the Chimney Rock area: faults formed by deformation bands and faults formed by subsequent shearing of joints. The ENE-striking map scale faults in the area are interpreted to have been produced during early deformation band formation (Davatzes et al., 2003). WNW-stiking joint sets formed after the first phase of ENE-striking faults, and are interpreted to have produced localized shearing that led to the formation of the WNW-striking faults in the area (Davatzes et al., 2003). The ENE-striking faults accommodated the first phase of NNW extension in the area. The WNW-striking faults accommodated a younger phase of NNE extension in the area (Davatzes et al., 2003). In addition to the younger phase of WNW-striking faults developed in the area, further development of the ENE-striking faults is observed to have developed in a younger phase of deformation (Davatzes et al., 2003). The WNW-striking faults produced by shearing of joints (Davatzes et al., 2003), are interpreted to have an increased fault parallel permeability compared to the ENE-striking deformation bands in the Chimney Rock area (Davatzes et al., 2003).

Understanding the paleo-migration of fluids and/or hydrocarbons on local and regional scales has important implications for carbon sequestration in the porous sandstone units. Previous work has identified diagenetic history of the water-rock interactions in the Navajo Sandstone, developing geochemical and paleo-hydrological models to explain the mobilization and precipitation of iron (Chan et al., 2000, 2004, 2005, 2006, 2007; Beitler et al., 2003, 2005; Parry et al., 2004). The models identify mobilization of iron as reducing fluids entered the sandstone reservoir, and precipitation of iron when the iron-bearing fluid interacts with oxidizing fluids. Modeling by Beitler et al. (2003, 2005) and Parry et al., (2004) shows reducing fluids and/or hydrocarbons migrated along conduits created by Laramide-aged (~55 Ma) blind thrusting

in the region. Potter and Chan (2011) identify multiple mobilization and precipitation events throughout the diagenetic history of the Jurassic Navajo Sandstone. Hematite grain coating formed by the weathering of ferromagnesian minerals approximately 190 Ma (Chan et al., 2000, 2004, 2005, 2006, 2007; Beitler et al., 2003, 2005; Parry et al., 2004), due to infiltration of meteoric water. Widespread color alteration in the Navajo Sandstone due to fluid migration along conduits created by Laramide-age blind thrust faulting approximately 80-55 Ma (Beitler et al., 2003, 2005; Parry et al., 2004; Seiler, 2008). At some time after the large bleaching even recorded by the Navajo Sandstone, microconcretions formed in cement of the Navajo Sandstone as oxidizing fluid infiltrated the reservoir and mobilized the previously precipitated iron (Beitler et al., 2003, 2005; Parry et al., 2004). At Spencer Flat, south of the San Rafael Swell focus area, rind macroconcretions are found to encase the microconcretions indicating another mobilization and precipitation event following the formation of the microconcretions (Potter and Chan, 2011). Evidence for another bleaching event is recorded after the macroconcretions due to color preservation on the interior of the macroconcretions (Potter and Chan, 2011). Northeast-striking joints, formed during the Miocene (< 23.3 Ma) in response to Basin and Range deformation (Davis, 1999), created conduits for infiltration of fluid (Beitler et al., 2005). Down-cutting of the Colorado River (< 10 Ma) created a hydraulic low producing asymmetrical mineralization and Liesegang banding in the Jurassic units of Spencer Flat (Potter and Chan, 2011). Multiple mobilization and precipitation events during the diagenetic history of the Navajo Sandstone (Potter and Chan, 2011) highlights paleo-migration of fluids and/or hydrocarbons through pore space, and along faults and fractures on local and regional scales (Vrolijk, 2005).

Description of Formations

Jurassic Navajo Sandstone

The Jurassic Navajo Sandstone was deposited as wind-blown sands over a large portion of the western United States (Blakey et al., 1988, 1994; Verlander 1995; Morris, 2000), and represents the largest preserved coastal and inland eolian system in the geologic record of North America. The sands are interpreted to have been recycled from Precambrian age belts, cratonic blocks, plutonic assemblages, and Paleozoic and Triassic sandstones (Peterson, 1988; Gehrels and Dickinson, 1995; Dickinson and Gehrels, 2003). The formation consists of cross strata derived from migrating and climbing dunes within the Jurassic sand sea (Figure 3) (Loope et al., 2001).

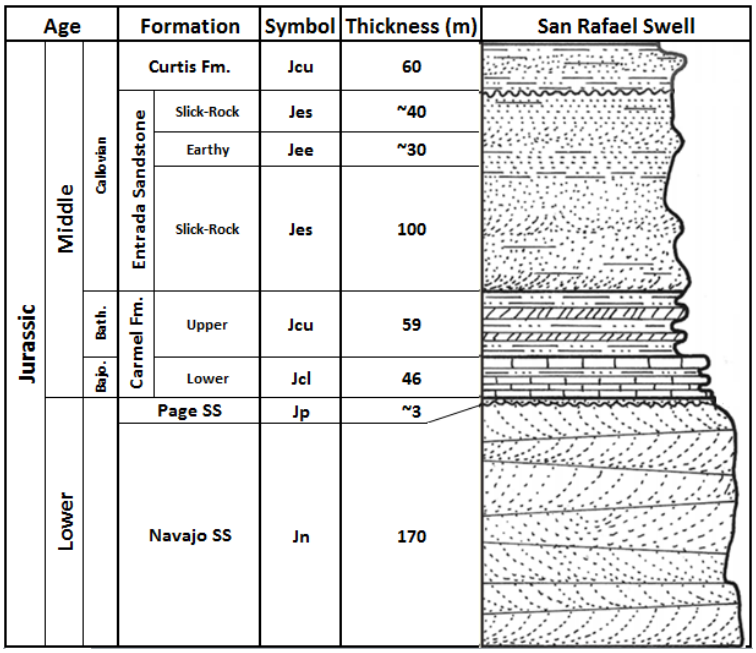

Figure 3. Generalized stratigraphic column of the San Rafael Swell focus area. (Modified from Doelling, 2002).

Regional isopach thickness values have been documented in the Navajo Sandstone at 100 m structural contours (Hunt, 1956; Beitler et al., 2003) (Figure 5). The Navajo Sandstone in the San Rafael Swell area is observed to thin eastward from ~ 180 (Doelling, 2002) to 70 m Monument Uplift area, the Navajo Sandstone thickens in proximity to the fold axis, with thinning observed north and south of the uplift from ~139 (O'Sullivan, 1998) to 100 m approximated from isopach thickness maps (Figure 4).

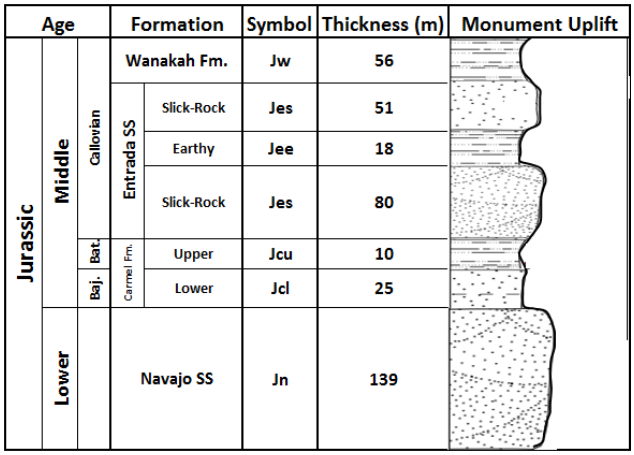

Figure 4. Generalized stratigraphic column of the Monument Uplift focus area. (Modified from O'Sullivan, 1998).

In the San Rafael Swell and Monument Uplift focus areas, the Navajo Sandstone is fine- to medium-grained with massive bedding and distinct cross-stratification. The color has been altered from red to pale yellow in both focus areas presumably by migration of reducing fluids through the formation (Chan et al., 2000; Parry et al., 2004, 2009; Beitler et al., 2005), with calcite mineralization observed in fractures only in the San Rafael Swell focus area.

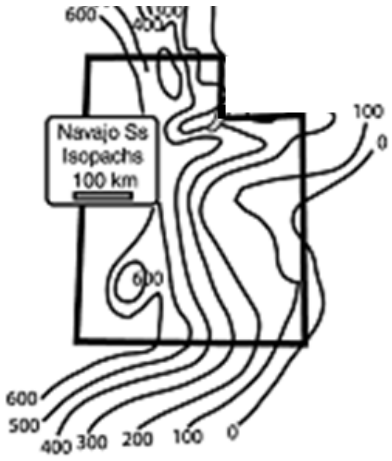

Figure 5. Navajo Sandstone 100 m structural contours (Beitler et al., 2003, modified after Hunt, 1956)

Jurassic Page Sandstone

The eolian Jurassic Page Sandstone is interpreted to have developed on the southeastern edge of the Carmel Sea, during fluctuations of the shoreline (Jones and Blakey, 1993). The chert nodules at the J-2 unconformable contact with the Navajo Sandstone area interpreted to be the result of marine encroachment into an eolian environment during storm activity (Blakey et al., 1983). The marine encroachment is the result of ephemeral stream flooding that extended into the Page Erg, thus resulting in debris flow characteristics consistent with the entrainment of sand and mud, due to the loss of fluid to the erg substrate (Jones and Blakey, 1997).

The Page Sandstone is found locally in the San Rafael Swell focus area and constitutes the lowest member of the Carmel Formation when present. The sandstone was deposited along a narrow north-northeast strip extending across eastern Utah and north-central Arizona as an intermittent erg deposit (Pipiringos and O'Sullivan, 1978). The Page Sandstone constitutes the lowest member of the Carmel Formation when present. The Page Sandstone unconformably overlies the Navajo Sandstone with an average thickness of approximately 3 m (Figure 3) (Doelling, 2002). The Page Sandstone is fine- to very fine-grained, with cross-stratification indicating north-northeast paleo-wind (Pipiringos and O'Sullivan, 1978; Jones and Blakey, 1993). The color has been altered from the red sandstone observed south of the San Rafael Swell focus area, to yellow red chert nodules present at the base.

Jurassic Carmel Formation

The Jurassic Carmel Formation was deposited in a variety of environments ranging from fluvial, eolian, coastal sabkha, to restricted and open marine environments as mudstone, siltstone, irregular sandstone beds, and eolian sandsheets and dunes (Blakey et al., 1983). The sabkha deposits consist of commonly contorted beds of red, ripple-laminated strata. Shallow marine

carbonate deposits range in color from tan to gray, and consist of mudstone to grainstone (Blakey et al., 1996).

The contact between the Carmel Formation and the Navajo Formation, or the Page Sandstone in the San Rafael Swell focus area, is the J-2 unconformity (Pipiringos and O'Sullivan, 1978; Peterson and Piperingos, 1979; Peterson, 1994). The J-2 unconformity is interpreted to have formed during the middle Jurassic (Pipiringos and O'Sullivan, 1978) and is distinguished by the presence of chert nodules near the contact.

The Carmel Formation in the San Rafael Swell focus area is observed to thin south-eastward from ~105m (Doelling, 2002) to 80m approximated from isopach thickness maps created for the region in this study (Figure 3). In the Monument Uplift focus area, the Carmel Formation is ~35m (Figure 4) (O'Sullivan, 1998). Color alteration and calcitic mineralization along faults and fractures is observed in the San Rafael Swell focus area, yet is absent in the Monment Uplift focus area.

Jurassic Entrada Sandstone

The Jurassic Entrada Sandstone was deposited in tidal flats, offshore bars, and barrier islands (Harris et al., 2004). The different deposits can be separated unconformably into two members, the upper Earthy, and lower Slickrock members. The Earthy and Slickrock members consist of thin-bedded brown to red mudstones and siltstones that are fine- to very fine-grained in the Slickrock Member, and thin-bedded mudstones and siltstones in the Earthy Member.

In the San Rafael Swell focus area the Slickrock member of the Entrada Sandstone varies from red to pale yellow, with pale yellow in areas of alteration. In the Monument Uplift focus area the Slickrock member is observed to be unaltered, maintaining the reddish orange hue. The Slickrock member is observed in the San Rafael Swell focus area to locally overlie the Earthy member.

The Entrada Sandstone in the San Rafael Swell and Monument Uplift focus areas exhibit consistent thickness from west to east from ~150-170 m (Figures 3-4) (O'Sullivan, 1998; Doelling, 2002). Color alteration and calcitic mineralization is observed in fractures and faults in the San Rafael Swell focus area, yet are absent in the Monument Uplift focus area. In some localities of the San Rafael Swell focus area, color alteration boundaries are observed in non-fractured portions of the formation.

Jurassic Curtis Formation

The Jurassic Curtis Formation was deposited in the shallow portion of the Jurassic seaway, and consists of fossiliferous limestone, sandstone, and shale (Kocurek and Dott, 1983; Kriesa and Moiola, 1986; Nuccio and Condon, 1996). The formation is light gray to green, with a basal conglomerate overlain by sandstone and shale beds (Harris et al., 2004). The Curtis Formation is present in the San Rafael Swell focus area, but is replaced by the Wanakah Formation eastward in the Monument Uplift focus area. Correlations between the Jurassic Curtis and Wanakah Formations are not part of this study.

In the San Rafael Swell focus area, the sandstone units of the Curtis Formation consist of fine to very fine-grained sandstones with ripple cross laminations indicating bimodal paleocurrent orientation to the NE-SW (Caputo, 1988; Harris et al., 2004; Wilcox, 2007). The Curtis Formation unconformably overlies the Entrada Sandstone, and transitions to thinly bedded mudstones higher up in the formation due to drowning of the sandstone deposits during transgressive sequences (Kocurek and Dott, 1983; Kriesa and Moiola, 1986). The Curtis Formation is ~60 m thick in the San Rafael Swell focus area (Figure 3). Color alteration of host rock and/or mineralization not observed along fractures in the field areas.

METHODS

To best correlate natural analog exposures to processes at depth analog exposures were studied on three different scales: macroscopic, mesoscopic, and microscopic. The maximum areal extent of the macroscopic scale analysis is approximately 250x200 km in the San Rafael Swell focus area, with a resolution of 30 m, and a minimum structural feature size of ~1 km. The maximum areal extent of the macroscopic scale analysis in the Monument Uplift focus area is approximately 190x140 km, with a resolution of 30 m, and a minimum structural feature size of ~1 km. Mesoscopic scale analysis focuses on outcrop scale features ranging from cm-m within individual field areas of the San Rafael Swell and Monument Uplift focus areas. Microscopic scale analysis focuses on petrographical analysis of thin sections for mineral components and pore space degradation.

The San Rafael Swell focus area is separated into three 6.5 x 9.0 km field areas, SRS North, SRS Central, and SRS South. The northwest corner of the SRS North field area is located at 38°55’34.82” N, -110°29’13.30” E. The northwest corner of the SRS Central field area is located at 38°48’33.76” N, -110°31’38.50” E. The northwest corner of the SRS South field area is located at 38°41’27.24” N, -110°42’18.27” E. The Monument Uplift focus area is separated into four 6.5 x 9.0 km field areas, MU North, MU Central A, MU Central B, and MU South. The northwest corner of the MU North field area is located at 37°50’05.40” N, -109°38’47.39” E. The northwest corner of the MU Central A field area is located at 37°41’26.20” N, -109°40’28.75” E. The northwest corner of the MU Central B field area is located at 37°33’18.64” N, -109°40’17.96” E. The northwest corner of the MU South field area is located at 37°21’19.72” N, -109°40’11.31” E.

Macroscopic Scale Analysis

Advanced Spaceborne Thermal Emission and Reflection Radiometer (ASTER) satellite imagery was used to identify and map areas of specific alteration related to the migration of fluid and/or hydrocarbons through fractures, and along faults in the focus areas. The identification and mapping of alteration related to migration of fluid and/or hydrocarbons in each of the focus areas was independent of data reported previously by others.

The ASTER multi-spectral satellite images are predominantly used for detailed mineral indexing through spectral analysis (Hewson et al., 2005; Petrovic et al., 2008). Similar styles of band ratio calculation and band combination methods were used to highlight argillic alteration (Volesky et al., 2003). Due to the interest in clays potentially formed by the migration of fluids, spectral analysis was used to identify areas where kaolinite and color alteration of Jurassic units was present over a 4000x4000 pixel area with a 30 m resolution (Kalinowski and Oliver, 2004).

Detailed regional contour and isopach formation thickness maps were created using IHS Petra™ software to aid in developing depth contour and curvature maps. The depth contour and curvature maps area useful in identify heterogeneities in each of the formations that could potentially impact the integrity of top sealing formations. Extensive commercial drilling throughout each of the focus areas allows for digital gridding of a 210x160 km area in the San Rafael Swell focus area, and a 148 x110 km area in the Monument Uplift focus area using formation top data recorded in geophysical well log data (Appendix A).

Formation top data from 497 oil and gas exploration drill holes and production wells in the San Rafael Swell focus area, and 294 oil and gas exploration drill holes and production wells in the Monument Uplift focus area (Appendix A), were used in creating the contour and isopach thickness maps with an average distance between nearest neighboring wells of 2.88 km to 3.13 km respectively for grid optimization. A highly connected features (least squares) gridding method was used with a grid size of 1400-1500 m recommended by IHS Petra™. Contours were

smoothed using grid flexing with a factor of four, and a search radius of 20 units was used as a weighting function for disconnected features. Major faults are classified in this study as exhibiting 5+ km trace length (Williams and Hackman, 1971; Haynes et al., 1972; Witkind, 1988, 1995; Hintze et al., 2000; Doelling, 2002) were incorporated into the contour mapping, with a fault gap tolerance of one, minimizing the amount of void space on either side of the faults in the depth contour maps. It is important to note however, that even though the faults exhibit 5+ km trace length, the throw on these faults is disproportionately low, and would fall below seismic resolution. Wells were selected based on formation top data for the Jurassic Entrada Sandstone. For wells that did not have formation top data for the Jurassic units down-section of the Entrada Sandstone, extrapolation of the formation top depth for the Jurassic Navajo Sandstone and Carmel Formation was based on the recorded top depth in nearest neighboring wells (Appendix A). In both focus areas, the extrapolation of formation tops was necessary for geometric modeling of each of the Jurassic formation tops because it is necessary for each gridded surface to be calculated from the same XY control points, otherwise the surface of the individually gridded formation tops would have different slope values calculated from nearest neighbors, resulting in false features displaying the lower formations as cross-cutting through the upper formations.

Commercial drilling throughout Utah has resulted in a large amount of public accessible geophysical borehole data provided by the Utah Division of Oil, Gas and Mining (DOGM) (http://oilgas.ogm.utah.gov/). In addition to the geophysical data acquired during drilling, the data also consists of marked formation tops used in this study to create depth contours of both of the focus areas. In order to correlate observations in the naturally exposed analogs of the San Rafael Swell and Monument Uplift to structures and processes at depth, a reconstruction of both of the uplifts was produced to approximate the morphology of each of the folds at depth, prior to uplift and sequential erosion.

Reconstruction of each monocline using formation top data from wells in the region were used to extrapolate the surface of the Jurassic formations to model an approximate paleo-surface that would have existed at depth prior to erosion. Although the geometric reconstruction is shown for the current elevation datum, it is intended for analysis of the effects of fractures and faults on the sealing integrity of a monocline, or anticline at depth. The three Jurassic formations geometrically modeled are the Jurassic Navajo Sandstone, Carmel Formation, and Entrada Sandstone. Separation of the Slickrock Member from the Earthy Member in the Jurassic Entrada Sandstone is not possible at the macroscopic scale due to the limited resolution of the formation top data that does not distinguish between the individual members.

Geometric reconstruction of both the San Rafael Swell and Monument Uplift focus areas highlight the morphological differences between the structural sinks and highs of the two monoclines, leading to the understanding of potential sources for migrating fluids and/or hydrocarbons into the structural highs from sinks. Formation top data from 497 oil and gas drill holes and production wells (Appendix A) in the San Rafael Swell focus area were used in the reconstruction of the Jurassic units within San Rafael Swell. The top surface of the Jurassic Navajo Sandstone is reconstructed through extrapolation up-section from the formation top depth of the Permian White Rim Sandstone in drilling records, along the axis of the San Rafael Swell where the Jurassic units have been eroded. A mean difference of depth in meters was calculated between the Navajo and White Rim Sandstones based on stratigraphic formation top data from well logs, and applied the mean difference up-section to the wells in the central portion of the San Rafael Swell, producing a reconstructed top surface of the Navajo Sandstone in areas where erosion has occurred.

Formation top data from 294 oil and gas exploration drill holes and production wells (Appendix A) in the Monument Uplift focus area were used in the geometrical reconstruction of the Jurassic units within Monument Uplift. Similar to the San Rafael Swell, the Jurassic units are

eroded away along the axis of the Monument Uplift. The top surface of the Jurassic Navajo Sandstone was reconstructed by extrapolating from the current depth of the Pennsylvanian Hermosa Formation, recorded in nearby wells to apply a mean difference of depth between the two formations based on stratigraphic formation top data from well logs. The mean difference in depth was applied up-section to the wells west of Comb Ridge, the existing eastern flank of the Monument Uplift exposing the folded Jurassic units.

Major faults that were identified from previously mapped fault traces in the San Rafael Swell and Monument Uplift focus areas (Williams and Hackman, 1971; Haynes et al., 1979; Witkind, 1988, 1995; Hintze et al., 2000; Doelling, 2002), were approximated to have an average dip of 60° for normal faults (Hubbert, 1951), and were projected three-dimensionally, in order to identify faults that could potentially intersect nearby antithetic faults at depth, to help constrain the nature of possible upward migration potentials for fluid and/or hydrocarbons along multiple fault boundaries.

Mesoscopic Scale Analysis

Individual field areas identified through the analysis of processed satellite imagery were analyzed one and two dimensionally for possible connectivity of fractures in successive stratigraphic layers from both bedding and pavement orientations (Figure 6). Analysis of outcrops in the identified field areas was accomplished by using 2- to 5- m scanline sampling of outcrop exposures. This data was used to quantify fracture patterns and faulting that may enhance the connectivity of migration pathways between successive stratigraphic layers in the Jurassic formations. Fracture orientation, spacing, trace length, density per length, and aperture were measured, noting the presence or absence of mineralization for the low-permeability caprocks and porous sandstone reservoir rocks in exposed analog monoclinal folds. The data acquired from scanline sampling was used to increase understanding as to how faults and

fractures affect the sealing integrity of caprocks, and migration of fluid and/or hydrocarbons in the underlying reservoir rocks.

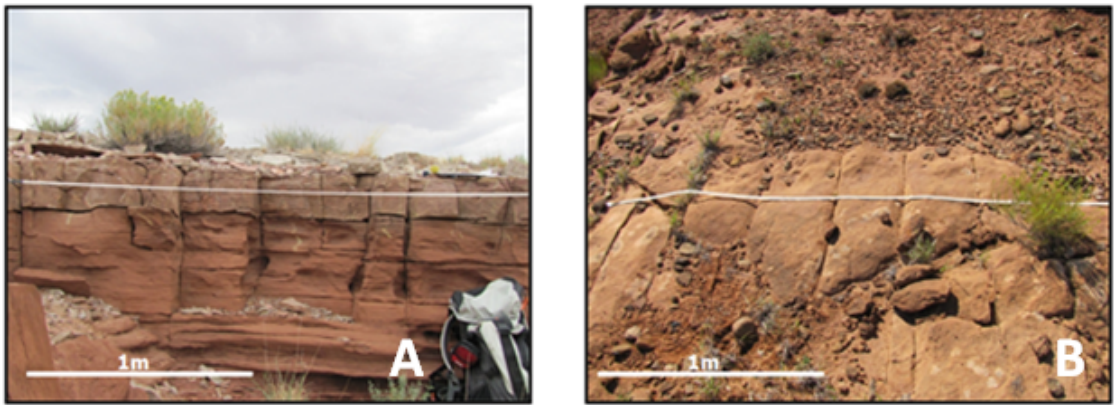

Figure 6. Bedding scanline on vertical exposure (A) in the SRS South field area, view is eastward. Pavement scanline on bedding plane exposure (B) in the SRS Central field area view is eastward. Both photos are the Paria Member of the Jurassic Carmel Formation.

Microscopic Scale Analysis

Rock samples were collected for the Jurassic Navajo Sandstone, Page Sandstone (San Rafael Swell focus area only), Carmel Formation, Entrada Sandstone (Slickrock and Earthy members), and Curtis Formation (San Rafael Swell focus area only) in the San Rafael Swell and Monument Uplift focus areas. Samples exhibiting evidence of fluid migration in the form of color alteration of host rock or mineralization within fractures, were collected from each Jurassic unit. Additionally, samples were collected from each Jurassic unit where color alteration and/or mineralization of fractures were minimal or not present for comparison with altered samples. Billets were produced for each of the samples and stained for pore space analysis, with the petrographic thin sections professionally produced by Burnham Petrographics. The petrographic thin sections were used to evaluate percentages of altered feldspar, calcite, and oxide in the pore space interpreted to be associated with migration of fluid and/or hydrocarbons.

The degree of cementation within pore space, or degradation (Laubach, 2003), was analyzed statistically through the use of graphical analysis software, Image J, in which the photomicrographs from each of the samples were analyzed by pixilation of features at the microscopic scale. The statistical analysis was used to investigate the degradation of each sample, and enhance the porosity values used in volumetric calculations in the geometric modeling.

RESULTS

Macroscopic Scale Characterization

Areas that exhibited the possible presence of kaolinite and color alteration of host rock on the eastern limb of the San Rafael Swell on the basis of analysis of ASTER data were field checked for accuracy of spectral analysis methods. Individual target field areas within the San Rafael Swell were chosen based on the combination of host rock alteration in blue and kaolinite alteration in orange. Alteration features include mineralized veins in fractures, color alteration of host rock, color alteration along fractures, and mineralization associated with faults and fractures (Figure 7) that were observed in areas that exhibited both host rock and kaolinite alteration. The names of individual field areas were based on local geographical features in the area.

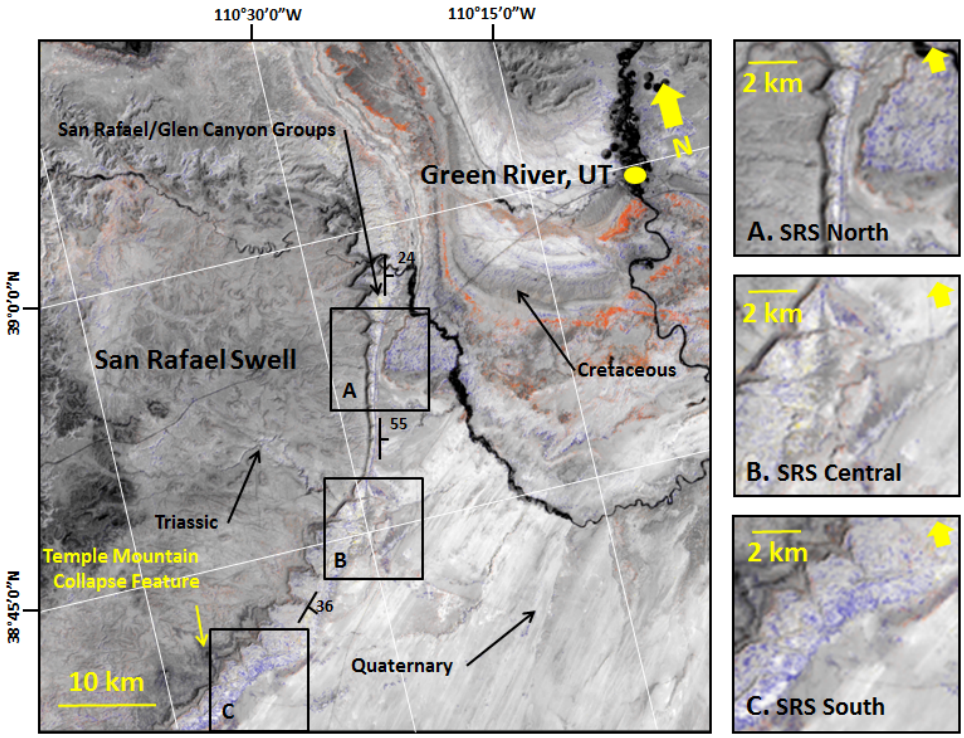

Figure 7. Processed ASTER 30 m satellite image (4000x4000 pixel) with kaolinite (orange) and host rock alteration (blue) overlays. (A) SRS North field area (North) (B) SRS Central field area (Central) (C) SRS South field area (South).

The Monument Uplift was chosen as a secondary focus area because of the structural and stratigraphic similarities, and contrasting alteration features between the two folds (Figure 8). Individual field areas within the Monument Uplift were chosen based on surface exposure of the Jurassic units along the eastern flank of the Monument Uplift rather than by presence of alteration, because extensive clay and host rock alteration is absent (Figure 8), as are calcite mineralization veins within fractures, and color alteration halos surrounding open and closed fractures. Although alteration of host rock is observed in the Navajo Sandstone in blue, and kaolinite is present along stream channels in orange, the Monument Uplift focus area does not exhibit the combination of the two types of alteration in the same localities.

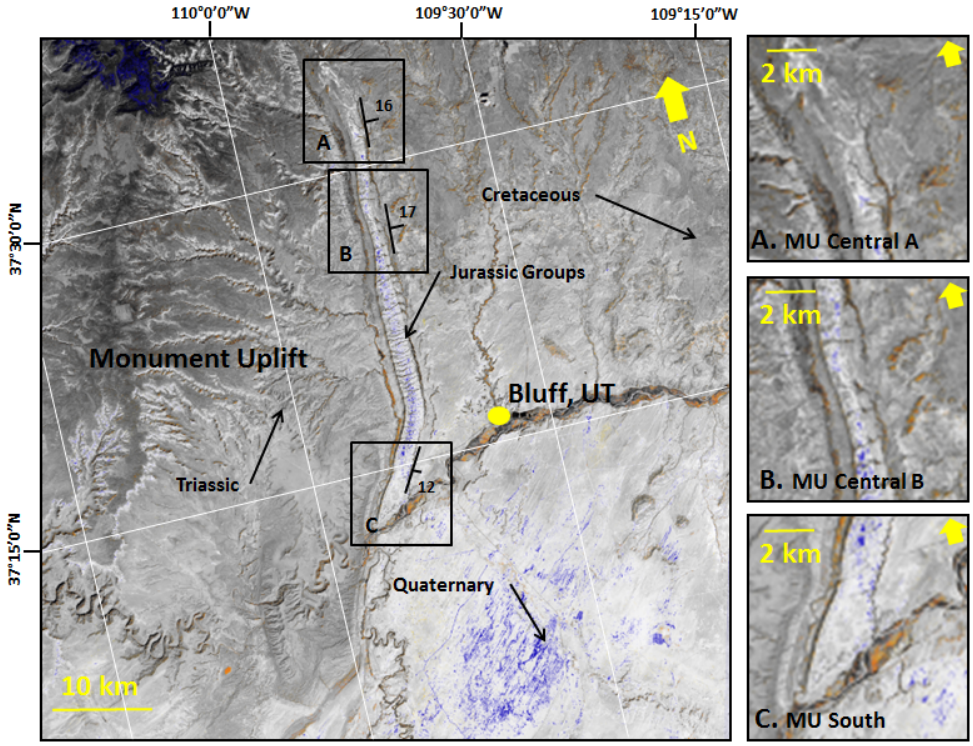

Figure 8. Processed ASTER 30 m satellite image (4000x4000 pixel) with kaolinite (orange) and host rock alteration (blue) overlays. (A) MU Central A field area. (B) MU Central B field area. (C) MU South field area. The MU North field area is not shown here.

San Rafael Swell Focus Area

The depth contour map of the Jurassic Navajo Sandstone, Carmel Formation, and Entrada Sandstone illustrate the geometrical reconstruction of the San Rafael Swell in meters of total vertical depth above mean sea level (TVD SS) (Figures 9-11). The geometric reconstruction reveals an approximate 4 km difference between the structural low located in the southern Uinta Basin, and the reconstructed structural high along the axis of the San Rafael Swell in the Jurassic Navajo Sandstone, Carmel Formation, and Entrada Sandstone.

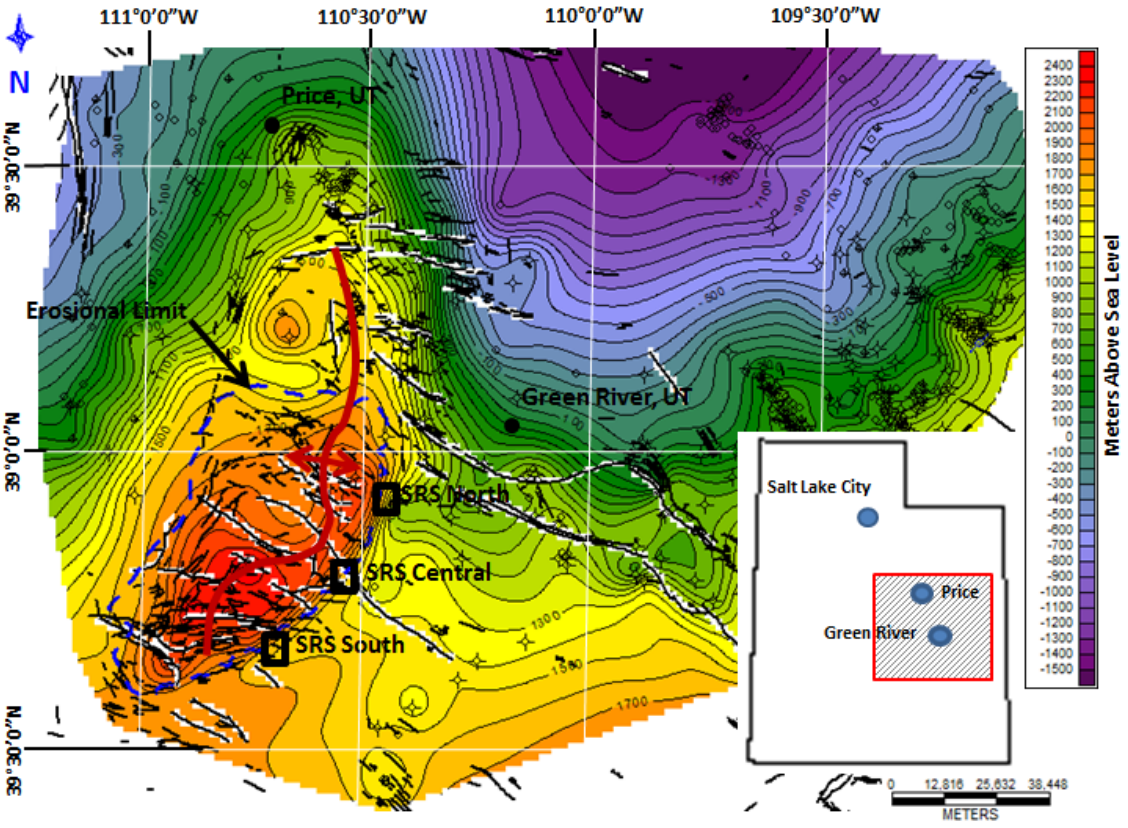

Figure 9. Geometrical reconstruction of the Jurassic Navajo Sandstone top surface in the San Rafael Swell focus area and the adjacent southern Uintah Basin. Red represents the structural high, purple represents the structural low at 100 m contour intervals (TVD SS). The blue dashed area represents the erosional limit in the reconstruction. Field areas are identified in boxes, SRS North field area, SRS Central field area, and SRS South field area. (Faults adapted from Williams and Hackman, 1971; Haynes et al., 1979; Witkind, 1988, 1995; Hintze et al., 2000; Doelling, 2002).

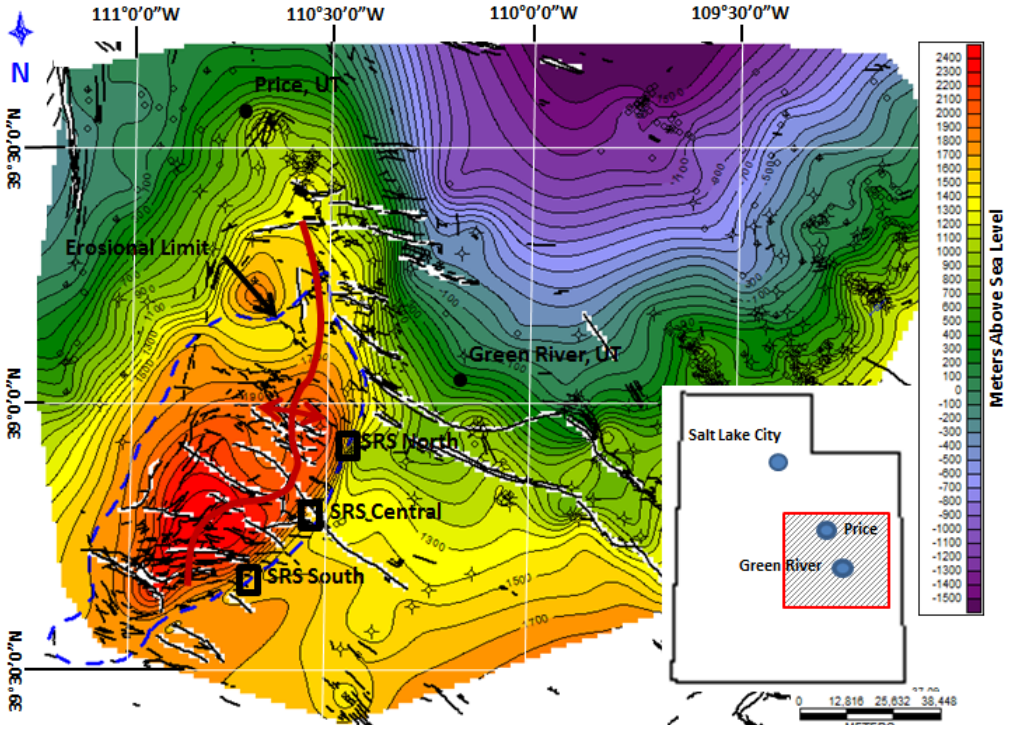

Figure 10. Geometrical reconstruction of the Jurassic Carmel Formation top surface in the San Rafael Swell focus area and the adjacent southern Uintah Basin. Red represents the structural high, purple represents the structural low at 100 m contour intervals (TVD SS). The blue dashed area represents the erosional limit in the reconstruction. Field areas are identified in boxes, SRS North, SRS Central, and SRS South. (Faults adapted from Williams and Hackman, 1971; Witkind, 1988, 1995; Haynes et al., 1979; Hintze et al., 2000; Doelling et al., 2002).

Curvature is defined as the reciprocal of the radius of curvature (Roberts, 2001). A dip curvature map of the reconstructed Jurassic Navajo Sandstone in the San Rafael Swell focus area was calculated using IHS Petra™ software grid application (Roberts, 2001). The highest curvature values are located along the south-eastern flank of the San Rafael Swell and other smaller anticlines in the region (Figure 12). SRS Central and SRS South field areas exhibit higher curvature than SRS Central field area, and is interpreted this to be due to local faulting in the area.

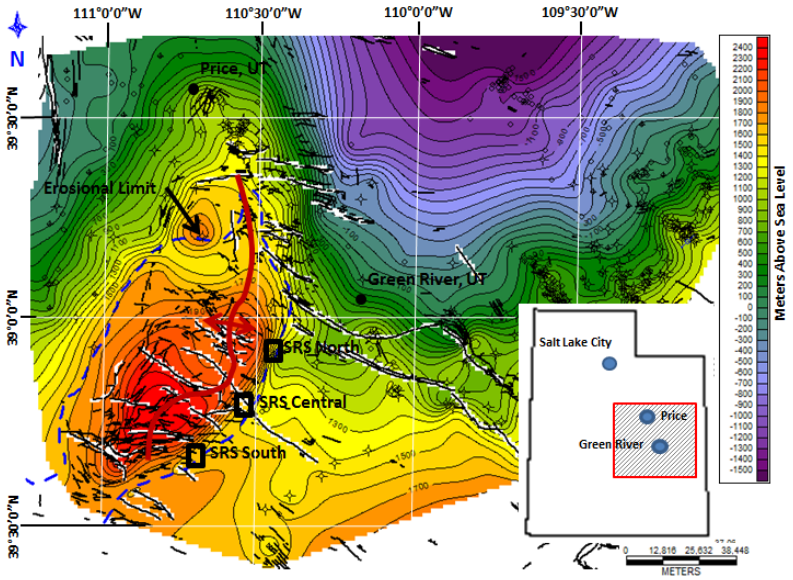

Figure 11. Geometrical reconstruction of the Jurassic Entrada Sandstone top surface in the San Rafael Swell focus area and the adjacent southern Uintah Basin. Red represents the structural high, purple represents the structural low at 100 m contour intervals (TVD SS). The blue dashed area represents the erosional limit in the reconstruction. Field areas are identified in boxes, SRS North, SRS Central, and SRS South. (Faults adapted from Williams and Hackman, 1971; Haynes et al., 1979; Witkind, 1988, 1995; Hintze et al., 2000; Doelling, 2002).

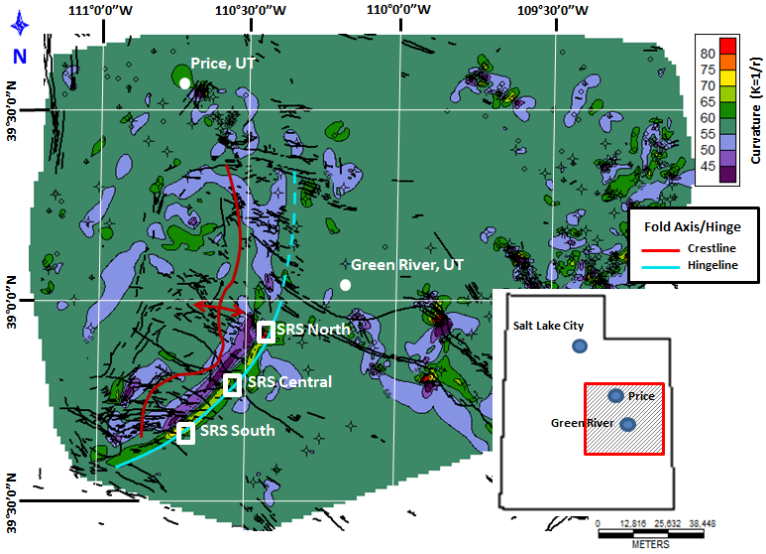

Figure 12. Dip curvature map calculated from reconstruction of San Rafael Swell for the Navajo Sandstone. Curvature is the reciprocal of curvature radius, K=1/r (Roberts, 2001). The hingeline identified by maximum curvature. Field areas are identified in boxes, SRS North, SRS Central, and SRS South. (Faults and fold axis adapted from Williams and Hackman, 1971; Witkind, 1988, 1995; Haynes et al., 1979; Hintze et al., 2000; Doelling et al., 2002).

Monument Uplift Focus Area

The depth contour map of the Jurassic Navajo Sandstone, Carmel Formation, and Entrada Sandstone, illustrate a geometrical reconstruction of the Monument Uplift in meters of total vertical depth above mean sea level (TVD SS) (Figures 13-15). The geometric reconstruction reveals an approximate 1.5 km difference between the structural low located in the Paradox Basin, and the reconstructed structural high along the axis of the Monument Uplift in the Jurassic Navajo Sandstone, Carmel Formation, and Entrada Sandstone.

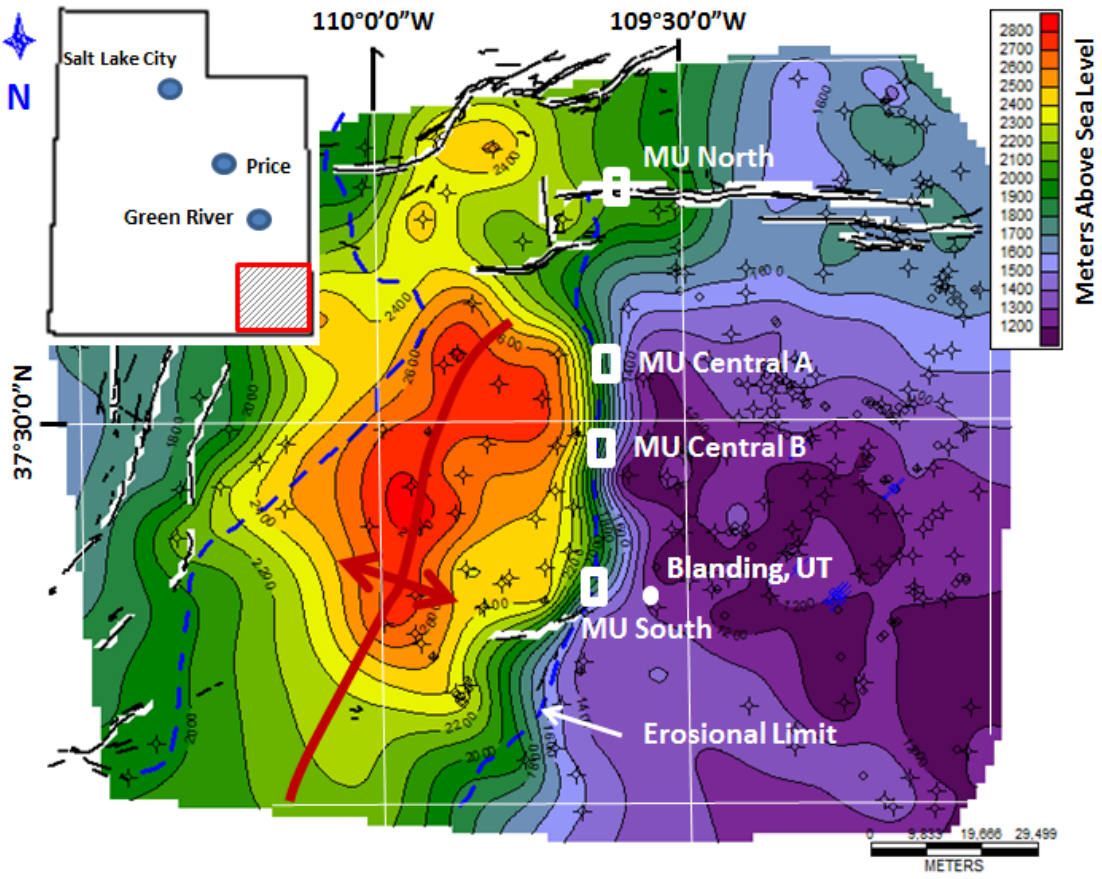

Figure 13. Geometrical reconstruction of the Jurassic Navajo Sandstone top surface in the Monument Uplift focus area and the adjacent Paradox Basin. Red represents the structural high, purple represents the structural low at 100 m contour intervals (TVD SS). The blue dashed area represents the erosional limit in the reconstruction. Field areas are identified in boxes, MU North, MU Central A, MU Central B, and MU South. (Faults adapted from Haynes et al., 1979, and Hintze et al., 2000).

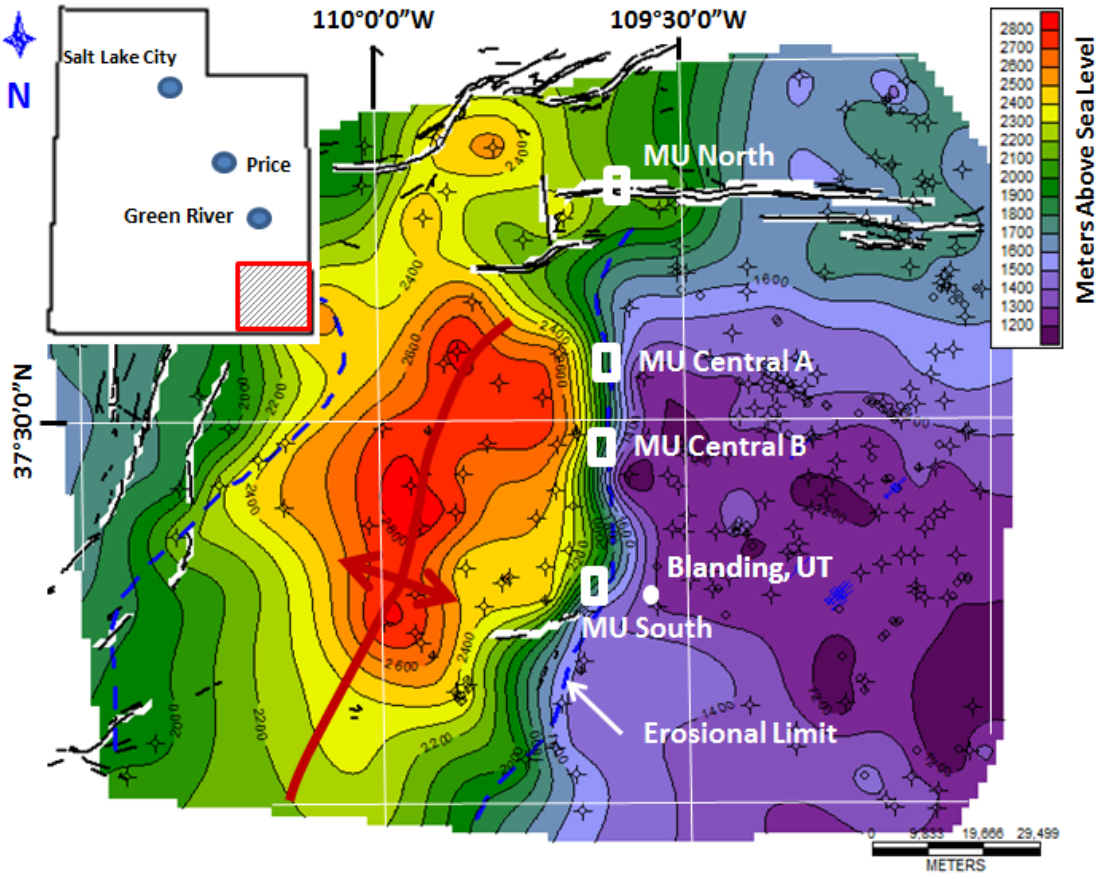

Figure 14. Geometrical reconstruction of the Jurassic Carmel Formation top surface in the Monument Uplift focus area and the adjacent Paradox Basin. Red represents the structural high, purple represents the structural low at 100 m contour intervals (TVD SS). The blue dashed area represents the erosional limit in the reconstruction. Field areas are identified in boxes, MU North, MU Central A, MU Central B, and MU South. (Faults adapted from Haynes et al., 1979, and Hintze et al., 2000).

A dip curvature of the reconstructed Jurassic Navajo Sandstone in the Monument Uplift focus area was calculated using IHS Petra™ software grid application (Roberts, 2001). Curvature is represented by the same color scale as was presented in the San Rafael Swell curvature map (Figure 12), and reveals significantly lower curvature in the Monument Uplift focus area (Figure 16).

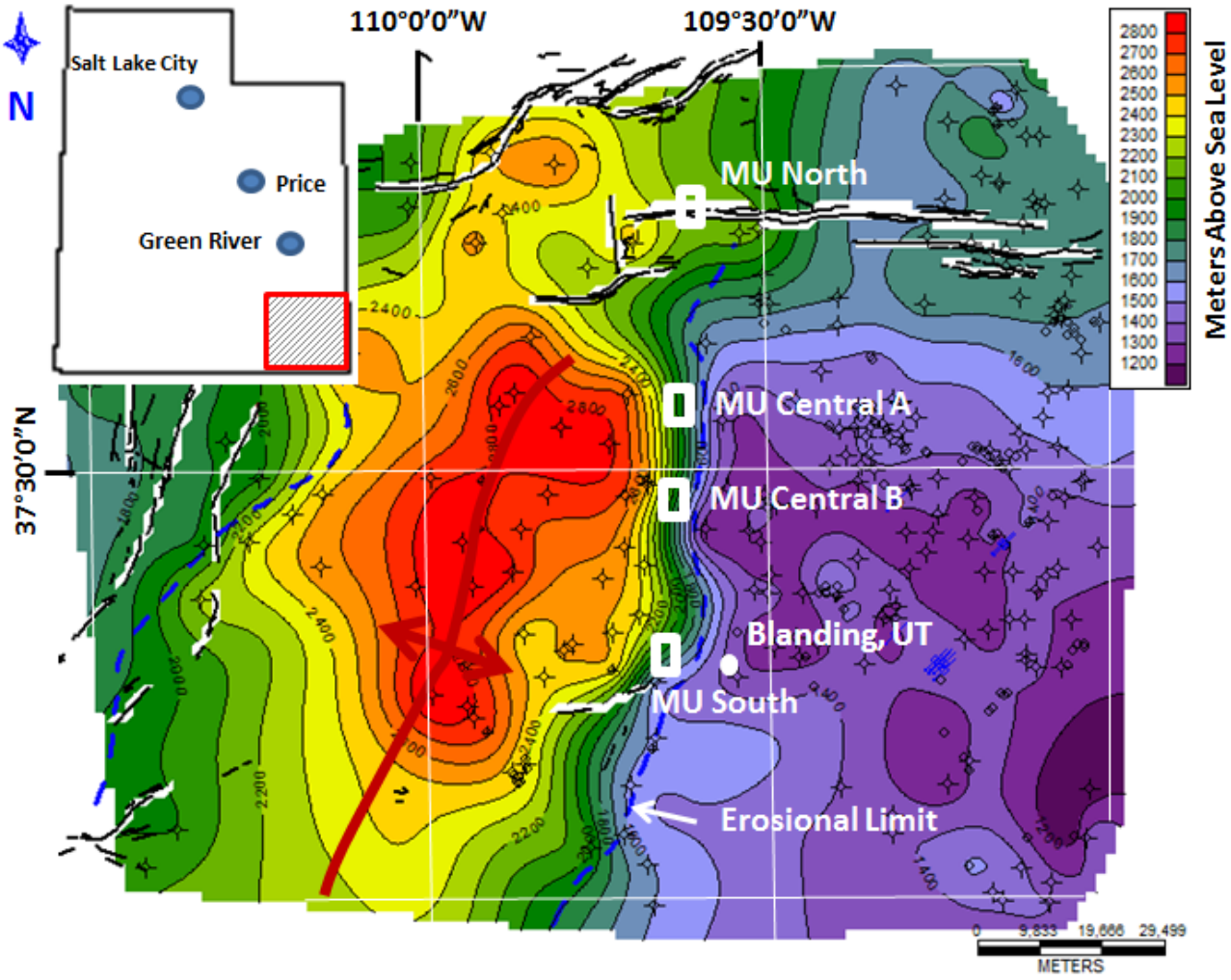

Figure 15. Geometrical reconstruction of the Jurassic Entrada Sandstone top surface in the Monument Uplift focus area and the adjacent Paradox Basin. Red represents the structural high, purple represents the structural low at 100 m contour intervals (TVD SS). The blue dashed area represents the erosional limit in the reconstruction. Field areas are identified in boxes, MU North, MU Central A, MU Central B, and MU South. (Faults adapted fromHaynes et al., 1979, and Hintze et al., 2000).

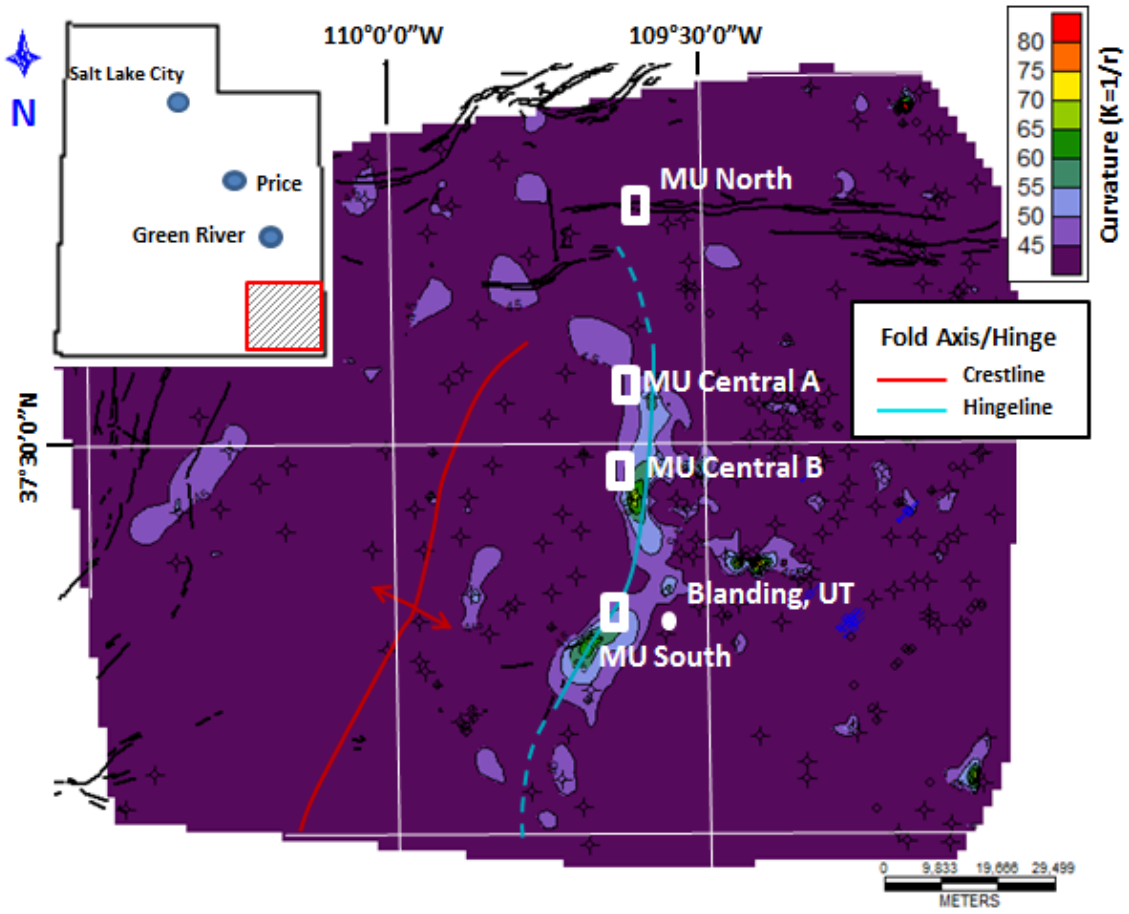

Figure 16. Dip curvature map calculated from reconstruction of San Rafael Swell for the Navajo Sandstone. Curvature is the reciprocal of curvature radius, K=1/r (Roberts, 2001). The hingeline is identified by maximum curvature. Field areas are identified in boxes, MU North field area, MU Central A field area, and MU Central B field area, and MU South field area. (Faults and fold axis adapted from Haynes et al., 1979, and Hintze et al., 2000).

Mesoscopic Scale Characterization

The nature of fracture transitions were examined in erosional exposures of sandstone, siltstone, mudstone, and shale sequences. The scanline station and outcrop sampling locations were plotted in each of the field areas previously identified in the processed satellite data. Mean fracture orientations were calculated for each of the stations using Orient 2.1 (Vollmer, 2010), presented in a rose diagram format.

San Rafael Swell Focus Area

Field areas are defined in this study as broad areas of interest identified for further inspection. Three field areas within the San Rafael Swell focus area were analyzed one and two dimensionally for fracture orientation, spacing, mineralization within fractures, trace length, fracture density, and aperture (Appendix B). The field areas are located along the eastern flank of the San Rafael Swell are named by geographic locality and include SRS North, SRS Central, and SRS South. Areas within a field area where measurements were recorded are identified as stations. A total of 32 stations, with n=738 fracture orientations analyzed in the Jurassic Navajo Sandstone, Page Sandstone, Carmel Formation, Entrada Sandstone, and Curtis Formation (Appendix B). Each of the field areas in the San Rafael Swell focus area exhibit euhedral calcite mineralization within fractures that indicate calcite growth in fractures developed at depth, and are not related to surficial meteoric fluxes (P. Mozeley, personal comm., 2011).

The SRS North field area lies along the steeply dipping limb on the eastern flank of the San Rafael Swell, dipping 42-55° east. Major faults classified in this study as exhibiting surface trace length >5 km are not found in proximity to the SRS North field area (Doelling, 2002). The SRS Central field area is a moderately dipping limb on the eastern flank of the San Rafael Swell, dipping 17-24° east. Major faults are mapped in the SRS Central field area (Doelling, 2002), and are interpreted to be associated with alteration of host rock and calcite mineralization within fractures (Figure 7). The SRS South field area is a shallow dipping limb on the southeastern flank of the San Rafael Swell, dipping 8-17° southeast. Major faults are mapped near the SRS South field area (Doelling, 2002), with alteration of host rock and mineralization of fractures in the area interpreted to be associated with the collapse feature near Temple Mountain (Kerr et al., 1957) (Figure 7). Hydrothermal solutions are interpreted to have removed the underlying Kaibab

Limestone (Kerr et al., 1957), allowing for host rock alteration and mineralization along faults and fractures in the area (Hawley et al., 1968).

SRS North Field Area

In the SRS North filed area a total of seven stations, with n=108 fracture orientations (Figure 17) were measured in the Jurassic Navajo Sandstone, Page Sandstone, Carmel Formation, Entrada Sandstone, and Curtis Formation (Figure 18). Station locations and sample numbers and listed with mean fracture orientations (Table 1). Orientations for each formation and local faults in the area are presented with rose diagrams, with the mean fracture orientation and dispersion of fracture strikes represented in each of the areas (Figure 19).

Extensive color alteration of rock matrix is observed in the Jurassic Navajo Sandstone and Slickrock member of the Entrada Sandstone throughout the field area. Color alteration of host rock occurs in the Carmel Formation as 2-4 cm symmetric halos on both sides of open and closed fractures (Figure 18a). Fracture aperture in the field area ranges from <1mm to 4 mm with euhedral calcite mineralization of the fracture observed in the Jurassic Navajo Sandstone (Figure 20b), Carmel Formation, and Entrada Sandstone. Euhedral growth of calcite crystals in open fractures is an indicator for mineral growth in an open fracture at depth (Figure 20c). Fractures in the Jurassic Curtis Formation are predominantly open with ≤ 1mm aperture.

Fracture orientations are uniform between each of the Jurassic units with exception for the Curtis Formation. Fractures extend across individual bedding planes within the Jurassic units, and in many cases transect depositional contacts. Fracture frequency within each lithology decreases with increasing bed thickness (Figure 21), with deformation bands occurring sporadically in 0.5-1.0 m zones within the eolian Navajo and Entrada Sandstones. Strong uniformity is observed in fracture orientations within the Navajo Sandstone, Carmel Formation, and Entrada Sandstone, with variation from the northwest to southeast orientation observed in the

Curtis Formation (Figure 19). Fracture orientations are uniform in the Navajo Sandstone, Carmel Formation, and Entrada Sandstone to may enhance connectivity of migration pathways through the potential sealing Carmel Formation.

The northwest strike of faults (Figure 19) in the area is interpreted to have developed in response joint shearing during a younger phase of deformation than the original Laramide age ENE faults (Davatzes et al., 2003). Fracture orientations in the Entrada Sandstone, Carmel Formation and Navajo Sandstone are consistent with the joint shear interpretation (Figure 19). It is unclear why the joint shear faults and fractures did not develop in the Curtis Formation, but it is possible that the mechanism for fracture development in the Curtis Formation was related to pressure solution seams that formed orthogonal to maximum stress. An increase in fault parallel permeability would be predicted for the Navajo Sandstone, Carmel Formation, and Entrada Sandstone that would provide conduit for fluid migration through the seal. The shale beds in the Curtis Formation would potentially provide seal against upward migration of fluid and/or hydrocarbon due to the lack of joint shear in the ENE striking fractures.

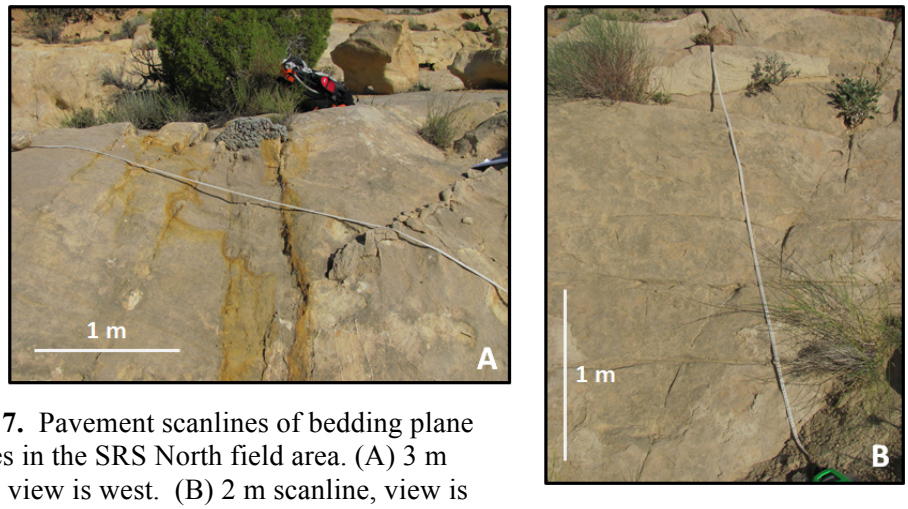

Figure 17. Pavement scanlines of bedding plane exposures in the SRS North field area. (A) 3 m scanline, view is west. (B) 2 m scanline, view is north. Both photos are the Slickrock Member of the Jurassic Entrada Sandstone.

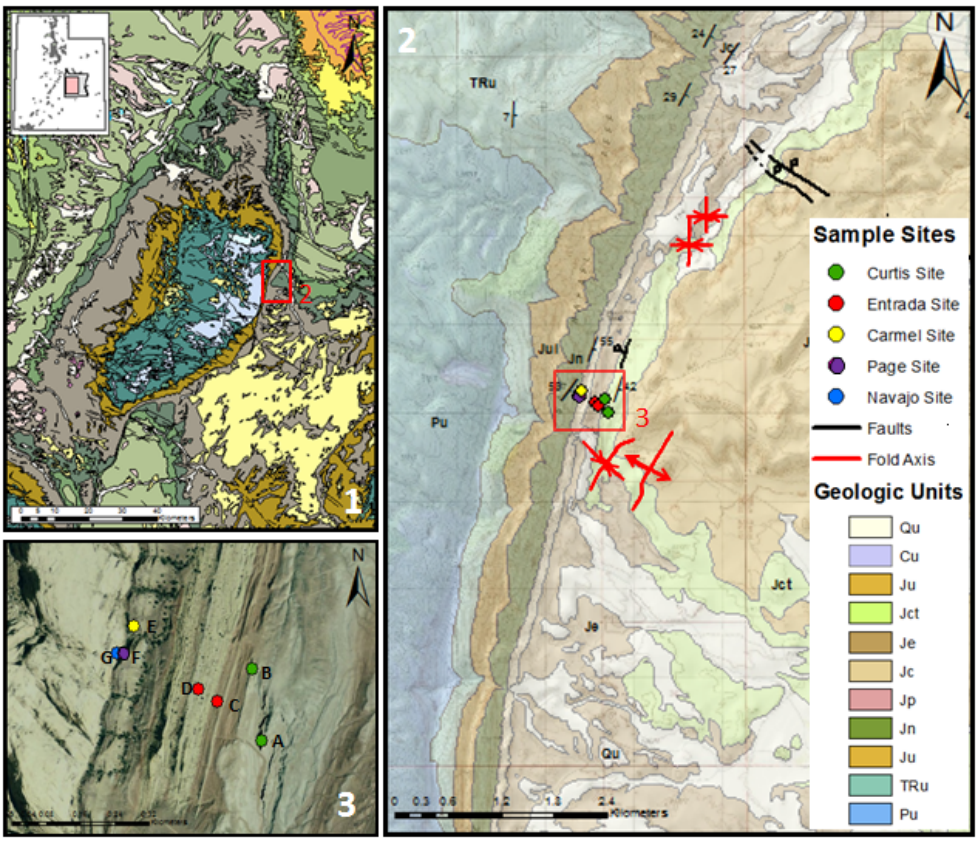

Figure 18. (1) Regional geologic map showing field area location (Adapted from Hintze et al., 2000). (2) Geologic map of SRS North field area showing sample sites (Modified from Doelling, 2002). (3) Sample sites with locations labeled.

Table 1. SRS North field area mean fracture orientations.

San Rafael Swell - North						
Location	**Formation**	**Station**	**n**	**Mean Strike**	**Mean Dip**	**GPS Location**
A	Curtis	SQ-CU-1A	16	252	72 S	12S 0547637 4304196
B	Curtis	SQ-CU-1B	12	16	46 W	12S 0547616 4304353
C	Entrada	SQ-EN-1A	14	318	78 SW	12S 0547533 4304282
D	Entrada	SQ-EN-2A	14	321	75 SW	12S 0547491 4304308
E	Carmel	SQ-CA-1A	24	332	34 W	12S 0547340 4304445
F	Page	SQ-PA-1A	14	316	80 SW	12S 0547316 4304388
G	Navajo	SQ-NA-1A	14	314	81 SW	12S 0547316 4304388

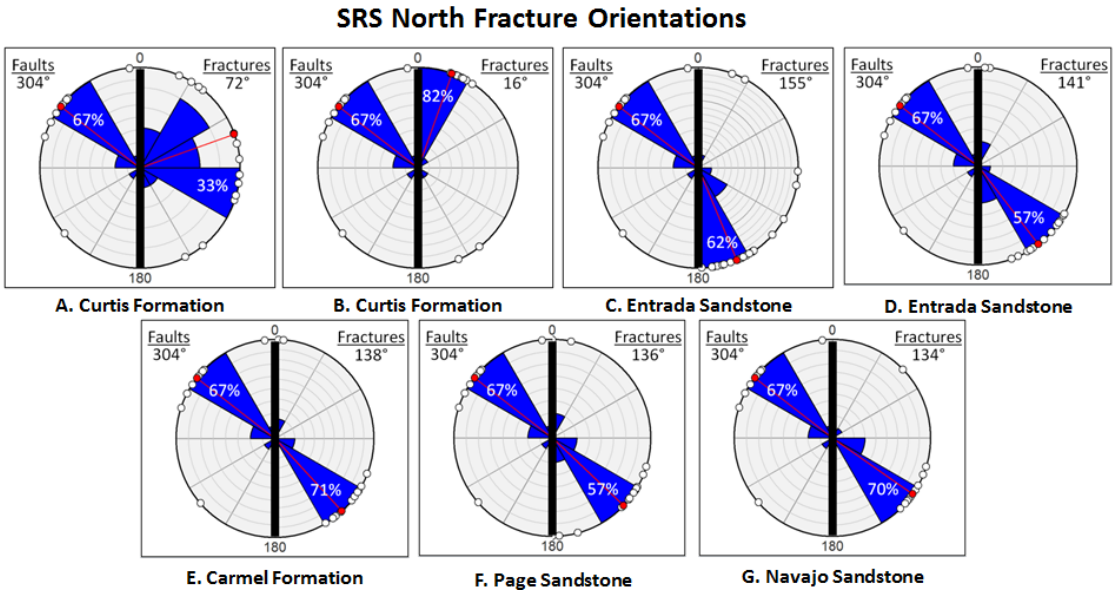

Figure 19. SRS North fracture orientations (right side) plotted with orientations of nearby faults (left side). Labels correlate to station locations in Table 1. (Fault orientation measured from previously mapped faults (Doelling, 2002, and Hintze et al., 2000). Rose diagrams created using Orient 2.1.1 (Vollmer, 2010).

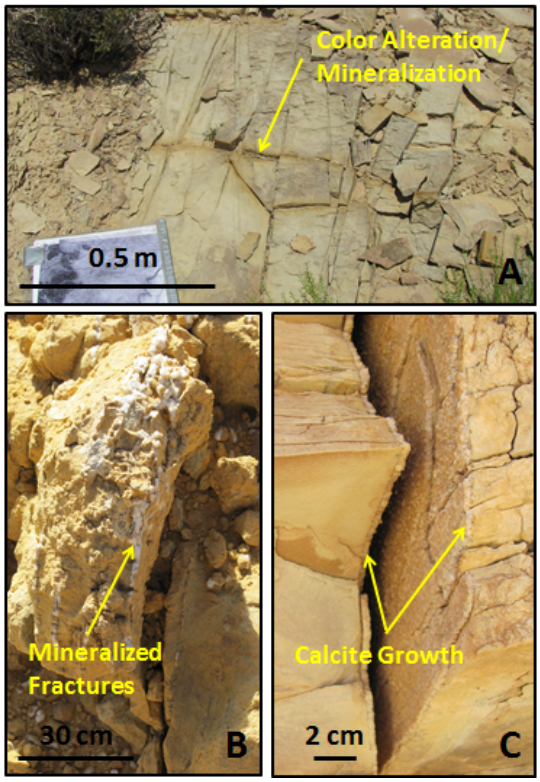

Figure 20. Alteration features in the SRS North field area. (A) Color alteration halo and mineralization of fractures in upper Carmel Formation, view is west. (B) Calcite mineralization of fractures in the Navajo Sandstone, view is south. (C) Symmetrical calcite growth on each side of open fracture in upper Carmel Formation, view is southeast.

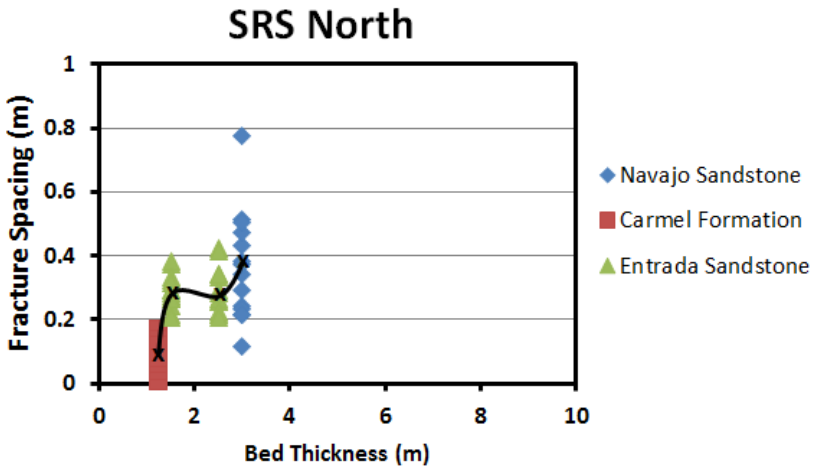

Figure 21. Fracture spacing data plotted against bed thickness for the SRS North field area.

S*RS Central Field Area*

A total of 13 stations, with n=282 fracture orientations were measured in the SRS Central field area (Figure 22), for the Jurassic Navajo Sandstone, Carmel Formation, and Entrada Sandstone Figure 24). Station locations and sample numbers and listed with mean fracture orientations (Table 2). Orientations for each formation are presented with rose diagrams, with the mean fracture orientation and dispersion of fracture strikes represented in each of the areas (Figure 23).

Extensive color alteration of rock matrix is observed in the Jurassic Navajo Sandstone, and Slickrock member of the Entrada Sandstone throughout the field area. Color alteration of host rock in the Jurassic Carmel Formation and Earthy member of Entrada Sandstone occur as 1 to 6 cm wide symmetric halos on both sides of open and closed fractures (Figure 25a). Fracture aperture in the field area ranges from <1mm to 5 mm, with euhedral calcite mineralization within fractures observed in the Jurassic Navajo Sandstone, Carmel Formation, and Entrada Sandstone (Figure 25b). The Jurassic Curtis Formation is not present in the SRS Central field area.

Fracture orientations are uniform between each of the Jurassic units, with an increase in fracture frequency compared SRS North and SRS South field areas. Fractures extend across individual bedding planes within the Jurassic formations, and in many cases continue across formation contacts (Figure 25c). Fracture frequency within the Jurassic Navajo and Entrada Sandstones, is consistently higher than observations in the SRS North and SRS South field areas, interpreted to result from proximity of extensive oblique normal faulting in the area (Figure 26) (Doelling, 2002). Deformation bands occur in 1-20 m wide zones within the Jurassic Navajo and Entrada Sandstones. The deformation bands in the area are prominent in the Slickrock member of the Entrada Sandstone, tipping out into the Earthy member. Increased fracture density exists in 2-5 m damage zones of smaller faults, synthetic to the larger oblique normal faults in the field area. Fracture orientations are strongly uniform within the Navajo Sandstone, Carmel Formation, and Entrada Sandstone (Figure 23). The uniformity of fracture orientations in the Navajo Sandstone, Carmel Formation, and Entrada Sandstone may enhance the connectivity of migration pathways through the potential sealing Carmel Formation.

The northwest strike of faults (Figure 23) in the area is interpreted to have developed in response joint shearing during a younger phase of deformation than the original Laramide age ENE faults (Davatzes et al., 2003). Fracture orientations in the Entrada Sandstone, Carmel Formation and Navajo Sandstone are consistent with the joint shear interpretation (Figure 23). ENE fractures consistent with Laramide age deformation (Davatzes et al., 2003; Erslev and Koenig, 2009) are present at a lesser degree in each of the formations. The dominant northwest striking joint shear are interpreted to have overprinted the ENE fractures in this area. An increase in fault parallel permeability would be predicted for the Navajo Sandstone, Carmel Formation, and Entrada Sandstone that would provide conduit for fluid migration through the potential sealing Carmel Formation.

Table 2. SRS Central field area mean fracture orientations.

San Rafael Swell - Central						
Location	**Formation**	**Station**	**n**	**Mean Strike**	**Mean Dip**	**GPS Location**
A	Entrada	SP-EN-4B	24	315	85 SW	12S 0545012 4295136
B	Entrada	SP-EN-4A	34	302	69 N	12S 0545012 4295134
C	Entrada	SP-EN-3B	10	282	87 N	12S 0545012 4295134
D	Entrada	SP-EN-3A	26	287	72 S	12S 0545168 4288187
E	Entrada	SP-EN-2A	26	266	76 S	12S 0544872 4287553
F	Entrada	SP-EN-1B	12	268	78 S	12S 0544872 4287537
G	Carmel	SP-CA-1B	30	306	81 N	12S 0545012 4295130
H	Carmel	SP-CA-2A	16	320	87 SW	12S 0545099 4288042
I	Carmel	SP-CA-1A	40	27	73 W	12S 0544166 4288092
J	Carmel	SP-CA-2A	16	317	87 SW	12S 0543352 4289272
K	Navajo	SP-NA-3A	10	314	81 NW	12S 0545012 4295130
L	Navajo	SP-NA-2A	14	326	84 NW	12S 0543352 4289272
M	Navajo	SP-NA-1A	24	340	87 SW	12S 0544166 4288092

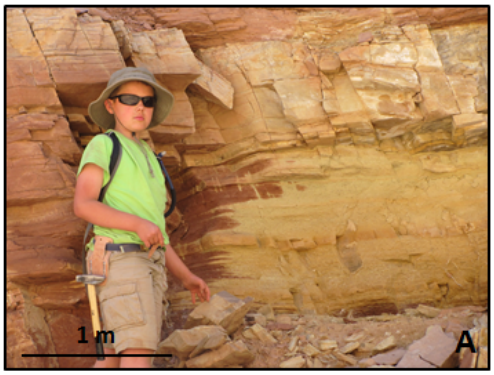

Figure 22. Alteration and mineralization of fractures in outcrop in the SRS Central field area (A) Alteration in Jurassic Carmel Formation, view is east. (B) Mineralized fractures in Winsor Member of Jurassic Carmel Formation, view is east.

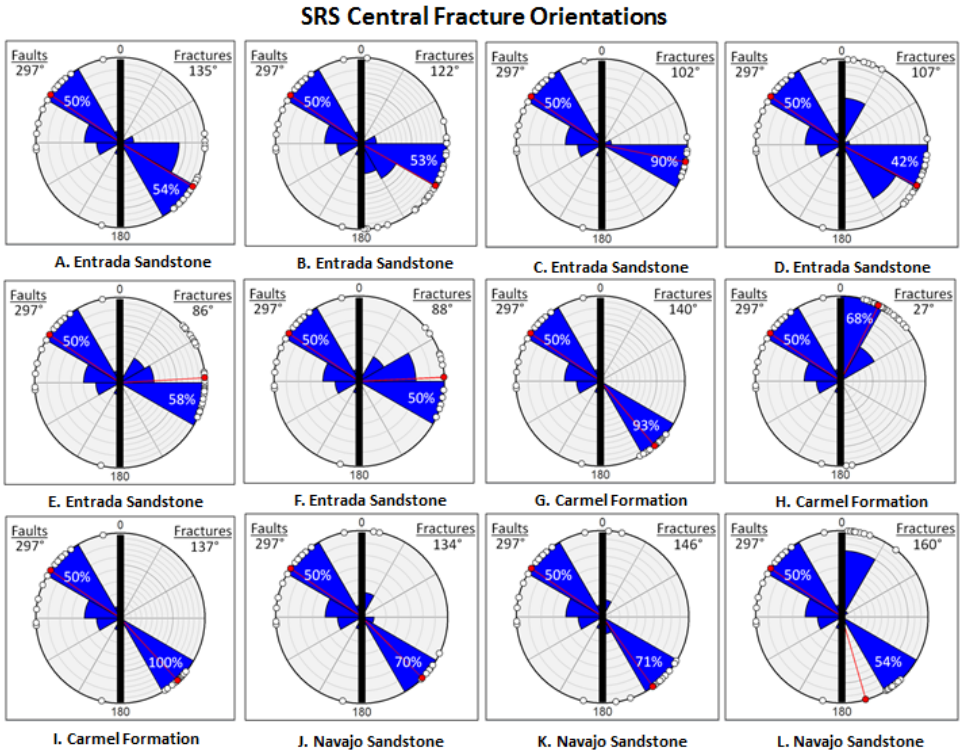

Figure 23. SRS Central fracture orientations (right side) plotted with orientations of nearby faults (left side). Labels correlate to station locations in Table 2. (Fault orientation measured from previously mapped faults (Doelling, 2002, and Hintze et al., 2000). Rose diagrams created using Orient 2.1.1 (Vollmer, 2010).

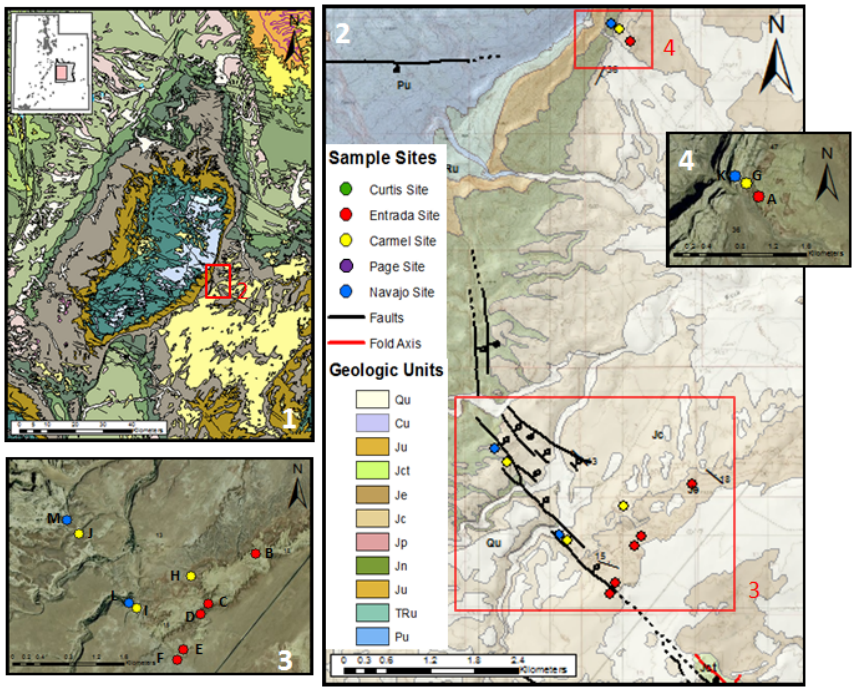

Figure 24. (1) Regional geologic map showing field area location (Adapted from Hintze et al., 2000). (2) Geologic map of SRS Central field area showing sample sites (Modified from Doelling, 2002). (3-4) Sample sites with locations labeled. Major faulting in the field area transects the eastern flank of the San Rafael Swell.

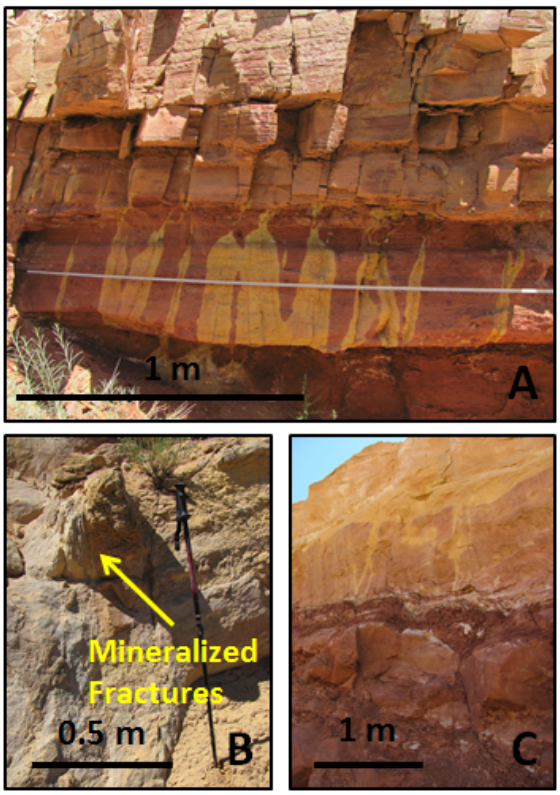

Figure 25. Alteration features in the SRS Central field area. (A) Color alteration halo and mineralization of fractures in upper Carmel Formation, view is northwest. (B) Calcite mineralization of fractures in the Entrada Sandstone, view is south. (C) Fractures extending through bedding planes in Carmel Formation and Entrada Sandstone.

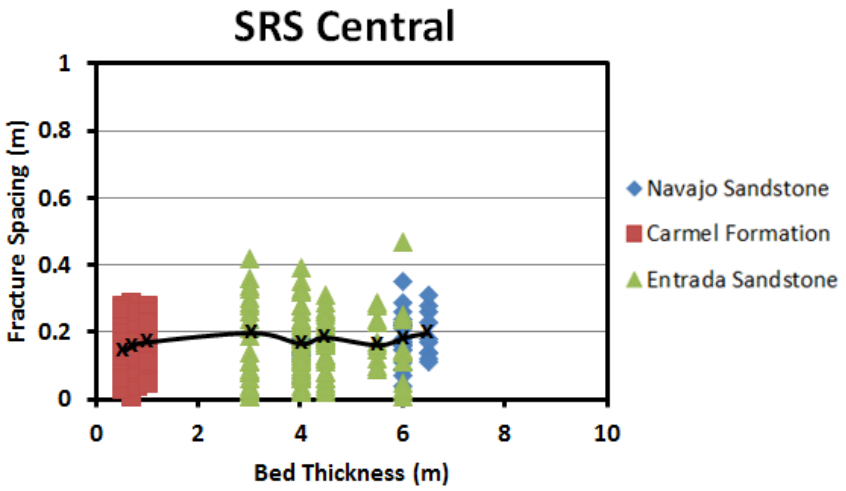

Figure 26. Fracture spacing data plotted against bed thickness for the SRS Central field area.

SRS South Field Area

A total of 12 stations, with n=348 fracture orientations were analyzed in the SRS South field area (Figure 27), for the Jurassic Navajo Sandstone, Page Sandstone, Carmel Formation, and Entrada Sandstone (Figure 29). Station locations and sample numbers and listed with mean fracture orientations (Table 3). Orientations for each formation are presented with rose diagrams, with the mean fracture orientation and dispersion of fracture strikes represented in each of the areas (Figure 30).

Extensive color alteration of rock matrix is observed in the Jurassic Navajo Sandstone, Slickrock member of the Entrada Sandstone, and Page Sandstone throughout the field area. Color alteration of host rock in the Carmel Formation occurs as 1 to 5 cm symmetric halos on both sides of open and closed fractures (Figure 29b). Extensive color alteration in the Carmel Formation occurs in damage zones up section from small faults in the Navajo Sandstone. Fracture aperture in the field area ranges from <1mm to 4 mm, with calcite mineralization of the fracture observed in the Jurassic Navajo Sandstone, Page Sandstone, Carmel Formation, and Entrada Sandstone (Figure 28a).

Fracture orientations are variable between each of the Jurassic units. Fractures extend across individual bedding planes within the Jurassic formations, and in many cases continue across depositional contacts (Figure 28b). The mean fracture frequency within each lithology decreases with increasing bed thickness (Figure 31), with deformation bands occurring sporadically in 0.5-1.0 m zones within the eolian Navajo and Entrada Sandstones. Variation in fracture orientation is recorded in each of the Jurassic units (Figure 30), and is likely due to the Temple Mountain collapse feature where hydrothermal solutions are interpreted to have removed the underlying Kaibab Limestone (Kerr et al., 1957). This mode of fluid migration in the SRS South area was different than the SRS Central and SRS North field areas, and color alteration of

host rock and mineralization along fractures may be due to dissolution of carbonates at depth in the SRS South field area.

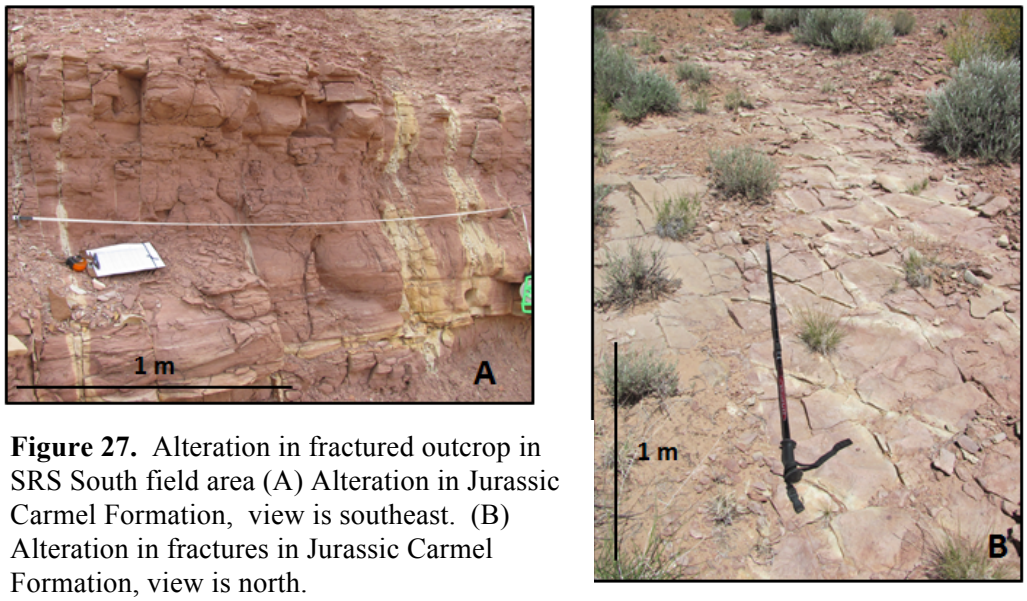

Figure 27. Alteration in fractured outcrop in SRS South field area (A) Alteration in Jurassic Carmel Formation, view is southeast. (B) Alteration in fractures in Jurassic Carmel Formation, view is north.

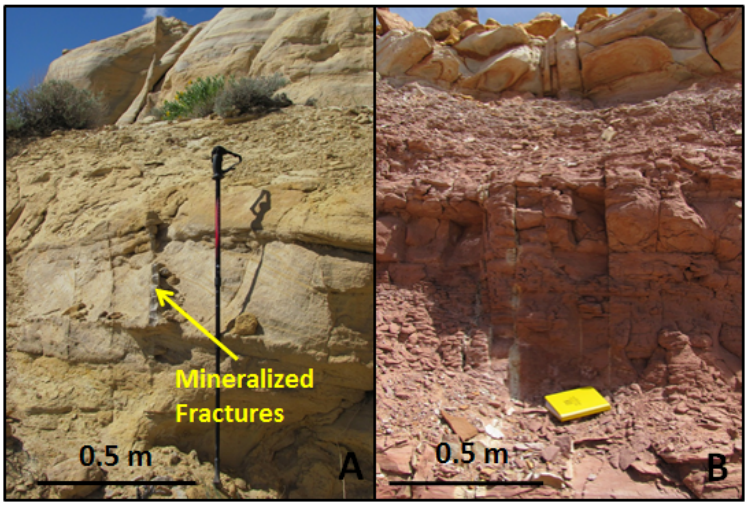

Figure 28. Alteration features in the SRS South field area. (A) Calcite mineralization of fractures in the Entrada Sandstone, view is northeast. (B) Fractures extending through bedding planes in Carmel Formation and Entrada Sandstone.

Table 3. SRS South field area mean fracture orientations.

San Rafael Swell - South						
Location	**Formation**	**Station**	**n**	**Mean Strike**	**Mean Dip**	**GPS Location**
A	Entrada	TM-EN-1A	6	331	85 W	12S 0533036 4278758
B	Carmel	TM-CA-2A	34	267	85 N	12S 0528693 4277439
C	Carmel	TM-CA-1B	26	297	72 NE	12S 0529012 4277610
D	Carmel	TM-CA-2B	34	268	85	12S 0528693 4277439
E	Carmel	TM-CA-3B	36	310	87	12S 0528747 4277720
F	Carmel	TM-CA-3A	76	305	88	12S 0527217 4276692
G	Page	TM-PA-2A	12	283	88	12S 0528747 4277720
H	Page	TM-PA-1A	40	26	72	12S 0528622 4277719
I	Page	TM-PA-1B	24	321	87	12S 0527217 4276692
J	Navajo	TM-NA-2A	6	314	86	12S 0528747 4277720
K	Navajo	TM-NA-1B	22	266	86	12S 0528526 4277719
L	Navajo	TM-NA-1A	32	311	87	12S 0527217 4276692

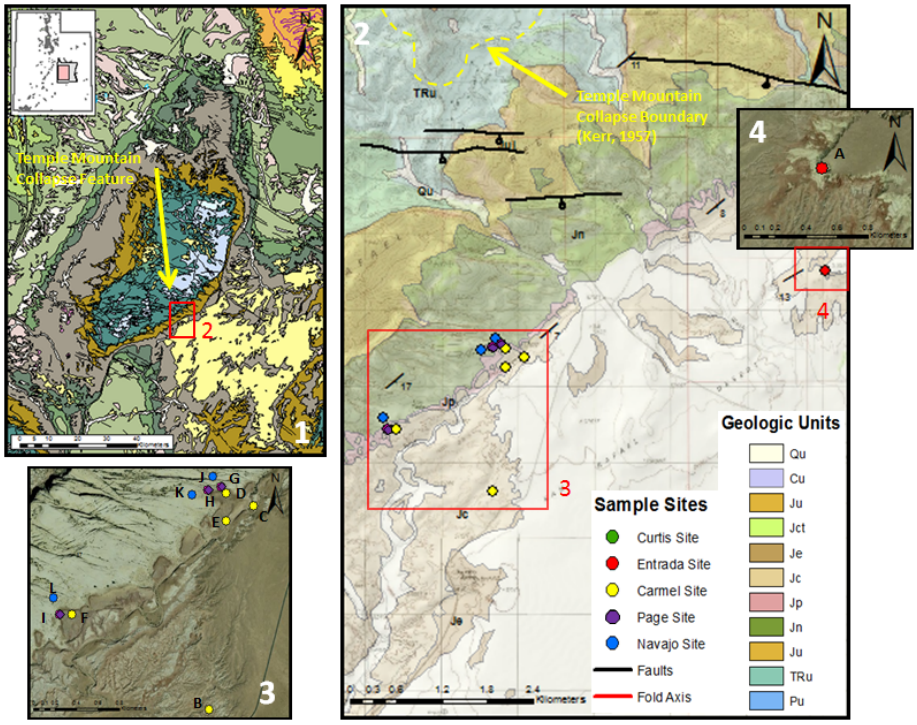

Figure 29. (1) Regional geologic map showing field area location (Adapted from Hintze et al., 2000). (2) Geologic map of SRS South field area showing sample sites (Modified from Doelling, 2002). (3-4) Sample sites with locations labeled.

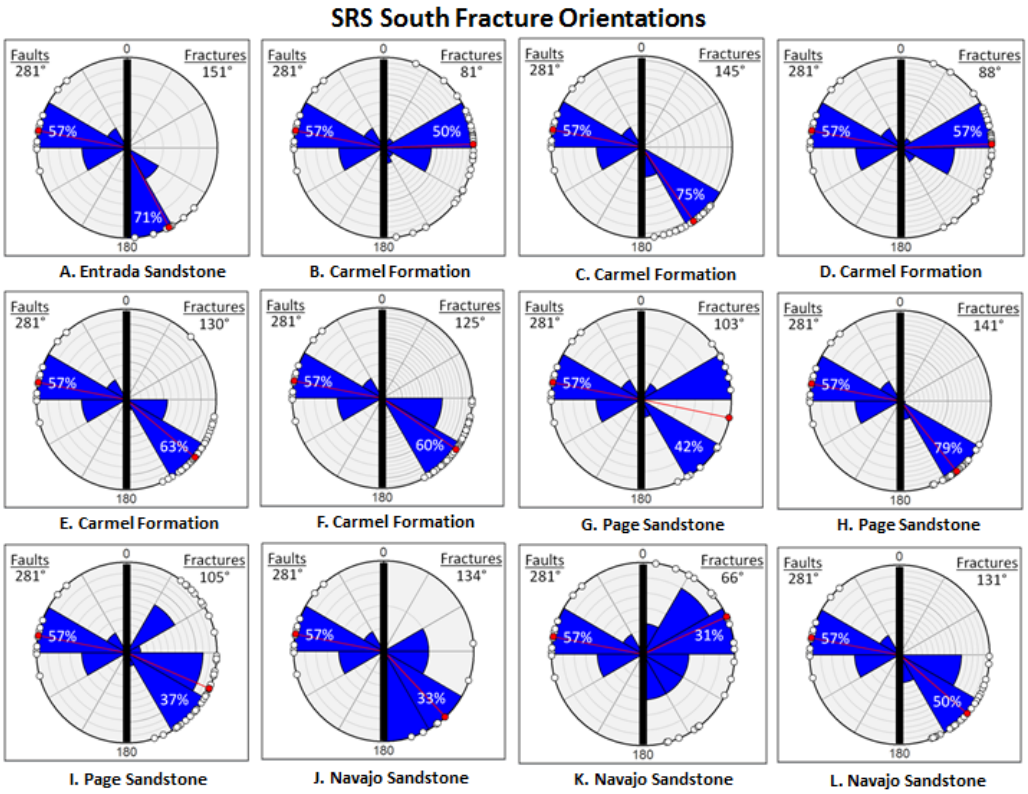

Figure 30. SRS South fracture orientations (right side) plotted with orientations of nearby faults (left side). Labels correlate to station locations in Table 3. (Fault orientation measured from previously mapped faults (Doelling, 2002, and Hintze et al., 2000). Rose diagrams created using Orient 2.1.1 (Vollmer, 2010).

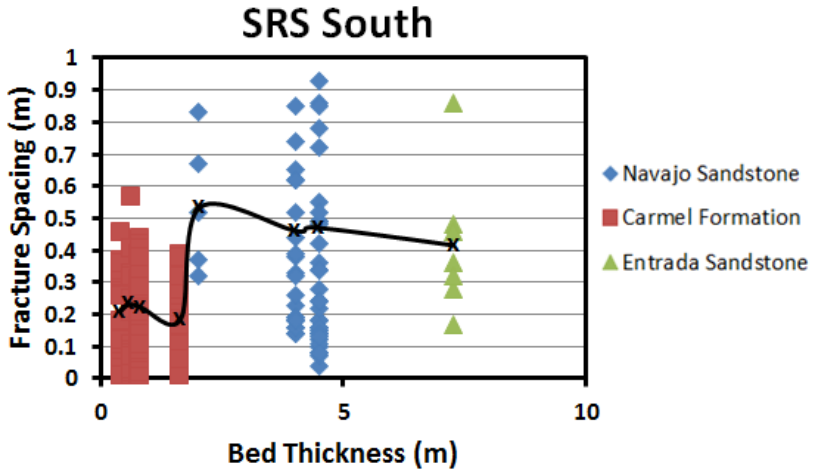

Figure 31. Fracture spacing data plotted against bed thickness for the SRS South field area.

Monument Uplift Focus Area

Four field areas within the Monument Uplift focus area were analyzed for fracture orientation, spacing, mineralization within fractures, trace length, fracture density and aperture (Appendix B). The field areas are located along the eastern flank of the Monument Uplift are named by geographic locality and include MU Central A, MU Central B, MU South, and MU North named by geographic locality. A total of 13 stations, with n=229 fracture orientations were analyzed in the Jurassic Navajo Sandstone, Carmel Formation, and Entrada Sandstone (Appendix B).

The MU Central A, MU Central B, and MU South field areas are on the eastern flank of the Monument Uplift, with a shallow dip of 4-18° east. Major faults classified in this study as exhibiting surface trace length >5 km and throw >10-15m are not found in proximity to the Butler Wash field areas. The MU North field area lies along a shallow dipping limb on the eastern flank of the Monument Uplift, dipping 11-14° east. Major faults are mapped in the MU North Field area (Haynes et al., 1979; Hintze et al., 2000), and are interpreted to be associated with alteration of host rock and calcite mineralization within fractures.

MU North Field Area

A total of four stations, with n=88 fracture orientations were analyzed in the MU North field area (Figure 32), in the Jurassic Navajo Sandstone, Carmel Formation, and Entrada Sandstone (Figure 35). Station locations and sample numbers are listed with mean fracture orientations (Table 4). Orientations for each formation are presented with rose diagrams, with the mean fracture orientation and dispersion of fracture strikes represented in each of the areas (Figure 33).

Table 4. MU North field area mean fracture orientations.

Monument Uplift - North					
Location	**Formation**	**n**	**Mean Strike**	**Mean Dip**	**GPS Location**
A	Entrada	20	31	76	12S 0625023 4183765
B	Entrada	28	301	73	12S 0625164 4184035
C	Carmel	20	264	36	12S 0624760 4183679
D	Navajo	20	345	52	12S 0619695 4187523

Figure 32. Alteration and deformation banding in MU North Field area. Unit is the Entrada Sandstone, view is north.

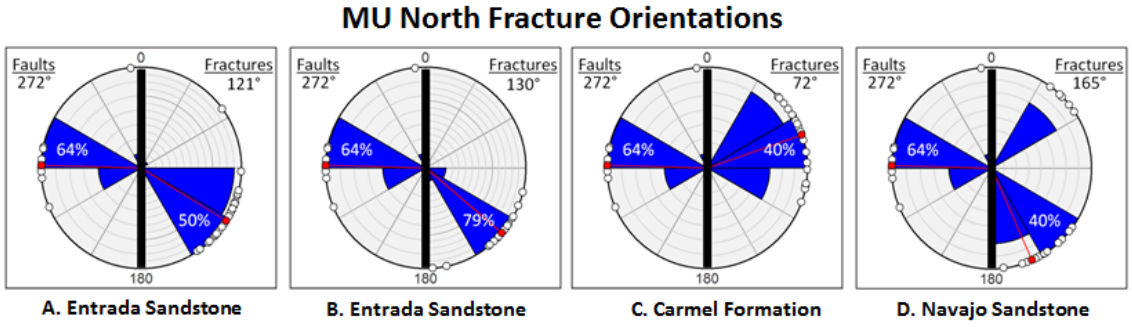

Figure 33. MU North fracture orientations (right side) plotted with orientations of nearby faults (left side). Labels correlate to station locations in Table 7. (Fault orientation measured from previously mapped faults (Haynes et al, 1979, and Hintze et al., 2000). Rose diagrams created using Orient 2.1.1 (Vollmer, 2010).

Extensive color alteration of rock matrix is observed in the Jurassic Navajo Sandstone, and Slickrock member of the Entrada Sandstone throughout the field area. Color alteration in the Jurassic Carmel Formation occurs as 1-3 cm symmetric halos on both sides of open and closed fractures. Fracture aperture in the field area ranges from < 1mm to 4 mm with calcite mineralization within fractures observed in the Jurassic Navajo Sandstone, Carmel Formation, and Entrada Sandstone.

Fracture orientations are uniform between the Navajo and Entrada Sandstones, with an increase in fracture frequency compared to MU Central A, Central, and South field areas. Fractures extend across individual bedding planes within the Jurassic units, and in many cases across depositional contacts. Fracture frequency within the sandstone lithologies, namely the Jurassic Navajo and Entrada Sandstones, is consistently higher than observations in the Butler Wash field areas, and is interpreted to be due to proximity to normal faulted graben in the area (Figure 34). Deformation bands cut two to 4-m wide zones in the eolian Navajo and Entrada Sandstones. Fracture orientations are varied between the Navajo Sandstone, and Carmel Formation (Figure 33). In the other field areas the variation in fracture orientation is interpreted to potentially minimize the connectivity of fractures, yet in the MU North field area, similar style of variation in fracture orientation did not appear to minimize fluid flow along fractures. The variation in fracture orientation in the MU North field area may not have been as important of a factor in fluid and/or hydrocarbon migration as the higher fracture frequency and proximity to a major fault zone.

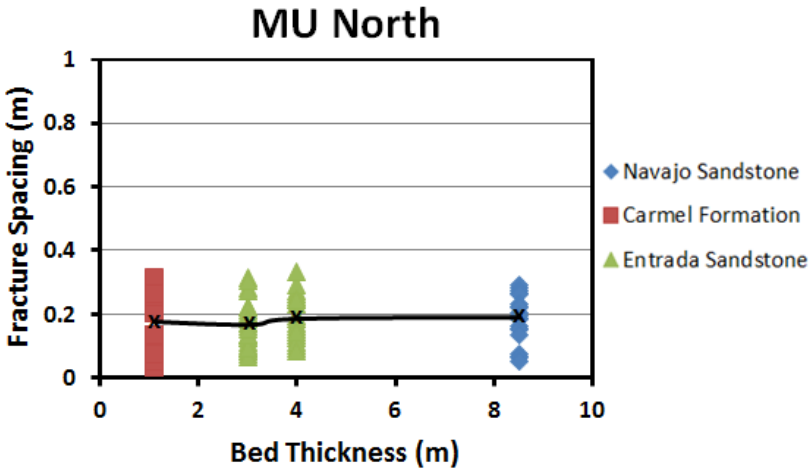

Figure 34. Fracture spacing data plotted against bed thickness for the MU North field area.

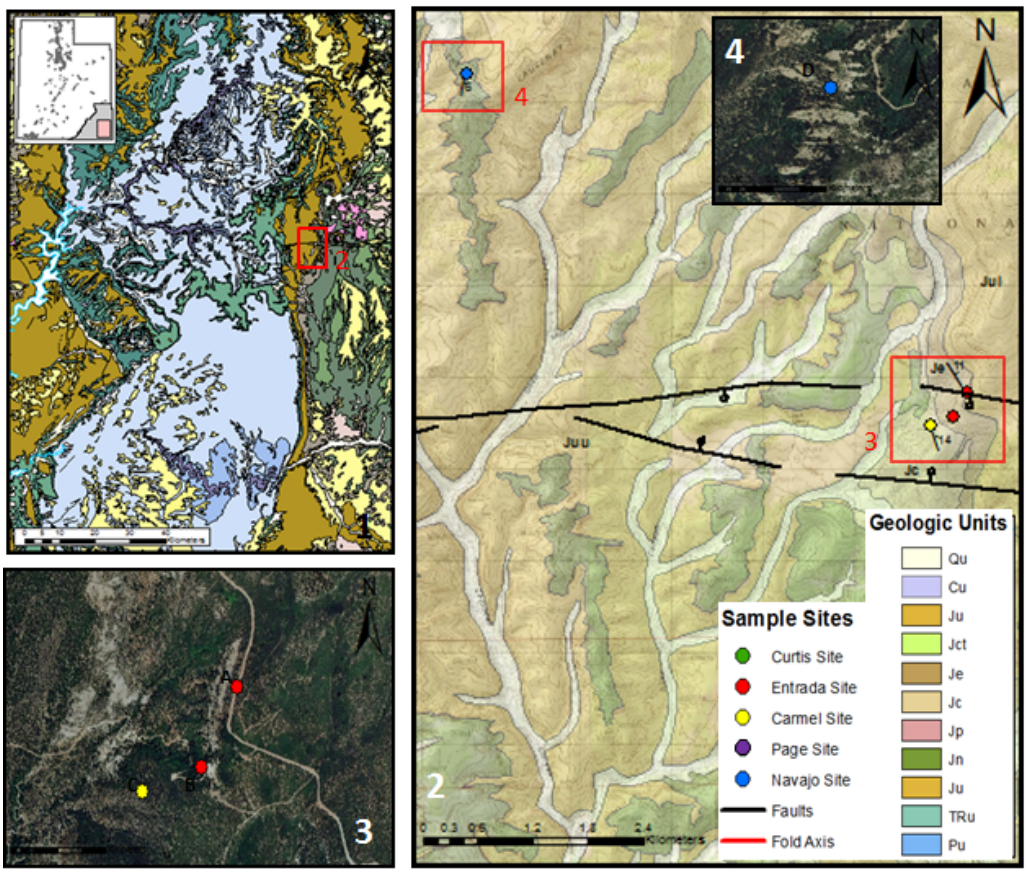

Figure 35. (1) Regional geologic map showing field area location (Adapted from Haynes et al., 1979, and Hintze et al., 2000). (2) Geologic map of MU North field area showing sample sites (Modified from Haynes et al., 1979, and Hintze et al., 2000). (3-4) Sample sites with locations labeled.

MU Central A Field Area

A total of three stations, with n=34 fracture orientations were analyzed in the MU Central A field area (Figure 36) for the Jurassic Navajo Sandstone, Carmel Formation, and Entrada Sandstone (Figure 38). Station locations and sample numbers and listed with mean fracture orientations (Table 5). Orientations for each formation are presented with rose diagrams, with the mean fracture orientation and dispersion of fracture strikes represented in each of the areas (Figure 39).

Extensive color alteration of host rock is observed only in the Jurassic Navajo Sandstone throughout the field area, with the unaltered reddish brown hue in the Earthy and Slickrock members of the Entrada Sandstone preserved. The color alteration in the Carmel Formation observed in the San Rafael Swell focus area is not observed in the MU Central A field area. Fracture aperture in the field area range from <1 mm to 6 mm. Fractures are open and do not exhibit the calcite mineralization that was observed in the San Rafael Swell focus area.

Fracture orientations are uniform between the Jurassic units with alteration of Jurassic units absent, with exception of the Navajo Sandstone. Fractures extend across individual bedding planes within the Jurassic Formations, and in some cases continue across depositional contacts. Mean fracture frequency decreases with increasing bed thickness (Figure 37). Deformation bands were not observed in the eolian Navajo and Entrada Sandstones in the MU Central A field area. Fracture orientations are uniform between the Navajo and Entrada Sandstones with variation in fracture orientation observed in the Carmel Formation (Figure 39). The mean fault orientation appears consistent with the orientation of fractures but the faults used to obtain the mean orientation are distant from the field area and are not likely related to the joint shear observed in the San Rafael Swell focus area. The lack of faults in the area and variation in fracture orientation in the Navajo Sandstone, and Carmel Formation is interpreted to minimize the

connectivity of migration pathways through the potential sealing Carmel Formation, allowing for color alteration of the Navajo Sandstone, but not the Entrada Sandstone.

Faults have not been identified in the field area (Haynes et al., 1979; Hintze et al., 2000), but orientation of fractures in the Navajo and Entrada Sandstones are consistent with regional fault and fracture orientations due to Laramide deformation (Erslev and Koenig, 2009).

Figure 36. Carmel Formation bedding exposure in MU Central A field area.

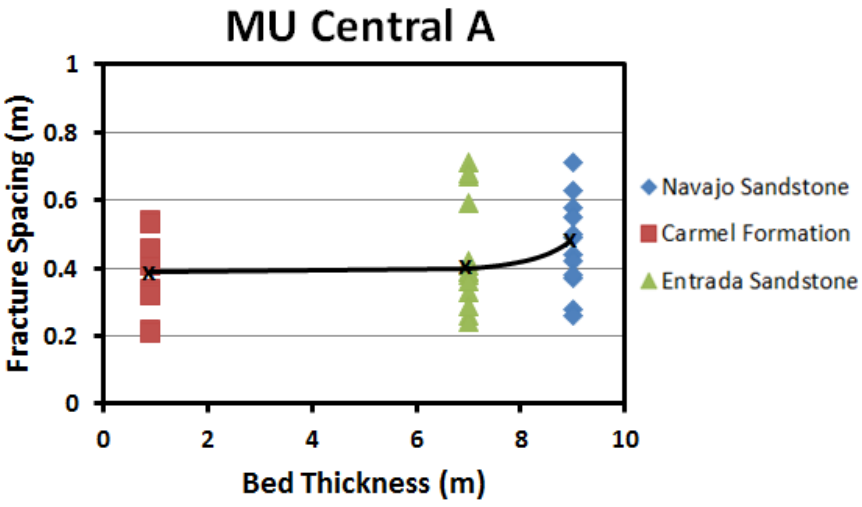

Figure 37. Fracture spacing data plotted against bed thickness for the MU Central A field area.

Table 5. MU Central A field area mean fracture orientations.

Monument Uplift - Central A						
Location	**Formation**	**Station**	**n**	**Mean Strike**	**Mean Dip**	**GPS Location**
A	Entrada	BL-EN-2B	12	252	75 NW	12S 0619514 4160720
B	Carmel	BL-CA-3B	10	293	88 N	12S 0619259 4161032
C	Navajo	BL-NA-2B	12	265	87 N	12S 0618464 4160572

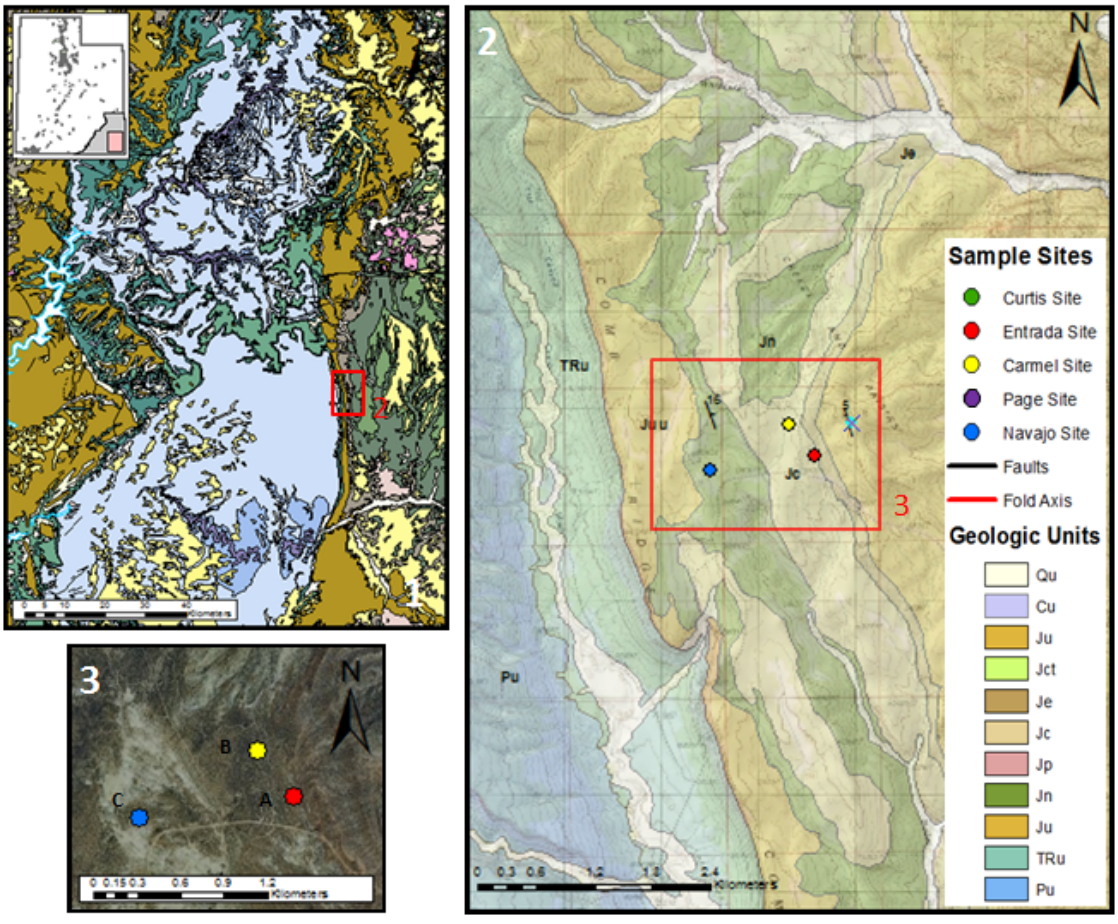

Figure 38. (1) Regional geologic map showing field area location (Adapted from Haynes et al., 1979, and Hintze et al., 2000). (2) Geologic map of MU Central A field area showing sample sites (Modified from Haynes et al., 1979, and Hintze et al., 2000). (3) Sample sites with locations labeled.

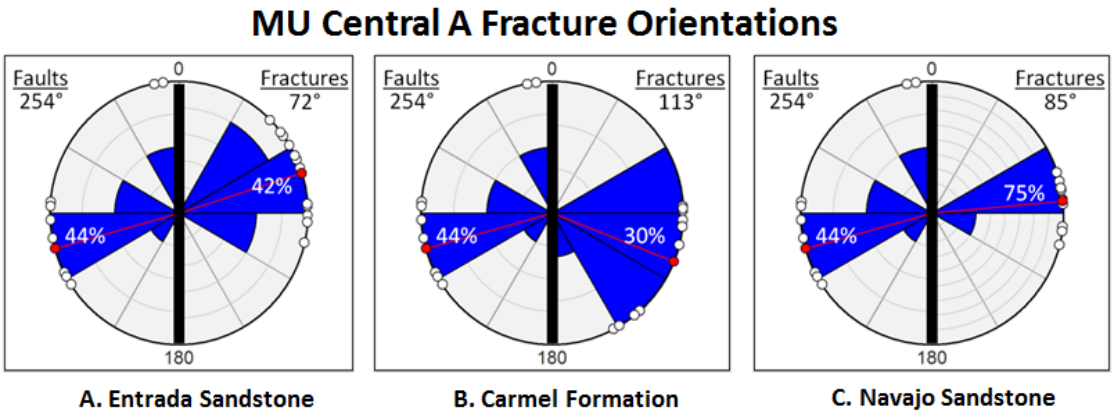

Figure 39. MU Central A fracture orientations (right side) plotted with orientations of nearby faults (left side). Labels correlate to station locations in Table 4. (Fault orientation measured from previously mapped faults (Haynes et al., 1979, and Hintze et al., 2000). Rose diagrams created using Orient 2.1.1 (Vollmer, 2010).

MU Central B Field Area

A total of three stations, with n=50 fracture orientations were analyzed in the MU Central B field area (Figure 40), for the Jurassic Navajo Sandstone, Carmel Formation, and Entrada Sandstone (Figure 43). Station locations and sample numbers are listed with mean fracture orientations (Table 6). Orientations for each formation are presented with rose diagrams, with the mean fracture orientation and dispersion of fracture strikes represented in each of the areas (Figure 41).

Extensive color alteration of host rock is observed only in the Jurassic Navajo Sandstone throughout the field area, with the unaltered reddish brown in the Earthy and Slickrock members of the Entrada Sandstone. Fracture aperture in the field area ranges from ≤ 1 mm, fractures are open and do not exhibit the calcite mineralization that was observed in the San Rafael Swell focus area.

Variation in fracture orientations are observed in the Jurassic units, with alteration constrained to the Navajo Sandstone. Fractures truncate at individual bedding planes within the Jurassic units and depositional contacts. Mean fracture frequency within each lithology decreases

with increasing bed thickness (Figure 42). Deformation bands were not observed in the eolian Navajo and Entrada Sandstones in the MU Central B field area. Uniformity of fracture orientations exist between the Navajo Sandstone and Carmel Formation, with variation in the Entrada Sandstone (Figure 41). The mean fault orientation appears consistent with the orientation of fractures, with exception of the Entrada Sandstone, but the faults used to obtain the mean orientation are distant from the field area and are not likely related to the joint shear observed in the San Rafael Swell focus area. The lack of faults in the area and variation in fracture orientations is interpreted to potentially minimize the connectivity of migration pathways through the potential sealing Carmel Formation.

Faults with considerable offset have not been identified in the field area (Haynes et al., 1979; Hintze et al., 2000), but strikes of fractures in the Jurassic Navajo Sandstone and Carmel Formation are consistent with regional fault and fracture orientations due to Laramide deformation (Erslev and Koenig, 2009). It is possible that the change in fracture orientation for the Entrada Sandstone is due to a fault or a stratigraphic detachment in this area (Figure 41).

Figure 40. Jurassic Carmel Formation in MU Central B field area. Contact between Sandstone and overlying Carmel Formation, view is southeast. Note the color alteration in the Navajo Sandstone, and the lack of color alteration in the Carmel Formation.

Table 6. MU Central B field area mean fracture orientations.

Monument Uplift - Central B						
Location	**Formation**	**Station**	**n**	**Mean Strike**	**Mean Dip**	**GPS Location**
A	Entrada	BL-EN-2A	22	7	84 W	12S 0621228 4152526
B	Carmel	BL-CA-3A	10	297	88 N	12S 0620122 4152241
C	Navajo	BL-NA-2A	18	283	87 N	12S 0620122 4152241

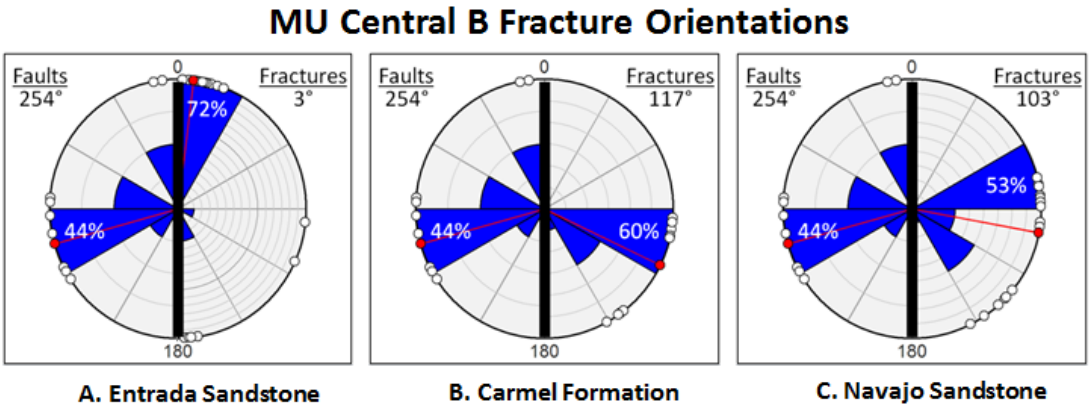

Figure 41. MU Central B fracture orientations (right side) plotted with orientations of nearby faults (left side). Labels correlate to station locations in Table 5. (Fault orientation measured from previously mapped faults (Haynes et al, 1979, and Hintze et al., 2000). Rose diagrams created using Orient 2.1.1 (Vollmer, 2010).

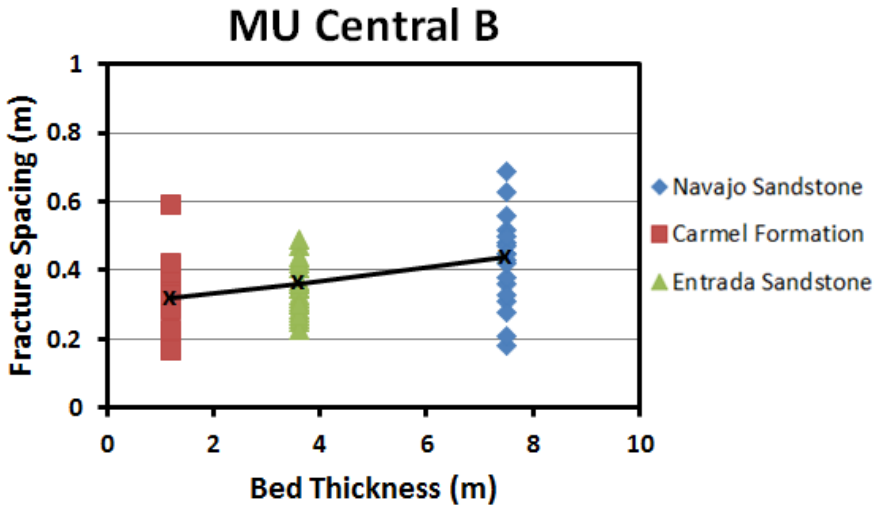

Figure 42. Fracture spacing data plotted against bed thickness for the MU Central B field area.

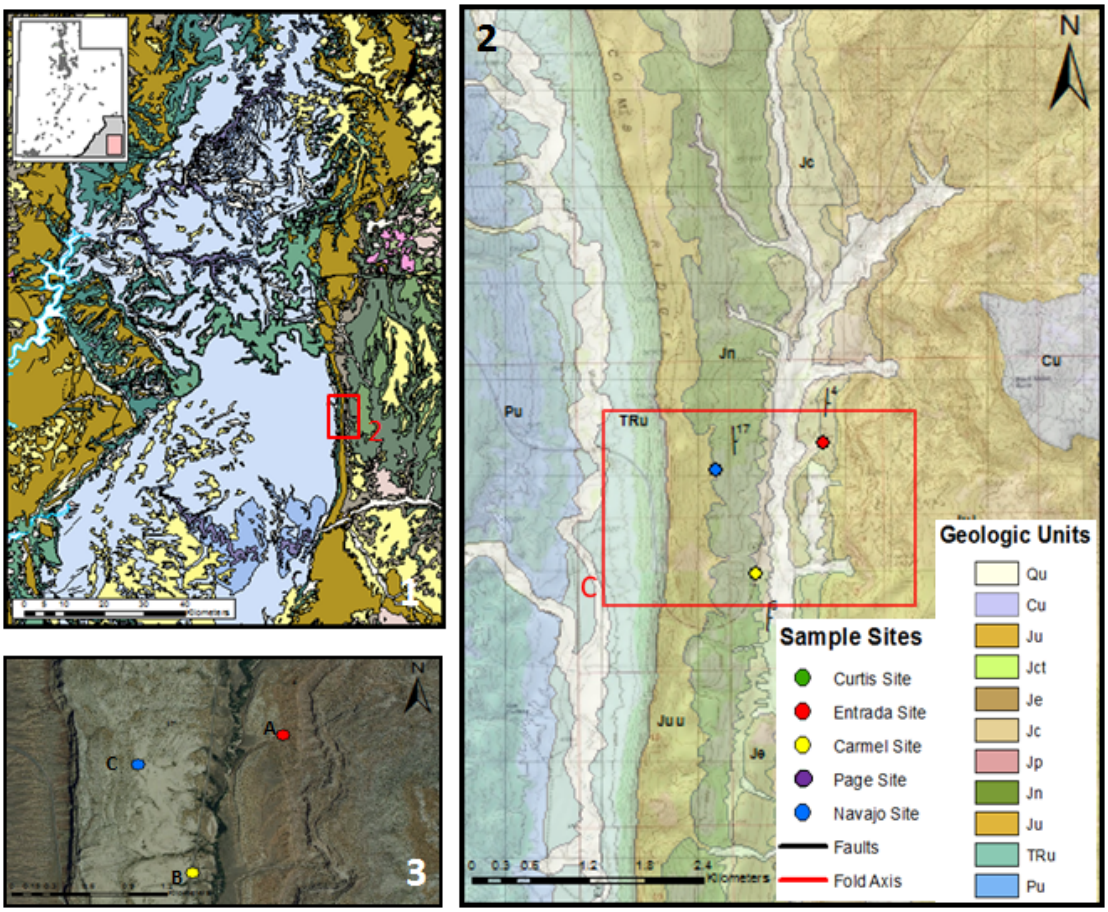

Figure 43. (1) Regional geologic map showing field area location (Adapted from Haynes et. al, 1979, and Hintze et al., 2000. (2) Geologic map of MU Central B field area showing sample sites (Modified from Haynes et al., 1979, and Hintze et al., 2000). (3) Sample sites with locations labeled.

MU South Field Area

A total of three stations, with n=57 fracture orientations were analyzed in the MU South field area (Figure 44), for the Jurassic Navajo Sandstone, Carmel Formation, and Entrada Sandstone (Figure 46). Station locations and sample numbers are listed with mean fracture orientations (Table 7). Orientations for each formation are presented with rose diagrams, with the mean fracture orientation and dispersion of fracture strikes represented in each of the areas (Figure 45).

Extensive color alteration of rock matrix is observed only in the Jurassic Navajo Sandstone throughout the field area, with the unaltered reddish brown hue in both the Earthy and Slickrock members of the Entrada Sandstone. The color alteration in the Carmel Formation observed in the San Rafael Swell focus area is not observed in the MU South field area. Fracture aperture in the field area range from ≤ 1 mm. Fractures are open and do not exhibit the calcite mineralization that was observed in the San Rafael Swell focus area.

Fracture orientations are varied in the Jurassic units, with alteration constrained to the Navajo Sandstone. Fractures truncate at individual bedding planes within the Jurassic Formations and depositional contacts. Mean fracture frequency decreases in the Navajo Sandstone, yet fracture frequencies in the Entrada Sandstone are comparable to the Carmel Formation in the MU Central A and MU South field areas (Figure 47). This change may be due to the change in axis of the Monument Uplift, creating a bend in the orientation of the Jurassic units along the eastern flank of the monocline. Deformation bands were not observed in the eolian Navajo and Entrada Sandstones in the MU South field area. Fracture orientations are varied between the Navajo Sandstone, and Entrada Sandstone (Figure 45). The variation in fracture orientations and the lack of faults in the area is interpreted to potentially minimize the connectivity of migration pathways through the potential sealing Carmel Formation. Further work would be required to analyze the effect of the change in axis of the monocline has on the fracture orientations in the Entrada Sandstone.

Faults with considerable offset have not been identified in the field area (Haynes et al., 1979; Hintze et al., 2000). Fractures in the Jurassic Navajo Sandstone are consistent with regional fault and fracture orientations due to Laramide deformation (Erslev and Koenig, 2009). The fracture orientation in the Entrada Sandstone (Figure 45) is almost identical to the orientation in the MU Central B field area (Figure 41). More work in these areas would be needed to determine the nature of the variability in the Entrada Sandstone.

Table 7. MU South field area mean fracture orientations.

Monument Uplift - South						
Location	**Formation**	**Station**	**n**	**Mean Strike**	**Mean Dip**	**GPS Location**
A	Entrada	BL-EN-1A	22	358	84	12S 0621443 4129031
B	Carmel	BL-CA-1A	19	275	86	12S 0621257 4129380
C	Navajo	BL-NA-1A	16	303	84	12S 0621132 4129038

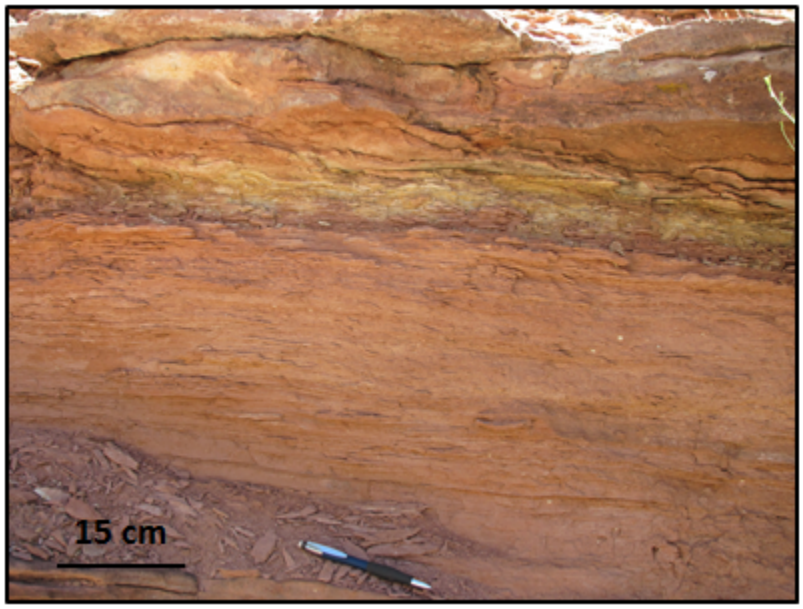

Figure 44. Jurassic Carmel Formation in MU South field area. Note lack of fractures and color alteration in the thin-bedded mudstones and siltstones.

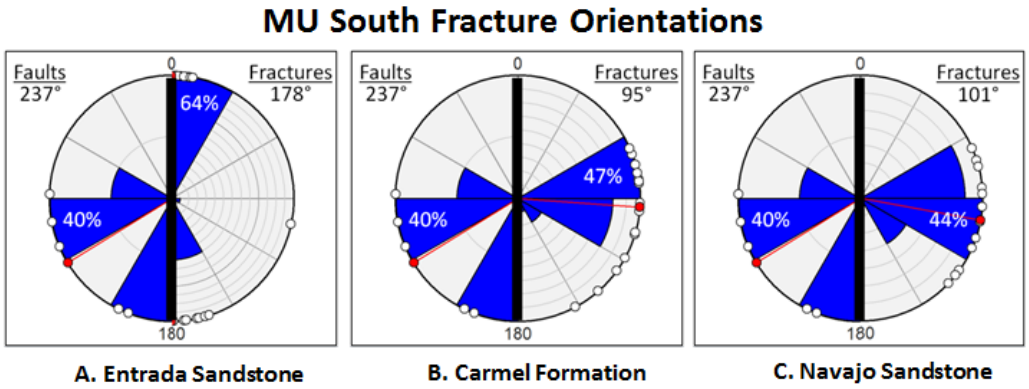

Figure 45. MU South fracture orientations (right side) plotted with orientations of nearby faults (left side). Labels correlate to station locations in Table 6. (Fault orientation measured from previously mapped faults (Haynes et al, 1979, and Hintze et al., 2000). Rose diagrams created using Orient 2.1.1 (Vollmer, 2010).

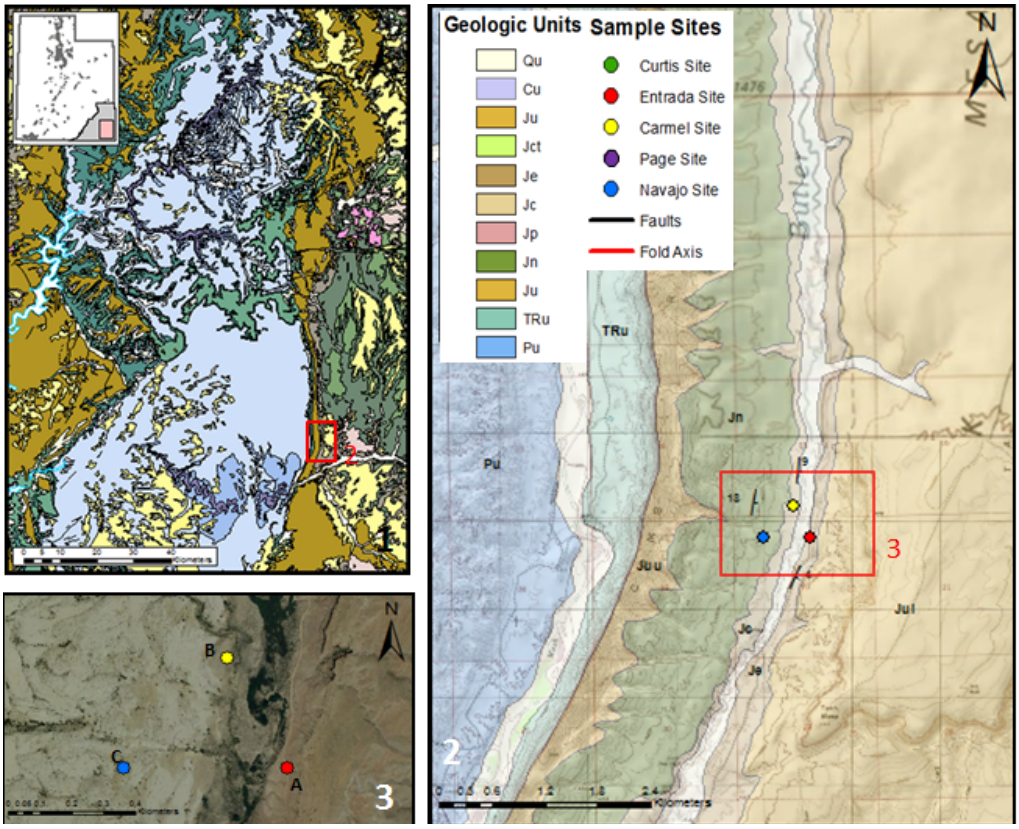

Figure 46. (1) Regional geologic map showing field area location (Adapted from Haynes et al., 1979, and Hintze et al., 2000). (2) Geologic map of MU South field area showing sample sites (Modified from Haynes et al., 1979, and Hintze et al., 2000). (3) Sample sites with locations labeled.

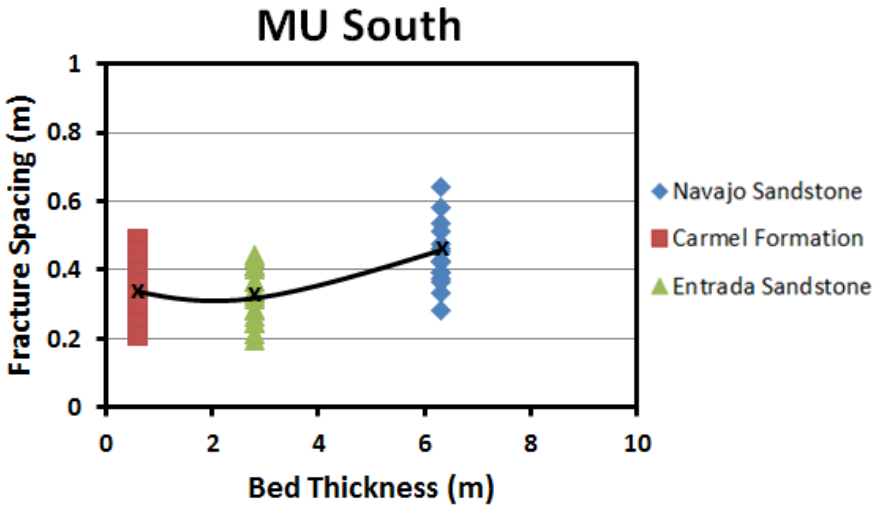

Figure 47. Fracture spacing data plotted against bed thickness for the MU South field area.

Fracture Spacing and Density

The raw fracture spacing data from the scanline measurements for the San Rafael Swell focus area (Figures 21, 26, 31), and the Monument Uplift focus area (Figures 34, 37, 42, 47) were used to calculate a mean fracture spacing for each field area. The mean fracture spacing data for each field area is plotted it against mean bed thickness for each of the field areas in the Jurassic Navajo Sandstone, Carmel Formation, and Entrada Sandstone, and separated the data into lithologic units of sandstone and siltstone/mudstone (Figure 48). The Navajo and Entrada Sandstones are identified lithologically as sandstone, and variable Carmel Formation as siltstone and mudstone.

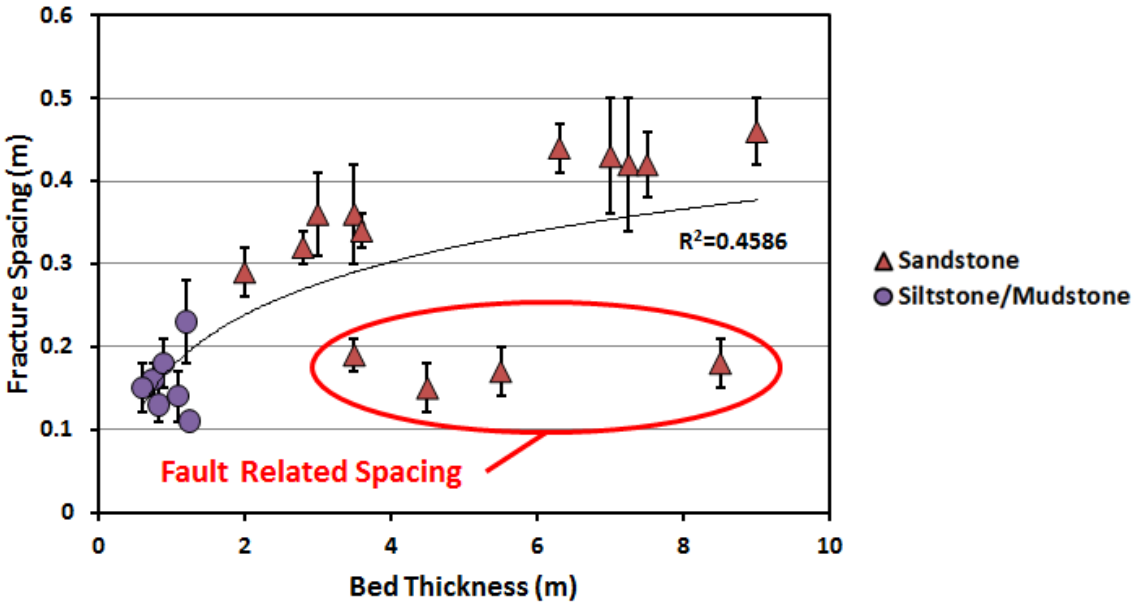

Figure 48. Mean fracture spacing plot vs. bed thickness for sandstone, and siltstone/mudstone lithologies. Sandstones in the SRS Central and MU North field areas that exhibit anomalously low fracture spacing are circled in red.

In the SRS Central and MU North field areas, the Navajo and Entrada sandstones exhibit fracture frequency comparable to the siltstone and mudstone of the Carmel Formation,

independent of bed thickness (Figure 48). The increased fracture frequency of the sandstone in these two areas may be the result of proximity to a major fault zone classified in this study as having a trace length >5 km, and an approximated >10-15 m throw (Haynes et al., 1979; Hintze et al., 2000; Doelling, 2002).

The damage zones in these areas would have a broad areal extent, increasing the fracture density observed in the sandstone. The fracture frequency in the sandstone in the SRS Central and MU North field areas is similar to the fracture spacing of the mudstone, and siltstone. Similar fracture frequency independent of lithology would allow for increased connectivity of fractures, increasing the fluid migration pathways in the SRS Central and MU North field areas, resulting in higher degradation of pore space, and increased amounts of feldspar alteration (Table 8).

Based on the high fracture frequency in the SRS Central and MU North field areas, two major populations in the data were identified; one population exhibits a logarithmic trend of increasing fracture spacing with increasing bedding thickness, and another population with fracture spacing comparable to siltstone, and mudstone values, independent of bed thickness and lithology. The overall population exhibits a flattening of fracture spacing values above 5 m bedding thickness was fit with a logarithmic style trendline (Figure 49). An R^2 value of 0.9238 was calculated for the fracture spacing data points, justifying the interpretation that fracture spacing increases logarithmically with increasing bed thickness in the general population.

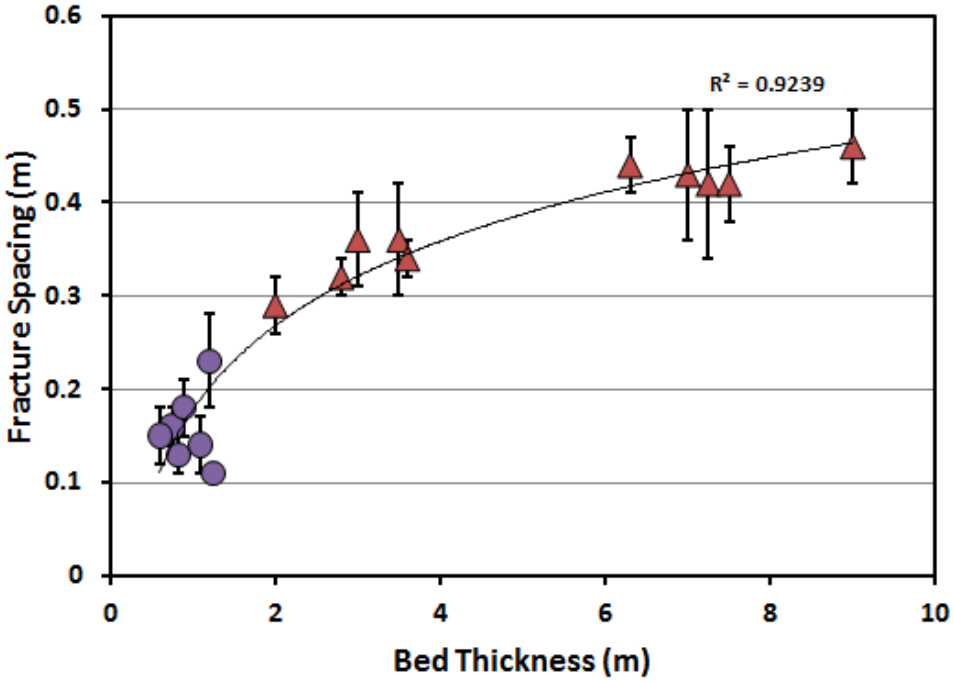

Figure 49. Mean fracture spacing plot vs. bed thickness for sandstone, and siltstone/mudstone lithologies with anomalous sandstone data points removed.

Microscopic Scale

In order to petrographically evaluate the evidence for the migration of fluids in these results, I examined the degradation of pore space compared to the amount of observed alteration. The mineral components and the degree of cementation within pore space, or degradation (Laubach, 2003), was statistically analyzed in ten field samples by using graphical analysis software Image J (National Institute of Health, 2010). Using the Image J statistical analysis software, individual grains were pixelated and the percent area was calculated from the pixelated area, with the mineral components normalized (Table 8). Different color pixels were assigned to each of the mineral components for quartz, feldspar, altered feldspar, calcite, oxide, and pore space (Figures 50-52).

Table 8. Mineral component table showing normalized percentages for samples from San Rafael Swell and Monument Uplift focus areas. Pore space reflects remaining open pore space in each sample.

Mineral Components									
Sample	Field Area	Formation	Lithology	Quartz	Feldspar	Authogenic Clay	Calcite	Oxide	Pore Space
SP-NA-1A	SRS Central	Navajo	Sandstone	76.9	2.2	4.4	16.3	0.3	7.8
SQ-NA-1A	SRS North	Navajo	Sandstone	83.6	1.8	2.7	3.2	10.5	1.6
TM-NA-1B	SRS South	Navajo	Sandstone	95.2	2.1	1.3	0.1	1.3	11.1
DR-NA-1A	MU North	Navajo	Sandstone	93.5	2.7	2.9	0.7	0.2	9
SQ-PA-1A	SRS North	Page	Sandstone	82.8	2.4	4.6	2.4	9.4	1.4
TM-PA-1A	SRS South	Page	Sandstone	90.0	3.0	5.5	0.3	1.3	9.3
SP-CA-2A	SRS Central	Carmel	Siltstone	72.0	1.5	4.9	21.5	0.1	4.7
SQ-EN-2A	SRS North	Entrada	Sandstone	84.9	7.9	3.5	2.0	1.9	3.1
SP-EN-2B	SRS Central	Entrada	Sandstone	82.4	1.0	7.9	6.2	3.0	2.8
DR-EN-1B	MU North	Entrada	Sandstone	77.7	2.1	5.3	14.1	0.9	0.8

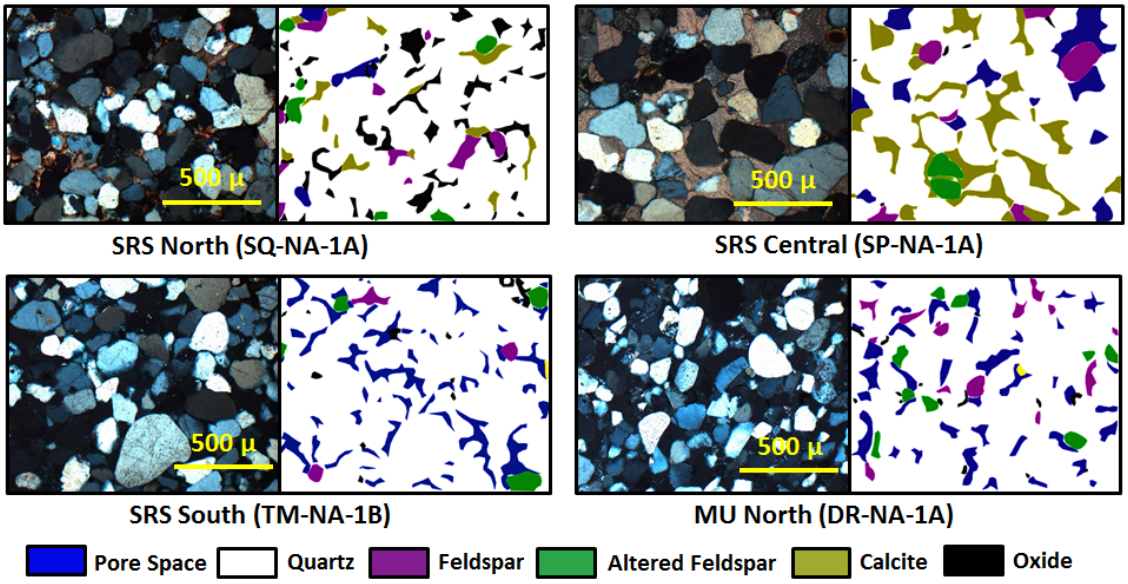

Figure 50. Photomicrograph with corresponding component analysis of Jurassic Navajo Sandstone in the San Rafael Swell and Monument Uplift focus areas.

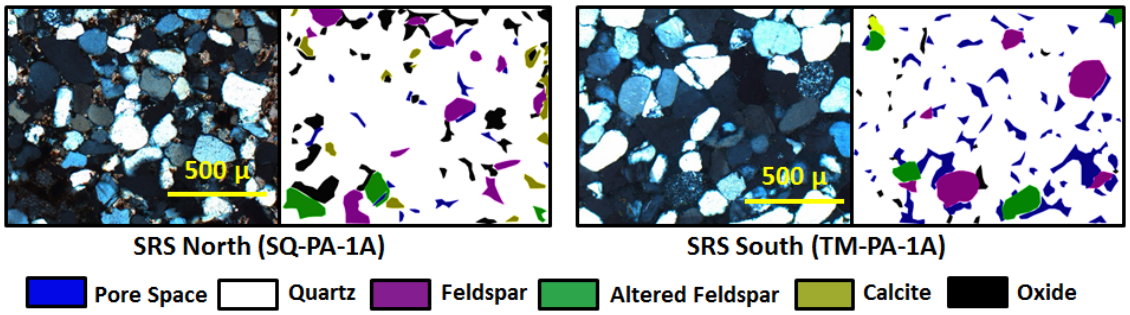

Figure 51. Photomicrograph with corresponding component analysis of Jurassic Page Sandstone in the San Rafael Swell and Monument Uplift focus areas.

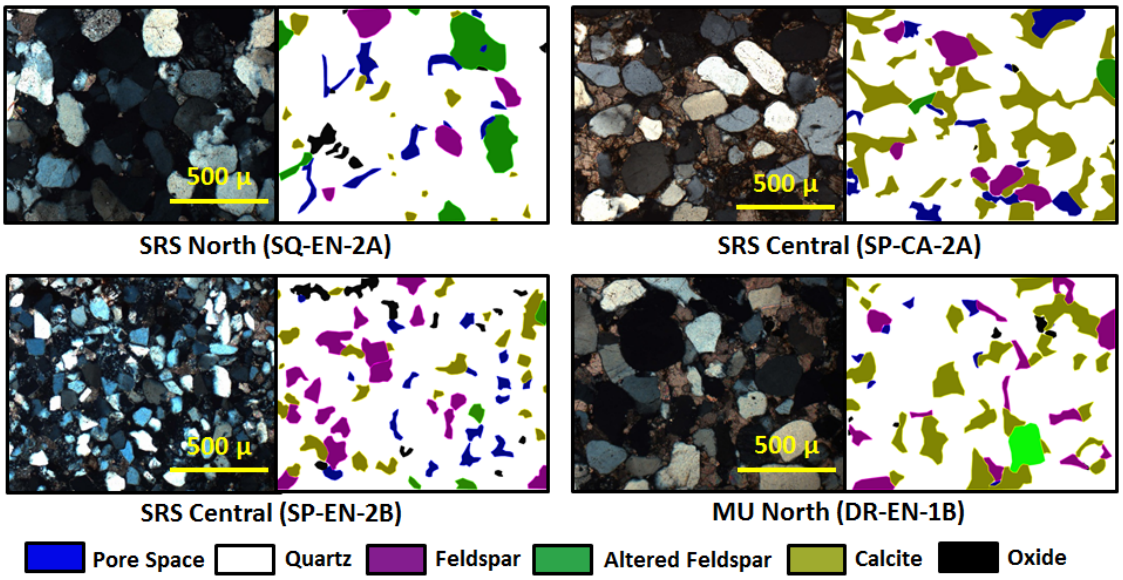

Figure 52. Photomicrograph with corresponding component analysis of the Carmel Formation and Entrada Sandstone in the San Rafael Swell and Monument Uplift focus areas.

In both of the focus areas, the Navajo Sandstone is a well-sorted quartz arenite with an average of 87% quartz, 2% feldspar, 3% altered feldspar, 5% calcite, and 3% oxide, calculated from petrographic analysis of four samples collected in the field (Figure 50). These values compare well to other observations in the region where an average 89% quartz, ~5% K-Feldspar, ~5% altered feldspar, and ~1% calcite were reported (Parry et al., 2007), with exception of a slightly lower feldspar value and higher calcite values recorded in this study. This slight

variation in mineralogy is attributed to field areas exhibiting large percentages of calcite mineralization within pore space and is investigated here, testing the hypothesis that the increased amounts of calcite in pore space is due to increased migration of fluid and/or hydrocarbons in major fault zones, classified in this study by having a 5+ km trace length (Doelling, 2002), and >10-15 m throw. Porosity is variable at 2-11%, which is lower than the 10-30% range reported in the region (Parry et al., 2007).

In the San Rafael Swell focus area, the Page Sandstone is a well-sorted quartz arenite with an average 86% quartz, 3% feldspar, 5% altered feldspar, 1% calcite, and 5% oxide calculated from petrographic analysis of two samples collected in the field (Figure 51).

A clastic sample from the Carmel Formation in the San Rafael Swell focus area is composed of 72% quartz, 2% feldspar, 5% altered feldspar, 21% calcite, and <1% oxide calculated from petrographic analysis of one sample collected in the field (Figure 52).

In each of the focus areas, the Entrada Sandstone is a well-sorted quartz arenite with an average 82% quartz, 4% feldspar, 6% altered feldspar, 7% calcite, and 2% oxide, calculated from petrographic analysis of three samples collected in the field (Figure 52). These values compare well to other observations in the region where average 83% quartz, 6-8% K-Feldspar, 4-8% Plagioclase, with variable amounts of calcite interpreted to due to facies control (Hicks, 2011). Porosity is variable at 1-3%, lower than the 14-17% range reported in the region (Hicks, 2011). I interpret the lower values of porosity to be due to calcite filling pore space in proximity to major fault zones.

The degradation of pore space is estimated by dividing the sum of the percentage of calcite and oxide in the sample by the amount of total pore space. Total pore space is identified as the sum of the amount of pore space, calcite, and oxide in the sample (Figure 53). This method is adapted from the degradation index calculation developed by Laubach (2003), where post kinematic cement was identified and compared to porosity in the sample (Figure 54). This

calculation provides a degradation value reflecting the percentage of the pore space filled in by calcite or oxide. The degradation value is compared to the amount of feldspar alteration in the samples calculated by dividing the amount of altered and unaltered feldspar alteration by the total amount of feldspar in the sample.

Two groupings were identified when comparing pore-space degradation to feldspar alteration (Figure 53). One grouping exhibits high amounts of pore space degradation and feldspar alteration. The other group exhibits low amounts of pore space degradation, and medial feldspar alteration. With exception for the data points in the SRS North field area, high percentages of degradation and feldspar alteration consistently exist in proximity to major fault zones in the SRS Central and MU North field areas. The split data points in the MU North field area are due to varying distances from the major faulting in the area (Figure 46b). The MU North sample exhibiting moderate feldspar alteration and low amounts of pore space degradation is ~ 5 km from a major fault zone.

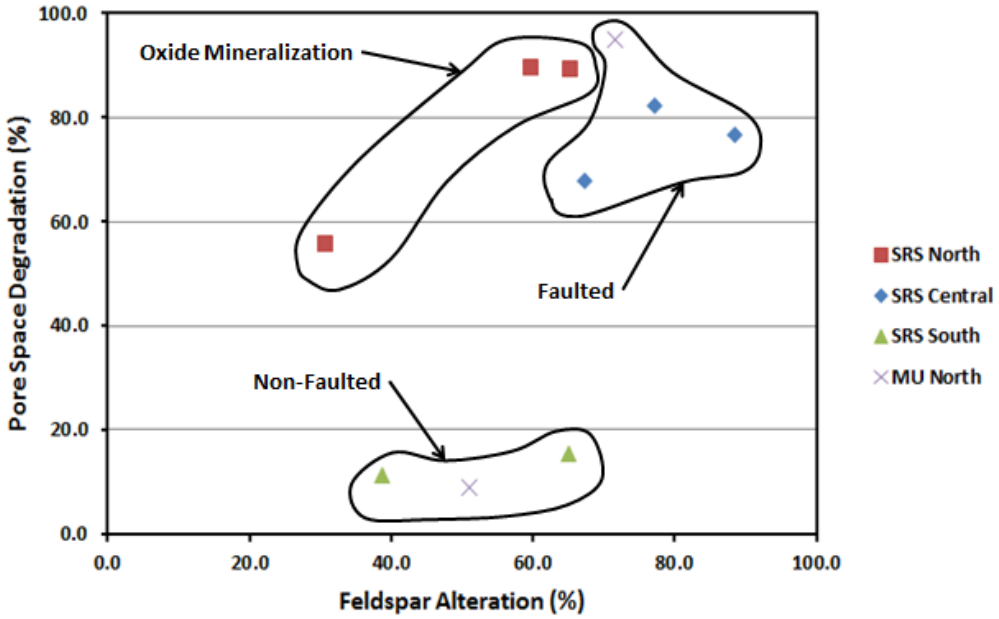

Figure 53. Pore space degradation vs. feldspar alteration observed in Navajo Sandstone, Carmel Formation, and Entrada Sandstone samples in both the San Rafael Swell and Monument Uplift focus areas.

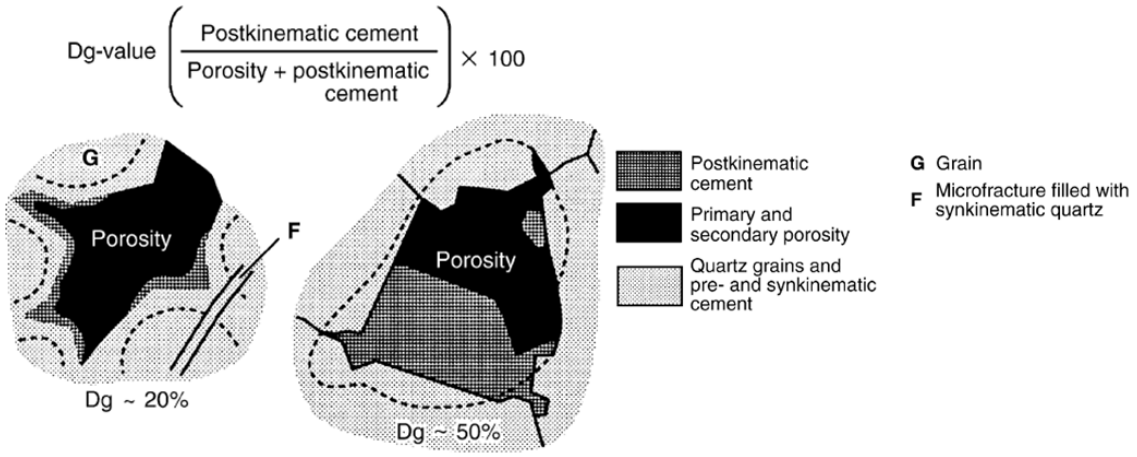

Figure 54. Degradation index method schematic (Laubach, 2003).

The sample exhibiting a high degree of feldspar alteration associated with high degradation of pore space is located within 20m of the MU North fault trace. In the SRS North field area, the dominant mode of pore space degradation is due to oxide mineralization within pore space, rather than mineralization of calcite. The high amounts of oxide mineralization are related to the location of the SRS North field area in relation to the potential migration pathways of fluid migrating from the structural low to the geometrically reconstructed structural high (Figure 9). The SRS North field area is north of the reconstructed apex in the San Rafael Swell, and may have been in the direct path of fluid and/or hydrocarbons migrating up-dip from the structural low to the northwest of the field area. The SRS North field area has potentially recorded the front of the fluid and/or hydrocarbon migration in which the oxide minerals were mobilized down-section by the migrating plume front through pore space, removing the iron from the porous sandstone reservoir by the reducing fluids. The oxide minerals are present in the SRS Central field area, but in smaller abundances. The SRS Central field area is located farther away from the structural low, and most of the oxides in the fluid were likely removed prior to fluid migration along faults and fractures.

There are three different styles of calcite mineralization observed in the fractures: 1). Open fracture with calcite growth occurring along the edges of the fracture (Figure 55a); 2). Closed fracture fully mineralized with calcite (Figure 55b); 3). Alteration occurring along a closed fracture mineralized with calcite cross-cut by an orthogonal open fracture absent of calcite mineralization (Figure 55c). In addition to the amounts of alteration observed in proximity to major fault zones, I examine the alteration and multiple phases of deformation (Table 2) and mineralization within the an oolitic grainstone of the Jurassic Carmel Formation from the SRS Central field area (Figure 55). Different styles of mineralization within fractures are observed, but it is unclear as to why the different mineralization styles exist in similar fractures.

Evidence for fluid migration is also observed along the sides of fractures in the Carmel Formation. Color alteration in the Carmel Formation forms as halos with variable radii on either side of the fractures, altering the reddish siltstones and mudstones to a pale yellow to pale orange. One sample from the SRS South field area of an oolitic grainstone in the Carmel Formation was petrographically analyzed at the red to pale yellow color alteration boundary (Figure 56). The boundary between the two colors is distinct in the photomicrograph, with the color alteration of the host rock on the left side of the photomicrograph. Magnification clearly shows the presence of authogenic clay in pore space that may have been created by the migration of fluid and/or hydrocarbons (Figure 56a-b).

Dissolution reactions, altering feldspar to kaolinite during migration of CO_2, has been shown to increase secondary porosity in the formation (Watson and Gibson-Poole, 2005). Additionally, the color alteration shown on the left side of the photomicrograph is adjacent to a mineralized fracture, indicating that in addition to the migration of fluid and/or hydrocarbons along an open fracture, secondary pore space is being created within the fabric, increasing the potential for upward migration of fluids along the fractured boundary. The timing of the fluid

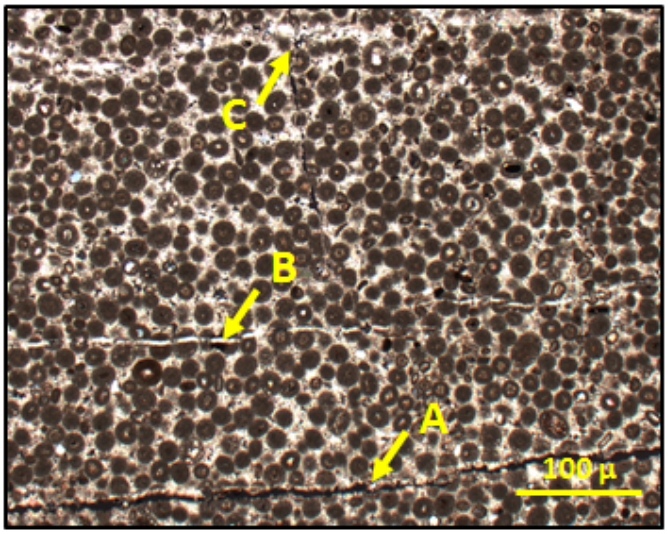

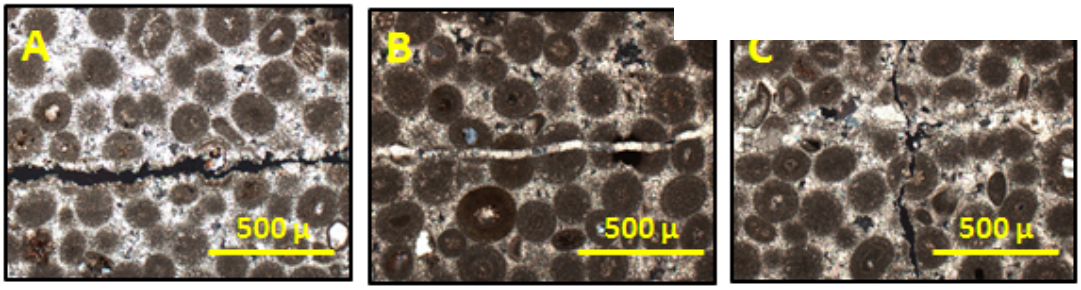

Figure 55. Multiple generations of deformation and mineralization in the oolitic grainstone of the Jurassic Carmel Formation (SP-CA-1A). (A) 10x magnification shows open fracture with calcite growth along edges. (B) Closed fracture with calcite mineralization. (C) Alteration along closed fracture orthogonally cross-cut by open fractures, absent of calcite mineralization.

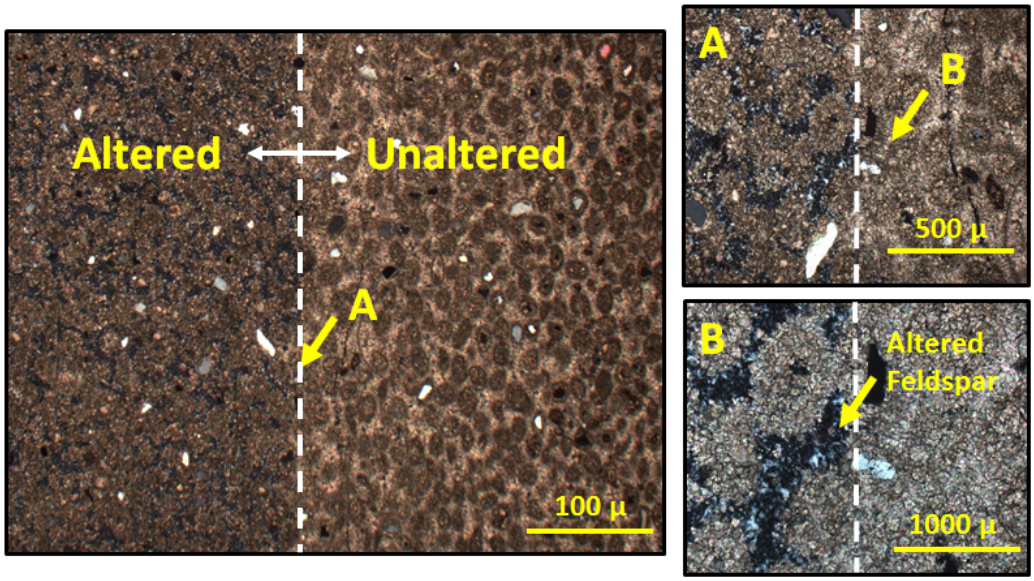

Figure 56. Magnification of color alteration zones in an oolitic grainstone of the Carmel Formation (TM-CA-2A) shows a distinct boundary between color indicating authogenic clay filling pore space.

migration would rely on studying micro- and macro-concretions in the underlying Navajo Sandstone (Potter and Chan, 2011), and is beyond the scope of this study.

Synthesis

The three-scale approach used in this study records the migration of fluids along fractures in proximity to major fault zones (Figure 48), and the resultant alteration and/or mineralization at the microscopic scale in two focus areas with similar structural characteristics (Figures 50-52, 55-56). An increase in fracture frequency in potential reservoir rock is interpreted to directly enhance the connectivity of fractures within a formation, allowing for seal bypass to occur in fine-grained units resulting in an increase in the amount of fluid and/or hydrocarbon migrating to the surface. This observation is verified by the increase in pore space degradation, and feldspar alteration, observed in proximity to major faults zones. Based on the observations at SRS Central and MU North, we interpret that faults are an effective bypass for fluids and/or hydrocarbons in this area, and the major fault zones in the area are examined (Williams and Hackman, 1971; Haynes et al., 1979; Witkind, 1988, 1995; Hintze et al., 2000; Doelling, 2002), to depict the effects that major fault zones can have on fluid migration with respect to proposed CO_2 sequestration projects. Previous work has identified multiple phases of fluid migration (Potter and Chan, 2011) along faults, fractures, and through pore space in the Colorado Plateau (Chan et al., 2000, 2004, 2005, 2006, 2007; Beitler et al., 2003, 2005; Parry et al., 2004).

San Rafael Swell Focus Area

Correlation of the geometrical reconstruction of the Jurassic units (Figure 9-11), uniformity of fracture orientations from reservoir to seal (Figure 23), increased fracture frequency in SRS Central field area (Figure 48), and increased pore space degradation in the SRS Central field area (Figure 53) highlight areas where evidence of fluid migration is documented in

proximity to major faults. The faults in the San Rafael Swell focus area were classified by trace length, identifying faults with trace lengths of over five km, and an estimated throw > 10-15 m as major fault zones that could create migration pathways from through the overlying seal, but could still fall below seismic resolution (Figures 57-58). Fault traces in the region were mapped previously by others (Hintze et al., 2000; Doelling, 2002), with previously unnamed faults in the area labeled by nearest geographical feature (Table 9). The fault trace data were loaded into IHS Petra ™ and merged with the geometrically reconstructed surfaces of the Jurassic units.

Antithetic dipping fault and deformation bands are observed in orthorhombic fault arrays in the San Rafael Swell (Shipton et al., 2002; Johansen and Fossen, 2008). Surface traces of faults that have been classified as major faults in this study with some exhibiting antithetic dips (Williams and Hackman, 1971; Haynes et al., 1979; Witkind, 1988, 1995; Hintze et al., 2000; Doelling, 2002). An increased potential for fluid migration along a fault plane is anticipated

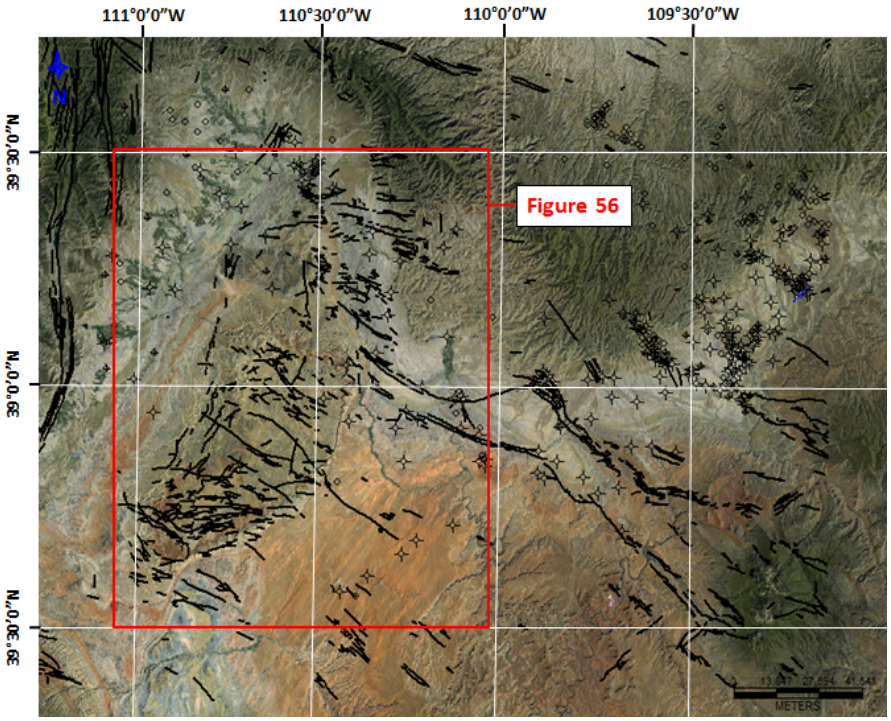

Figure 57. Regional fault map with major faults (5 km+) shown in the San Rafael Swell focus area. (Fault traces adapted from Williams and Hackman, 1971; Haynes et al., 1979; Witkind, 1988, 1995; Hintze et al., 2000; Doelling, 2002).

Table 9. San Rafael Swell focus area fault reference table. Previously unnamed faults (*) referenced by nearest topographic features.

SRS Focus Area Fault Reference Table					
Fault Label	Fault Name	Abbreviation	Location (Lat/Long)	Approximate Fault Trace Length (km)	Reference Map
A	*Grassy Trail Creek Fault	GTCF	39.4 N -110.5 W	13	Huntington 30x60 (Witkind, 1988)
B	*Coon Spring Fault	CSF	39.4 N -110.4 W	10	Huntington 30x60 (Witkind, 1988)
C	*Stove Gulch Fault	SGF	39.3 N -110.5 W	38	Huntington 30x60 (Witkind, 1988)
D	*Big Horn Fault	BHF	39.2 N -110.2 W	18	Huntington 30x60 (Witkind, 1988)
E	*Chimney Rock Fault	CRF	39.2 N -110.5 W	11	Huntington 30x60 (Witkind, 1988)
F	*Left Fork Fault	LFF	39.2 N -110.4 W	15	Huntington 30x60 (Witkind, 1988)
G	*Dry Mesa Fault	DMF	39.2 N -110.4 W	10	Huntington 30x60 (Witkind, 1988)
H	*Lost Spring Fault	LSF	39.1 N -110.4 W	16	Huntington 30x60 (Witkind, 1988)
I	Little Grand Wash Fault Zone	LGWFZ	38.9 N -110.2 W	47	San Rafael 30x60 (Doelling, 2002)
J	*Saleratus Wash Fault	SWF	39.0 N -110.3 W	17	San Rafael 30x60 (Doelling, 2002)
K	Salt Wash Graben Fault Zone	SWGFZ	38.9 N -110.1 W	33	San Rafael 30x60 (Doelling, 2002)
L	*Jackass Flat Fault	JFF	39.0 N -110.6 W	18	San Rafael 30x60 (Doelling, 2002)
M	*Drowned Hole Fault	DHF	38.9 N -110.5 W	10	San Rafael 30x60 (Doelling, 2002)
N	*Sinkhole Flat Fault	SFF	38.9 N -110.6 W	16	San Rafael 30x60 (Doelling, 2002)
O	*Sagebrush Bench Fault	SBF	38.9 N -110.6 W	10	San Rafael 30x60 (Doelling, 2002)
P	*Straight Wash Fault	SWF	38.9 N -110.6 W	23	San Rafael 30x60 (Doelling, 2002)
Q	*Neilson Draw Fault	NDF	38.8 N -110.7 W	26	San Rafael 30x60 (Doelling, 2002)
R	*Eardley Canyon Fault	ECF	38.8 N -110.6 W	9	San Rafael 30x60 (Doelling, 2002)
S	*Iron Wash Fault	IWF	38.7 N -110.4 W	24	San Rafael 30x60 (Doelling, 2002)
T	*Cat Canyon Fault	CCF	38.8 N -110.9 W	15	Salina 30x60 (Doelling, 2004)
U	*Block Mountain Fault	BMF	38.8 N - 110.7 W	8	San Rafael 30x60 (Doelling, 2002)
V	*Square Top Fault	STF	38.8 N -110.9 W	15	Salina 30x60 (Doelling, 2004)
W	*North Temple Wash Fault	NTWF	38.7 N -110.7 W	7	San Rafael 30x60 (Doelling, 2002)
X	*Man Draw Fault	MDF	38.8 N - 110.6 W	12	San Rafael 30x60 (Doelling, 2002)
Y	*Temple Wash Fault	TWF	38.7 N -110.8 W	18	San Rafael 30x60 (Doelling, 2002)
Z	*Big Ridge Fault	BRF	38.6 N -110.6 W	19	San Rafael 30x60 (Doelling, 2002)
AA	*Muddy Creek Fault	MCF	38.6 N -111.0 W	20	Salina 30x60 (Doelling, 2004)
BB	*Horse Creek Fault	HCF	38.6 N -110.7 W	8	San Rafael 30x60 (Doelling, 2002)
CC	*Wild Horse North Fault	WHNF	38.5 N -110.8 W	14	Geologic Map of Utah (Hintze, 2000)
DD	*Wild Horse South Fault	WHSF	38.5 N -110.9 W	13	Geologic Map of Utah (Hintze, 2000)

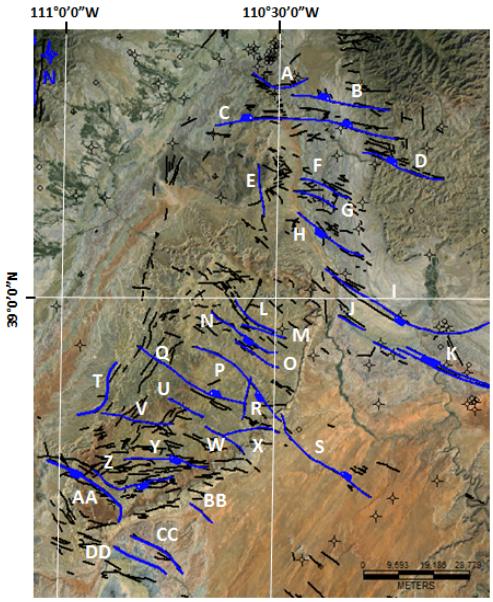

Figure 58. Simplified San Rafael Swell focus area fault map. Fault information on Table 9. (Fault traces adapted from Williams and Hackman, 1971; Witkind, 1988, 1995; Haynes et al., 1979; Hintze et al., 2000; Doelling et al., 2002).

if projected surface traces of mapped antithetic faults intersected at with individual fault planes at depth. Intersecting fault planes at depth can also create linear pathways to enhance vertical or horizontal flow.

The fault planes are color coded to represent the number of antithetic faults a single fault intersected at depth (Figure 59a). Assuming that faults with multiple intersections with antithetic faults at depth would allow for increased fluid migration, a fault leakage potential map was created with boundaries of varying intensity by correlating fault traces at the surface to structural contours for the Navajo Sandstone (Figure 59b). The resultant fault leakage potential map indicates areas in which the highest leakage potential existed in the San Rafael Swell focus area. This interpretation is justified by increased degradation of pore space through mineralization of calcite in the SRS Central field area, and degradation of pore space through mineralization of oxides in the SRS North field area. The degradation of pore space in the samples is a proxy for paleo-migration of fluid through pore space. The calcite and oxide present in the two field areas is interpreted to have migrated up-section along Little Grand Wash fault zone, Salt Wash Graben fault zone, and the SRS Central fault (Table 9).

To highlight the potential connectivity of faults at depth, a color gradient was applied to the fault planes at the depth of intersection to each of the major faults exhibiting one or more intersection(s) with antithetic faults at depth. The red line indicates the approximated depth that the faults plane intersects an antithetic fault (Figure 60). It is assumed at each intersection, fluids are allowed to migrate laterally along the fault plane, in addition to the upward migration through seals along the connected fault planes. This map does not predict where leakage would occur, but it can be used as a tool to evaluate the potential risk of leakage in certain areas.

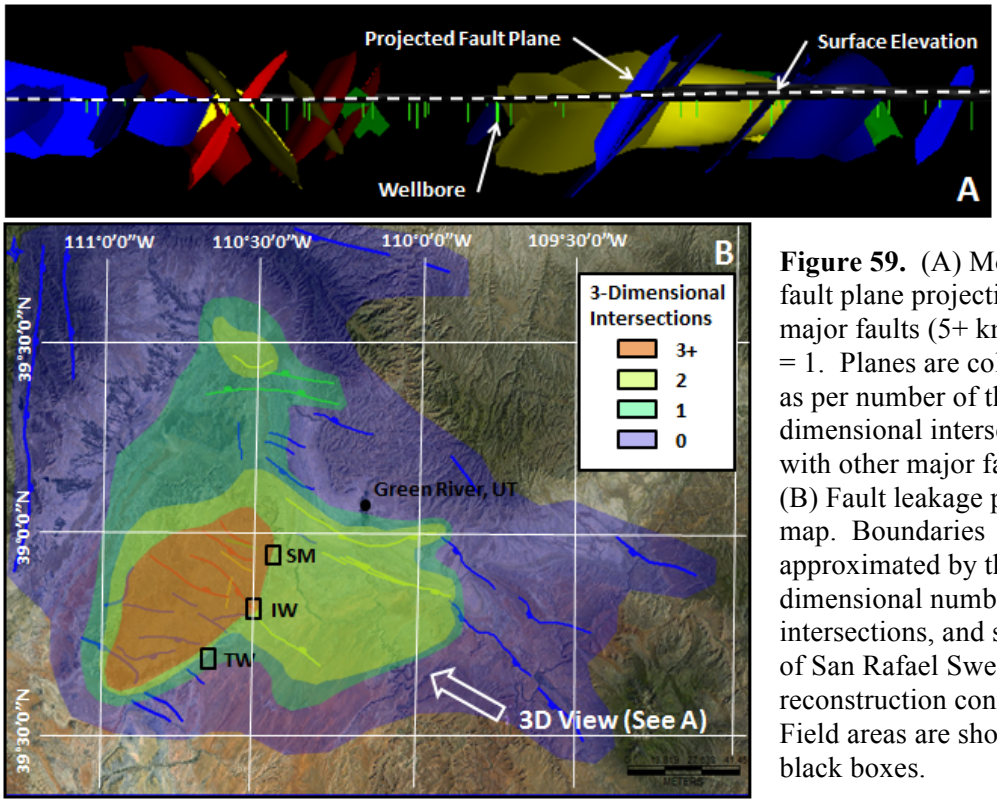

Figure 59. (A) Modeled fault plane projections of major faults (5+ km), V.E. = 1. Planes are color coded as per number of three-dimensional intersections with other major faults. (B) Fault leakage potential map. Boundaries approximated by three-dimensional number of fault intersections, and structure of San Rafael Swell reconstruction contours. Field areas are shown in black boxes.

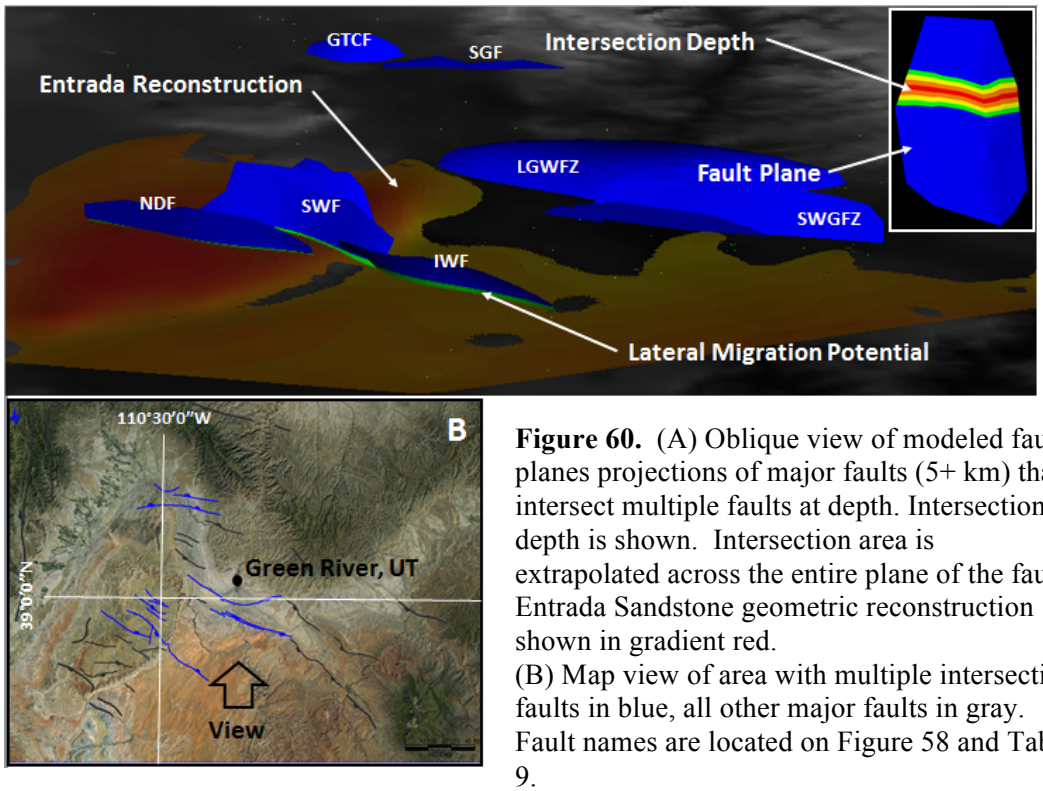

Figure 60. (A) Oblique view of modeled fault planes projections of major faults (5+ km) that intersect multiple faults at depth. Intersection depth is shown. Intersection area is extrapolated across the entire plane of the fault. Entrada Sandstone geometric reconstruction shown in gradient red. (B) Map view of area with multiple intersection faults in blue, all other major faults in gray. Fault names are located on Figure 58 and Table 9.

High leakage potential of the major faults in the area is consistent with the extensive color alteration of host rock and mineralization that led to the interpretation of fluid migration in the SRS Central field area. The approximated fault plane projections show a lateral extent of leakage of approximately 70 km that would allow fluids and/or hydrocarbons to bypass top sealing formations near the structural high of the monocline, with alteration assumed to extending laterally along the fault plane (Figure 60).

Evidence of fluid migration up-dip along a fault plane is preserved as springs and tufa deposits along the Little Grand Wash fault zone, located south of Green River, Utah (Shipton et al., 2004; Heath et al., 2009). In addition to the springs and tufa deposits, oil seep exposures along strike of the Little Grand Wash fault have been geochemically characterized to source from the Permian Phosphoria formation in the Uinta Basin, Utah (Lillis et al., 2003). The combination of fault plane projection and contouring of formation top data for the Permian Phosphoria Formation, exhibit a potential migration pathway for oil sourcing from the Uinta Basin (Figure 61). As shown in the three-dimensional model, upward migration to the southwest is likely, intersecting the Little Grand Wash fault zone, allowing for vertical migration along the fault zone to result in oil seeps at the surface approximately 100 km distant from the source.

The projected fault traces were also used to identify the possible origination depths of the antithetic dipping faults. The intersection color gradient on the planes on the major faults highlights the strong correlation between the approximated intersecting depths of the antithetic faults to the Paradox Formation top depth collected from drilling wells (Figure 62). The approximate down-dip intersections of the major faults based on an assumed 60° dip (Hubbert, 1951) in the San Rafael Swell focus area, are observed to intersect at, or near, the formation top depth of the Paradox Formation, indicating that reactivation of major faults in the area may be possible due to migration of salt at depth.

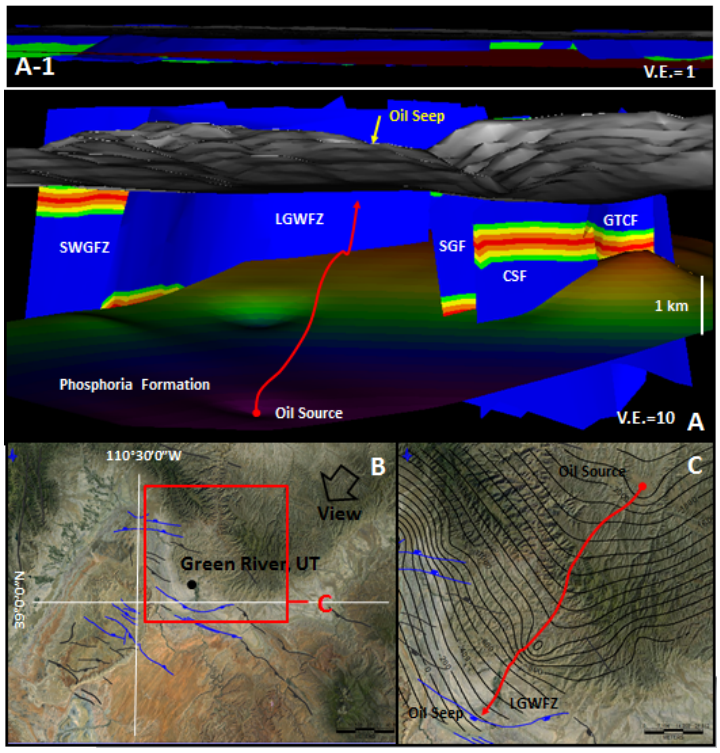

Figure 61. (A) Oblique view of modeled fault planes projections of major faults (5+ km) that intersect multiple faults at depth. Red line shows pathway from Phosphoria oil source, to surface seep at Little Grand Wash Fault Zone (LGWFZ), V.E.=10. (A-1) No vertical exaggeration. (B) Map view of area with multiple intersection faults in blue, all other major faults in gray. (C) Map view of migration pathway (red line), approximately 100 km in length. Fault names are located on Figure 56 and Table 9.

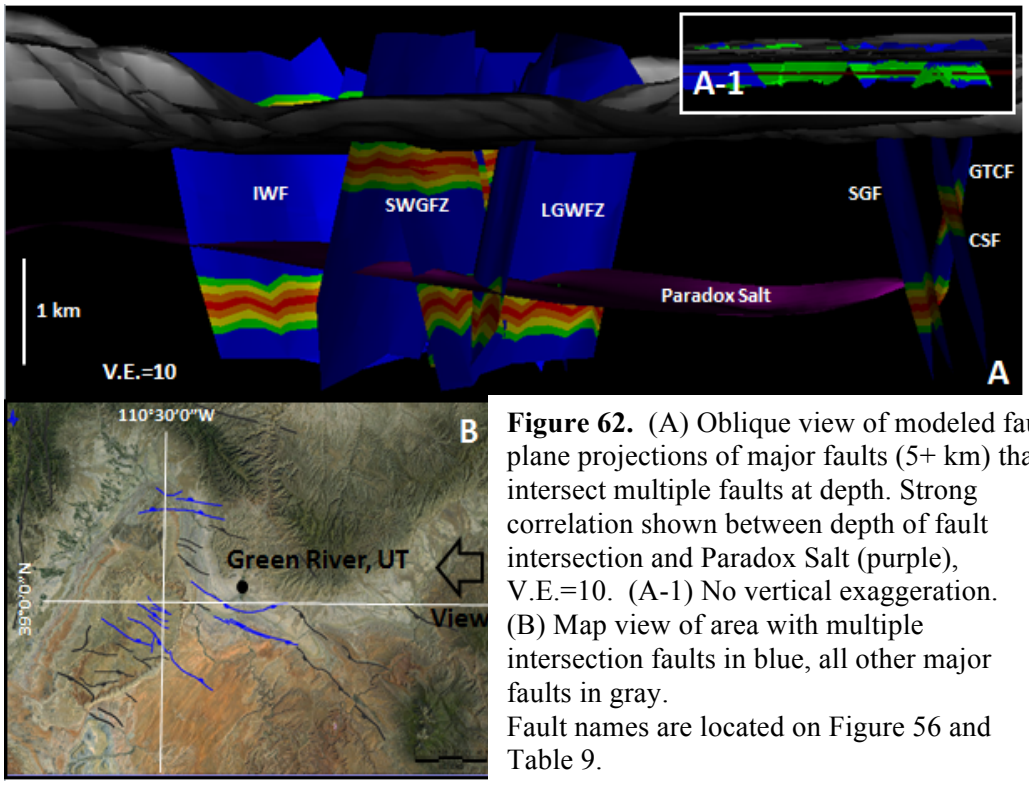

Figure 62. (A) Oblique view of modeled fault plane projections of major faults (5+ km) that intersect multiple faults at depth. Strong correlation shown between depth of fault intersection and Paradox Salt (purple), V.E.=10. (A-1) No vertical exaggeration. (B) Map view of area with multiple intersection faults in blue, all other major faults in gray.
Fault names are located on Figure 56 and Table 9.

Monument Uplift Focus Area

Correlation of the geometrical reconstruction of the Jurassic units (Figures 13-15), with increased fracture frequency and increased pore-space degradation in the MU North field area (Figures 48-53) highlight areas where evidence of fluid migration is documented in proximity to major faults. The faults in the Monument Uplift focus area were classified by trace length, identifying faults with trace lengths of over five km, and an estimated throw > 10-15 m as major fault zones that could create migration pathways from through the overlying sealing Carmel Formation (Figure 63). Fault traces in the region were mapped previously by others (Haynes et al., 1979; Hintze et al., 2000), with previously unnamed faults in the area labeled by nearest geographical feature (Table 10). The fault trace data were loaded into IHS Petra ™ and merged with the geometrically reconstructed surfaces of the Jurassic units.

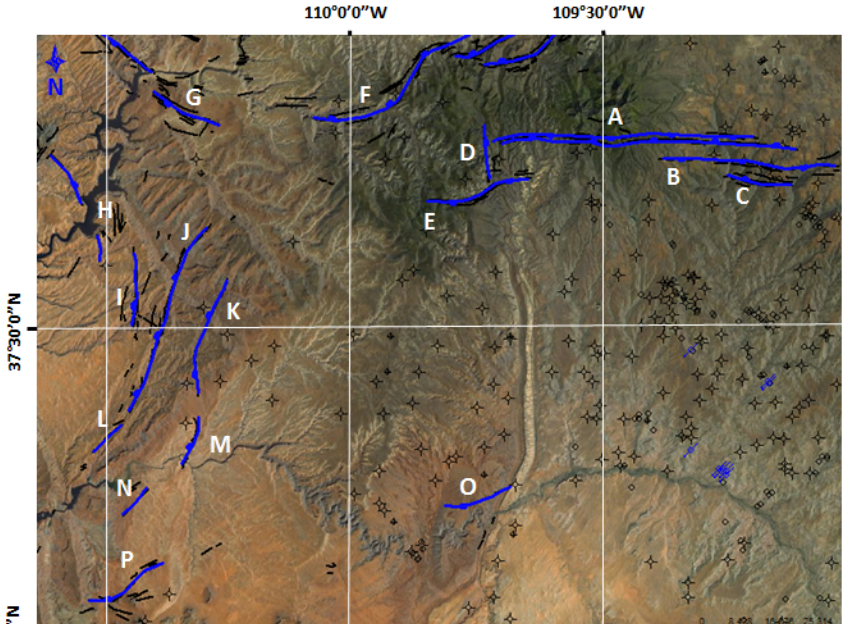

Figure 63. Simplified regional fault map with major faults (5 km+) shown in the Monument Uplift focus area. (Fault traces adapted from Haynes et al., 1979, and Hintze et al., 2000).

Table 10. Monument Uplift focus area fault reference table. Previously unnamed faults (*) referenced by nearest topographic features.

MU Focus Area Fault Reference Table					
Fault Label	Fault Name	Abbreviation	Location (Lat/Long)	Approximate Fault Trace Length (km)	Reference Map
A	*Duckett Graben Fault Zone	DGFZ	37.6 -109.5	35	Geologic Map of Utah (Hintze, 2000)
B	*Montezuma Canyon Fault	MCF	37.8 -109.2	31	Geologic Map of Utah (Hintze, 2000)
C	*Horsehead Canyon Fault	HCF	37.7 -109.2	9	Geologic Map of Utah (Hintze, 2000)
D	*Notch Canyon Fault	NCF	37.8 -109.7	10	Geologic Map of Utah (Hintze, 2000)
E	*South Elk Ridge Fault	SERF	37.7 -109.7	18	Geologic Map of Utah (Hintze, 2000)
F	*North Long Point Fault	NLPF	37.9 -109.9	34	Geologic Map of Utah (Hintze, 2000)
G	*White Canyon Fault	WCF	37.8 -110.3	13	Geologic Map of Utah (Hintze, 2000)
H	*Good Hope Mesa Fault	GHMF	37.7 -110.5	20	Geologic Map of Utah (Hintze, 2000)
I	*Mancos Mesa Fault	MMF	37.6 -110.4	10	Geologic Map of Utah (Hintze, 2000)
J	*Red Canyon Fault	RCF	37.5 -110.3	35	Geologic Map of Utah (Hintze, 2000)
K	*Steer Pasture Fault	SPF	37.5 -110.3	21	Geologic Map of Utah (Hintze, 2000)
L	*Mikes Mesa Fault	MMF	37.3 -110.5	7	Geologic Map of Utah (Hintze, 2000)
M	*Whirlwind Draw Fault	WDF	37.3 -110.3	9	Geologic Map of Utah (Hintze, 2000)
N	*Rockhouse Gulch Fault	RGF	37.2 -110.4	7	Geologic Map of Utah (Hintze, 2000)
O	*Lime Ridge Fault	LRF	37.2 -109.7	12	Geologic Map of Utah (Hintze, 2000)
P	*Copper Canyon Fault	CCF	37.1 -110.4	13	Geologic Map of Utah (Hintze, 2000)

The projected fault planes were color coded by the number of antithetic faults a single fault intersected at depth (Figure 64a). A fault leakage potential map was created with boundaries of varying intensity by correlating fault traces at the surface to structural contours for the Navajo Sandstone (Figure 64b). The resultant fault leakage potential map effectively indicates areas in which the highest leakage potential existed prior to erosion of the Monument Uplift.

To highlight the potential connectivity of faults at depth a color gradient is applied to the depth planes to represent an approximate depth of intersection for each of the major faults exhibiting one or more intersection(s) with antithetic faults at depth. The red line indicates the approximated depth that the faults intersect antithetic faults (Figure 65). It is assumed that at each intersection, fluids are allowed to migrate laterally along the fault plane, in addition to upward migration through seals. The high leakage potential of the major faults in the area is consistent with the extensive alteration, and mineralization due to fluid migration in the MU North field area. The approximated fault plane projections show a lateral extent of leakage of approximately 75 km that may allow fluids and/or hydrocarbons to bypass top sealing formations near the structural high of the monocline, extending laterally along the fault trace. This map does

not predict where leakage would occur, but it can be used as a tool to evaluate the potential risk of leakage in certain areas.

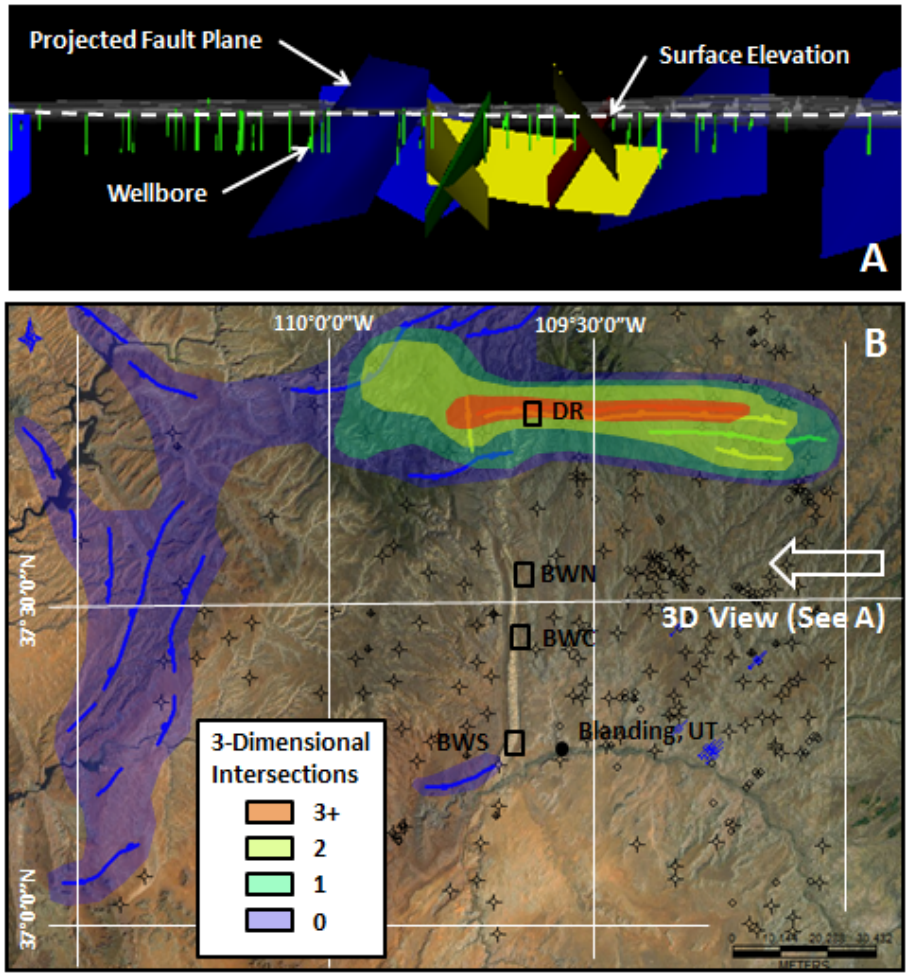

Figure 64. (A) Modeled fault planes projections of major faults (5+ km). Planes are color coded as per number of 3-dimensional intersections with other major faults.
(B) Fault leakage potential map. Boundaries approximated by 3-dimensional number of fault intersections, and structure of MU reconstruction contours.
Field areas are shown in black boxes.

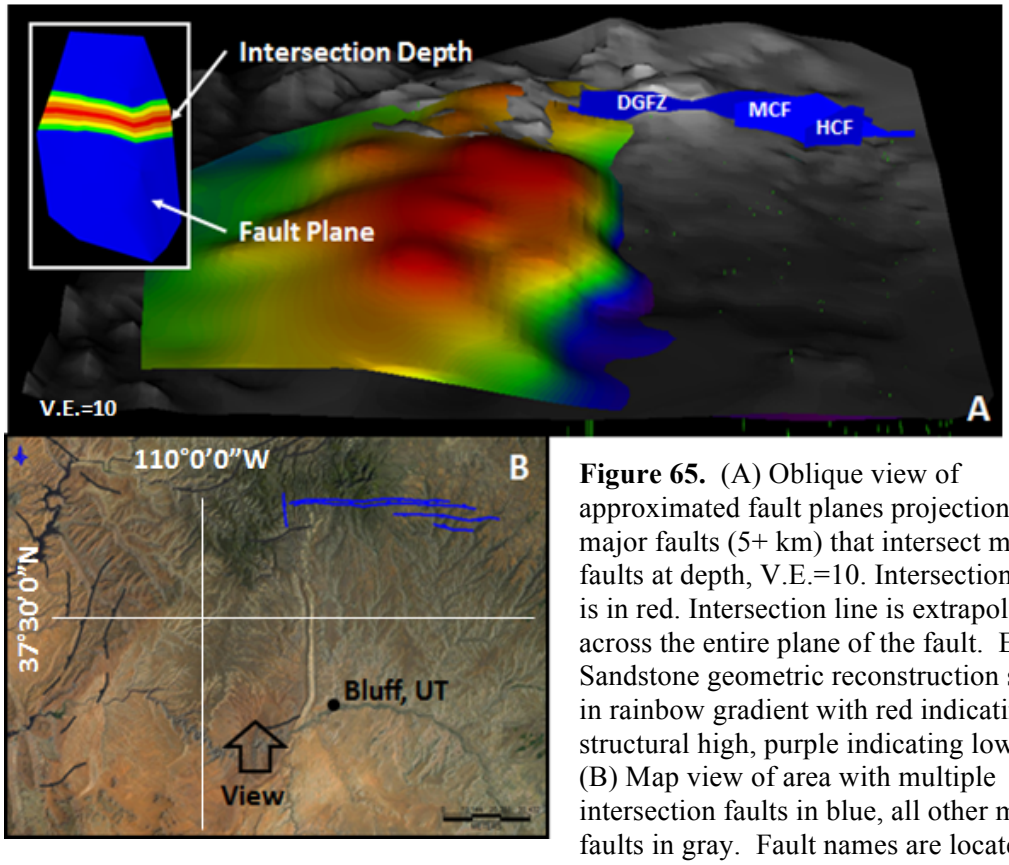

Figure 65. (A) Oblique view of approximated fault planes projections of major faults (5+ km) that intersect multiple faults at depth, V.E.=10. Intersection depth is in red. Intersection line is extrapolated across the entire plane of the fault. Entrada Sandstone geometric reconstruction shown in rainbow gradient with red indicating structural high, purple indicating low. (B) Map view of area with multiple intersection faults in blue, all other major faults in gray. Fault names are located on Figure 61 and Table 10.

Oil seeps and extensive tufa deposits such as those that occur along the Little Grand Wash fault in the San Rafael Swell focus area are not observed in the Monument Uplift focus area. However, the Elaterite Basin in the Canyonlands National Park located approximately 60 km northwest from the MU North field area, exhibits heavy oil seeps from the Jurassic Wingate Formation (Doelling, 1965; Bowman, 1969). The heavy oils have been geochemically altered, preventing detailed analysis of source, but three-dimensional contouring of the Pennsylvanian formation tops indicates that hydrocarbons could potentially migrate to the northwest (Figure 66). A Further work would need to be accomplished to determine a direct correlation in potential migration paths in the Monument Uplift focus area and surface seeps in Elaterite Basin.

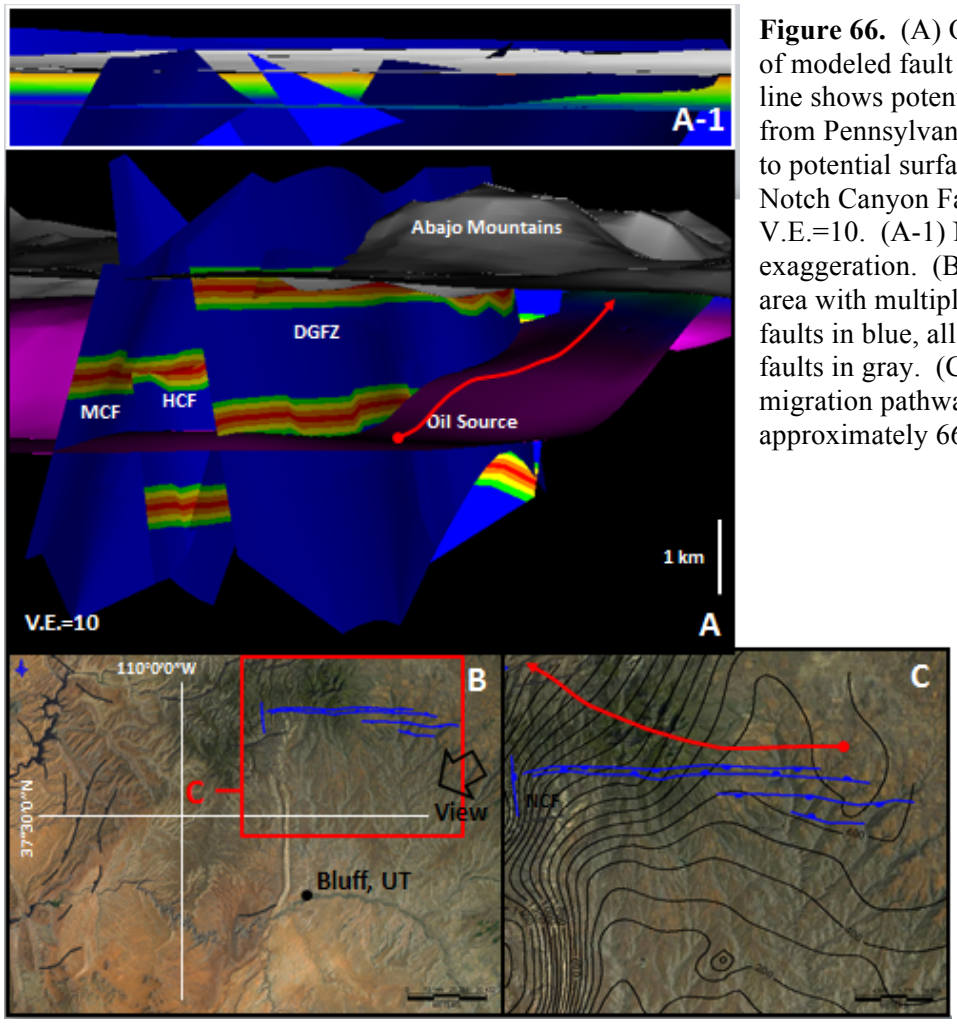

Figure 66. (A) Oblique view of modeled fault planes. Red line shows potential pathway from Pennsylvanian oil source, to potential surface seep at Notch Canyon Fault (NCF). V.E.=10. (A-1) No vertical exaggeration. (B) Map view of area with multiple intersection faults in blue, all other major faults in gray. (C) Map view of migration pathway (red line), approximately 66 km in length.

A weaker correlation in the Monument Uplift focus area between fault intersection and the Paradox Formation top depth, than was observed in the San Rafael Swell focus area (Figure 67). However, the MU North field area was the only area in the Monument Uplift focus area to exhibit extensive alteration due to fluid migration. The increase in alteration may be due to the proximity of the MU North field area to the local major faulting in the area.

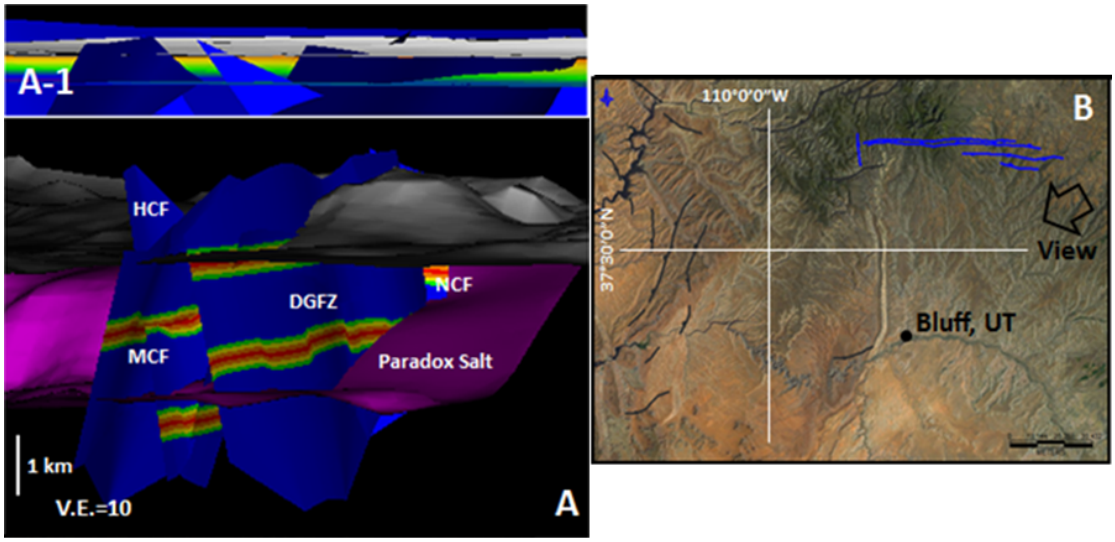

Figure 67. (A) Oblique view of modeled fault planes projections of major faults (5+ km) that intersect multiple faults at depth, V.E.=10.
(A-1) No vertical exaggeration. Strong correlation shown between depth of fault intersection and Paradox Salt (purple).
(B) Map view of area with multiple intersection faults in blue, all other major faults in gray. Fault names are located on Figure 61 and Table 10.

DISCUSSION

Fluid Migration Potential

To justify the boundaries created in the fault leakage potential maps (Figures 59, 64) indicating areas of increased leakage of fluid in major fault zones, the fault leakage boundaries are correlated to areas from which oil and/or gas have been produced historically from multiple formations to create a fluid migration potential map. A total of 438 wells were used in the analysis for hydrocarbon production with 56 wells with an unknown status, and three injection wells removed from the list. The areas that have historically produced oil or gas, are highlighted in red on the fluid migration potential map (Figure 68).

A total of 43% of the 438 wells analyzed in the San Rafael Swell focus area historically produced considerable quantities of oil or gas, with 91% of the producing wells falling within the blue/white zones indicating low to very low fluid migration potentials (Figure 68). The other 9% of producing wells that fall within the yellow zone of fluid migration are interpreted to be the product of either hydrocarbons trapped in structural traps with intact seals, or large enough influx of migrating hydrocarbons to offset the loss along faults. This relationship between fault leakage potential boundaries coupled with areas exhibiting historic production of oil and/or gas justify the idea that seal bypass has occurred in areas of increased fault leakage potential, allowing for the continued upward migration of hydrocarbons to the surface. Additionally, robust approximations of potential intersections with antithetic faults at depth, effectively identifies areas with adequate seal integrity for hydrocarbon preservation at depth.

To examine the effect of seal bypass in relation to hydrocarbon migration, the areas of historic oil and gas production are placed as an overlay on the geometric reconstruction of the Jurassic Navajo Sandstone (Figure 69). Potential migration pathways of hydrocarbons that

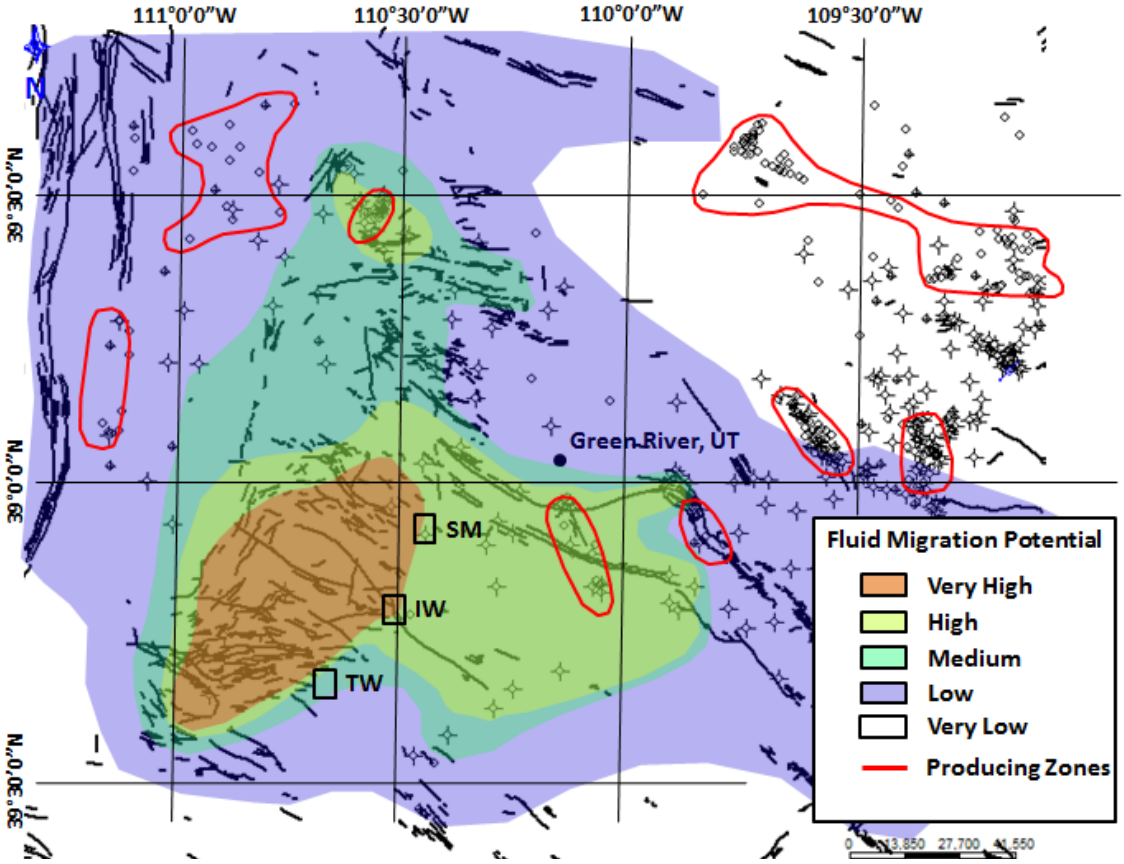

Figure 68. Fluid migration potential map with the historical producing zones highlighted in red. 91% of the wells in the producing zones fall within the low to very low migration potential zones. Field areas identified in black boxes. SRS North, SRS Central, and SRS South field areas.

source from the Pennsylvanian Phosphoria Formation are drawn in blue, with the flow directions based on the structural contours of the Jurassic Entrada Sandstone from the geometric reconstruction of the area using formation tops from the geophysical well logs (Figure 69). Wells that historically produce gas or oil are zoned in red. The producing wells consistently lie along migration pathways in areas that have a low fault leakage potential along major faults.

In order to contrast and compare the fluid migration potential observed in the San Rafael Swell focus area, the fault leakage potential zones for the Monument Uplift focus area (Figure 64) are overlain on the well location map in the Monument Uplift focus area (Figure 70). A total of

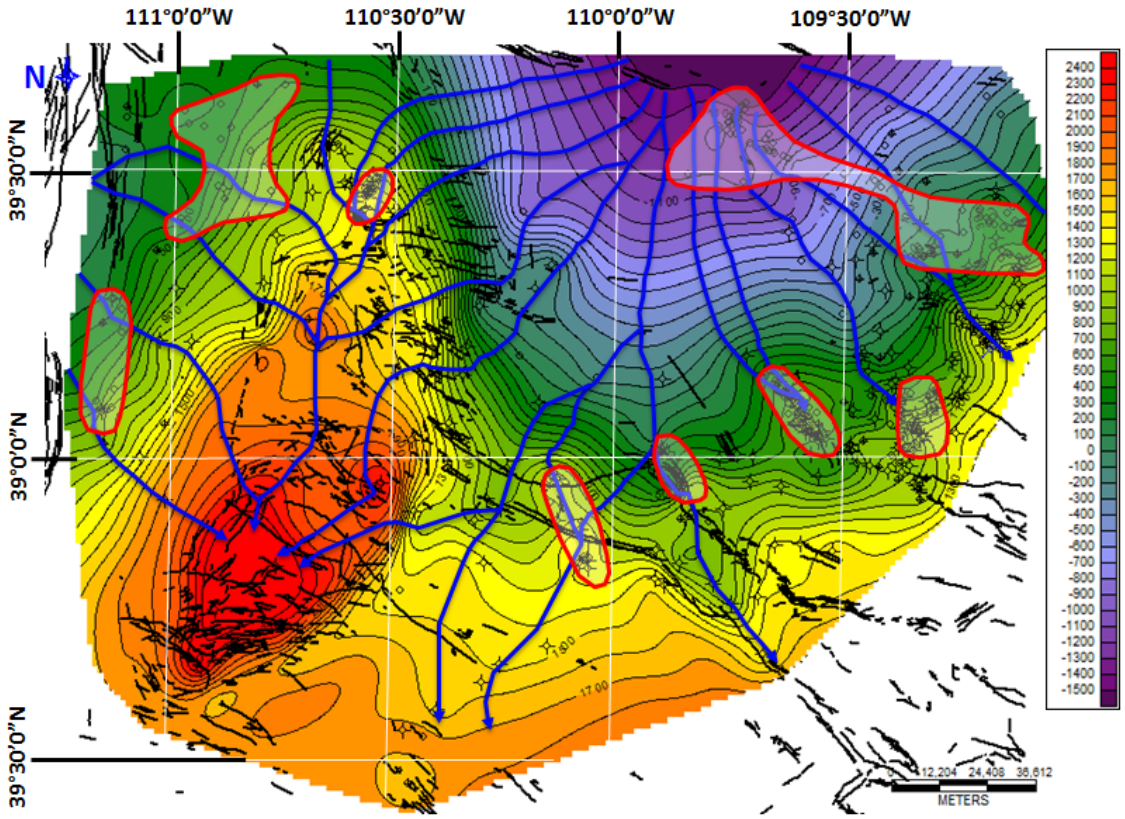

Figure 69. Potential migration pathways of Pennsylvanian Phosphoria Formation traced orthogonal to structural contours of the Entrada Sandstone in the San Rafael Swell geometrical reconstruction. The historical producing zones are highlighted in red.

271 wells were used in the analysis for hydrocarbon production with 14 wells with an unknown status, and 9 injection wells removed from the list. The areas that have historically produced oil or gas are highlighted in red on the fluid migration potential map.

A total of 26% of the 271 wells analyzed in the area were found to have historically produced considerable quantities of oil or gas, with 100% of the producing wells falling within the blue/white zones indicating low to very low fluid migration potentials. This relationship between fault leakage potential boundaries coupled with areas exhibiting historic production of oil and/or gas again justify the theory in the Monument Uplift focus area that seal bypass has occurred in areas of increased fault leakage potential, allowing for the continued upward migration of hydrocarbons to the surface. Additionally, robust approximations of potential

intersections with antithetic faults at depth, effectively identifies areas with adequate seal integrity for hydrocarbon preservation at depth in the Paradox Basin.

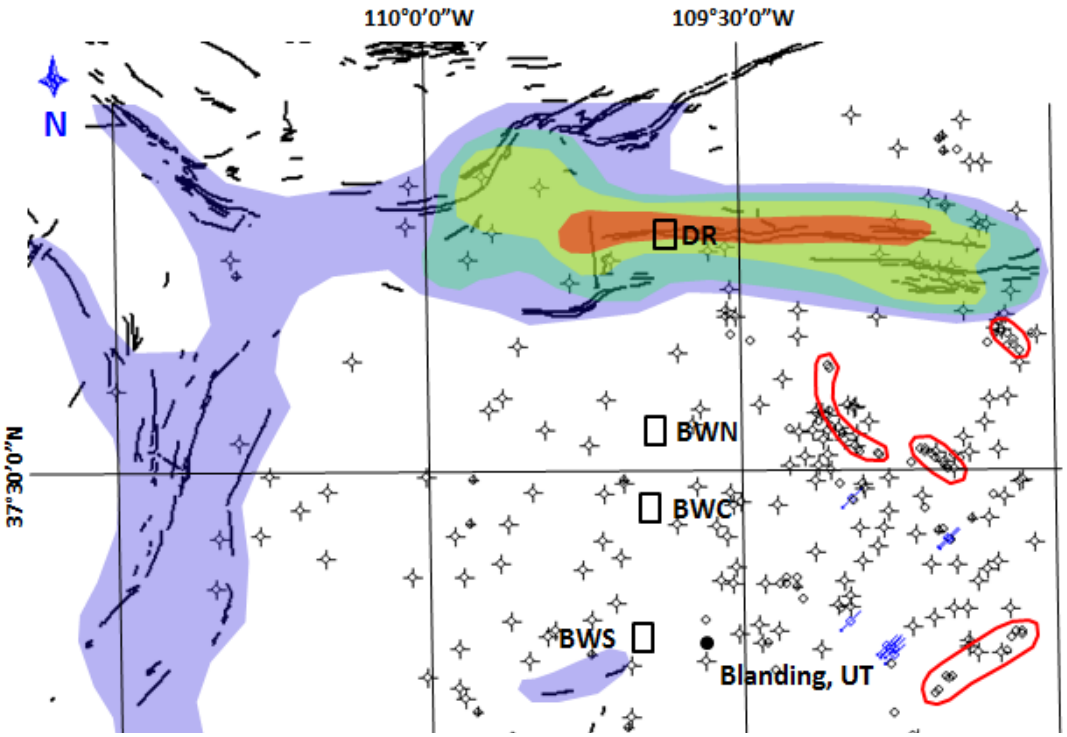

Figure 70. Fluid migration potential map with the historical producing zones highlighted in red. 100% of the wells in the producing zones fall within the low to very low migration potential zones. Field areas identified in black boxes. MU North, MU Central A, MU Central B, and MU South field areas.

Potential migration pathways of hydrocarbons sourcing from the Pennsylvanian units are drawn in blue, with flow directions based on the structural contours of the Jurassic Entrada Sandstone, from the geometric reconstruction of the area using formation tops from the geophysical well logs (Figure 71).

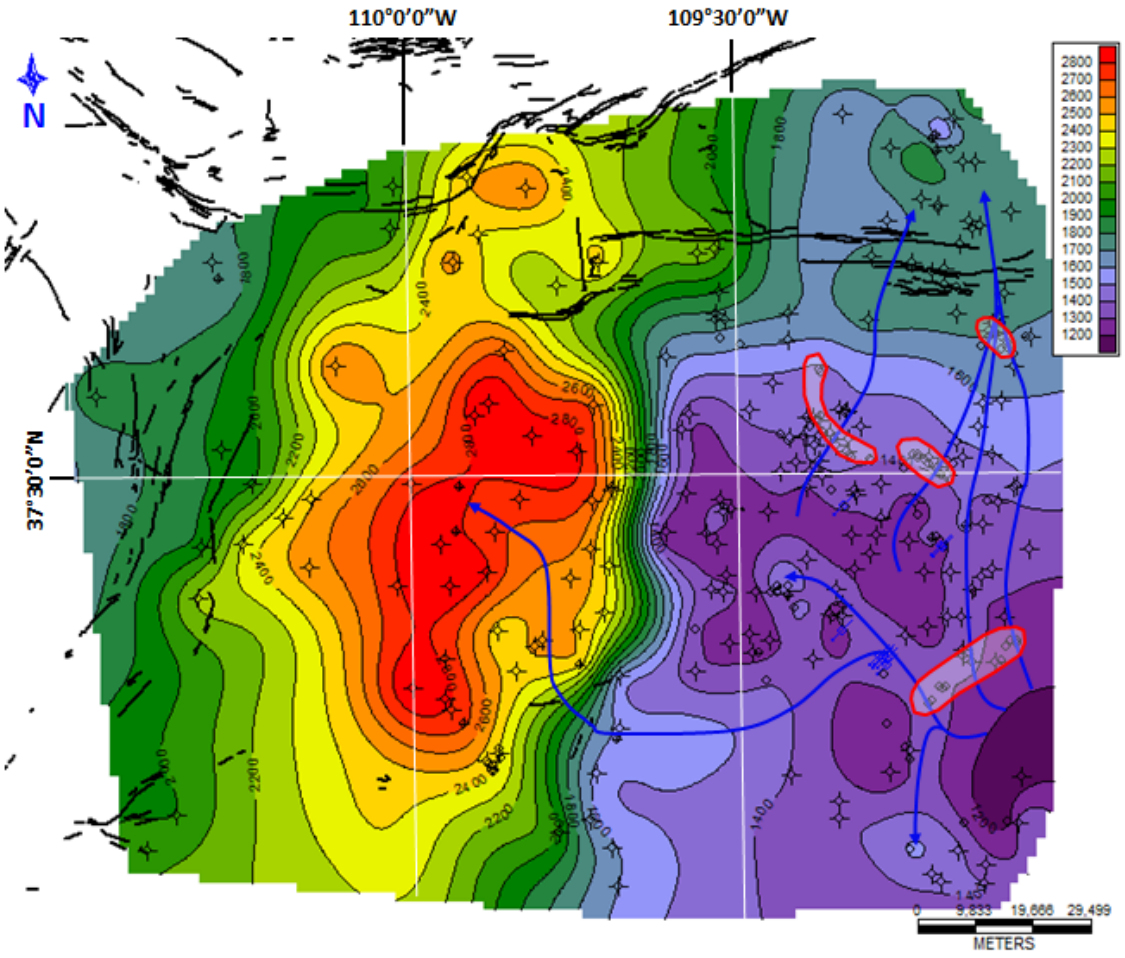

Figure 71. Potential migration pathways of Pennsylvanian units traced orthogonal to structural contours of the Entrada Sandstone in the Monument Uplift geometrical reconstruction. The historical producing zones are highlighted in red.

A producing capability of a well is defined by structural, sedimentalogical and stratigraphic parameters, yet it is interesting to note that the producing wells consistently lie along migration pathways in areas that have a low fault leakage potential along major faults. The lack of extensive alteration of the Jurassic formations in the Monument Uplift focus area and absence of mineralization of calcite along fractures, may be due to a structural low directly west of the eastern flank of the Monument Uplift (Figure 71). The structural low may have minimized migration of fluids and/or hydrocarbons towards the Monument Uplift structural high.

Additionally, the San Rafael Swell focus area exhibited approximately 4 km of elevation contrast between the structural high located in the San Rafael Swell, and the structural low located beneath the Uinta Basin. This strong elevation contrast in San Rafael Swell focus area would have been a driving factor for fluid migration toward the structural high. The elevation contrast of the Monument Uplift focus area is approximately 1.5 km, much lower than the contrast observed in the San Rafael Swell focus area. The lower elevation contrast, coupled with the structural low paralleling the eastern flank of the Monument Uplift may have caused the fluid and/or hydrocarbons to migrate northward, intersecting the MU North Fault, and may explain the presence of alteration and mineralization in the MU North field area that was absent in the other three field areas in the Monument Uplift focus area.

CO_2 Plume and Fault Interaction Through Time

Using the geometric reconstruction of the San Rafael Swell as a hypothetical CO_2 injection site intended for geologic storage of CO_2, a hypothetical injection site is placed in the apex of the reconstruction of the Jurassic Navajo Sandstone, and assumed that the injected CO_2 was free to flow through pore space at a constant rate, with no leakage occurring to the formations above (Figure 72). This is a purely geometric model to envision how the probability of a CO_2 plume at a storage site at the scale of the San Rafael Swell or Monument Uplift focus areas would intersect an increasing area of faults through time. The areal extent of the plume was calculated based on a 100 year injection at 20,000 tonnes/day is an amount released daily by a 1 GW/day coal fired power plant (Blunt, 2010). Using volumetric calculations derived from the geometric reconstruction a porosity of 10%, and a saturation of 30% was assumed (Doctor et al., 2000) to determine a 100 year areal extent of ~293 km^2 (Figure 72). The 100 year CO_2 plume is displayed with major faults with a trace length of 5+ km and over 10-15 m of throw (Doelling, 2002) (Figure 72b), and with smaller mapped faults in the area added (Figure 72c).

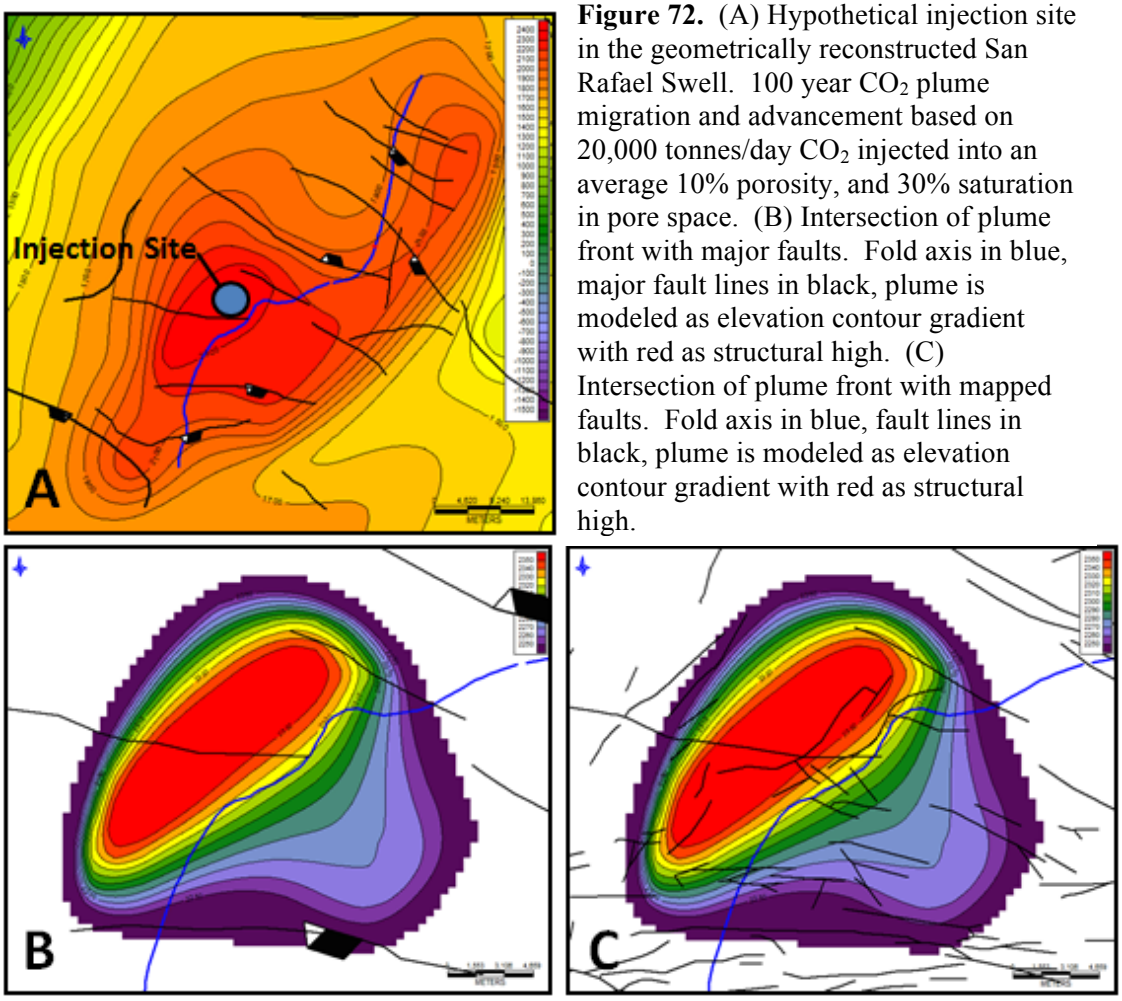

Figure 72. (A) Hypothetical injection site in the geometrically reconstructed San Rafael Swell. 100 year CO_2 plume migration and advancement based on 20,000 tonnes/day CO_2 injected into an average 10% porosity, and 30% saturation in pore space. (B) Intersection of plume front with major faults. Fold axis in blue, major fault lines in black, plume is modeled as elevation contour gradient with red as structural high. (C) Intersection of plume front with mapped faults. Fold axis in blue, fault lines in black, plume is modeled as elevation contour gradient with red as structural high.

When only major faults are considered, the CO_2 plume front intersects ~33 linear km of fault surface in the Navajo Sandstone, with an approximate fault plane surface area of 4.95 km^2. When all mapped faults in the area are considered the plume front intersects ~138 linear km of fault surface in the Navajo Sandstone, a ~400% increase in fault surface area is observed, with an approximate fault plane surface area of 20.7 km^2. The fault plane surface area potentially intersected by a migrating CO_2 plume illustrates the importance of not only considering major faults registered through seismic imaging, but it is also important to consider the effects of faults that lie below current seismic resolution on a proposed CO_2 injection site.

In addition to the smaller faults considered in the plume model (Figure 72), the uniformity of fracture orientations in the Navajo Sandstone and Carmel Formation and the observed connectivity of fractures across lithologic boundaries in the San Rafael Swell focus area increases the potential for upward migration of fluid and/or hydrocarbons across low-permeability top seals. The area closest to the hypothetical injection location in the San Rafael Swell is the SRS Central field area, exhibiting uniformity of fracture orientations (Table 2), and similar fracture spacing in the Navajo Sandstone and Carmel Formation (Figure 48). Mean fracture spacing in the Navajo Sandstone is 0.17 m, and 0.16 m in the Carmel Formation. Applying these values along a single plane orthogonal to the dominant fracture orientation in the hypothetical CO_2 plume would result in $1.26 * 10^5$ fractures in the Navajo Sandstone, and $1.34 * 10^5$ fractures in the Carmel Formation. The difference in fracture spacing for the Navajo Sandstone and Carmel Formation, approximates direct connectivity of fractures to exist every 2.72 m. This value indicates that approximately 8000 fractures would allow for direct migration of fluids and/or hydrocarbons across the lithologic boundary between the Navajo Sandstone and Carmel Formation along a single plane. This value reflects a direct connection of fractures only, and approximates fluid migration to occur along 6% of fractures along a single plane (Figure 73).

Fluids and/or hydrocarbons have been shown to migrate through the matrix of the Carmel Formation along fracture boundaries, creating secondary pore space, and altering of feldspar (Figure 56). In the SRS Central field area, color alteration halos due to migration of fluids and/or hydrocarbons through the matrix, extended 1 to 6 cm on either side of the fracture. Applying the mean of 3.5 cm to the fracture connectivity calculation allows for connectivity of 10 fractures per every 5 linear meters. This increases the number of fractures allowing for fluid migration to $4.2 * 10^4$, indicating that approximately 32% of fractures along a single plane would allow for migration of fluid and/or hydrocarbons (Figure 73).

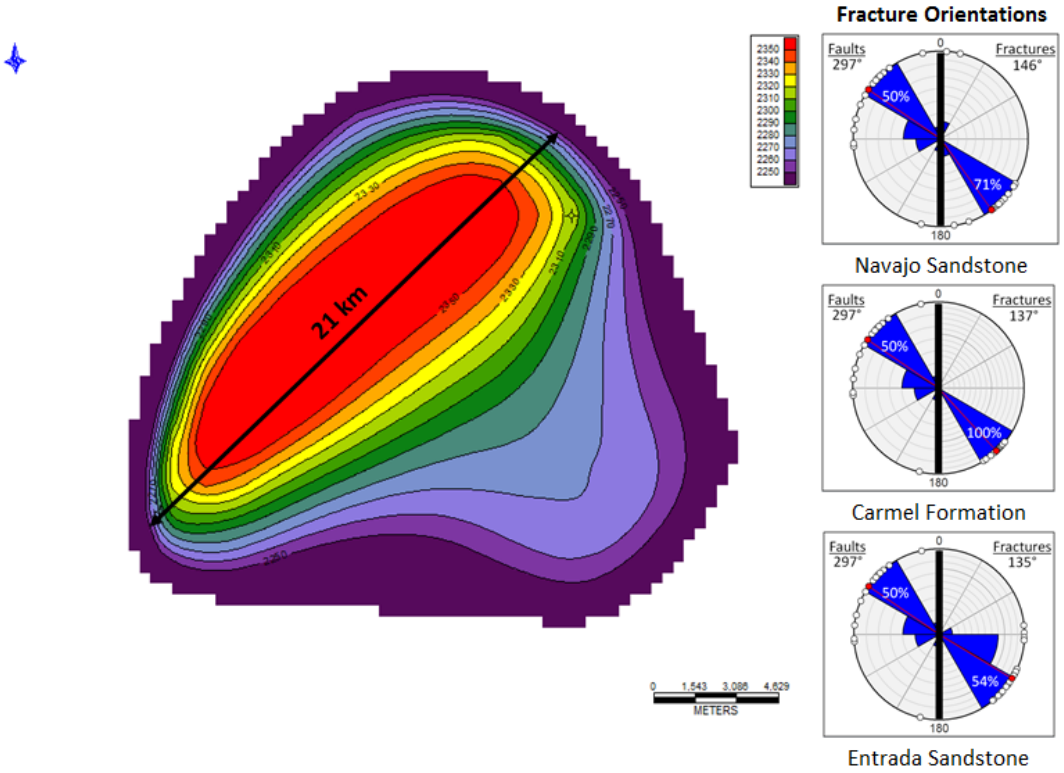

Figure 73. Connectivity of fractures calculated on single plane (21.5 km) across the 100 year CO_2 plume in the Navajo Sandstone. Fracture orientations from SRS Central field area.

CONCLUSIONS

The goal of this study was to correlate observations, at three different scales, exposures of a natural analog anticline to subsurface conditions of a potential injection target for geologic storage of CO_2 at depth, in order to predict potential migration pathways and seal bypass mechanisms. Color alteration of host rock and mineralization within fractures were used as indicators of migration of fluid and/or hydrocarbons through the formations at natural analog exposures in the San Rafael Swell and Monument Uplift focus areas.

Projection of the surface traces of faults at depth were modeled to provide insight into potential intersections with antithetic faults at depth. Faults with modeled multiple intersections at depth may result in a higher potential of fluid migration along the fault plane, bypassing sealing formations, and increasing leakage from a reservoir. The projection of modeled fault planes at depth also may give insight into the origination points of faults at depth in the area. The modeled faults in the San Rafael Swell focus area are strongly correlated to the upward migration of the Paradox Formation, with many of the projected faults in the area intersecting at or near the Paradox Formation top.

Fluid migration along the fault plane and damage zone increases the probability of fluid leakage through sealing formations along fault zones. The fault leakage potential map is effective in highlighting areas in which seal bypass may have occurred, minimizing effectiveness of a sealing formation regardless of thickness. Additionally, prior to injection of CO_2 in produced oil and gas fields, it is necessary to identify the migration potential of the field in order to differentiate a sealed reservoir from a leaking reservoir in which the influx was greater than the outflow. The producing oil and gas fields that are located in the medium to high zones of potential fault leakage may be the result of a high influx of hydrocarbons into an area with a compromised seal.

Formation top data recorded by hydrocarbon exploration in the two areas can be used to construct effective contour maps useful in determining the potential migration pathways of fluids and/or hydrocarbons migrating up-dip from the source. The migration traces show produced oil and gas reservoirs that may be adequate for future injection of CO_2 due to the presence of an intact sealing formation necessary for successful geologic storage of CO_2. The migration pathway and fault leakage potential maps effectively predicted oil seeps along the Little Grand Wash fault zone outside of Green River, Utah that source 100+ km to the northwest in the Pennsylvanian Phosphoria Formation.

Petrographic analysis of samples from both of the focus areas allows for calculation of pore space degradation. Percentage of degradation records the paleo-migration of fluids through the porous sandstones, and supports both the migration pathway and fault leakage potential maps. Areas of increased degradation are interpreted to be due to close proximity to a fracture zone with multiple intersections with antithetic faults at depth, or due to location up section from the migrating fluids and/or hydrocarbons.

Geometrical reconstruction of both focus areas allowed for volumetric calculations of the Jurassic Navajo and Entrada Sandstones necessary for modeling of a hypothetical CO_2 injection into the geometrical reconstruction of the San Rafael Swell. The modeling of a 100 year plume migrating through the Navajo Formation did not account for the sedimentalogical or stratigraphical heterogeneity of formations, but did effectively illustrate the importance of accounting not only for potential leakage along major faults, but also for faults with throw less than 10-15 m that are below the resolution of current seismic imaging methods.

Multiple scale analysis of faults and fractures in areas of proposed CO_2 storage sites is shown in this study to be an important consideration prior to injection of CO_2 at depth. The risk factors that increase the potential of fluid migration at a CO_2 sequestration site include: 1) Fluid migration through potential sealing formations, namely the Jurassic Carmel formation, can occur

on microscopic scale fractures; 2) Presence of authogenic clay near fractures indicate migration of fluid extending into the matrix adjacent to fractures, increasing potential connectivity; 3) Euhedral calcite mineralization in the Carmel formation indicates open fractures at depth in the formation identified as a seal in the Gordon Creek test injection; 4) Fracture orientations are uniform from the Navajo Sandstone into the overlying Carmel Formation and Entrada Sandstone; 5) Fracture orientations are uniform with fault orientations in the surrounding areas allowing for linear horizontal flow that would increase connectivity of migration pathways; 6) Fracture frequency increases in proximity to major fault zones with sub-seismic resolution independent of lithology; 7) Potential connectivity of migration pathways increases with decreasing scale of analysis. Utilizing the methods proposed in this study will allow for enhanced prediction of potential fluid migration pathways.

Recommendations

Surveying a wide range outcrop exposures over two large areas allows for regional analysis of two reservoir and seal pairs that have been identified in the Gordon Creek test injection. The potential risks associated with sequestration into the Navajo and Entrada Sandstones were identified using a variety of methods. Future work in the San Rafael Swell area should be separated into three main parts: 1) Outcrop scale analysis of fractures and faults; 2) Microscopic scale analysis of fractures from outcrop, core samples, and laboratory simulations of CO_2 injection into reservoir and caprock samples; 3) Correlation of fracture and fault analysis in the San Rafael Swell area to CO_2 injection sites using well data and 4-D seismic.

Fault leakage potential maps and fluid migration potential maps coupled with migration pathway maps in geometrically reconstructed formation top surfaces will assist in determining adequacy of proposed areas for CO_2 injection into saline aquifers at depth for long-term geologic storage. In contrast, the mapping will allow for further evaluation in areas where failure of the

seal is likely to occur. The SRS Central field area provides one of the best proxy for failure of a sealing formation allowing for leakage into the overlying strata. Mineralized fractures, color alteration adjacent to fractures, and euhedral mineralization of calcite in open fractures in the SRS Central field area provide an opportunity for continued analysis on both an outcrop and microscopic scale.

Petrographic analysis of samples from natural analogues can be used to calculate degradation of pore space, and record the type of mineralization that occurred at depth prior to uplift and erosion of an exposed analog. Degradation of pore space highlights the effects of faults in a potential storage site, and records seal bypass occurring along fault zones in the record of paleo-fluid flow. Additionally, the petrographic analysis identifies degradation of pore space not related to proximity to a major fault such as is seen in the SRS North field area. Further analysis of the dominant oxides present in pore space may allow for a better understanding of the upward migration of fluid through pore space in the area, and help in determining the potential lateral extent of migrating fluids along a damage zone.

REFERENCES

Allis, R.G., Chidsey, T.C., Gwynn, W., Morgan, C., White, S., Adams, M., and Moore, J., 2001, Natural CO_2 reservoirs on the Colorado Plateau and Southern Rocky Mountain candidates for CO_2 sequestration, *in* Proceedings, *First National Conference on Carbon Sequestration*, Washington, D.C., May 14-17, p. 19. www.netl.doe.gov/publications/proceedings/01/carbon.../6a2.pdf (April, 2010).

Allis, R.G., Chidsey, T.C., Morgan, C., Moore, J., and White, S.P., 2003, CO_2 sequestration potential beneath large power plants in the Colorado Plateau-Southern Rocky Mountain region, USA, *in* Proceedings, *Second National Conference on Carbon Sequestration*, Alexandria, VA, May 5-8, p. 1-25. www.netl.doe.gov/publications/proceedings/03/carbon.../003.pdf (April, 2010).

Allimendinger, R.W., Farmer, H., Hauser, E., Sharp, J., Von Tish, D., Oliver, J., and Kaufman, S., 1986, Phanerozoic tectonics of the Basin and Range-Colorado Plateau transition from COCORP data and geologic data, *in*, Barazangi, M., Brown, L., eds., Reflection Seismology: The Continental Crust: *American Geophysical Union Geodynamics Series*, v. 14, p. 257-268.

Baars, D.L., and Stevenson, G.M., 1982, Subtle stratigraphic traps in Paleozoic rocks of Paradox Basin, *in* Halbouty, M.T., eds., Deliberate Search for the Subtle Trap: *American Association of Petroleum Geologists Memoir 32*, p. 131-158.

Baer, J., and Rigby, J., 1978, Geology of the Crystal Geyser and environmental implications of its effluent, Grand County, Utah: *Utah Geology*, v. 5, p. 125-130.

Behrens, R.A., and Tran, T.T., 1999, Incorporating Seismic Data of Intermediate Vertical Resolution Into Three-Dimensional Reservoir Models: A New Method: *Society of Petroleum Engineers*, v. 2, no. 4, p. 325-333, doi 10.2118/57481-PA

Beitler, B., Chan, M.A., and Parry, W.T., 2003, Bleaching of Jurassic Navajo Sandstone on Colorado Plateau Laramide highs: evidence of exhumed hydrocarbon supergiants? *Geology*, v. 31, p. 1041-1044.

Beitler B., Parry, W.T., and Chan M.A., 2005, Fingerprints of fluid flow: Chemical diagenetic history of the Jurassic Navajo Sandstone, southern Utah, U.S.A: *Journal of Sedimentary Research*, v. 75, p. 547-561, doi: 10.2110/jsr.2005.045.

Benson, S., and Cook, P., 2005, Underground geologic storage, *in* Metz, B., Davidson, O., de Coninck, H.C., Loos, M., Meyer, L.A., eds., IPCC, 2005: *IPCC Special Report on Carbon Dioxide Capture and Storage*. Prepared by Working Group III of the Intergovernmental Panel on Climate Change Cambridge UniversityPress, Cambridge, United Kingdom and New York, NY, USA, 442 pp. www.ipcc.ch/pdf/special-reports/srccs/srccs_chapter5.pdf (May, 2010).

Berg, R. R., and Gangi, A. F., 1999, Primary migration by oil-generation microfracturing in low-permeability source rocks: Application to the Austin chalk, Texas: *American Association of Petroleum Geologists Bulletin*, v. 83, no. 5, p. 727-756.

Bird, P., 1998, Kinematic history of the Laramide orogeny in latitudes 35°-49°, western United States: *Tectonics*, v. 17, no. 5, p. 780-801.

Blakey, R.C., Peterson, F., Caputo, M.W., Geesaman, R.C., and Voorhees, B.J., 1983, Paleogeography of Middle Jurassic continental, shoreline, and shallow marine sedimentation, southern Utah, *in* Reynolds, M.W. and Dolley, E.D., eds., Mesozoic Paleogeography of the West Central United States: *Society of Economic Paleontologists and Mineralogists, Rocky Mountain Sect., Symp.*, v. 2, p. 77-100.

Blakey, R.C., Peterson, F., and Kocurek, G., 1988, Synthesis of late Paleozoic and Mesozoic eolian deposits of the Western Interior of the United States: *Sedimentary Geology*, v. 56, p. 3-125.

Blakey, R.C., 1994, Paleogeographic and tectonic controls on some Lower and Middle Jurassic erg deposits, Colorado Plateau, *in* Caputo, M.V., Peterson, J.A., and Franczyk, K.J., eds., Mesozoic systems of the Rocky Mountain region, USA, p. 273-298.

Blakey, R.C., Havholm, K.G., and Jones, L.S., 1996, Stratigraphic analysis of eolian interactions with marine and fluvial deposits, Middle Jurassic Page Sandstone and Carmel Formation, Colorado Plateau, U.S.A: *Journal of Sedimentary Research*, v. 66, no. 2, p. 324-342.

Blunt, M., 2010, Carbon dioxide storage: *Grantham Institute for Climate Change Briefing Paper*, December, n. 4.
http://www3.imperial.ac.uk/climatechange/publications (March, 2011).

Bowman, J.L., 1969, Oil Impregnated sandstone between Dirty Devil and Colorado and Green Rivers, Garfield and Wayne Counties, Utah, *in* Proceedings, *Petroleum Geologists' Annual Meeting*, Albuquerque, New Mexico, February 26, 18 p.
http://ds.heavyoil.utah.edu/dspace/handle/123456789/7889 (November, 2010).

Bump, A., 2003, Late Cretaceous-early Tertiary Laramide deformation of the northern Colorado Plateau, Utah and Colorado: *Journal of Structural Geology*, v. 25, no. 3, p. 421-440.

Burnside, N. M., 2010, U-Th dating of travertines on the Colorado Plateau: implications for the leakage of geologically stored CO_2 [PhD Dissertation]: *University of Glasgow*, 306 p.
http://theses.gla.ac.uk/1988/ (January, 2011).

Caine, J.S., Evans, J.P., and Forster, C.P., 1996, Fault zone architecture and permeability structure: *Geology*, v. 24, p. 1125-1128.

Caputo, M.V., 1988, Origin of sedimentary facies in the upper San Rafael group (Middle Jurassic), east-central Utah [PhD Dissertation]: *University of Cincinatti*, Ohio, 708 p.

Cartwright, J., Huuse, M., and Aplin, A., 2007, Seal bypass systems: *American Association of Petroleum Geologists Bulletin*, v. 91, n. 8, p. 1141-1166.

Celia, M.A., Bachu, S., Nordbotten, J.M., Gasda, S.E., and Dahle, H.K., 2004, Quantitative estimation of CO_2 leakage from geological storage: Analytical models, numerical models, and data needs, *in* Proceedings, *7th International Conference on Greenhouse Gas Control Technologies*, Vancouver, Canada, September 5-9. uregina.ca/ghgt7/PDF/papers/peer/228.pdf (March, 2010).

Chan, M.A., Beitler, B., Parry, W.T., Ormo, J., and Komatsu, G., 2004, A possible terrestrial analogue for hematite concretions on Mars: *Nature*, 429, p. 731-734.

Chan, M.A., Beitler, B., Parry, W.T., Ormo, J., and Komatsu, G., 2005, Red rock and red planet diagenesis: comparison of Earth and Mars concretions: *Geological Society of America Today*, v.15, p. 8.

Chan, M.A., Johnson, C.M., Beard, B.L., Bowman, J.R., and Parry, W.T., 2006, Iron isotopes constrain the pathways and formation mechanisms of terrestrial oxide concretions: a tool for tracing iron cycling on Mars?: *Geosphere*, v. 2, p. 324-332.

Chan, M.A., Parry, W.T., and Bowman, J.R., 2000, Diagenetic hematite and manganese oxides and fault-related fluid flow in Jurassic sandstones, southeastern Utah: *American Association of Petroleum Geologists Bulletin*, v. 84, p. 1281-1310.

Chan, M.A., Ormo, J., Park, A.J., Stich, M., Souza-Egipsy, V., and Komatsu, G., 2007, Models of iron oxide concretion formation: field, numerical, and laboratory comparisons: *Geofluids*, v. 7, p. 1-14.

Curtis, J. B., 2002, Fractured Shale-Gas Systems: *American Association of Petroleum Geologists Bulletin*, v. 86, n. 11, p. 1921-1938. doi: 10.1306/61EEDDBE-173E-11D7-8645000102C1865D.

Davatzes, N.C., Aydin, A., and Eichhubl, P., 2003, Overprinting faulting mechanisms during the development of multiple fault sets in sandstone, Chimney Rock fault array, Utah, USA: *Tectonophysics*, v. 363, p. 1-18.

Davis, G.H., 1999, Structural geology of the Colorado Plateau region of southern Utah, with special emphasis on deformation band shear zones: *Geological Society of America Special Paper 342*, 157 p.

Deming, D., 1994, Factors necessary to define a pressure seal: *American Association of Petroleum Geologists Bulletin*, v. 78: p. 1005-1009.

Dickinson, W.R., 1989, Tectonic setting of Arizona through geologic time, in Jenney, J.P., and Reynolds, S.J., eds., Geologic Evolution of Arizona: *Tucson, Arizona Geological Society Digest 17*, p. 1-16.

Dickinson, W.R., 2004, Evolution of the North American Cordillera: *Annual Review of Earth and Planetary Sciences*, v. 32, p. 13-45, doi:10.1146 /annurev.earth.32.101802.120257.

Dickinson, W.R., and Gehrels, G.E., 2003, U-Pb ages of detrital zircons from Permian and Jurassic eolian sandstones of the Colorado Plateau, USA: Paleogeographic implications: *Sedimentary Geology*, v. 163, p. 29-66.

Dickinson, W.R., Klute, M.A., Hayes, M.J., Janecke, S.U., Lundin, E.R., McKittrick,M.A., and Olivares, M.D., 1988, Paleogeographic and paleotectonic setting of Laramide sedimentary basins in the central Rocky Mountain region: *Geological Society of America Bulletin*, v. 100, p. 1023-1039, doi:10.1130/0016-7606(1988)100<1023:PAPSOL>2.3.CO;2.

Dockrill, B., and Shipton, Z.K., 2010, Structural controls on leakage from a natural CO_2 geologic storage site: central Utah, *U.S.A. Journal of Structural Geology*, v. 32, i. 11, p.1768-1782. doi:10.1016/j.jsg.2010.01.007 >>.

Doctor, R., Palmer, A., Coleman, D., Davison, J., Hendriks, C., Kaarstad, O., Ozaki, M., and Austell, M., 2000, Transport of CO_2, *in* Metz, B., Pichs-Madrugea, and Timashev, S., eds., Carbon Dioxide Capture and Storage: *Intergovernmental Panel on Climate Change Working Group III*, p. 179-193.

Doelling, H.H., 1965, Reconnaissance study of bituminous sandstone deposits, trans-Dirty Devil and Garfield Counties, Utah: *Report of the Utah Geological and Mineralogical Survey*. repository.icse.utah.edu/dspace/bitstream/123456789/.../Utah-Tar-159.pdf (February, 2011).

Doelling, H.H., 1994, Tufa deposits in western Grand County: *Survey Notes – Utah Geological Survey*, v. 26, p. 8-10, 13.

Doelling, H.H., 2002, Interim Geologic Map of the San Rafael Desert 30' x 60' Quadrangle, Emery and Grand Counties, Utah: *Utah Geological Survey Open-File Report 404*. geology.utah.gov/maps/geomap/30x60/pdf/ofr-404.pdf (March, 2010).

Erslev, E.A., and Koenig, N.V., 2009, Three-dimensional kinematics of Laramide, basement-involved Rocky Mountain deformation, USA: Insights from minor faults and GIS-enhanced structure maps, *in* Kay, S., Ramos, V., and Dickinson, W.R., eds., Backbone of the Americas: Shallow subduction, plateau uplift and ridge and terrane collision: *Geological Society of America Memoirs*, v. 204, p. 125-150.

Esser, R., Levey, R., Mcpherson, B., O'Dowd, W., Litynski, J., and Plasynski, S., 2010, Preparing for a carbon constrained world; overview of the United States regional carbon sequestration partnerships programme and its Southwest Regional Partnership, *in* Proceedings, *Petroleum Geology Conference Series*, v. 7, p. 1189-1195, doi: 10.1144/0071189.

Gehrels, G.E., and Dickinson, W.R., 1995, Detrital zircon provenance of Cambrian to Triassic miogeoclinal and eugeoclinal strata in Nevada: *American Journal of Science*, v. 295, p. 18-48.

Harris, A.G., Tuttle, E., and Tuttle, S.D., 2004, Capitol Reef National Park: *Geology of National Parks* ed. 6, p. 55-66.

Halloway, S., 2001, Storage of fossil fuel derived carbon dioxide beneath the surface of the earth: *Annual Review of Energy and the Environment*, v. 26, p. 145-166.

Hawley, C.C., Robeck, R.C., and Dyer, H.B., 1968, Geology altered rocks and ore deposits of the San Rafael Swell, Emery County, Utah: *United States Geological Survey Bulletin 1239*, 115 p.

Haynes, D.D., Vogel, J.D., and Wyant, D.G., 1979, Geology, structure, and uranium deposits of the Cortez quadrangle, Colorado and Utah: *United States Geological Survey Map I-629*, scale 1x2°, 2 sheets. http://geology.utah.gov/online/usgs/i/i-629.pdf (March, 2010).

Heath, J.E., Lachmar, T.E., Evans, J.P., Kolesar, P.T., and Williams, A.P., 2009, Hydrogeochemical characterization of leaking carbon dioxide-charged fault zones in east-central Utah, with implications for geologic carbon storage, *in* McPherson, B., and Sundquist, E., eds., The Science and Technology of Carbon Sequestration: *American Geophysical Union Monograph 18*, p. 147-158.

Hewson, R.D., Cudahy T.J., Mizuhiko S., Ueda, K., and Mauger, A.J., 2005, Seamless geological map generation using ASTER in the Broken Hill–Curnamona province of Australia: *Remote Sensing of Environment*, v. 99, p. 159-172.

Hiatt, E.E., and Budd, D.A., 2001, Sedimentary phosphate formation in warm shallow waters: new insights into the palaeoceanography of the Permian Phosphoria Sea from analysis of phosphate oxygen isotopes: *Sedimentary Geology*, v. 145, p. 119-133.

Hicks, T.C., 2011, Facies analysis and reservoir characterization of subtidal, intertidal, and supratidal zones of the mudstone-rich entrada sandstone, south-central Utah [Ms Thesis]: Brigham Young University, 142 p. contentdm.lib.byu.edu/ETD/image/etd4215.pdf (May, 2011).

Hintze, L.F., 1993, Geologic history of Utah: Brigham Young University Geology Studies *Special Publication 7*, 202 p.

Hintze, L.F. and Kowallis, B.J., 2009, Geologic History of Utah: *Brigham Young University Geology Studies Special Publication 9*, 225 p.

Hintze, L.F., Willis, G.C., Laes, D.Y.M., Sprinkel, D.A., and Brown, K.D., 2000, Digital Geologic Map of Utah: *Utah Geological Survey Digital State Map*, scale 1:500000, 2 sheets. geology.utah.gov/maps/geomap/statemap/pdf/digitalgeoutah.pdf (February, 2010).

Hubbert, M.K., 1951, Mechanical basis for certain familiar geologic structures: *Geological Society of America Bulletin*, v. 62, no. 4, p. 355-372, doi: 10.1130/0016-7606(1951) 62[355:MBFCFG]2.0.CO;2.

Hunt, C.B., 1956, Cenozoic geology of the Colorado Plateau: *United States Geological Survey Professional Paper 279*, p. 99.

Johansen, T.E.S., and Fossen, H., 2008, Internal geometry of fault damage zones in interbedded siliciclastic sediments, *in* Wibberly, C.A.J., Kurz, W., Imber, J., Holdsworth, R.E., and Collettini, C., eds., The Internal Structure of Fault Zones: *Implications for mechanical and fluid-flow properties*, v. 299, p. 35-36, doi: 10.1144/SP299.3.

Jones, L.S., and Blakey, R.C., 1993, Erosional remnants and adjacent unconformities along an eolian-marine boundary of the Page Sandstone and Carmel Formation, Middle Jurassic, south-central Utah: *Journal of Sedimentary Petrology*, v. 63, no. 5, p. 852-859.

Jones, L.S., and Blakey, R.C., 1997, Eolian-fluvial interaction in the Page Sandstone (Middle Jurassic) in south-central Utah, USA – a case study of erg margin processes: *Sedimentary Geology*, v. 109, p. 181-198.

Kalinowski,A., and Oliver, S., 2004, ASTER mineral indexing processing manual: Remote Sensing Applications, Geoscience Australia, October, 37 p. http://www.google.com/url?sa=t&rct=j&q=kalinowski%20and%20oliver%2C%202000&source=web&cd=2&ved=0CCIQFjAB&url=http%3A%2F%2Fwww.ga.gov.au%2Fimage_cache%2FGA7833.pdf&ei=vLTvTr3gB-XIsQLonulM&usg=AFQjCNG-YaqPaq7x-h1EI8MW0MThVRjZtA (March, 2010).

Kelley, V., 1955, Monoclines of the Colorado Plateau: *Geological Society of America Bulletin*, v. 66, n. 7, p. 789-804, doi: 10.1130/0016-7606(1955)66[789:MOTCP]2.0.CO;2.

Kerr, P.F., Bodine, M.W., Kelley, D.R., and Keys, W.S., 1957, Collapse features, Temple Mountain uranium area, Utah: *Geological Society of America Bulletin*, v. 68, no. 8, p. 933-982, doi: 10.1130/0016-7606(1957)68[933:CFTMUA]2.0.CO;2.

Kocurek, G.A., and Dott, R.H., 1983, Jurassic paleogeography and paleoclimate of the central and southern Rocky Mountains region, *in* Reynolds, M.W., and Dolly, E.D., eds., Mesozoic paleogeography of west-central United States: *Society of Economic Paleontologists and Mineralogists (Rocky Mountain Section)*, p. 101-113.

Kocurek, G., 2003, Limits on extreme eolian systems: Sahara of Mauritania and Jurassic Navajo Sandstone examples, *in* Chan, M. A., and Archer, A. W., eds., Extreme depositional environments: Mega end members in geologic time: *Geological Society of America Special Paper 370*: Boulder, CO, Geological Society of America, p. 44-53.

Krantz, W.R., 1988, Multiple fault sets and three-dimensional strain: Theory and application: *Journal of Structural Geology*, v. 10, p. 225-237.

Kreisa, R.D., and Moiola, R.J., 1986, Sigmoidal tidal bundles and other tide-generated sedimentary structures of the Curtis Formation, Utah: *Geological Society of America Bulletin*, v. 97, p. 381-387.

LaBarre, E.L., and Davis, T.L., 2008, Fault and natural fracture identification from multicomponent seismic at Rulison Field, Colorado*, 2008 SEG Annual Meeting Expanded Abstracts*, v. 27, p. 948.

Laubach, S.E., 2003, Practical approaches to identifying sealed and open fractures: *American Association of Petroleum Geologists Bulletin*, v. 87, no. 4, p. 561-579, doi:10.1190/1.3063795.

Laubach, S.E., Olson, J.E., and Gross, M.R., 2009, Mechanical and fracture stratigraphy: *American Association of Petroleum Geologists Bulletin*, v. 93, no. 11, p. 1413-1426, doi: 10.1306/07270909094.

Lillis, P.G., Warden, A., and King, J.D., 2003, Petroleum Systems of the Uinta and Piceance Basins-Geochemical Characteristics of Oil Types, *in* Norton, G.A., and Groat, C.G., eds., Petroleum Systems and Geologic Assessment of Oil and Gas in the Uinta-Piceance Province Utah and Colorado: *United States Geological Survey Uinta-Piceance Assessment Team*, United States Geological Survey Digital Data Series DDS-69-B, ch. 3, p. 25.

Loope, D.B., Kettler, R.M., and Weber, K.A., 2010, Follow the water: Connecting a CO_2 reservoir and bleached sandstone to iron-rich concretions in the Navajo Sandstone of south-central Utah, *USA: Geology*, v. 38, no. 11, p. 999-1002.

Loope, D.B., Rowe, C.M, and Joeckel, R.M., 2001, Annual monsoon rains recorded by Jurassic dunes: *Nature*, v. 412, p. 64-66.

Maerten, L., 2000, Variation in slip on intersecting normal faults: Implications for paleostress inversion: *Journal of Geophysical Research*, v. 105, p. 553-565. doi: 10.1029/2000JB900264.

Maerten, L., Pollard, D.D., and Maerten, F., 2001, Digital mapping of three-dimensional structures of the Chimney Rock fault system, central Utah: *Journal of Structural Geology*, v. 23,
p. 585-592.

Maughan, E.K., 1983, Geological setting of oil shales in the Permian Phosphoria Formation and some of the geochemistry of these rocks, *in* Proceedings, *American Chemical Society Meeting, Seattle, WA*, March 20-25, 2 p.

McPherson, B. J., and Grigg, R., 2010, SWP Phase 3 Deployment Project: Overview and Summary: Southwest Regional, *in* Proceedings, *Regional Carbon Sequestration Partnerships Annual Review Meeting, Pittsburgh, PA.*, October 5–7, 75 p. http://www.netl.doe.gov/publications/proceedings/10/rcsp/presentations/Wed%20am/Dawn%20Deel/McPherson.%20Grigg.swp.%20phase3.annual.pitt.rcsp.oct2010.shorte.pdf (December, 2010).

Morris, T.H., Manning, V.W., and Ritter, S.M., 2000, Geology of Capitol Reef National Park, Utah, *in* Sprinkel, D.A., Chidsey, T.C., and Anderson, P.B., eds., Geology of Utah's Parks and Monuments: *Utah Geological Association Publication 28*, p. 85-106.

Narr, W., 1996, Estimating average fracture spacing in subsurface rock: *American Association of Petroleum Geologists Bulletin*, v. 80, no. 10, p. 1565-1586.

National Institute of Health, 2010, Image J, Image Processing and Analysis in Java, http://rsbweb.nih.gov/ij/download.html (December, 2010).

Nuccio, V.F., and Condon, S.M., 1996, Burial and thermal history of the Paradox Basin, Utah and Colorado, and petroleum potential of the Middle Pennsylvanian Paradox Formation: *United States Geological Survey Bulletin 2000-O*, 41 p.

O'Sullivan, R.B., 1998, Correlation of Jurassic San Rafael Group and related rocks from Blanding, Utah to Dove Creek, Colorado: *United States Geological Survey Geologic Investigations Series Map I-2764*, 21 p.

Parry, W.T., Chan, M.A., and Beitler, B.B., 2004, Chemical bleaching indicates episodes of fluid flow in deformation bands in sandstone: *American Association of Petroleum Geologists Bulletin*, v. 88, p. 1–17.

Parry, W.T., Chan, M.A., and Nash, B.P, 2009, Diagenetic characteristics of the Jurassic Navajo Sandstone in the Covenant Oil Field, Central Utah Thrust Belt: *American Association of Petroleum Geologists Bulletin*, v. 93, p. 1039-1061.

Parry, W.T., Forster, C.B., Evans, J.P., Bowen, B.B., and Chan, M.A., 2007, Geochemistry of CO_2 sequestration in the Jurassic Navajo Sandstone, Colorado Plateau, Utah: *Environmental Geosciences*, v. 14, no. 2, p. 91-109.

Peterson, F., and Pipiringos, G.N., 1979, Stratigraphic relations of the Navajo Sandstone to Middle Jurassic Formations, southern Utah and northern Arizona: *U.S. Geological Survey Professional Paper 1035-b*, p. 1-43.

Peterson, F., 1988, Pennsylvanian to Jurassic eolian transportation systems in the western United States, in Late Paleozoic and Mesozoic eolian deposits of the western interior of the United States: *Sedimentary Geology*, v. 56, p. 207-260.

Peterson, F., 1994, Sand dunes, sabkhas, streams, and shallow seas: Jurassic paleogeography in the southern part of the Western Interior Basin, *in* Caputo, M.V., Peterson, J.A., and Franczyk, K. J., eds., Mesozoic Systems of the Rocky Mountain Region, USA. Denver, *Rocky Mountain Section SEPM*, p. 233-265.

Petrovic, A., Khan, S.D., and Chafetz, H.S., 2008, Remote detection and geochemical studies for finding hydrocarbon induced alterations in Lisbon Valley, Utah: *Marine and Petroleum Geology*, v. 25, no. 8, p. 696-705.

Pipiringos, G.N., and O'Sullivan, R.B., 1978, Principal unconformities in Triassic and Jurassic rocks, Western Interior United States; a preliminary survey: *United States Geological Survey Professional Paper 1035-A*, 29 p.

Poole, F.G., and Sandberg, C.A., 1991, Mississippian paleogeography and conodont biostratigraphy of the Western United States, *in* Cooper, J.D., and Stevens, C.H., eds., Paleozoic Paleogeography of the Western United States—II: Pacific Section, *Society of Economic Paleontologists and Mineralogists Book 67*, v. 1, p. 107-136.

Poole, F.G., Stewart, J.H., Palmer, A.R., Sandberg, C.A., Madrid, R.J., Ross, R.J., Jr., Hintze, L.F., Miller, M.M., and Wrucke, C.T., 1992, Latest Precambrian to latest Devonian time; development of a continental margin, *in* Burchfiel, B.C., Lipman, P.W., and Zoback, M.L., eds., The Cordilleran Orogen, Conterminous U.S.: *Geological Society of America, The Geology of North America*, v. G-3, p. 9-56.

Potter, S.L., and Chan, M.A., 2011, Joint controlled fluid flow patterns and iron mass transfer in Jurassic Navajo Sandstone, Southern Utah, USA: *Geofluids*, v. 11, p. 184-198.

Roberts, A., 2001, Curvature attributes and their application to 3D interpreted horizons: First Break, v. 19, i. 2, p. 85-100, doi: 10.1046/j.0263-5046.2001.00142.x. https://petraftp.ihsenergy.com/curvature.pdf (January, 2011).

Roy, M., Jordan, T.H., and Pederson, J., 2009, Colorado Plateau magmatism and uplift by warming of heterogeneous lithosphere: *Nature*, v. 459, p. 978-982, doi:10.1038/nature08052.

Seiler, W.M., 2008, Jurassic Navajo Sandstone of Coyote Buttes, Utah/Arizona: Coloration and Diagenetic History, Preservation of a Dinosaur Trample Surface, and a Terrestrial Analog to Mars [M.S. Thesis]: *University of Utah*, Salt Lake City, Utah, 256 p.

Shipton, Z.K., 1999, Fault displacement profiles and off-fault deformation: interpreting the records of fault growth at the Chimney Rock fault array, Utah, USA [PhD thesis]: *Edinburgh University*, Edinburgh, Scotland, 224 p.

Shipton, Z.K., and Cowie, P.A., 2001, Analysis of three-dimensional damage zone development over a micron to km scale range in the high-porosity Navajo Sandstone, Utah: *Journal of Structural Geology*, v. 23, p. 1825-1844.

Shipton, Z.K, and Cowie, P.A., 2003, A conceptual model for the origin of fault damage zone structures in high-porosity sandstone: *Journal of Structural Geology*, v. 25, p. 333-344.

Shipton, Z. K., Evans, J.P., Kirschner, D., Kolesar, P. T., Williams, A. P., and Heath. J., 2004, Analysis of CO_2 leakage through "low-permeability" faults from natural reservoirs in the Colorado Plateau, east-central Utah, *in* Baines, S. J., and Worden, R. H., eds., Geological Storage of Carbon Dioxide: Reducing Greenhouse Gas Emissions: *Geological Society, London, Special Publications*, v. 233, p. 43-58, doi: 10.1144/GSL.SP.2004.233.01.05.

Shipton, Z.K., Evans, J.P., Robeson, K.R., Forster, C.B., and Snelgrove, S., 2002, Structural heterogeneity and permeability in faulted eolian sandstone: Implications for subsurface modeling of faults: *American Association of Petroleum Geologists Bulletin*, v. 85, no. 5, p. 863-883.

Sibson, R.H., 1994, Crustal stress, faulting and fluid flow, *in* Parnell, J., eds., Geofluids: Origin, Migration and Evolution of Fluids in Sedimentary Basins: *Geological Society Special Publication*, no. 78, p 69-84.

Stephens, N.P., and Carroll, A.R., 1999, Salinity stratification in the Permian Phosphoria sea; a proposed paleoceanographic model: *Geology*, v. 27, no. 10, p. 899-902.

Stewart, J.H., Poole, F.G., and Wilson, R.F., 1972, Stratigraphy and origin of the Triassic Moenkopi Formation and related strata in the Colorado Plateau region: *U.S. Geological Survey Professional Paper 691*, 195 p.

Verlander, J.E., 1995, The Navajo Sandstone: *Geology Today*, v. July-August, p. 143-146.

Volesky, J.C., Stern, R.J., and Johnson, P.R., 2003, Geological control of massive sulfide mineralization in the Neoproterozoic Wadi Bidah shear zone, southwestern Saudi Arabia, inferences from orbital remote sensing and filed studies: *Precambrian Research*, v. 123, p. 235-247.

Vollmer, F.W., 2010, Orient 2.1.1 Orientation Data Analysis Software. www.frederickvollmer.com (September, 2010).

Vrolijk, P., Myers, R., Sweet, M.L., Shipton, Z.K., Dockrill, B., Evans, J.P., Heath, J., and Williams, A.P., 2005, Anatomy of reservoir-scale normal faults in central Utah: stratigraphic controls and implications for fault zone evolution and fluid flow, *in* Pederson, J., and Dehler, C.M., eds., *Geological Society of America Field Guide: Interior Western United States*, v. 6, p. 261-282, doi:10.1130/2005.fld006(13).

Watson, N.W., and Gibson-Poole, C.M., 2005, Reservoir selection for optimized geological injection and storage of carbon dioxide: A combined geochemical and stratigraphic perspective, *in* Proceedings, *Fourth National Conference on Carbon Sequestration*, Alexandria, Virginia, May 2-5. www.netl.doe.gov/publications/.../Tech%20Session%20Paper%20110.pdf (August, 2010).

White, S.P., Allis, R.G., Moore, J., Chidsey, T., Morgan, C., Gwynn, W., and Adams, M., 2001, Numerical simulation of CO_2 sequestration in natural CO2 reservoirs on the Colorado Plateau, in Proceedings, *First National Conference on Carbon Sequestration*, Washington D.C., May 14-17. www.netl.doe.gov/publications/proceedings/03/carbon-seq/PDFs/220.pdf (March, 2010).

Williams, P.L., and Hackman, R.J., 1971, Geologic Map of the Salina 1 X 2 Quadrangle, Utah: *U.S. Geological Survey map i-591a*. http://geology.utah.gov/online/usgs/i/i-591.pdf (February, 2010).

Witkind, I. J., 1988, Geologic Map of the Huntington 30' X 60' Quadrangle, Carbon, Emery, Grand, and Uinta Counties, Utah: *U.S. Geological Survey map i-1764*. http://geology.utah.gov/maps/geomap/30x60/pdf/i-1764.pdf (January, 2010).

Witkind, I.J., 1995, Geologic Map of the Price 1 X 2 Quadrangle, Utah: *U.S. Geological Survey map i-2462*. http://geology.utah.gov/online/usgs/i/i-2462.pdf (August, 2011).

Wilcox, W.T., 2007, Sequence stratigraphy of the Curtis, Summerville and Stump Formations, Utah and northwest Colorado [M.S. thesis]: *Miami University*, Oxford, Ohio, 388 p.

Woodward, L.A., 1973, Structural framework and tectonic evolution of the Four Corners region of the Colorado Plateau, *in* James, H.L., eds., Guidebook of Monument Valley and vicinity Arizona and Utah: *New Mexico Geological Society*, 24th Field Conference, p. 94-98.

Zhang, Y., Oldenburg, C.M., Finsterle, S., Jordan, P., and Zhang, K., 2009, Probability estimation of CO_2 leakage through faults at geologic carbon sequestration sites: *Energy Procedia*, v. 1, i. 1, p. 41-46.

APPENDICES

Appendix A. Well Samples

Navajo Sandstone Well Information

API WELL #	TOP DEPTH	OPERATOR	WELL NAME	COUNTY	LOCATION
43-007-10355	828	EQUITY OIL COMPANY	FARNHAM DOME U 2	CARBON	15S-12E
43-007-10791	1949	PACIFIC TRANS SUPPLY	NORTH SPRINGS 1	CARBON	15S-9E
43-007-10819	660	PAN AMERICAN PETROLEUM COR	USA FARNHAM DOME 1	CARBON	15S-12E
43-007-10820	1154	PAN AMERICAN PETROLEUM COR	USA-LILLIE C CULLEN 1	CARBON	15S-13E
43-007-11029	1193	SHELL OIL COMPANY	MILLER CREEK 1	CARBON	15S-10E
43-007-15114	945	CARBON DIOXIDE AND CHEM CO	FARNHAM DOME 2	CARBON	15S-11E
43-007-15115	632	AMERIGAS INC	FARNHAM DOME 3	CARBON	15S-11E
43-007-15116	621	CARBON DIOXIDE AND CHEM CO	FARNHAM DOME 4	CARBON	15S-11E
43-007-15394	855	EQUITY OIL COMPANY	GOVT MOUNDS 3	CARBON	15S-12E
43-007-15395	849	EQUITY OIL COMPANY	FARNHAM DOME 1-A	CARBON	15S-12E
43-007-15606	754	MCADAMS J F	GRASSY TRAIL CREEK U 3	CARBON	15S-12E
43-007-15922	2685	SKELLY OIL CO	GORDON CREEK UNIT 5	CARBON	14S-7E
43-007-16107	2754	SKELLY OIL CO	GORDON CREEK UNIT 1	CARBON	14S-7E
43-007-20071	3488	ARCO OIL & GAS COMPANY	HIAWATHA U 1	CARBON	15S-7E
43-007-30012	1087	MOUNTAIN FUEL SUPPLY CO	SUNNYSIDE UNIT 1	CARBON	15S-13E
43-007-30036	863	EQUITY OIL COMPANY	MOUNDS 3-A	CARBON	15S-12E
43-007-30040	1733	CONOCOPHILLIPS COMPANY	DRUNKARDS WASH 31-1 (D-1)	CARBON	14S-10E
43-007-30044	2561	GORDON CREEK LLC	GORDON CREEK U 1	CARBON	14S-8E
43-007-30061	841	SWEPI/WESTERN DIVISION	FEDERAL 1-19	CARBON	15S-12E
43-007-30084	733	GENESIS PETROLEUM US INC	STATE 36-13	CARBON	15S-12E
43-007-30093	2199	CONOCOPHILLIPS COMPANY	ARCADIA-TELONIS 1 (D2)	CARBON	14S-9E
43-007-30100	2177	CONOCOPHILLIPS COMPANY	UTAH D-6	CARBON	14S-9E
43-007-30103	764	GENESIS PETROLEUM US INC	STATE 36-2	CARBON	15S-12E
43-007-30290	1692	CONOCOPHILLIPS COMPANY	UTAH D3	CARBON	15S-10E
43-007-30314	1842	CONOCOPHILLIPS COMPANY	UTAH D4	CARBON	14S-9E
43-007-30351	2135	CONOCOPHILLIPS COMPANY	FAUSETT D5	CARBON	14S-9E
43-007-30361	1789	ANADARKO PETROLEUM CORP	HELPER ST SWD 1	CARBON	14S-10E
43-007-30431	1838	CONOCOPHILLIPS COMPANY	UTAH D8	CARBON	15S-9E
43-007-30438	2196	CONOCOPHILLIPS COMPANY	UTAH D-9	CARBON	14S-9E
43-007-30555	1717	ANADARKO PETROLEUM CORP	FED F-2 SWD	CARBON	14S-10E
43-007-30567	1390	CONOCOPHILLIPS COMPANY	SAMPINOS D14	CARBON	15S-10E

43-007-30656	1886	MARATHON OIL COMPANY	SITLA SWD 1	CARBON	15S-9E
43-007-30721	2345	ANADARKO PETROLEUM CORP	CLAWSON SPRING ST SWD 1	CARBON	15S-8E
43-007-30818	853	SAVOY ENERGY LLC	EDP 1	CARBON	15S-12E
43-007-30912	1733	KERR-MCGEE OIL & GAS ONSHORE L.P.	WELLINGTON FED 44-6 SWD	CARBON	14S-11E
43-007-30967	1675	KERR-MCGEE OIL & GAS ONSHORE L.P.	WELLINGTON FED 22-04 SWD	CARBON	14S-11E
43-007-31262	828	SAVOY ENERGY LLC	SAVOY 2	CARBON	15S-12E
43-007-31263	866	SAVOY ENERGY LLC	SAVOY 1	CARBON	15S-12E
43-007-31374	1349	KERR-MCGEE OIL & GAS ONSHORE L.P.	WELLINGTON FED 41-25 SWD	CARBON	14S-10E
43-007-31375	1333	KERR-MCGEE OIL & GAS ONSHORE L.P.	WELLINGTON FED 31-30 SWD	CARBON	14S-11E
43-015-10019	487	AMAX PETROLEUM CORP	AMAX-SINCLAIR GOVT 29-4B	EMERY	22S-15E
43-015-10021	629	AMAX PETROLEUM CORP	GREEN RIVER DESERT U 9-7	EMERY	22S-15E
43-015-10022	362	AMAX PETROLEUM CORP	GREEN RIVER DESERT U 24-1	EMERY	22S-13E
43-015-10028	0	AMERADA	USA COLMAN 1	EMERY	23S-9E
43-015-10116	110	GENERAL PETROLEUM CORP	45-56	EMERY	24S-15E
43-015-10182	36	STANDARD OIL CO OF CALIF	LOOKOUT POINT UNIT 1	EMERY	25S-16E
43-015-10183	76	STANDARD OIL CO OF CALIF	MOONSHINE WASH U 1	EMERY	25S-15E
43-015-10229	98	CONTINENTAL OIL COMPANY	MOONSHINE WASH U 2	EMERY	25S-15E
43-015-10350	30	EL PASO NATURAL GAS CO	PACK SADDLE FED 1	EMERY	18S-12E
43-015-10358	713	EQUITY OIL COMPANY	MOUNDS 2	EMERY	16S-12E
43-015-10359	664	EQUITY OIL COMPANY	MOUNDS FED 4	EMERY	16S-12E
43-015-10360	558	EQUITY OIL COMPANY	STATE 1	EMERY	16S-12E
43-015-10374	1983	FOREST OIL CORP	FOREST GOVT 25-1 ARNOLD	EMERY	16S-14E
43-015-10460	9	HANCOCK-UTAH DEVELOPMENT	CEDAR MOUNTAIN U 1	EMERY	19S-12E
43-015-10500	535	HUMBLE OIL & REFINING CO	GOVT-WHEATLEY 1	EMERY	16S-12E
43-015-10502	170	HUMBLE OIL & REFINING CO	NEQUOIA ARCH U 7	EMERY	26S-14E
43-015-10634	1079	KRALIK OIL CO	STATE 1	EMERY	18S-9E
43-015-10698	695	MCADAMS J F	GRASSY TRAIL CREEK U 4	EMERY	16S-12E
43-015-10800	1925	PACIFIC NATURAL GAS EXPLOR	RANGE CREEK UNIT 1-27	EMERY	17S-16E
43-015-10825	757	PAN AMERICAN PETROLEUM COR	FEDERAL MOUNDS 1	EMERY	16S-11E
43-015-10826	166	PAN AMERICAN PETROLEUM COR	NEQUOIA ARCH UNIT 9	EMERY	26S-13E
43-015-10827	226	PAN AMERICAN PETROLEUM COR	NEQUOIA ARCH UNIT 10	EMERY	26S-13E
43-015-10828	97	PAN AMERICAN PETROLEUM COR	USA-C M BROWN 1	EMERY	25S-12E
43-015-10900	2063	PHILLIPS PETROLEUM CO	GOVERNMENT 1	EMERY	17S-8E
43-015-10928	796	PLACID OIL COMPANY	MARSH FLAT UNIT 1	EMERY	17S-14E
43-015-10961	442	READ R H JR	SUCKLE GOVERNMENT 1	EMERY	17S-12E

43-015-10963	542	RESERVE OIL & GAS	CEDAR SIDING UNIT 1	EMERY	16S-13E
43-015-10969	9	REYNOLDS MINING CORP	CEDAR MOUNTAIN UNIT 1	EMERY	19S-12E
43-015-11138	373	TEXAS EASTERN SKYLINE OIL	GREEN RIVER UNIT 1	EMERY	21S-16E
43-015-11184	108	SUPERIOR OIL COMPANY	N SPRING WASH 31-15	EMERY	25S-15E
43-015-11328	844	UNION OIL CO OF CALIFORNIA	DESERT LAKE UNIT 1	EMERY	17S-10E
43-015-11329	1632	UNION OIL CO OF CALIFORNIA	WASHBOARD WASH USA 1	EMERY	16S-9E
43-015-11398	224	UTAH PLATEAU URANIUM CO	FEDERAL 1	EMERY	22S-8E
43-015-11399	224	UTAH PLATEAU URANIUM CO	FEDERAL 1-X (WSW)	EMERY	22S-8E
43-015-15104	67	ORPHAN-NO RESPONSIBLE OPERATOR	ENGLISH 1-X	EMERY	26S-7E
43-015-15105	73	STANDARD ENERGY CORP	H L RATH 1-A	EMERY	26S-7E
43-015-15603	611	PRIDE VENTURES LLC	BOLINDER C-1	EMERY	16S-12E
43-015-15604	719	GENESIS PETROLEUM US INC	FEDERAL 1	EMERY	16S-12E
43-015-15605	694	MEGADON ENTERPRISES INC	GRASSY TRAILS 2	EMERY	16S-12E
43-015-15607	695	PRIDE VENTURES LLC	FEDERAL 2	EMERY	16S-12E
43-015-15676	1471	NORTHSTARGAS LC	PAN AM 3	EMERY	20S-7E
43-015-15677	1503	PAN AMERICAN PETROLEUM COR	FERRON UNIT FEE 4 (14-2)	EMERY	20S-7E
43-015-20053	1500	DIAMOND SHAMROCK EXPL	WITTER FED 1	EMERY	18S-15E
43-015-20091	513	AUSTRAL OIL CO INC	FEDERAL 1-27	EMERY	18S-11E
43-015-20145	1497	TENNECO OIL COMPANY	FERRON UNIT 5	EMERY	20S-7E
43-015-20190	1209	CHEVRON USA INC	CLARENCE WILLSON FEE 1(24-28)	EMERY	16S-10E
43-015-20214	24	UNION OIL CO OF CALIFORNIA	TEMPLE WASH STATE 1	EMERY	24S-13E
43-015-20215	54	UNION OIL CO OF CALIFORNIA	TEMPLE WASH GOVT 019-1	EMERY	25S-12E
43-015-20224	26	UNION OIL CO OF CALIFORNIA	TEMPLE WASH GOVT 998-A-1	EMERY	25S-13E
43-015-20312	255	UTAH OIL REFINING CO	1	EMERY	19S-13E
43-015-20330	210	LEONARD PETROLEUM CO	1	EMERY	21S-9E
43-015-20342	477	EQUITY OIL COMPANY	FEDERAL 1	EMERY	22S-15E
43-015-20350	212	DELHI-TAYLOR OIL CORP	RUSSELL 1	EMERY	25S-12E
43-015-20352	62	MOUNTAIN FUEL SUPPLY CO	S LAST CHANCE 1-A	EMERY	26S-7E
43-015-20367	119	MARALO LLC	LAST CHANCE UNIT 1	EMERY	26S-7E
43-015-30001	1163	CALIFORNIA-TIME PET CO	BARRIER BANK 1	EMERY	19S-14E
43-015-30003	437	TOLEDO MINING CO	TOLEDO FEDERAL 1	EMERY	20S-14E
43-015-30004	525	GLOBE MINERALS INC	COON SPRINGS 1	EMERY	16S-12E
43-015-30005	24	MODERN MINERALS CORP	SKYLINE STATE 1	EMERY	19S-12E
43-015-30006	15	MODERN MINERALS CORP	SKYLINE FEDERAL 1	EMERY	18S-12E
43-015-30007	27	REYNOLDS & CARVER	FEDERAL 1	EMERY	25S-14E

43-015-30008	500	TEXAS EASTERN SKYLINE OIL	SKYLINE FED WOODSIDE 8-1	EMERY	19S-14E
43-015-30009	27	FLYING DIAMOND OIL CORP	IRON WASH FED 1	EMERY	24S-13E
43-015-30014	2333	CHEVRON USA INC	NORRIS FED 1	EMERY	18S-16E
43-015-30016	62	ENERGETICS OPERATING CO	RESERVE FED 23X-7	EMERY	26S-7E
43-015-30017	148	TEXAS GAS EXPLORATION CORP	FEDERAL 11-24-13 (WSW)	EMERY	24S-13E
43-015-30027	0	TRUE OIL COMPANY	TRUE FEDERAL 44-30	EMERY	17S-13E
43-015-30028	649	TRUE OIL COMPANY	TRUE FEDERAL 11-35	EMERY	20S-8E
43-015-30029	366	TRUE OIL COMPANY	TRUE FEDERAL 14-10	EMERY	22S-8E
43-015-30032	489	TRUE OIL COMPANY	TRUE FEDERAL 22-11	EMERY	19S-11E
43-015-30033	52	TRUE OIL COMPANY	TRUE FEDERAL 34-7	EMERY	20S-10E
43-015-30036	61	WALDEN ENERGY VENTURES LLC	ENERGETICS FED 21-20	EMERY	26S-7E
43-015-30039	884	HAMON OPERATING COMPANY	USA FED 8-1	EMERY	19S-9E
43-015-30046	1631	NORTHSTARGAS LC	FERRON CREEK 2	EMERY	20S-7E
43-015-30047	186	BUSH WILLIAM G	BUSH 1	EMERY	19S-10E
43-015-30059	2103	TIGER OIL CO	JACK CURTIS 41-15	EMERY	18S-7E
43-015-30066	69	COLUMBIA GAS DEVELOP CORP	PARADOX 1-23	EMERY	24S-13E
43-015-30070	1519	NORTHSTARGAS LC	J LEMON 1	EMERY	20S-7E
43-015-30078	174	MEGADON ENTERPRISES INC	FEDERAL 2-20	EMERY	26S-17E
43-015-30079	515	MEGADON ENTERPRISES INC	GEYSER DOME 1-14	EMERY	22S-15E
43-015-30092	2212	TEXAS INTERNATIONAL PETRO	FEDERAL 41-33	EMERY	18S-7E
43-015-30097	556	GENESIS PETROLEUM US INC	FEDERAL 11-33	EMERY	16S-12E
43-015-30100	635	GENESIS PETROLEUM US INC	STATE 2-43X	EMERY	16S-12E
43-015-30111	620	GENESIS PETROLEUM US INC	STATE 2-23	EMERY	16S-12E
43-015-30118	601	GENESIS PETROLEUM US INC	FEDERAL 11-41	EMERY	16S-12E
43-015-30120	568	GENESIS PETROLEUM US INC	FEDERAL 11-13	EMERY	16S-12E
43-015-30121	700	GENESIS PETROLEUM US INC	FEDERAL 4-32	EMERY	16S-12E
43-015-30122	78	AMOCO PRODUCTION COMPANY	LUCKY FLATS 1	EMERY	17S-12E
43-015-30123	570	TEXAS EASTERN SKYLINE OIL	FEDERAL 10-33	EMERY	16S-12E
43-015-30125	587	TEXAS EASTERN SKYLINE OIL	FEDERAL 10-13	EMERY	16S-12E
43-015-30126	722	TEXAS EASTERN SKYLINE OIL	FEDERAL 5-32	EMERY	16S-12E
43-015-30128	553	SAMEDAN OIL CORPORATION	FEDERAL 14-31	EMERY	16S-12E
43-015-30138	557	GENESIS PETROLEUM US INC	FEDERAL 14-11	EMERY	16S-12E
43-015-30142	554	GENESIS PETROLEUM US INC	FEDERAL 12-13	EMERY	16S-12E
43-015-30149	596	GENESIS PETROLEUM US INC	FEDERAL 11-11	EMERY	16S-12E
43-015-30151	496	TEXAS EASTERN	DUSTY TRAIL 1	EMERY	16S-13E

		SKYLINE OIL			
43-015-30156	136	AMOCO PRODUCTION COMPANY	DESERT LAKE U 1	EMERY	17S-12E
43-015-30159	61	UNION TEXAS PETROLEUM	LITTLE FLAT TOP UNIT 1-25	EMERY	25S-14E
43-015-30162	110	UNION TEXAS PETROLEUM	WILDCAT BUTTE UNIT 1-2	EMERY	26S-13E
43-015-30167	566	GENESIS PETROLEUM US INC	FEDERAL 11-42	EMERY	16S-12E
43-015-30170	569	GENESIS PETROLEUM US INC	FEDERAL 11-23	EMERY	16S-12E
43-015-30172	544	GENESIS PETROLEUM US INC	FEDERAL 11-43	EMERY	16S-12E
43-015-30174	351	AMOCO PRODUCTION COMPANY	DESERT LAKE U 5	EMERY	17S-11E
43-015-30178	607	PRIDE VENTURES LLC	BOLINDER FED 3-12	EMERY	16S-12E
43-015-30180	616	GENESIS PETROLEUM US INC	FEDERAL 1-14	EMERY	16S-12E
43-015-30184	604	PRIDE VENTURES LLC	FEDERAL 12-32	EMERY	16S-12E
43-015-30192	1498	CHANDLER & ASSOCIATES INC	LAWRENCE 15-1	EMERY	18S-8E
43-015-30195	312	SAMEDAN OIL CORPORATION	HATT RANCH 27-33	EMERY	22S-14E
43-015-30202	507	ARCO OIL & GAS COMPANY	JEEP TRAIL U 1	EMERY	18S-10E
43-015-30221	1847	COASTAL PLAINS ENERGY INC	ORANGEVILLE U 4-1	EMERY	19S-7E
43-015-30232	212	CELSIUS ENERGY COMPANY	CELSIUS FED 8-1	EMERY	21S-9E
43-015-30237	186	BUSH WILLIAM G	BUSH 1-A	EMERY	19S-10E
43-015-30240	113	WILDROSE RESOURCES CORP	NEQUOIA STATE 16-1	EMERY	26S-14E
43-015-30251	860	ANDOVER PARTNERS	FEDERAL 1-17	EMERY	21S-8E
43-015-30272	1953	XTO ENERGY INC	SWD 1	EMERY	18S-7E
43-015-30323	2080	XTO ENERGY INC	SWD 2	EMERY	18S-7E
43-015-30338	1736	CONOCOPHILLIPS COMPANY	UTAH D7	EMERY	16S-9E
43-015-30356	1543	CONOCOPHILLIPS COMPANY	D-11	EMERY	16S-9E
43-015-30477	2317	ANADARKO PETROLEUM CORP	CLAWSON SPRING ST SWD 4	EMERY	16S-8E
43-015-30510	1826	XTO ENERGY INC	SWD 5	EMERY	17S-8E
43-015-30531	2069	CONOCOPHILLIPS COMPANY	PPCO D13	EMERY	16S-9E
43-015-30701	306	TWIN BRIDGES LLC	WOODSIDE 1	EMERY	19S-13E
43-015-30709	1128	SWEPI LP	CARBON CANAL 5-12	EMERY	16S-10E
43-019-10030	456	KERN COUNTY LAND CO	AMERADA GREEN RIVER U 1	GRAND	22S-16E
43-019-10116	698	POTASH COMPANY OF AMERICA	WRIGHT FED 1	GRAND	22S-19E
43-019-10122	101	BROADHEAD WALTER	KING FEDERAL 1 (WSW)	GRAND	24S-18E
43-019-10155	0	CALVERT EXPLORATION CO	BIG FLAT UNIT 7	GRAND	26S-20E
43-019-10231	973	CONTINENTAL OIL COMPANY	CISCO UNIT 1	GRAND	20S-21E
43-019-10233	728	CONTINENTAL OIL COMPANY	SALT VALLEY-FED 1	GRAND	22S-19E
43-019-10361	662	EQUITY OIL COMPANY	STRAT ST 1	GRAND	23S-19E

43-019-10666	549	LOCKHART L M	SARGEANT-GOVT 1	GRAND	21S-23E
43-019-10716	664	MENOR J E & AUBREY GEO	GOVERNMENT 1	GRAND	22S-19E
43-019-10817	148	PACIFIC WESTERN OIL CORP	SHARP STATE 1	GRAND	22S-17E
43-019-10831	141	PAN AMERICAN PETROLEUM COR	SALT WASH UNIT 1	GRAND	23S-17E
43-019-10989	165	S W ENERGY CORPORATION	FEDERAL ROSENBLATT 1	GRAND	23S-17E
43-019-11035	207	SHELL OIL COMPANY	LEGGETT 1	GRAND	24S-20E
43-019-11478	1103	GREAT WESTERN DRILLING CO	ROBERT S BRENNARD JR FED 1	GRAND	18S-24E
43-019-11485	678	PACIFIC WESTERN OIL CORP	THOMPSON 1	GRAND	21S-21E
43-019-11498	558	POTASH COMPANY OF AMERICA	POTASH CO OF AMERICA 2	GRAND	21S-19E
43-019-11500	712	EQUITY OIL COMPANY	DONOHUE 1	GRAND	23S-19E
43-019-11503	491	GRAND PYRAMID OIL INC	GRAND PYRAMID OIL INC 1	GRAND	22S-19E
43-019-11557	775	WHISNANT W P	W P WHISNANT ET AL 1	GRAND	23S-18E
43-019-15027	1168	LONE MTN PRODUCTION CO	CRITTENDEN 1	GRAND	17S-25E
43-019-15819	230	SMOOT RICHARD P	CF&I 22-16	GRAND	23S-17E
43-019-16532	1561	AUGUSTUS ENERGY PARTNERS LLC	SAN ARROYO 1	GRAND	16S-25E
43-019-20146	271	UNION OIL CO OF CALIFORNIA	DEVILS GARDEN USA 1	GRAND	23S-21E
43-019-30008	347	GILILLAND DAYMON D	LANSDALE GOVT 13	GRAND	19S-25E
43-019-30048	959	TEXACO INC	GOVERNMENT T-1	GRAND	21S-20E
43-019-30055	183	QUINTANA PETROLEUM CORP	YELLOW CAT USA 1-9	GRAND	23S-22E
43-019-30062	278	UNION OIL CO OF CALIFORNIA	STATE 1-P-2	GRAND	23S-21E
43-019-30070	1318	TEXACO INC	GOVERNMENT Y NCT-1	GRAND	21S-20E
43-019-30074	371	FERGUSON OIL CO	U-TEX ET AL 1-14	GRAND	22S-16E
43-019-30077	1613	J C THOMPSON OPERATOR LLC	WESTWATER U E5	GRAND	17S-24E
43-019-30110	719	CONOCO INC	CRESCENT UNIT 1	GRAND	22S-20E
43-019-30119	415	GOAL RESOURCES INC	GOAL STATE 5	GRAND	21S-24E
43-019-30124	250	MOUNTAIN FUEL SUPPLY CO	MT FUEL-SKYLINE GEYSER 1-25	GRAND	22S-16E
43-019-30207	1554	S W ENERGY CORPORATION	BLAZE A-1	GRAND	21S-18E
43-019-30215	1416	PHILLIPS PETROLEUM CO	BLAZE "C" 1	GRAND	21S-19E
43-019-30244	1536	PHILLIPS PETROLEUM CO	BLAZE "A" 3	GRAND	21S-18E
43-019-30251	237	HILLIARD OIL & GAS INC	KLONDIKE U 1	GRAND	23S-18E
43-019-30272	27	MOUNTAIN FUEL SUPPLY CO	KLONDIKE UNIT 2	GRAND	24S-19E
43-019-30312	1363	HAMILTON BROTHERS OIL CO	SALT VALLEY NW U 1	GRAND	21S-18E
43-019-30326	239	WEXPRO COMPANY	KLONDIKE UNIT 3	GRAND	23S-19E
43-019-30327	58	PEASE OIL & GAS COMPANY	FEDERAL SKYLINE 1A SW	GRAND	23S-17E
43-019-30414	580	LANSDALE A	FEDERAL 2-18	GRAND	18S-26E
43-019-30418	171	ARI-MEX OIL & EXPLOR	SKIP FEDERAL 1-7	GRAND	25S-21E

43-019-30455	524	TIGER OIL CO	STATE 12-11	GRAND	24S-20E
43-019-30681	305	MEGADON ENTERPRISES INC	STATE 1-16	GRAND	23S-17E
43-019-30732	280	TENNECO OIL COMPANY	TENNECO USA 11-1	GRAND	19S-22E
43-019-30752	142	MEGADON ENTERPRISES INC	FEDERAL 1-15	GRAND	23S-17E
43-019-30783	293	S W ENERGY CORPORATION	STATE 1-16A	GRAND	23S-17E
43-019-30918	967	MOBIL OIL CORPORATION	AMERICAN PETROFINA 1-30	GRAND	21S-22E
43-019-31063	1622	BWAB INCORPORATED	FEDERAL 12-42	GRAND	21S-18E
43-019-31394	1016	NAE LLC	STATE 1-32	GRAND	21S-19E
43-019-31401	1317	NAE LLC	STATE MSC 16-1	GRAND	21S-20E
43-019-31404	1131	NAE LLC	STATE MSC 35-1	GRAND	21S-19E
43-019-31462	371	DELTA PETROLEUM CORP	GREENTOWN ST 36-11	GRAND	21S-16E
43-019-31463	693	DELTA PETROLEUM CORP	SALT VLY ST 25-12	GRAND	22S-19E
43-019-31469	1158	SAMSON RESOURCES COMPANY	TIDEWATER ST 32-3	GRAND	21S-19E
43-019-31496	736	ENCANA OIL & GAS (USA) INC	LITTLE GRAND 35-2	GRAND	22S-18E
43-019-31502	433	SAMSON RESOURCES COMPANY	POWER LINE 12-1	GRAND	23S-18E
43-019-31503	179	PACIFIC ENERGY & MINING CO	FEDERAL 28-11	GRAND	22S-17E
43-019-31505	368	DELTA PETROLEUM CORP	GREENTOWN ST 36-11S	GRAND	21S-16E
43-019-31507	331	DELTA PETROLEUM CORP	GREENTOWN FED 35-12	GRAND	21S-16E
43-019-31511	1155	TIDEWATER OIL & GAS COMPANY LLC	CACTUS ROSE FED 29-44-2119	GRAND	21S-19E
43-019-31519	333	DELTA PETROLEUM CORP	GREENTOWN ST 36-24H	GRAND	21S-16E
43-019-31533	454	RUNNING FOXES PETROLEUM INC.	CISCO 30-15-4	GRAND	20S-24E
43-019-31535	320	NAE LLC	CACTUS ROSE 36-43-2217	GRAND	22S-17E
43-019-31547	413	PACIFIC ENERGY & MINING CO	GREENTOWN FED 26-43H	GRAND	21S-16E
43-019-31551	331	DELTA PETROLEUM CORP	GREENTOWN FED 35-12D	GRAND	21S-16E
43-019-31569	275	DELTA PETROLEUM CORP	GREENTOWN ST 31-362216H	GRAND	22S-16E
43-019-31575	462	PACIFIC ENERGY & MINING CO	FEDERAL 11-24	GRAND	22S-16E
43-019-31595	980	NAE LLC	SVA 23-33-2119	GRAND	21S-19E
43-019-50002	1006	FIDELITY E&P COMPANY	GUNNISON VLY FEE 22-9	GRAND	21S-17E
43-037-20173	0	ROSEN OIL CO	GRAYS PASTURE 1	SAN JUAN	27S-19E
43-037-30031	0	LARUE E B JR	EB LA RUE PETROGLYPH 1	SAN JUAN	27S-21E
43-037-30650	0	MEGADON ENTERPRISES INC	LION MESA 5-28	SAN JUAN	27S-21E
43-047-10577	3576	WHITING OIL & GAS CORPORATION	UTE TRIBAL 32-5A	UINTAH	14S-20E
43-047-20508	2345	PHILLIPS PETROLEUM CO	TWO WATERS UNIT 1	UINTAH	14S-25E
43-047-39428	2893	FOUNDATION ENERGY MANAGEMENT LLC	MAIN CYN FED 12-8-15-23	UINTAH	15S-23E
43-047-39463	3744	QEP ENERGY COMPANY	FR 9P-17-14-20	UINTAH	14S-20E

43-055-10025	0	AMAX PETROLEUM CORP	MORONI SLOPES-GOVT 1	WAYNE	27S-8E
43-055-10035	182	AMERADA	NEQUOIA ARCH U 5	WAYNE	27S-14E
43-055-11209	56	SUPERIOR OIL COMPANY	HANKSVILLE UNIT 31-30	WAYNE	27S-13E
43-055-30025	182	COLUMBIA GAS DEVELOP CORP	PARADOX 1-9	WAYNE	27S-12E
43-055-30027	134	TIGER OIL CO	FEDERAL 11-4	WAYNE	27S-7E
43-055-30032	405	CHEVRON USA INC	HANKSVILLE UNIT 1	WAYNE	27S-11E

Carmel Formation Well Information

API WELL #	TOP DEPTH	OPERATOR	WELL NAME	COUNTY	LOCATION
43-007-10791	1741	PACIFIC TRANS SUPPLY	NORTH SPRINGS 1	CARBON	15S-9E
43-007-10820	1065	PAN AMERICAN PETROLEUM COR	USA-LILLIE C CULLEN 1	CARBON	15S-13E
43-007-11029	1008	SHELL OIL COMPANY	MILLER CREEK 1	CARBON	15S-10E
43-007-15115	520	AMERIGAS INC	FARNHAM DOME 3	CARBON	15S-11E
43-007-15116	493	CARBON DIOXIDE AND CHEM CO	FARNHAM DOME 4	CARBON	15S-11E
43-007-15394	756	EQUITY OIL COMPANY	GOVT MOUNDS 3	CARBON	15S-12E
43-007-15395	751	EQUITY OIL COMPANY	FARNHAM DOME 1-A	CARBON	15S-12E
43-007-16107	2379	SKELLY OIL CO	GORDON CREEK UNIT 1	CARBON	14S-7E
43-007-20071	3228	ARCO OIL & GAS COMPANY	HIAWATHA U 1	CARBON	15S-7E
43-007-30012	997	MOUNTAIN FUEL SUPPLY CO	SUNNYSIDE UNIT 1	CARBON	15S-13E
43-007-30040	1528	CONOCOPHILLIPS COMPANY	DRUNKARDS WASH 31-1 (D-1)	CARBON	14S-10E
43-007-30044	2332	GORDON CREEK LLC	GORDON CREEK U 1	CARBON	14S-8E
43-007-30093	1968	CONOCOPHILLIPS COMPANY	ARCADIA-TELONIS 1 (D2)	CARBON	14S-9E
43-007-30100	1954	CONOCOPHILLIPS COMPANY	UTAH D-6	CARBON	14S-9E
43-007-30103	682	GENESIS PETROLEUM US INC	STATE 36-2	CARBON	15S-12E
43-007-30314	1632	CONOCOPHILLIPS COMPANY	UTAH D4	CARBON	14S-9E
43-007-30431	1632	CONOCOPHILLIPS COMPANY	UTAH D8	CARBON	15S-9E
43-007-30438	2012	CONOCOPHILLIPS COMPANY	UTAH D-9	CARBON	14S-9E
43-007-30555	1648	ANADARKO PETROLEUM CORP	FED F-2 SWD	CARBON	14S-10E
43-007-30567	1214	CONOCOPHILLIPS COMPANY	SAMPINOS D14	CARBON	15S-10E
43-007-30656	1677	MARATHON OIL COMPANY	SITLA SWD 1	CARBON	15S-9E
43-007-30818	764	SAVOY ENERGY LLC	EDP 1	CARBON	15S-12E
43-007-30912	1534	KERR-MCGEE OIL & GAS ONSHORE L.P.	WELLINGTON FED 44-6 SWD	CARBON	14S-11E
43-007-30967	1516	KERR-MCGEE OIL & GAS ONSHORE L.P.	WELLINGTON FED 22-04 SWD	CARBON	14S-11E

43-007-31262	610	SAVOY ENERGY LLC	SAVOY 2	CARBON	15S-12E
43-007-31263	610	SAVOY ENERGY LLC	SAVOY 1	CARBON	15S-12E
43-015-10019	420	AMAX PETROLEUM CORP	AMAX-SINCLAIR GOVT 29-4B	EMERY	22S-15E
43-015-10021	571	AMAX PETROLEUM CORP	GREEN RIVER DESERT U 9-7	EMERY	22S-15E
43-015-10022	284	AMAX PETROLEUM CORP	GREEN RIVER DESERT U 24-1	EMERY	22S-13E
43-015-10182	0	STANDARD OIL CO OF CALIF	LOOKOUT POINT UNIT 1	EMERY	25S-16E
43-015-10183	26	STANDARD OIL CO OF CALIF	MOONSHINE WASH U 1	EMERY	25S-15E
43-015-10229	56	CONTINENTAL OIL COMPANY	MOONSHINE WASH U 2	EMERY	25S-15E
43-015-10358	618	EQUITY OIL COMPANY	MOUNDS 2	EMERY	16S-12E
43-015-10359	580	EQUITY OIL COMPANY	MOUNDS FED 4	EMERY	16S-12E
43-015-10360	466	EQUITY OIL COMPANY	STATE 1	EMERY	16S-12E
43-015-10374	1921	FOREST OIL CORP	FOREST GOVT 25-1 ARNOLD	EMERY	16S-14E
43-015-10460	0	HANCOCK-UTAH DEVELOPMENT	CEDAR MOUNTAIN U 1	EMERY	19S-12E
43-015-10500	439	HUMBLE OIL & REFINING CO	GOVT-WHEATLEY 1	EMERY	16S-12E
43-015-10504	738	HUMBLE OIL & REFINING CO	SPHINX UNIT 1A	EMERY	19S-14E
43-015-10658	453	LEMM & MAIATICO	WOODSIDE FED 1	EMERY	18S-14E
43-015-10800	1268	PACIFIC NATURAL GAS EXPLOR	RANGE CREEK UNIT 1-27	EMERY	17S-16E
43-015-10825	671	PAN AMERICAN PETROLEUM COR	FEDERAL MOUNDS 1	EMERY	16S-11E
43-015-10826	91	PAN AMERICAN PETROLEUM COR	NEQUOIA ARCH UNIT 9	EMERY	26S-13E
43-015-10827	173	PAN AMERICAN PETROLEUM COR	NEQUOIA ARCH UNIT 10	EMERY	26S-13E
43-015-10900	1692	PHILLIPS PETROLEUM CO	GOVERNMENT 1	EMERY	17S-8E
43-015-10928	668	PLACID OIL COMPANY	MARSH FLAT UNIT 1	EMERY	17S-14E
43-015-10961	377	READ R H JR	SUCKLE GOVERNMENT 1	EMERY	17S-12E
43-015-10963	453	RESERVE OIL & GAS	CEDAR SIDING UNIT 1	EMERY	16S-13E
43-015-10969	0	REYNOLDS MINING CORP	CEDAR MOUNTAIN UNIT 1	EMERY	19S-12E
43-015-11138	326	TEXAS EASTERN SKYLINE OIL	GREEN RIVER UNIT 1	EMERY	21S-16E
43-015-11182	586	SUPERIOR OIL COMPANY	GRAND FAULT UNIT 14-24	EMERY	21S-15E
43-015-11328	779	UNION OIL CO OF CALIFORNIA	DESERT LAKE UNIT 1	EMERY	17S-10E
43-015-11329	1545	UNION OIL CO OF CALIFORNIA	WASHBOARD WASH USA 1	EMERY	16S-9E
43-015-11398	37	UTAH PLATEAU URANIUM CO	FEDERAL 1	EMERY	22S-8E
43-015-11399	37	UTAH PLATEAU URANIUM CO	FEDERAL 1-X (WSW)	EMERY	22S-8E
43-015-15104	0	ORPHAN-NO RESPONSIBLE OPERATOR	ENGLISH 1-X	EMERY	26S-7E
43-015-15603	522	PRIDE VENTURES LLC	BOLINDER C-1	EMERY	16S-12E
43-015-15604	604	GENESIS PETROLEUM US INC	FEDERAL 1	EMERY	16S-12E
43-015-15607	631	PRIDE VENTURES LLC	FEDERAL 2	EMERY	16S-12E

43-015-15676	1181	NORTHSTARGAS LC	PAN AM 3	EMERY	20S-7E
43-015-15677	1269	PAN AMERICAN PETROLEUM COR	FERRON UNIT FEE 4 (14-2)	EMERY	20S-7E
43-015-20145	1229	TENNECO OIL COMPANY	FERRON UNIT 5	EMERY	20S-7E
43-015-20190	1034	CHEVRON USA INC	CLARENCE WILLSON FEE 1(24-28)	EMERY	16S-10E
43-015-20312	207	UTAH OIL REFINING CO	1	EMERY	19S-13E
43-015-20330	0	LEONARD PETROLEUM CO	1	EMERY	21S-9E
43-015-20342	422	EQUITY OIL COMPANY	FEDERAL 1	EMERY	22S-15E
43-015-20350	91	DELHI-TAYLOR OIL CORP	RUSSELL 1	EMERY	25S-12E
43-015-20352	0	MOUNTAIN FUEL SUPPLY CO	S LAST CHANCE 1-A	EMERY	26S-7E
43-015-20367	0	MARALO LLC	LAST CHANCE UNIT 1	EMERY	26S-7E
43-015-30001	1067	CALIFORNIA-TIME PET CO	BARRIER BANK 1	EMERY	19S-14E
43-015-30003	360	TOLEDO MINING CO	TOLEDO FEDERAL 1	EMERY	20S-14E
43-015-30004	435	GLOBE MINERALS INC	COON SPRINGS 1	EMERY	16S-12E
43-015-30005	0	MODERN MINERALS CORP	SKYLINE STATE 1	EMERY	19S-12E
43-015-30006	0	MODERN MINERALS CORP	SKYLINE FEDERAL 1	EMERY	18S-12E
43-015-30007	0	REYNOLDS & CARVER	FEDERAL 1	EMERY	25S-14E
43-015-30015	0	ENERGETICS OPERATING CO	FEDERAL 41X11	EMERY	26S-6E
43-015-30016	0	ENERGETICS OPERATING CO	RESERVE FED 23X-7	EMERY	26S-7E
43-015-30017	67	TEXAS GAS EXPLORATION CORP	FEDERAL 11-24-13 (WSW)	EMERY	24S-13E
43-015-30021	1838	ENERGY RESERVES GROUP	USA THOMAS WALSH FED 1	EMERY	19S-15E
43-015-30028	504	TRUE OIL COMPANY	TRUE FEDERAL 11-35	EMERY	20S-8E
43-015-30029	210	TRUE OIL COMPANY	TRUE FEDERAL 14-10	EMERY	22S-8E
43-015-30032	401	TRUE OIL COMPANY	TRUE FEDERAL 22-11	EMERY	19S-11E
43-015-30036	0	WALDEN ENERGY VENTURES LLC	ENERGETICS FED 21-20	EMERY	26S-7E
43-015-30039	692	HAMON OPERATING COMPANY	USA FED 8-1	EMERY	19S-9E
43-015-30046	1460	NORTHSTARGAS LC	FERRON CREEK 2	EMERY	20S-7E
43-015-30047	0	BUSH WILLIAM G	BUSH 1	EMERY	19S-10E
43-015-30059	1835	TIGER OIL CO	JACK CURTIS 41-15	EMERY	18S-7E
43-015-30070	1256	NORTHSTARGAS LC	J LEMON 1	EMERY	20S-7E
43-015-30079	457	MEGADON ENTERPRISES INC	GEYSER DOME 1-14	EMERY	22S-15E
43-015-30092	1943	TEXAS INTERNATIONAL PETRO	FEDERAL 41-33	EMERY	18S-7E
43-015-30100	550	GENESIS PETROLEUM US INC	STATE 2-43X	EMERY	16S-12E
43-015-30111	535	GENESIS PETROLEUM US INC	STATE 2-23	EMERY	16S-12E
43-015-30120	483	GENESIS PETROLEUM US INC	FEDERAL 11-13	EMERY	16S-12E
43-015-30121	614	GENESIS PETROLEUM US INC	FEDERAL 4-32	EMERY	16S-12E

43-015-30126	638	TEXAS EASTERN SKYLINE OIL	FEDERAL 5-32	EMERY	16S-12E
43-015-30142	478	GENESIS PETROLEUM US INC	FEDERAL 12-13	EMERY	16S-12E
43-015-30149	511	GENESIS PETROLEUM US INC	FEDERAL 11-11	EMERY	16S-12E
43-015-30151	418	TEXAS EASTERN SKYLINE OIL	DUSTY TRAIL 1	EMERY	16S-13E
43-015-30174	236	AMOCO PRODUCTION COMPANY	DESERT LAKE U 5	EMERY	17S-11E
43-015-30178	530	PRIDE VENTURES LLC	BOLINDER FED 3-12	EMERY	16S-12E
43-015-30181	404	T-REX CORP	T-REX FEDERAL 1-27	EMERY	18S-11E
43-015-30192	1248	CHANDLER & ASSOCIATES INC	LAWRENCE 15-1	EMERY	18S-8E
43-015-30202	382	ARCO OIL & GAS COMPANY	JEEP TRAIL U 1	EMERY	18S-10E
43-015-30221	1612	COASTAL PLAINS ENERGY INC	ORANGEVILLE U 4-1	EMERY	19S-7E
43-015-30232	0	CELSIUS ENERGY COMPANY	CELSIUS FED 8-1	EMERY	21S-9E
43-015-30237	55	BUSH WILLIAM G	BUSH 1-A	EMERY	19S-10E
43-015-30241	897	WINDSOR ENERGY US CORP	CLAWSON ET AL 1	EMERY	19S-8E
43-015-30251	590	ANDOVER PARTNERS	FEDERAL 1-17	EMERY	21S-8E
43-015-30272	1705	XTO ENERGY INC	SWD 1	EMERY	18S-7E
43-015-30323	1823	XTO ENERGY INC	SWD 2	EMERY	18S-7E
43-015-30338	1523	CONOCOPHILLIPS COMPANY	UTAH D7	EMERY	16S-9E
43-015-30356	1369	CONOCOPHILLIPS COMPANY	D-11	EMERY	16S-9E
43-015-30531	1857	CONOCOPHILLIPS COMPANY	PPCO D13	EMERY	16S-9E
43-019-10116	688	POTASH COMPANY OF AMERICA	WRIGHT FED 1	GRAND	22S-19E
43-019-10122	61	BROADHEAD WALTER	KING FEDERAL 1 (WSW)	GRAND	24S-18E
43-019-10231	967	CONTINENTAL OIL COMPANY	CISCO UNIT 1	GRAND	20S-21E
43-019-10233	681	CONTINENTAL OIL COMPANY	SALT VALLEY-FED 1	GRAND	22S-19E
43-019-10361	526	EQUITY OIL COMPANY	STRAT ST 1	GRAND	23S-19E
43-019-10716	622	MENOR J E & AUBREY GEO	GOVERNMENT 1	GRAND	22S-19E
43-019-10817	110	PACIFIC WESTERN OIL CORP	SHARP STATE 1	GRAND	22S-17E
43-019-10989	134	S W ENERGY CORPORATION	FEDERAL ROSENBLATT 1	GRAND	23S-17E
43-019-11485	671	PACIFIC WESTERN OIL CORP	THOMPSON 1	GRAND	21S-21E
43-019-11498	554	POTASH COMPANY OF AMERICA	POTASH CO OF AMERICA 2	GRAND	21S-19E
43-019-11500	591	EQUITY OIL COMPANY	DONOHUE 1	GRAND	23S-19E
43-019-11557	767	WHISNANT W P	W P WHISNANT ET AL 1	GRAND	23S-18E
43-019-15819	182	SMOOT RICHARD P	CF&I 22-16	GRAND	23S-17E
43-019-16532	1547	AUGUSTUS ENERGY PARTNERS LLC	SAN ARROYO 1	GRAND	16S-25E
43-019-20146	242	UNION OIL CO OF CALIFORNIA	DEVILS GARDEN USA 1	GRAND	23S-21E
43-019-30008	338	GILILLAND DAYMON D	LANSDALE GOVT 13	GRAND	19S-25E

43-019-30048	928	TEXACO INC	GOVERNMENT T-1	GRAND	21S-20E
43-019-30055	159	QUINTANA PETROLEUM CORP	YELLOW CAT USA 1-9	GRAND	23S-22E
43-019-30074	335	FERGUSON OIL CO	U-TEX ET AL 1-14	GRAND	22S-16E
43-019-30077	1578	J C THOMPSON OPERATOR LLC	WESTWATER U E5	GRAND	17S-24E
43-019-30124	203	MOUNTAIN FUEL SUPPLY CO	MT FUEL-SKYLINE GEYSER 1-25	GRAND	22S-16E
43-019-30207	1516	S W ENERGY CORPORATION	BLAZE A-1	GRAND	21S-18E
43-019-30215	1373	PHILLIPS PETROLEUM CO	BLAZE "C" 1	GRAND	21S-19E
43-019-30244	1500	PHILLIPS PETROLEUM CO	BLAZE "A" 3	GRAND	21S-18E
43-019-30251	204	HILLIARD OIL & GAS INC	KLONDIKE U 1	GRAND	23S-18E
43-019-30326	199	WEXPRO COMPANY	KLONDIKE UNIT 3	GRAND	23S-19E
43-019-30327	21	PEASE OIL & GAS COMPANY	FEDERAL SKYLINE 1A SW	GRAND	23S-17E
43-019-30328	821	TXO PRODUCTION CORP	KLOTZ FEDERAL 1	GRAND	21S-22E
43-019-30415	752	LANSDALE A	FEDERAL 3-31	GRAND	17S-26E
43-019-30418	122	ARI-MEX OIL & EXPLOR INC	SKIP FEDERAL 1-7	GRAND	25S-21E
43-019-30681	191	MEGADON ENTERPRISES INC	STATE 1-16	GRAND	23S-17E
43-019-30752	94	MEGADON ENTERPRISES INC	FEDERAL 1-15	GRAND	23S-17E
43-019-30918	947	MOBIL OIL CORPORATION	AMERICAN PETROFINA 1-30	GRAND	21S-22E
43-019-31063	1583	BWAB INCORPORATED	FEDERAL 12-42	GRAND	21S-18E
43-019-31394	991	NAE LLC	STATE 1-32	GRAND	21S-19E
43-019-31401	1280	NAE LLC	STATE MSC 16-1	GRAND	21S-20E
43-019-31404	1091	NAE LLC	STATE MSC 35-1	GRAND	21S-19E
43-019-31463	663	DELTA PETROLEUM CORP	SALT VLY ST 25-12	GRAND	22S-19E
43-019-31469	1076	SAMSON RESOURCES COMPANY	TIDEWATER ST 32-3	GRAND	21S-19E
43-019-31505	321	DELTA PETROLEUM CORP	GREENTOWN ST 36-11S	GRAND	21S-16E
43-019-31507	288	DELTA PETROLEUM CORP	GREENTOWN FED 35-12	GRAND	21S-16E
43-019-31519	288	DELTA PETROLEUM CORP	GREENTOWN ST 36-24H	GRAND	21S-16E
43-019-31547	369	PACIFIC ENERGY & MINING CO	GREENTOWN FED 26-43H	GRAND	21S-16E
43-019-31569	250	DELTA PETROLEUM CORP	GREENTOWN ST 31-362216H	GRAND	22S-16E
43-019-31575	416	PACIFIC ENERGY & MINING CO	FEDERAL 11-24	GRAND	22S-16E
43-047-16197	2853	BEARTOOTH OIL & GAS CO	FENCE CYN U 1	UINTAH	15S-22E
43-047-30121	2881	CHORNEY OIL CO	SE FLANK UINTA 1-5	UINTAH	15S-23E
43-047-34102	3563	WHITING OIL & GAS CORPORATION	UTE TRIBAL 29-6A	UINTAH	14S-20E
43-047-34103	3564	WHITING OIL & GAS CORPORATION	UTE TRIBAL 29-7A	UINTAH	14S-20E
43-047-34742	3509	UINTAH INVESTORS LLC	N HILL CREEK 1-9-15-20	UINTAH	15S-20E
43-047-34830	3519	UINTAH INVESTORS LLC	N HILL CREEK 10-10-15-20	UINTAH	15S-20E
43-047-34922	3464	UINTAH INVESTORS LLC	N HILL CREEK 4-1-	UINTAH	15S-20E

			15-20		
43-047-34953	3509	UINTAH INVESTORS LLC	N HILL CREEK 14-11-15-20	UINTAH	15S-20E
43-047-35054	3403	UINTAH INVESTORS LLC	NHC 4-13-15-20	UINTAH	15S-20E
43-047-35140	3643	UINTAH INVESTORS LLC	N HILL CREEK 1-6-15-20	UINTAH	15S-20E
43-047-35283	3432	UINTAH INVESTORS LLC	N HILL CREEK 2-12-15-20	UINTAH	15S-20E
43-047-35390	3441	UINTAH INVESTORS LLC	NHC 9-11-15-20	UINTAH	15S-20E
43-047-35880	3479	QEP ENERGY COMPANY	FR 9P-36-14-19	UINTAH	14S-20E
43-047-36795	3620	WHITING OIL & GAS CORPORATION	FLAT ROCK 3-29-14-20	UINTAH	14S-20E
43-047-37376	3473	QEP ENERGY COMPANY	FR 3P-36-14-19	UINTAH	14S-19E
43-047-38349	3438	QEP ENERGY COMPANY	FR 11P-36-14-19	UINTAH	14S-19E
43-047-38506	3709	WHITING OIL & GAS CORPORATION	UTE TRIBAL 6-16-14-20	UINTAH	14S-20E
43-047-38992	3440	QEP ENERGY COMPANY	FR 7P-36-14-19	UINTAH	14S-20E
43-047-39052	3636	WHITING OIL & GAS CORPORATION	UTE TRIBAL 15-25-14-19	UINTAH	14S-20E
43-047-39168	3647	QEP ENERGY COMPANY	FR 14P-20-14-20	UINTAH	14S-20E
43-047-39428	2883	FOUNDATION ENERGY MANAGEMENT LLC	MAIN CYN FED 12-8-15-23	UINTAH	15S-23E
43-047-39665	3633	WHITING OIL & GAS CORPORATION	UTE TRIBAL 1-30-14-20	UINTAH	14S-20E
43-047-39739	3555	WHITING OIL & GAS CORPORATION	UTE TRIBAL 3-30-14-20	UINTAH	14S-20E
43-047-39740	3543	WHITING OIL & GAS CORPORATION	UTE TRIBAL 11-30-14-20	UINTAH	14S-20E
43-047-39811	3716	QEP ENERGY COMPANY	FR 4P-21-14-20	UINTAH	14S-20E
43-055-10035	147	AMERADA	NEQUOIA ARCH U 5	WAYNE	27S-14E
43-055-10590	134	HUMBLE OIL & REFINING CO	NEQUOIA ARCH U 1	WAYNE	27S-14E
43-055-30027	0	TIGER OIL CO	FEDERAL 11-4	WAYNE	27S-7E

Entrada Sandstone Well Information

API WELL #	TOP DEPTH	OPERATOR	WELL NAME	COUNTY	LOCATION
43-007-10355	597	EQUITY OIL COMPANY	FARNHAM DOME U 2	CARBON	15S-12E
43-007-10791	1518	PACIFIC TRANS SUPPLY	NORTH SPRINGS 1	CARBON	15S-9E
43-007-10819	611	PAN AMERICAN PETROLEUM COR	USA FARNHAM DOME 1	CARBON	15S-12E
43-007-11029	823	SHELL OIL COMPANY	MILLER CREEK 1	CARBON	15S-10E
43-007-15115	419	AMERIGAS INC	FARNHAM DOME 3	CARBON	15S-11E
43-007-15116	402	CARBON DIOXIDE AND CHEM CO	FARNHAM DOME 4	CARBON	15S-11E
43-007-15394	677	EQUITY OIL COMPANY	GOVT MOUNDS 3	CARBON	15S-12E
43-007-15395	619	EQUITY OIL COMPANY	FARNHAM DOME 1-A	CARBON	15S-12E
43-007-15922	2054	SKELLY OIL CO	GORDON CREEK UNIT 5	CARBON	14S-7E

43-007-16107	2051	SKELLY OIL CO	GORDON CREEK UNIT 1	CARBON	14S-7E
43-007-20071	2974	ARCO OIL & GAS COMPANY	HIAWATHA U 1	CARBON	15S-7E
43-007-30012	893	MOUNTAIN FUEL SUPPLY CO	SUNNYSIDE UNIT 1	CARBON	15S-13E
43-007-30022	1387	PEASE OIL & GAS COMPANY	PRICE STATE 2	CARBON	14S-10E
43-007-30040	1329	CONOCOPHILLIPS COMPANY	DRUNKARDS WASH 31-1 (D-1)	CARBON	14S-10E
43-007-30084	546	GENESIS PETROLEUM US INC	STATE 36-13	CARBON	15S-12E
43-007-30093	1712	CONOCOPHILLIPS COMPANY	ARCADIA-TELONIS 1 (D2)	CARBON	14S-9E
43-007-30100	1686	CONOCOPHILLIPS COMPANY	UTAH D-6	CARBON	14S-9E
43-007-30103	552	GENESIS PETROLEUM US INC	STATE 36-2	CARBON	15S-12E
43-007-30314	1433	CONOCOPHILLIPS COMPANY	UTAH D4	CARBON	14S-9E
43-007-30431	1431	CONOCOPHILLIPS COMPANY	UTAH D8	CARBON	15S-9E
43-007-30438	1651	CONOCOPHILLIPS COMPANY	UTAH D-9	CARBON	14S-9E
43-007-30567	1021	CONOCOPHILLIPS COMPANY	SAMPINOS D14	CARBON	15S-10E
43-007-30912	1342	KERR-MCGEE OIL & GAS ONSHORE L.P.	WELLINGTON FED 44-6 SWD	CARBON	14S-11E
43-015-10019	287	AMAX PETROLEUM CORP	AMAX-SINCLAIR GOVT 29-4B	EMERY	22S-15E
43-015-10021	468	AMAX PETROLEUM CORP	GREEN RIVER DESERT U 9-7	EMERY	22S-15E
43-015-10022	146	AMAX PETROLEUM CORP	GREEN RIVER DESERT U 24-1	EMERY	22S-13E
43-015-10183	0	STANDARD OIL CO OF CALIF	MOONSHINE WASH U 1	EMERY	25S-15E
43-015-10229	0	CONTINENTAL OIL COMPANY	MOONSHINE WASH U 2	EMERY	25S-15E
43-015-10357	363	EQUITY OIL COMPANY	BULL CANYON ST 1	EMERY	18S-10E
43-015-10358	508	EQUITY OIL COMPANY	MOUNDS 2	EMERY	16S-12E
43-015-10359	467	EQUITY OIL COMPANY	MOUNDS FED 4	EMERY	16S-12E
43-015-10360	357	EQUITY OIL COMPANY	STATE 1	EMERY	16S-12E
43-015-10374	1779	FOREST OIL CORP	FOREST GOVT 25-1 ARNOLD	EMERY	16S-14E
43-015-10500	346	HUMBLE OIL & REFINING CO	GOVT-WHEATLEY 1	EMERY	16S-12E
43-015-10504	667	HUMBLE OIL & REFINING CO	SPHINX UNIT 1A	EMERY	19S-14E
43-015-10603	0	ORPHAN-NO RESPONSIBLE OPERATOR	A K WILSON 1	EMERY	24S-13E
43-015-10658	398	LEMM & MAIATICO	WOODSIDE FED 1	EMERY	18S-14E
43-015-10698	494	MCADAMS J F	GRASSY TRAIL CREEK U 4	EMERY	16S-12E
43-015-10800	1746	PACIFIC NATURAL GAS EXPLOR	RANGE CREEK UNIT 1-27	EMERY	17S-16E
43-015-10803	983	PACIFIC NATURAL GAS EXPLOR	SORENSEN FEE 42-9	EMERY	21S-7E
43-015-10825	486	PAN AMERICAN PETROLEUM COR	FEDERAL MOUNDS 1	EMERY	16S-11E
43-015-10827	0	PAN AMERICAN PETROLEUM COR	NEQUOIA ARCH UNIT 10	EMERY	26S-13E
43-015-10900	1405	PHILLIPS PETROLEUM CO	GOVERNMENT 1	EMERY	17S-8E

43-015-10928	573	PLACID OIL COMPANY	MARSH FLAT UNIT 1	EMERY	17S-14E
43-015-10961	258	READ R H JR	SUCKLE GOVERNMENT 1	EMERY	17S-12E
43-015-10963	354	RESERVE OIL & GAS	CEDAR SIDING UNIT 1	EMERY	16S-13E
43-015-11030	113	SHELL OIL COMPANY	CHAFFIN UNIT 1	EMERY	23S-15E
43-015-11033	0	SHELL OIL COMPANY	GRUVERS MESA 2	EMERY	25S-16E
43-015-11182	469	SUPERIOR OIL COMPANY	GRAND FAULT UNIT 14-24	EMERY	21S-15E
43-015-11328	549	UNION OIL CO OF CALIFORNIA	DESERT LAKE UNIT 1	EMERY	17S-10E
43-015-11329	1244	UNION OIL CO OF CALIFORNIA	WASHBOARD WASH USA 1	EMERY	16S-9E
43-015-11398	0	UTAH PLATEAU URANIUM CO	FEDERAL 1	EMERY	22S-8E
43-015-11399	0	UTAH PLATEAU URANIUM CO	FEDERAL 1-X (WSW)	EMERY	22S-8E
43-015-15603	415	PRIDE VENTURES LLC	BOLINDER C-1	EMERY	16S-12E
43-015-15604	503	GENESIS PETROLEUM US INC	FEDERAL 1	EMERY	16S-12E
43-015-15605	471	MEGADON ENTERPRISES INC	GRASSY TRAILS 2	EMERY	16S-12E
43-015-15607	501	PRIDE VENTURES LLC	FEDERAL 2	EMERY	16S-12E
43-015-15663	853	COASTAL PLAINS ENERGY INC	BEHLING FEE 41-22	EMERY	20S-7E
43-015-15676	888	NORTHSTARGAS LC	PAN AM 3	EMERY	20S-7E
43-015-15677	1034	PAN AMERICAN PETROLEUM COR	FERRON UNIT FEE 4 (14-2)	EMERY	20S-7E
43-015-20053	1376	DIAMOND SHAMROCK EXPL	WITTER FED 1	EMERY	18S-15E
43-015-20145	981	TENNECO OIL COMPANY	FERRON UNIT 5	EMERY	20S-7E
43-015-20190	864	CHEVRON USA INC	CLARENCE WILLSON FEE 1(24-28)	EMERY	16S-10E
43-015-20279	1064	KEWANEE OIL CO	STATE GRN 1	EMERY	20S-16E
43-015-20312	656	UTAH OIL REFINING CO	1	EMERY	19S-13E
43-015-30001	948	CALIFORNIA-TIME PET CO	BARRIER BANK 1	EMERY	19S-14E
43-015-30003	264	TOLEDO MINING CO	TOLEDO FEDERAL 1	EMERY	20S-14E
43-015-30004	304	GLOBE MINERALS INC	COON SPRINGS 1	EMERY	16S-12E
43-015-30014	2128	CHEVRON USA INC	NORRIS FED 1	EMERY	18S-16E
43-015-30021	1745	ENERGY RESERVES GROUP	USA THOMAS WALSH FED 1	EMERY	19S-15E
43-015-30028	360	TRUE OIL COMPANY	TRUE FEDERAL 11-35	EMERY	20S-8E
43-015-30032	290	TRUE OIL COMPANY	TRUE FEDERAL 22-11	EMERY	19S-11E
43-015-30039	494	HAMON OPERATING COMPANY	USA FED 8-1	EMERY	19S-9E
43-015-30046	1260	NORTHSTARGAS LC	FERRON CREEK 2	EMERY	20S-7E
43-015-30059	1603	TIGER OIL CO	JACK CURTIS 41-15	EMERY	18S-7E
43-015-30070	1007	NORTHSTARGAS LC	J LEMON 1	EMERY	20S-7E
43-015-30079	364	MEGADON ENTERPRISES INC	GEYSER DOME 1-14	EMERY	22S-15E
43-015-30080	2607	BOW VALLEY PETROLEUM INC	WILCOX 1-24	EMERY	16S-15E
43-015-30092	1715	TEXAS INTERNATIONAL PETRO	FEDERAL 41-33	EMERY	18S-7E

43-015-30097	364	GENESIS PETROLEUM US INC	FEDERAL 11-33	EMERY	16S-12E
43-015-30100	437	GENESIS PETROLEUM US INC	STATE 2-43X	EMERY	16S-12E
43-015-30111	427	GENESIS PETROLEUM US INC	STATE 2-23	EMERY	16S-12E
43-015-30118	406	GENESIS PETROLEUM US INC	FEDERAL 11-41	EMERY	16S-12E
43-015-30120	371	GENESIS PETROLEUM US INC	FEDERAL 11-13	EMERY	16S-12E
43-015-30121	490	GENESIS PETROLEUM US INC	FEDERAL 4-32	EMERY	16S-12E
43-015-30125	381	TEXAS EASTERN SKYLINE OIL	FEDERAL 10-13	EMERY	16S-12E
43-015-30126	507	TEXAS EASTERN SKYLINE OIL	FEDERAL 5-32	EMERY	16S-12E
43-015-30128	355	SAMEDAN OIL CORPORATION	FEDERAL 14-31	EMERY	16S-12E
43-015-30138	364	GENESIS PETROLEUM US INC	FEDERAL 14-11	EMERY	16S-12E
43-015-30142	356	GENESIS PETROLEUM US INC	FEDERAL 12-13	EMERY	16S-12E
43-015-30149	397	GENESIS PETROLEUM US INC	FEDERAL 11-11	EMERY	16S-12E
43-015-30151	304	TEXAS EASTERN SKYLINE OIL	DUSTY TRAIL 1	EMERY	16S-13E
43-015-30167	374	GENESIS PETROLEUM US INC	FEDERAL 11-42	EMERY	16S-12E
43-015-30170	376	GENESIS PETROLEUM US INC	FEDERAL 11-23	EMERY	16S-12E
43-015-30172	347	GENESIS PETROLEUM US INC	FEDERAL 11-43	EMERY	16S-12E
43-015-30174	104	AMOCO PRODUCTION COMPANY	DESERT LAKE U 5	EMERY	17S-11E
43-015-30178	431	PRIDE VENTURES LLC	BOLINDER FED 3-12	EMERY	16S-12E
43-015-30181	289	T-REX CORP	T-REX FEDERAL 1-27	EMERY	18S-11E
43-015-30192	1009	CHANDLER & ASSOCIATES INC	LAWRENCE 15-1	EMERY	18S-8E
43-015-30221	1411	COASTAL PLAINS ENERGY INC	ORANGEVILLE U 4-1	EMERY	19S-7E
43-015-30240	0	WILDROSE RESOURCES CORP	NEQUOIA STATE 16-1	EMERY	26S-14E
43-015-30241	675	WINDSOR ENERGY US CORP	CLAWSON ET AL 1	EMERY	19S-8E
43-015-30251	315	ANDOVER PARTNERS	FEDERAL 1-17	EMERY	21S-8E
43-015-30272	1479	XTO ENERGY INC	SWD 1	EMERY	18S-7E
43-015-30323	1590	XTO ENERGY INC	SWD 2	EMERY	18S-7E
43-015-30338	1304	CONOCOPHILLIPS COMPANY	UTAH D7	EMERY	16S-9E
43-015-30356	1169	CONOCOPHILLIPS COMPANY	D-11	EMERY	16S-9E
43-015-30531	1632	CONOCOPHILLIPS COMPANY	PPCO D13	EMERY	16S-9E
43-015-30709	809	SWEPI LP	CARBON CANAL 5-12	EMERY	16S-10E
43-019-10024	995	AMAX PETROLEUM CORP	S BAR-X GOVT 3	GRAND	17S-26E
43-019-10087	1175	BELCO DEVELOPMENT CORP	GOVT 1	GRAND	19S-21E
43-019-10088	577	BELCO DEVELOPMENT CORP	HARLEY GOVT 2	GRAND	18S-25E
43-019-10116	664	POTASH COMPANY OF AMERICA	WRIGHT FED 1	GRAND	22S-19E

43-019-10146	944	CABEEN EXPLORATION CORP	GOVT-ROBERTSON 1	GRAND	21S-22E
43-019-10219	1085	COLONIAL OIL CO	GOVT 1	GRAND	21S-18E
43-019-10231	835	CONTINENTAL OIL COMPANY	CISCO UNIT 1	GRAND	20S-21E
43-019-10233	568	CONTINENTAL OIL COMPANY	SALT VALLEY-FED 1	GRAND	22S-19E
43-019-10361	489	EQUITY OIL COMPANY	STRAT ST 1	GRAND	23S-19E
43-019-10390	285	G-K INDUSTRIES	STATE 1	GRAND	21S-24E
43-019-10463	1301	HANCOCK BURTON W	GOVERNMENT 6	GRAND	17S-25E
43-019-10610	1262	KANAB URANIUM CORP	GOVERNMENT 1	GRAND	21S-19E
43-019-10646	717	LARSEN GEORGE N	GEORGE LARSEN FED 1	GRAND	20S-23E
43-019-10666	422	LOCKHART L M	SARGEANT-GOVT 1	GRAND	21S-23E
43-019-10716	507	MENOR J E & AUBREY GEO	GOVERNMENT 1	GRAND	22S-19E
43-019-10775	252	NITRONICS CORPORATION	1 NITRONICS FEDERAL	GRAND	19S-25E
43-019-10815	1388	PACIFIC COAST GAS CORP	PACIFIC COAST 2	GRAND	19S-22E
43-019-10817	6	PACIFIC WESTERN OIL CORP	SHARP STATE 1	GRAND	22S-17E
43-019-10889	1448	PEASE WILLARD H	BOOK CLIFFS 2	GRAND	17S-24E
43-019-10890	1980	PEASE WILLARD H	JONES FEDERAL 1	GRAND	17S-24E
43-019-10932	510	PROMONTORY & FEDERAL	PROMONTORY & FED CISCO ST 10	GRAND	21S-23E
43-019-10950	358	PUMPELLY RAPHAEL SR	PUMPELLY-STAVA UTI 31-81	GRAND	20S-24E
43-019-10954	98	PUMPELLY RAPHAEL SR	STATE 36-33	GRAND	20S-24E
43-019-10989	26	S W ENERGY CORPORATION	FEDERAL ROSENBLATT 1	GRAND	23S-17E
43-019-10991	855	ROYSTER HARRY	FEDERAL 1	GRAND	17S-26E
43-019-10998	777	RESOURCE VENTURES CORP	FEDERAL 5	GRAND	17S-26E
43-019-11013	1960	DIAMOND SHAMROCK EXPL	TUSCHER CREEK 1	GRAND	19S-18E
43-019-11035	46	SHELL OIL COMPANY	LEGGETT 1	GRAND	24S-20E
43-019-11089	1855	AUGUSTUS ENERGY PARTNERS LLC	FEDERAL GILBERT 1	GRAND	16S-25E
43-019-11093	1377	SINCLAIR OIL CORPORATION	S SAN ARROYO 1	GRAND	16S-25E
43-019-11127	619	SKELLY OIL CO	A C MASSA 1	GRAND	18S-25E
43-019-11165	2224	SUNRAY DX OIL CO	DIAMOND RIDGE UNIT 3	GRAND	17S-22E
43-019-11166	2441	SUNRAY DX OIL CO	DIAMOND RIDGE UNIT 4	GRAND	16S-22E
43-019-11167	2614	SUNRAY DX OIL CO	DIAMOND RIDGE UNIT 5	GRAND	17S-22E
43-019-11280	418	TEXOTA OIL COMPANY	FEDERAL B-1	GRAND	18S-25E
43-019-11281	569	TEXOTA OIL COMPANY	FEDERAL 1-C	GRAND	19S-25E
43-019-11282	776	TEXOTA OIL COMPANY	FEDERAL D-1	GRAND	19S-24E
43-019-11283	421	TEXOTA OIL COMPANY	FEDERAL E-1	GRAND	18S-25E
43-019-11308	1545	TREND OIL CO	BRYSON CANYON UNIT 5-A	GRAND	17S-24E
43-019-11309	1895	TREND OIL CO	BRYSON CANYON UNIT 7	GRAND	17S-24E

43-019-11319	2003	UNDERWOOD RIP C	FEDERAL-GIBBS 1-29	GRAND	16S-24E
43-019-11367	481	UNITED TECHNICAL IND	FEDERAL 2	GRAND	20S-24E
43-019-11370	451	UNITED TECHNICAL IND	STRAT 3-A	GRAND	21S-23E
43-019-11412	591	UTEX OIL COMPANY	FEE 3	GRAND	20S-24E
43-019-11414	512	UTEX OIL COMPANY	STATE 6-A	GRAND	20S-24E
43-019-11416	483	UTEX OIL COMPANY	STATE 7	GRAND	20S-24E
43-019-11434	1155	WESTERN STATES REFINING	FEDERAL 10-1	GRAND	18S-24E
43-019-11479	628	GREAT WESTERN DRILLING CO	BRENNARD-FEDERAL 2	GRAND	18S-24E
43-019-11485	600	PACIFIC WESTERN OIL CORP	THOMPSON 1	GRAND	21S-21E
43-019-11487	236	RUDDICK A B	FEDERAL 1	GRAND	22S-24E
43-019-11494	328	TOLES & TOLES DRILLING	LARSEN-FEDERAL 1	GRAND	20S-24E
43-019-11498	570	POTASH COMPANY OF AMERICA	POTASH CO OF AMERICA 2	GRAND	21S-19E
43-019-11500	546	EQUITY OIL COMPANY	DONOHUE 1	GRAND	23S-19E
43-019-11503	431	GRAND PYRAMID OIL INC	GRAND PYRAMID OIL INC 1	GRAND	22S-19E
43-019-11504	671	GRAND COUNTY OIL CO	GRAND COUNTY OIL CO 1	GRAND	22S-19E
43-019-11545	564	TEX-AM OIL CO	GOVERNMENT 1	GRAND	21S-23E
43-019-11557	655	WHISNANT W P	W P WHISNANT ET AL 1	GRAND	23S-18E
43-019-11575	660	CARTER OIL CO	HARLEY BASHOR 1	GRAND	18S-25E
43-019-11576	347	TILTON & WILSON	GOVERNMENT 1	GRAND	18S-25E
43-019-15023	1068	LONE MTN PRODUCTION CO	BAR X UNIT 4	GRAND	17S-26E
43-019-15024	1104	LONE MTN PRODUCTION CO	BAR X UNIT 5	GRAND	17S-26E
43-019-15025	1169	LONE MTN PRODUCTION CO	BAR X 6	GRAND	17S-25E
43-019-15027	1098	LONE MTN PRODUCTION CO	CRITTENDEN 1	GRAND	17S-25E
43-019-15092	1654	BENSON-MONTIN-GREER DRL	HATCH 1	GRAND	16S-26E
43-019-15481	1244	HANCOCK BURTON W	WEST BAR-X U 1	GRAND	17S-25E
43-019-15482	1253	HANCOCK BURTON W	FEDERAL GOVT 1	GRAND	17S-25E
43-019-15648	1567	THOMPSON J C	FEDERAL 1	GRAND	17S-23E
43-019-15657	1558	J C THOMPSON OPERATOR LLC	WESTWATER U E2	GRAND	17S-24E
43-019-15658	1873	J C THOMPSON OPERATOR LLC	WESTWATER U E3	GRAND	17S-24E
43-019-15697	1780	DOUGHERTY H W	GOVT 1-A	GRAND	17S-24E
43-019-15819	44	SMOOT RICHARD P	CF&I 22-16	GRAND	23S-17E
43-019-15885	2019	AUGUSTUS ENERGY PARTNERS LLC	SAN ARROYO 2	GRAND	16S-25E
43-019-15886	1657	AUGUSTUS ENERGY PARTNERS LLC	SAN ARROYO 3	GRAND	16S-25E
43-019-15887	1417	AUGUSTUS ENERGY PARTNERS LLC	SAN ARROYO 4	GRAND	16S-26E
43-019-15888	1460	AUGUSTUS ENERGY PARTNERS LLC	SAN ARROYO 5	GRAND	16S-25E
43-019-15889	1981	AUGUSTUS ENERGY PARTNERS LLC	SAN ARROYO 6	GRAND	16S-25E

43-019-15933	2014	SUNRAY DX OIL CO	DIAMOND RIDGE UNIT 1	GRAND	17S-23E
43-019-16029	686	MAR/REG OIL COMPANY	A W CULLEN GOVT 1	GRAND	20S-23E
43-019-16046	2654	BEARTOOTH OIL & GAS CO	FENCE CANYON 3	GRAND	15.5S-23E
43-019-16203	2292	LONE MTN PRODUCTION CO	EAST CANYON UNIT 33-18	GRAND	16S-25E
43-019-16211	1901	TREND OIL CO	BRYSON CANYON 3	GRAND	17S-24E
43-019-16212	1597	TREND OIL CO	BRYSON CYN 6-A	GRAND	17S-24E
43-019-16260	518	UTEX OIL COMPANY	GRETCHEN STATE 1	GRAND	20S-24E
43-019-16514	344	PROMONTORY OIL CO	PROMONTORY-FED ST 31-1 (WSW)	GRAND	21S-24E
43-019-16532	1478	AUGUSTUS ENERGY PARTNERS LLC	SAN ARROYO 1	GRAND	16S-25E
43-019-20128	338	U CAL PETROLEUM G LTD	U-CAL STATE 31-1	GRAND	21S-24E
43-019-20146	105	UNION OIL CO OF CALIFORNIA	DEVILS GARDEN USA 1	GRAND	23S-21E
43-019-20198	509	BUSH WILLIAM G	USA FEDERAL 5-5	GRAND	21S-24E
43-019-20219	245	ALGREM L W JR	ALGREM ST 1	GRAND	19S-25E
43-019-20247	255	MOUNTAIN ENERGY & RESOURCES INC	LANSDALE GOVT 1	GRAND	18S-25E
43-019-20249	378	LANSDALE A	LANSDALE GOVT 3	GRAND	18S-25E
43-019-20383	358	CALTAH OIL CO	KENMORE 24-114	GRAND	21S-23E
43-019-20410	2128	SUNRAY DX OIL CO	DIAMOND RIDGE UNIT 7	GRAND	17S-23E
43-019-30001	454	GREEN BILLY J	FEDERAL GREEN 2	GRAND	20S-24E
43-019-30003	255	MOUNTAIN ENERGY & RESOURCES INC	LANSDALE GOVT 4	GRAND	19S-25E
43-019-30005	296	LANSDALE A	LANSDALE GOVT 6	GRAND	18S-25E
43-019-30007	265	LANSDALE A	LANSDALE GOVT 9	GRAND	19S-25E
43-019-30008	262	GILILLAND DAYMON D	LANSDALE GOVT 13	GRAND	19S-25E
43-019-30010	396	VIKING OIL COMPANY	S SIEBER NOSE 8	GRAND	20S-25E
43-019-30016	238	LANSDALE A	LANSDALE STATE 14	GRAND	19S-25E
43-019-30020	419	LANSDALE A	LANSDALE GOVT 17	GRAND	18S-25E
43-019-30021	261	LANSDALE A	LANSDALE GOVT 16	GRAND	18S-25E
43-019-30022	339	LANSDALE A	LANSDALE GOVT 18	GRAND	18S-25E
43-019-30026	469	LANSDALE A	LANSDALE GOVT 19	GRAND	18S-26E
43-019-30037	418	ORPHAN-NO RESPONSIBLE OPERATOR	LANSDALE GOVERNMENT 8	GRAND	18S-25E
43-019-30047	1982	AUGUSTUS ENERGY PARTNERS LLC	BITTER CREEK 1	GRAND	16S-25E
43-019-30048	789	TEXACO INC	GOVERNMENT T-1	GRAND	21S-20E
43-019-30055	19	QUINTANA PETROLEUM CORP	YELLOW CAT USA 1-9	GRAND	23S-22E
43-019-30061	2452	ARCO OIL & GAS COMPANY	BITTER CREEK ST 2	GRAND	16S-25E
43-019-30062	92	UNION OIL CO OF CALIFORNIA	STATE 1-P-2	GRAND	23S-21E
43-019-30070	1119	TEXACO INC	GOVERNMENT Y NCT-1	GRAND	21S-20E
43-019-30073	1444	ANSCHUTZ CORPORATION THE	FEDERAL 773-1	GRAND	19S-21E
43-019-30077	1531	J C THOMPSON OPERATOR LLC	WESTWATER U E5	GRAND	17S-24E

43-019-30078	1233	TOLEDO MINING CO	BULL CANYON GOVT 1	GRAND	20S-21E
43-019-30079	593	THUNDERBIRD OIL CO	LARSON FEDERAL 20-1A	GRAND	18S-25E
43-019-30080	1401	ANSCHUTZ CORPORATION THE	FEDERAL 773-2	GRAND	19S-21E
43-019-30082	703	ANDERSON & STROOCK	ST OF UT 1	GRAND	21S-22E
43-019-30104	1392	ANSCHUTZ CORPORATION THE	FEDERAL 262-1	GRAND	19S-23E
43-019-30107	959	ANSCHUTZ CORPORATION THE	FEDERAL 267-1	GRAND	19S-23E
43-019-30110	550	CONOCO INC	CRESCENT UNIT 1	GRAND	22S-20E
43-019-30115	747	RUNNING FOXES PETROLEUM INC.	FEDERAL 1-355	GRAND	20S-23E
43-019-30119	350	GOAL RESOURCES INC	GOAL STATE 5	GRAND	21S-24E
43-019-30121	408	ADAK ENERGY CORPORATION	CISCO FED 3	GRAND	21S-23E
43-019-30124	154	MOUNTAIN FUEL SUPPLY CO	MT FUEL-SKYLINE GEYSER 1-25	GRAND	22S-16E
43-019-30139	309	GOAL RESOURCES INC	GOAL RESOURCES ST 31-6	GRAND	21S-24E
43-019-30142	646	BROADHEAD WALTER	LANSDALE FEDERAL 2	GRAND	20S-24E
43-019-30158	1337	TEJAS GAS CORP	COLORADO-UT LIVESTOCK CO 1	GRAND	19S-22E
43-019-30171	2314	PACIFIC TRANS SUPPLY	FEDERAL 915-1	GRAND	17S-22E
43-019-30175	101	GOAL RESOURCES INC	GOAL STATE 36-7	GRAND	20S-24E
43-019-30177	902	ADAK ENERGY CORPORATION	TERTELING GOVT 1	GRAND	20S-21E
43-019-30184	812	ADAK ENERGY CORPORATION	ADAK-ANSCHUTZ FED 1	GRAND	20S-21E
43-019-30194	1583	ANSCHUTZ CORPORATION THE	FEDERAL 772-1	GRAND	19S-21E
43-019-30207	1404	S W ENERGY CORPORATION	BLAZE A-1	GRAND	21S-18E
43-019-30209	1039	GAS PRODUCING ENTERPRISES	FEDERAL 14-20-22	GRAND	20S-22E
43-019-30213	344	THUNDERBIRD OIL CO	STATE 32-5	GRAND	20S-24E
43-019-30215	1234	PHILLIPS PETROLEUM CO	BLAZE "C" 1	GRAND	21S-19E
43-019-30236	558	PEASE OIL & GAS COMPANY	CISCO SPRINGS FED 15	GRAND	20S-23E
43-019-30237	558	PEASE OIL & GAS COMPANY	CISCO SPRINGS FED 16	GRAND	20S-23E
43-019-30260	274	LANSDALE A	LANSDALE GOVT 3-30-A	GRAND	19S-25E
43-019-30279	1026	CSV OIL EXPLORATION CO	LANSDALE FED 14-1	GRAND	17S-25E
43-019-30284	1352	ANSCHUTZ CORPORATION THE	STATE 635-1	GRAND	19S-21E
43-019-30286	1000	PEASE OIL & GAS COMPANY	FEDERAL 1-5	GRAND	20S-23E
43-019-30306	835	UNITED ENERGY CORP	FEDERAL 29-3	GRAND	20S-22E
43-019-30312	1208	HAMILTON BROTHERS OIL CO	SALT VALLEY NW U 1	GRAND	21S-18E
43-019-30322	2118	STALLWORTH ROBERT B	FEDERAL 4-1	GRAND	18S-23E
43-019-30324	973	PEASE OIL & GAS COMPANY	FEDERAL 10-1	GRAND	20S-22E
43-019-30326	90	WEXPRO COMPANY	KLONDIKE UNIT 3	GRAND	23S-19E
43-019-30327	0	PEASE OIL & GAS COMPANY	FEDERAL SKYLINE 1A SW	GRAND	23S-17E

43-019-30328	710	TXO PRODUCTION CORP	KLOTZ FEDERAL 1	GRAND	21S-22E
43-019-30335	820	BEARTOOTH OIL & GAS CO	BAR CREEK 1	GRAND	17S-26E
43-019-30337	927	ANSCHUTZ CORPORATION THE	FEDERAL 267-3	GRAND	19S-23E
43-019-30338	1034	ANSCHUTZ CORPORATION THE	FEDERAL 266-1	GRAND	19S-23E
43-019-30340	1316	ANSCHUTZ CORPORATION THE	FEDERAL 263-1	GRAND	19S-23E
43-019-30343	1433	ANSCHUTZ CORPORATION THE	FEDERAL 258-1	GRAND	18S-24E
43-019-30346	1644	CORPORATION THE	FEDERAL 273-1	GRAND	18S-23E
43-019-30347	808	ELK PRODUCTION LLC	STATE 32-1	GRAND	20S-22E
43-019-30352	1623	ANSCHUTZ CORPORATION THE	FEDERAL 769-1	GRAND	19S-21E
43-019-30355	861	ELK PRODUCTION LLC	FEDERAL 23-1	GRAND	20S-21E
43-019-30359	788	ELK PRODUCTION LLC	FEDERAL 25-1	GRAND	20S-21E
43-019-30361	1394	PEAK OIL TOOL	MAGNUM 258-2	GRAND	18S-24E
43-019-30362	1394	ANSCHUTZ CORPORATION THE	FEDERAL 258-3	GRAND	18S-24E
43-019-30371	2118	ANSCHUTZ CORPORATION THE	FEDERAL 078-1	GRAND	18S-22E
43-019-30375	1300	THOMPSON J C	FEDERAL 1-104	GRAND	20S-21E
43-019-30383	1129	ANSCHUTZ CORPORATION THE	FEDERAL 335-3	GRAND	19S-23E
43-019-30388	802	ADAMS FRANK B	STATE 1-2	GRAND	20S-23E
43-019-30389	712	MOBIL OIL CORPORATION	MCCORMICK FEDERAL C 2	GRAND	21S-22E
43-019-30390	1403	HANCOCK BURTON W	HANCOCK GOVT 44	GRAND	17S-25E
43-019-30391	762	MCCONNELL B L OPERATING	CALF CANYON FED 6	GRAND	20S-21E
43-019-30393	1000	ELK PRODUCTION LLC	CALF CANYON 5	GRAND	20S-21E
43-019-30404	755	RUNNING FOXES PETROLEUM INC.	CISCO 3	GRAND	20S-23E
43-019-30406	1184	PEASE OIL & GAS COMPANY	CALF CANYON 3	GRAND	20S-21E
43-019-30413	568	LANSDALE A	FEDERAL 1-23	GRAND	18S-25E
43-019-30414	517	LANSDALE A	FEDERAL 2-18	GRAND	18S-26E
43-019-30415	672	LANSDALE A	FEDERAL 3-31	GRAND	17S-26E
43-019-30418	30	ARI-MEX OIL & EXPLOR INC	SKIP FEDERAL 1-7	GRAND	25S-21E
43-019-30421	3134	ANSCHUTZ CORPORATION THE	TEN MILE STATE 921-1	GRAND	16S-21E
43-019-30423	384	PACIFIC ENERGY & MINING CO	NUGGETT 14-4	GRAND	21S-23E
43-019-30424	765	PEASE OIL & GAS COMPANY	BAR CREEK UNIT 4	GRAND	17S-26E
43-019-30425	727	PEASE OIL & GAS COMPANY	BAR CREEK UNIT 5	GRAND	17S-26E
43-019-30427	1314	HANCOCK BURTON W	HANCOCK 33	GRAND	17S-25E
43-019-30428	784	PEASE OIL & GAS COMPANY	FEDERAL 31-3	GRAND	20S-22E
43-019-30429	814	ELK PRODUCTION LLC	FEDERAL 30-1	GRAND	20S-22E
43-019-30432	835	ELK PRODUCTION LLC	FEDERAL 24-3	GRAND	20S-21E
43-019-30436	951	ELK PRODUCTION LLC	FEDERAL 14-1A	GRAND	20S-21E

43-019-30449	1265	LINN BROS OIL & GAS INC	WILLOW CREEK E 4970-1	GRAND	20S-21E
43-019-30466	335	FLORIDA EXPLORATION CO	MOBIL 26-21-23-1	GRAND	21S-23E
43-019-30467	604	SUPRON ENERGY CORPORATION	GRYNBERG 36-20-23-1	GRAND	20S-23E
43-019-30475	453	RUNNING FOXES PETROLEUM INC.	CISCO FEDERAL 1	GRAND	21S-23E
43-019-30479	533	CARMACK DRILLING	LANSDALE-CARMACK 1-10	GRAND	20S-24E
43-019-30484	1058	ELK PRODUCTION LLC	FEDERAL 1-10	GRAND	20S-21E
43-019-30487	945	ELK PRODUCTION LLC	FEDERAL 14-2	GRAND	20S-21E
43-019-30492	847	NP ENERGY CORPORATION	FEDERAL 30-2	GRAND	20S-22E
43-019-30501	1153	CARMACK DRILLING	STATE 1-16	GRAND	21S-20E
43-019-30502	749	SUPRON ENERGY CORPORATION	MOBIL 11-21-22-1	GRAND	21S-22E
43-019-30503	701	SUPRON ENERGY CORPORATION	MOBIL 13-21-22-1	GRAND	21S-22E
43-019-30504	561	UNICON PRODUCING COMPANY	MOBIL 19-21-23-1	GRAND	21S-23E
43-019-30529	920	NP ENERGY CORPORATION	STATE 32-3	GRAND	20S-22E
43-019-30530	884	ELK PRODUCTION LLC	FEDERAL 24-2	GRAND	20S-21E
43-019-30536	792	BURTON/HAWKS INC	EAST CISCO FED 1-1	GRAND	20S-23E
43-019-30542	1103	STARNER DRILLING	CARMACK FEDERAL 1-14	GRAND	21S-20E
43-019-30547	390	ORPHAN-NO RESPONSIBLE OPERATOR	BUCKHORN-NUGGETT 14-22B	GRAND	21S-23E
43-019-30549	1070	PEASE OIL & GAS COMPANY	FEDERAL 10-1	GRAND	18S-24E
43-019-30550	696	PEASE OIL & GAS COMPANY	FEDERAL 13-2	GRAND	18S-24E
43-019-30555	783	AMBRA OIL & GAS COMPANY	INLAND FUELS FED 11-1	GRAND	20S-23E
43-019-30557	816	LINN BROS OIL & GAS INC	E CISCO FEDERAL 1-3	GRAND	20S-23E
43-019-30560	543	PETROVEST INTERNATIONAL	ESCONDITO 2	GRAND	21S-23E
43-019-30568	783	INLAND FUELS CORP	FEDERAL 11-2	GRAND	20S-23E
43-019-30586	940	ELK PRODUCTION LLC	FEDERAL 23-2	GRAND	20S-21E
43-019-30587	794	ELK PRODUCTION LLC	FEDERAL 25-2	GRAND	20S-21E
43-019-30663	776	JACOBS R L OIL & GAS CO	ST OF UT 36-1	GRAND	20S-21E
43-019-30681	130	MEGADON ENTERPRISES INC	STATE 1-16	GRAND	23S-17E
43-019-30691	635	SCHUSTER HOMES INC.	BROWNDIRT 2	GRAND	20S-23E
43-019-30693	661	SCHUSTER HOMES INC.	TXO MESA 23-1	GRAND	20S-23E
43-019-30706	3130	J C THOMPSON OPERATOR LLC	PETERSON SPRINGS 1	GRAND	17S-21E
43-019-30715	914	LINN BROS OIL & GAS INC	TUMBLEWEED 27-5	GRAND	20S-21E
43-019-30734	2392	LOCKRIDGE JOHN P	STATE 14-4	GRAND	19S-20E
43-019-30735	1420	TENNECO OIL COMPANY	LONG CANYON UNIT ST 16-4	GRAND	19S-23E
43-019-30744	539	HARRISON THOMAS D	PIONEER 2-1	GRAND	21S-23E
43-019-30745	1595	RESOURCE DEVELOPMENT TECHNOLOGY LLC	WILLOW CREEK EAST 30-5	GRAND	19S-21E

43-019-30747	843	LINN BROS OIL & GAS INC	BO-TX 2-36	GRAND	20S-21E
43-019-30752	94	MEGADON ENTERPRISES INC	FEDERAL 1-15	GRAND	23S-17E
43-019-30764	1067	PARKER ENERGY TECH INC	WESTERN FED 14-5	GRAND	20S-23E
43-019-30772	1664	TENNECO OIL COMPANY	SULPHER CANYON USA 1-15	GRAND	18S-23E
43-019-30783	197	S W ENERGY CORPORATION	STATE 1-16A	GRAND	23S-17E
43-019-30786	1082	JACOBS R L OIL & GAS CO	SULPHUR SPRINGS 4	GRAND	18S-24E
43-019-30801	850	ARI-MEX OIL & EXPLOR INC	FED CLAYTON 2	GRAND	20S-24E
43-019-30806	808	ADAMS & DIZDAR	ST OF UT 2 CABEEN	GRAND	20S-21E
43-019-30819	824	B L OIL AND GAS	20-1	GRAND	20S-23E
43-019-30828	226	BROADHEAD WALTER	STATE L B 1	GRAND	20S-24E
43-019-30835	1701	TENNECO OIL COMPANY	BUTLER CYN UNIT USA 33-12	GRAND	19S-17E
43-019-30855	940	BOG INC (BOWERS)	BO-TX 3-36	GRAND	20S-21E
43-019-30868	632	ADAMS FRANK B	FEDERAL 33-1	GRAND	19S-24E
43-019-30872	712	EQUITY OIL COMPANY	STATE 2-3	GRAND	21S-22E
43-019-30875	908	ELK PRODUCTION LLC	FEDERAL 18-1	GRAND	20S-22E
43-019-30876	796	PEASE OIL & GAS COMPANY	FEDERAL 31-2	GRAND	20S-22E
43-019-30877	837	NP ENERGY CORPORATION	FEDERAL 31-4	GRAND	20S-22E
43-019-30878	875	ELK PRODUCTION LLC	FEDERAL 14-4	GRAND	20S-21E
43-019-30881	960	ELK PRODUCTION LLC	FEDERAL 12-1	GRAND	20S-21E
43-019-30883	932	ELK PRODUCTION LLC	FEDERAL 13-3	GRAND	20S-21E
43-019-30887	1007	ELK PRODUCTION LLC	FEDERAL 15-4	GRAND	20S-21E
43-019-30894	573	PROSPECTOR ENERGY INC	PROSPECTOR CAPANSKY 18-2	GRAND	20S-24E
43-019-30900	860	ELK PRODUCTION LLC	FEDERAL 24-4	GRAND	20S-21E
43-019-30918	826	MOBIL OIL CORPORATION	AMERICAN PETROFINA 1-30	GRAND	21S-22E
43-019-30919	649	AMBRA OIL & GAS COMPANY	CISCO FED 25-1	GRAND	20S-23E
43-019-30940	770	AMBRA OIL & GAS COMPANY	CISCO FED 26-1	GRAND	20S-23E
43-019-30948	366	BOOKCLIFF PETROLEUM INC	W BITTER CREEK 27-33	GRAND	18S-25E
43-019-30950	550	SCHUSTER HOMES INC.	ISLAND FUEL 23-4	GRAND	20S-23E
43-019-30996	351	GILILLAND DAYMON D	WEST BITTER CREEK 27-44	GRAND	18S-25E
43-019-31003	640	PUMPELLY RAPHAEL SR	MARTHA EPPIE C 8	GRAND	20S-24E
43-019-31022	927	BUSH WILLIAM G	GOVERNMENT BUSH 12-1	GRAND	21S-21E
43-019-31063	1475	BWAB INCORPORATED	FEDERAL 12-42	GRAND	21S-18E
43-019-31077	1993	FOUNDATION ENERGY MANAGEMENT LLC	BRYSON CANYON FED 1-34-16-24	GRAND	16S-24E
43-019-31112	398	LADD PETROLEUM CORPORATION	SALT VALLEY 1	GRAND	24S-20E
43-019-31120	572	DAB OIL CO	CISCO 1	GRAND	20S-24E
43-019-31167	2033	SAGE ENERGY COMPANY	SAGE FEDERAL 31-31	GRAND	16S-25E

43-019-31186	442	BROADHEAD WALTER	BROADHEAD FED 7-5	GRAND	21S-24E
43-019-31209	1142	ELK PRODUCTION LLC	CALF CANYON 11	GRAND	20S-21E
43-019-31250	1874	AUGUSTUS ENERGY PARTNERS LLC	SAN ARROYO U 40	GRAND	16S-25E
43-019-31251	1555	AUGUSTUS ENERGY PARTNERS LLC	SAN ARROYO U 36-A	GRAND	16S-26E
43-019-31253	2062	AUGUSTUS ENERGY PARTNERS LLC	SAN ARROYO U 38	GRAND	16S-25E
43-019-31371	1093	LONE MTN PRODUCTION CO	BAR X UNIT 25	GRAND	17S-25E
43-019-31399	1128	NAE LLC	STATE 21-19 (32-16D)	GRAND	21S-19E
43-019-31444	785	ELK PRODUCTION LLC	FEDERAL 25-5	GRAND	20S-21E
43-019-31462	153	DELTA PETROLEUM CORP	GREENTOWN ST 36-11	GRAND	21S-16E
43-019-31463	567	DELTA PETROLEUM CORP	SALT VLY ST 25-12	GRAND	22S-19E
43-019-31466	341	NAE LLC	TIDEWATER ST 23-5	GRAND	21S-23E
43-019-31469	1011	SAMSON RESOURCES COMPANY	TIDEWATER ST 32-3	GRAND	21S-19E
43-019-31481	410	RUNNING FOXES PETROLEUM INC.	30-6	GRAND	20S-24E
43-019-31482	379	RUNNING FOXES PETROLEUM INC.	30-11	GRAND	20S-24E
43-019-31488	496	RUNNING FOXES PETROLEUM INC.	CP 1-5A	GRAND	21S-23E
43-019-31502	335	SAMSON RESOURCES COMPANY	POWER LINE 12-1	GRAND	23S-18E
43-019-31503	133	PACIFIC ENERGY & MINING CO	FEDERAL 28-11	GRAND	22S-17E
43-019-31505	145	DELTA PETROLEUM CORP	GREENTOWN ST 36-11S	GRAND	21S-16E
43-019-31507	138	DELTA PETROLEUM CORP	GREENTOWN FED 35-12	GRAND	21S-16E
43-019-31511	983	TIDEWATER OIL & GAS COMPANY LLC	CACTUS ROSE FED 29-44-2119	GRAND	21S-19E
43-019-31519	120	DELTA PETROLEUM CORP	GREENTOWN ST 36-24H	GRAND	21S-16E
43-019-31526	3268	ROYALE ENERGY INC.	TEN MILE CYN 22-1	GRAND	16S-21E
43-019-31530	359	RUNNING FOXES PETROLEUM INC.	CISCO 30-9-4	GRAND	20S-24E
43-019-31533	350	RUNNING FOXES PETROLEUM INC.	CISCO 30-15-4	GRAND	20S-24E
43-019-31534	404	RUNNING FOXES PETROLEUM INC.	CISCO 30-12-3	GRAND	20S-24E
43-019-31536	482	RUNNING FOXES PETROLEUM INC.	CISCO 6-11-2	GRAND	21S-24E
43-019-31547	189	PACIFIC ENERGY & MINING CO	GREENTOWN FED 26-43H	GRAND	21S-16E
43-019-31551	138	DELTA PETROLEUM CORP	GREENTOWN FED 35-12D	GRAND	21S-16E
43-019-31569	91	DELTA PETROLEUM CORP	GREENTOWN ST 31-362216H	GRAND	22S-16E
43-019-31575	271	PACIFIC ENERGY & MINING CO	FEDERAL 11-24	GRAND	22S-16E
43-019-31580	1946	AUGUSTUS ENERGY PARTNERS LLC	SAN ARROYO 1625-22O	GRAND	16S-25E
43-019-31595	799	NAE LLC	SVA 23-33-2119	GRAND	21S-19E
43-019-31622	302	WESTWATER FARMS LLC	HARLEY DOME 1	GRAND	19S-25E
43-047-10577	3522	WHITING OIL & GAS CORPORATION	UTE TRIBAL 32-5A	UINTAH	14S-20E
43-047-10692	2368	MARATHON OIL COMPANY	OHIO TWO WATERS UNIT 1	UINTAH	14S-25E

43-047-10764	2739	MOUNTAIN FUEL SUPPLY CO	MAIN CANYON 1	UINTAH	15S-23E
43-047-16197	2802	BEARTOOTH OIL & GAS CO	FENCE CYN U 1	UINTAH	15S-22E
43-047-20508	2280	PHILLIPS PETROLEUM CO	TWO WATERS UNIT 1	UINTAH	14S-25E
43-047-30097	2553	WEBB RESOURCES INC	FEDERAL 31-13	UINTAH	15S-24E
43-047-30121	2838	CHORNEY OIL CO	SE FLANK UINTA 1-5	UINTAH	15S-23E
43-047-30126	3022	FOUNDATION ENERGY MANAGEMENT LLC	SE FLANK UINTAH 1-28	UINTAH	15S-22E
43-047-30135	3156	TEXACO INC	J CHORNEY C-2	UINTAH	14S-22E
43-047-30271	2961	EXXON CORPORATION	CROOKED CANYON U 1	UINTAH	14S-23E
43-047-34102	3523	WHITING OIL & GAS CORPORATION	UTE TRIBAL 29-6A	UINTAH	14S-20E
43-047-34103	3530	WHITING OIL & GAS CORPORATION	UTE TRIBAL 29-7A	UINTAH	14S-20E
43-047-34742	3444	UINTAH INVESTORS LLC	N HILL CREEK 1-9-15-20	UINTAH	15S-20E
43-047-34830	3441	UINTAH INVESTORS LLC	N HILL CREEK 10-10-15-20	UINTAH	15S-20E
43-047-34922	3397	UINTAH INVESTORS LLC	N HILL CREEK 4-1-15-20	UINTAH	15S-20E
43-047-34953	3383	UINTAH INVESTORS LLC	N HILL CREEK 14-11-15-20	UINTAH	15S-20E
43-047-34954	3417	UINTAH INVESTORS LLC	N HILL CREEK 8-13-15-20	UINTAH	15S-20E
43-047-34955	3401	WIND RIVER RESOURCES CORP	N HILL CREEK 2-14-15-20	UINTAH	15S-20E
43-047-35054	3335	UINTAH INVESTORS LLC	NHC 4-13-15-20	UINTAH	15S-20E
43-047-35140	3566	UINTAH INVESTORS LLC	N HILL CREEK 1-6-15-20	UINTAH	15S-20E
43-047-35283	3373	UINTAH INVESTORS LLC	N HILL CREEK 2-12-15-20	UINTAH	15S-20E
43-047-35390	3374	UINTAH INVESTORS LLC	NHC 9-11-15-20	UINTAH	15S-20E
43-047-35442	3519	UINTAH INVESTORS LLC	NHC 3-6-15-20X	UINTAH	14S-20E
43-047-35625	3398	WHITING OIL & GAS CORPORATION	UTE TRIBAL 10-2-15-20	UINTAH	15S-20E
43-047-35880	3440	QEP ENERGY COMPANY	FR 9P-36-14-19	UINTAH	14S-20E
43-047-36795	3532	WHITING OIL & GAS CORPORATION	FLAT ROCK 3-29-14-20	UINTAH	14S-20E
43-047-37376	3374	QEP ENERGY COMPANY	FR 3P-36-14-19	UINTAH	14S-19E
43-047-37541	3685	QEP ENERGY COMPANY	WF 14C-29-15-19	UINTAH	15S-19E
43-047-38349	3339	QEP ENERGY COMPANY	FR 11P-36-14-19	UINTAH	14S-19E
43-047-38506	3622	WHITING OIL & GAS CORPORATION	UTE TRIBAL 6-16-14-20	UINTAH	14S-20E
43-047-38968	3247	ROYALE ENERGY INC.	V CYN 20-1	UINTAH	15S-21E
43-047-38992	3415	QEP ENERGY COMPANY	FR 7P-36-14-19	UINTAH	14S-20E
43-047-39052	3549	WHITING OIL & GAS CORPORATION	UTE TRIBAL 15-25-14-19	UINTAH	14S-20E
43-047-39168	3490	QEP ENERGY COMPANY	FR 14P-20-14-20	UINTAH	14S-20E
43-047-39226	3477	QEP ENERGY COMPANY	FR 13P-20-14-20	UINTAH	14S-20E
43-047-39299	3344	STEWART PETROLEUM CORP	TUMBLEWEED 18-9	UINTAH	15S-21E
43-047-39428	2843	FOUNDATION ENERGY MANAGEMENT LLC	MAIN CYN FED 12-8-15-23	UINTAH	15S-23E
43-047-39463	3624	QEP ENERGY COMPANY	FR 9P-17-14-20	UINTAH	14S-20E

43-047-39499	3512	WIND RIVER RESOURCES CORP	NHC 12-33-15-20	UINTAH	15S-20E
43-047-39665	3538	WHITING OIL & GAS CORPORATION	UTE TRIBAL 1-30-14-20	UINTAH	14S-20E
43-047-39739	3460	WHITING OIL & GAS CORPORATION	UTE TRIBAL 3-30-14-20	UINTAH	14S-20E
43-047-39740	3457	WHITING OIL & GAS CORPORATION	UTE TRIBAL 11-30-14-20	UINTAH	14S-20E
43-047-39741	3560	WHITING OIL & GAS CORPORATION	UTE TRIBAL 5-32-14-20	UINTAH	14S-20E
43-047-39809	3624	QEP ENERGY COMPANY	FR 6P-20-14-20	UINTAH	14S-20E
43-047-39811	3615	QEP ENERGY COMPANY	FR 4P-21-14-20	UINTAH	14S-20E
43-047-39942	3451	WHITING OIL & GAS CORPORATION	UTE TRIBAL 15-30-14-20	UINTAH	14S-20E
43-047-40349	3077	ROYALE ENERGY INC.	V CANYON 20-2	UINTAH	15S-21E
43-055-10265	0	CONOCO INC	S HANKSVILLE ST 1	WAYNE	27S-13E
43-055-10590	0	HUMBLE OIL & REFINING CO	NEQUOIA ARCH U 1	WAYNE	27S-14E

Appendix B. Fracture Orientations

SRS North Fracture Orientations

STATION	FORMATION	STRIKE	DIP	DIRECTION	FRACTURE SPACING (m)	ALTERATION (Y/N)
SQ-CU-1A	Curtis	274	81	S	0.13	N
SQ-CU-1A	Curtis	289	83	S	0.26	N
SQ-CU-1A	Curtis	250	83	W	0.32	N
SQ-CU-1A	Curtis	31	73	W	0.27	N
SQ-CU-1A	Curtis	321	76	E	0.33	N
SQ-CU-1A	Curtis	286	79	S	0.24	N
SQ-CU-1A	Curtis	39	68	W	0.14	N
SQ-CU-1A	Curtis	31	84	W	0.42	N
SQ-CU-1A	Curtis	256	84	S	0.43	N
SQ-CU-1A	Curtis	274	82	S	0.26	N
SQ-CU-1A	Curtis	265	85	W	0.34	N
SQ-CU-1A	Curtis	23	76	W	0.35	N
SQ-CU-1A	Curtis	333	79	E	0.27	N
SQ-CU-1A	Curtis	279	81	S	0.29	N
SQ-CU-1A	Curtis	23	72	W	0.31	N
SQ-CU-1A	Curtis	36	83	W	0.18	N
SQ-CU-1B	Curtis	24	47	W	0.26	N
SQ-CU-1B	Curtis	26	42	W	0.27	N
SQ-CU-1B	Curtis	24	46	W	0.33	N
SQ-CU-1B	Curtis	322	48	SW	0.39	N
SQ-CU-1B	Curtis	22	52	W	0.48	N
SQ-CU-1B	Curtis	23	51	W	0.44	N
SQ-CU-1B	Curtis	29	52	W	0.36	N
SQ-CU-1B	Curtis	33	48	W	0.22	N
SQ-CU-1B	Curtis	19	41	W	0.2	N
SQ-CU-1B	Curtis	336	58	SW	0.34	N
SQ-CU-1B	Curtis	26	47	W	0.33	N
SQ-CU-1B	Curtis	27	53	W	0.27	N
SQ-EN-1A	Entrada	322	84	S	0.42	Y
SQ-EN-1A	Entrada	302	78	SW	0.25	Y
SQ-EN-1A	Entrada	324	82	NE	0.25	Y
SQ-EN-1A	Entrada	318	81	NE	0.21	Y
SQ-EN-1A	Entrada	309	72	SW	0.26	Y
SQ-EN-1A	Entrada	291	79	SW	0.21	Y
SQ-EN-1A	Entrada	2	72	E	0.41	Y
SQ-EN-1A	Entrada	318	87	S	0.33	Y
SQ-EN-1A	Entrada	306	74	S	0.28	Y

SQ-EN-1A	Entrada	329	88	NE	0.34	Y
SQ-EN-1A	Entrada	324	77	NE	0.22	Y
SQ-EN-1A	Entrada	303	68	SW	0.2	Y
SQ-EN-1A	Entrada	299	84	SW	0.29	Y
SQ-EN-1A	Entrada	5	76	E	0.34	Y
SQ-EN-2A	Entrada	318	81	S	0.28	Y
SQ-EN-2A	Entrada	307	71	SW	0.32	Y
SQ-EN-2A	Entrada	330	88	NE	0.21	Y
SQ-EN-2A	Entrada	326	76	NE	0.37	Y
SQ-EN-2A	Entrada	304	74	SW	0.24	Y
SQ-EN-2A	Entrada	300	74	SW	0.26	Y
SQ-EN-2A	Entrada	7	71	E	0.38	Y
SQ-EN-2A	Entrada	328	84	S	0.27	Y
SQ-EN-2A	Entrada	299	73	SW	0.29	Y
SQ-EN-2A	Entrada	336	89	NE	0.26	Y
SQ-EN-2A	Entrada	340	73	NE	0.33	Y
SQ-EN-2A	Entrada	312	71	SW	0.29	Y
SQ-EN-2A	Entrada	305	69	SW	0.2	Y
SQ-EN-2A	Entrada	4	78	E	0.31	Y
SQ-CA-1A	Carmel	351	21	W	0.16	Y
SQ-CA-1A	Carmel	334	24	W	0.05	Y
SQ-CA-1A	Carmel	349	20	W	0.12	Y
SQ-CA-1A	Carmel	280	65	SW	0.01	Y
SQ-CA-1A	Carmel	331	31	W	0.14	Y
SQ-CA-1A	Carmel	341	30	W	0.07	Y
SQ-CA-1A	Carmel	346	34	W	0.09	Y
SQ-CA-1A	Carmel	301	58	SW	0.11	Y
SQ-CA-1A	Carmel	334	26	W	0.07	Y
SQ-CA-1A	Carmel	327	35	W	0.14	Y
SQ-CA-1A	Carmel	326	32	W	0.17	Y
SQ-CA-1A	Carmel	28	58	E	0.11	Y
SQ-CA-1A	Carmel	345	26	W	0.08	Y
SQ-CA-1A	Carmel	336	31	W	0.1	Y
SQ-CA-1A	Carmel	358	27	W	0.17	Y
SQ-CA-1A	Carmel	272	69	SW	0.17	Y
SQ-CA-1A	Carmel	341	36	W	0.12	Y
SQ-CA-1A	Carmel	336	34	W	0.04	Y
SQ-CA-1A	Carmel	352	38	W	0.17	Y
SQ-CA-1A	Carmel	312	62	SW	0.09	Y
SQ-CA-1A	Carmel	345	31	W	0.06	Y
SQ-CA-1A	Carmel	329	39	W	0.13	Y

SQ-CA-1A	Carmel	333	34	W	0.08	Y
SQ-PA-1A	Page	300	87	W	0.12	Y
SQ-PA-1A	Page	301	87	W	0.2	Y
SQ-PA-1A	Page	302	88	W	0.16	Y
SQ-PA-1A	Page	301	87	W	0.06	Y
SQ-PA-1A	Page	304	89	W	0.03	Y
SQ-PA-1A	Page	345	44	W	0.29	Y
SQ-PA-1A	Page	360	89	W	0.06	Y
SQ-PA-1A	Page	315	78	W	0.13	Y
SQ-PA-1A	Page	309	84	W	0.21	Y
SQ-PA-1A	Page	287	83	W	0.36	Y
SQ-PA-1A	Page	292	86	W	0.22	Y
SQ-PA-1A	Page	308	85	W	0.11	Y
SQ-PA-1A	Page	356	59	W	0.13	Y
SQ-PA-1A	Page	371	82	W	0.14	Y
SQ-NA-1A	Navajo	36	58	E	0.24	Y
SQ-NA-1A	Navajo	302	86	W	0.34	Y
SQ-NA-1A	Navajo	309	88	W	0.51	Y
SQ-NA-1A	Navajo	307	88	W	0.77	Y
SQ-NA-1A	Navajo	292	89	W	0.38	Y
SQ-NA-1A	Navajo	310	86	W	0.43	Y
SQ-NA-1A	Navajo	309	87	W	0.47	Y
SQ-NA-1A	Navajo	46	67	E	0.29	Y
SQ-NA-1A	Navajo	310	83	W	0.23	Y
SQ-NA-1A	Navajo	316	84	W	0.21	Y
SQ-NA-1A	Navajo	299	86	W	0.11	Y
SQ-NA-1A	Navajo	287	88	W	0.18	Y
SQ-NA-1A	Navajo	316	84	W	0.48	Y
SQ-NA-1A	Navajo	312	83	W	0.42	Y

SRS Central Fracture Orientations

STATION	FORMATION	STRIKE	DIP	DIRECTION	FRACTURE SPACING (m)	ALTERATION (Y/N)
SP-EN-4B	Entrada	114	88	SW	0.19	Y
SP-EN-4B	Entrada	126	86	SW	0.18	Y
SP-EN-4B	Entrada	128	84	SW	0.11	Y
SP-EN-4B	Entrada	116	89	SW	0.12	Y
SP-EN-4B	Entrada	132	87	SW	0.09	Y

SP-EN-4B	Entrada	136	88	SW	0.07	Y
SP-EN-4B	Entrada	121	88	SW	0.1	Y
SP-EN-4B	Entrada	140	87	SW	0.23	Y
SP-EN-4B	Entrada	128	89	SW	0.24	Y
SP-EN-4B	Entrada	264	88	N	0.32	Y
SP-EN-4B	Entrada	269	87	N	0.26	Y
SP-EN-4B	Entrada	124	86	SW	0.12	Y
SP-EN-4B	Entrada	118	86	SW	0.13	Y
SP-EN-4B	Entrada	132	83	SW	0.17	Y
SP-EN-4B	Entrada	134	81	SW	0.14	Y
SP-EN-4B	Entrada	119	83	SW	0.11	Y
SP-EN-4B	Entrada	136	86	SW	0.16	Y
SP-EN-4B	Entrada	141	83	SW	0.15	Y
SP-EN-4B	Entrada	118	88	SW	0.22	Y
SP-EN-4B	Entrada	116	85	SW	0.24	Y
SP-EN-4B	Entrada	132	89	SW	0.16	Y
SP-EN-4B	Entrada	272	88	N	0.14	Y
SP-EN-4B	Entrada	274	85	N	0.18	Y
SP-EN-4B	Entrada	119	86	SW	0.11	Y
SP-EN-4A	Entrada	300	59	S	0.13	Y
SP-EN-4A	Entrada	358	74	N	0.08	Y
SP-EN-4A	Entrada	276	57	S	0.03	Y
SP-EN-4A	Entrada	285	66	N	0.02	Y
SP-EN-4A	Entrada	296	56	S	0.05	Y
SP-EN-4A	Entrada	297	78	N	0.04	Y
SP-EN-4A	Entrada	269	72	NW	0.06	Y
SP-EN-4A	Entrada	357	81	NW	0.18	Y
SP-EN-4A	Entrada	270	75	NW	0.17	Y
SP-EN-4A	Entrada	286	81	N	0.23	Y
SP-EN-4A	Entrada	356	88	N	0.26	Y
SP-EN-4A	Entrada	299	78	N	0.19	Y
SP-EN-4A	Entrada	302	61	S	0.13	Y
SP-EN-4A	Entrada	295	80	N	0.11	Y
SP-EN-4A	Entrada	285	56	S	0.12	Y
SP-EN-4A	Entrada	320	55	S	0.06	Y
SP-EN-4A	Entrada	291	76	N	0.08	Y
SP-EN-4A	Entrada	358	21	SE	0.25	Y
SP-EN-4A	Entrada	312	65	S	0.23	Y
SP-EN-4A	Entrada	364	79	N	0.31	Y
SP-EN-4A	Entrada	266	64	S	0.29	Y
SP-EN-4A	Entrada	255	67	N	0.26	Y

SP-EN-4A	Entrada	306	58	S	0.21	Y
SP-EN-4A	Entrada	309	64	N	0.19	Y
SP-EN-4A	Entrada	278	78	NW	0.16	Y
SP-EN-4A	Entrada	342	84	NW	0.17	Y
SP-EN-4A	Entrada	278	78	NW	0.18	Y
SP-EN-4A	Entrada	291	81	N	0.12	Y
SP-EN-4A	Entrada	349	87	N	0.19	Y
SP-EN-4A	Entrada	287	75	N	0.22	Y
SP-EN-4A	Entrada	308	64	S	0.27	Y
SP-EN-4A	Entrada	299	82	N	0.16	Y
SP-EN-4A	Entrada	287	61	S	0.24	Y
SP-EN-4A	Entrada	321	62	S	0.18	Y
SP-EN-4A	Entrada	299	81	N	0.15	Y
SP-EN-3B	Entrada	281	87	NW	0.12	Y
SP-EN-3B	Entrada	286	88	NW	0.1	Y
SP-EN-3B	Entrada	265	83	NW	0.09	Y
SP-EN-3B	Entrada	288	89	NW	0.15	Y
SP-EN-3B	Entrada	289	86	NW	0.17	Y
SP-EN-3B	Entrada	274	87	NW	0.24	Y
SP-EN-3B	Entrada	292	84	NW	0.29	Y
SP-EN-3B	Entrada	276	83	NW	0.23	Y
SP-EN-3B	Entrada	285	88	NW	0.28	Y
SP-EN-3B	Entrada	281	88	NW	0.16	Y
SP-EN-3A	Entrada	21	88	S	0.23	Y
SP-EN-3A	Entrada	120	70	S	0.39	Y
SP-EN-3A	Entrada	118	82	S	0.14	Y
SP-EN-3A	Entrada	121	81	S	0.06	Y
SP-EN-3A	Entrada	86	77	S	0.02	Y
SP-EN-3A	Entrada	121	78	S	0.04	Y
SP-EN-3A	Entrada	108	77	S	0.06	Y
SP-EN-3A	Entrada	105	67	S	0.03	Y
SP-EN-3A	Entrada	4	88	S	0.02	Y
SP-EN-3A	Entrada	100	74	S	0.23	Y
SP-EN-3A	Entrada	18	64	S	0.28	Y
SP-EN-3A	Entrada	104	67	S	0.33	Y
SP-EN-3A	Entrada	115	71	S	0.21	Y
SP-EN-3A	Entrada	28	86	S	0.28	Y
SP-EN-3A	Entrada	124	74	S	0.17	Y
SP-EN-3A	Entrada	128	81	S	0.08	Y
SP-EN-3A	Entrada	132	80	S	0.09	Y
SP-EN-3A	Entrada	97	74	S	0.02	Y

SP-EN-3A	Entrada	134	82	S	0.07	Y
SP-EN-3A	Entrada	119	85	S	0.11	Y
SP-EN-3A	Entrada	120	71	S	0.13	Y
SP-EN-3A	Entrada	8	87	S	0.32	Y
SP-EN-3A	Entrada	109	77	S	0.35	Y
SP-EN-3A	Entrada	15	65	S	0.28	Y
SP-EN-3A	Entrada	111	68	S	0.22	Y
SP-EN-3A	Entrada	119	78	S	0.18	Y
SP-EN-2A	Entrada	106	75	S	0.28	Y
SP-EN-2A	Entrada	98	72	S	0.42	Y
SP-EN-2A	Entrada	91	73	S	0.08	Y
SP-EN-2A	Entrada	92	79	S	0.02	Y
SP-EN-2A	Entrada	104	81	S	0.01	Y
SP-EN-2A	Entrada	83	84	S	0.02	Y
SP-EN-2A	Entrada	91	68	S	0.03	Y
SP-EN-2A	Entrada	94	79	S	0.02	Y
SP-EN-2A	Entrada	109	81	S	0.01	Y
SP-EN-2A	Entrada	56	76	S	0.26	Y
SP-EN-2A	Entrada	48	78	S	0.36	Y
SP-EN-2A	Entrada	51	76	S	0.3	Y
SP-EN-2A	Entrada	50	73	S	0.19	Y
SP-EN-2A	Entrada	111	78	S	0.14	Y
SP-EN-2A	Entrada	104	71	S	0.11	Y
SP-EN-2A	Entrada	84	76	S	0.04	Y
SP-EN-2A	Entrada	95	84	S	0.08	Y
SP-EN-2A	Entrada	110	83	S	0.03	Y
SP-EN-2A	Entrada	89	86	S	0.06	Y
SP-EN-2A	Entrada	96	72	S	0.09	Y
SP-EN-2A	Entrada	101	75	S	0.11	Y
SP-EN-2A	Entrada	114	83	S	0.29	Y
SP-EN-2A	Entrada	64	81	S	0.34	Y
SP-EN-2A	Entrada	59	85	S	0.33	Y
SP-EN-2A	Entrada	61	89	S	0.21	Y
SP-EN-2A	Entrada	62	81	S	0.24	Y
SP-EN-1B	Entrada	71	82	SE	0.14	Y
SP-EN-1B	Entrada	51	41	SE	0.01	Y
SP-EN-1B	Entrada	96	88	SE	0.03	Y
SP-EN-1B	Entrada	101	86	SE	0.14	Y
SP-EN-1B	Entrada	109	87	SE	0.15	Y
SP-EN-1B	Entrada	72	86	SE	0.02	Y
SP-EN-1B	Entrada	75	87	SE	0.05	Y

SP-EN-1B	Entrada	56	47	SE	0.03	Y
SP-EN-1B	Entrada	106	86	SE	0.11	Y
SP-EN-1B	Entrada	109	84	SE	0.25	Y
SP-EN-1B	Entrada	115	83	SE	0.24	Y
SP-EN-1B	Entrada	79	86	SE	0.47	Y
SP-CA-1B	Carmel	219	63	W	0.09	N
SP-CA-1B	Carmel	111	83	N	0.11	N
SP-CA-1B	Carmel	114	82	N	0.12	Y
SP-CA-1B	Carmel	113	86	N	0.18	N
SP-CA-1B	Carmel	115	88	N	0.23	N
SP-CA-1B	Carmel	105	87	N	0.24	N
SP-CA-1B	Carmel	112	84	N	0.09	N
SP-CA-1B	Carmel	116	83	N	0.27	Y
SP-CA-1B	Carmel	117	86	N	0.21	Y
SP-CA-1B	Carmel	124	88	N	0.28	N
SP-CA-1B	Carmel	104	89	N	0.14	N
SP-CA-1B	Carmel	123	87	N	0.16	N
SP-CA-1B	Carmel	124	88	N	0.12	N
SP-CA-1B	Carmel	125	88	N	0.21	N
SP-CA-1B	Carmel	230	66	W	0.16	N
SP-CA-1B	Carmel	116	84	N	0.07	N
SP-CA-1B	Carmel	118	83	N	0.13	Y
SP-CA-1B	Carmel	119	87	N	0.12	N
SP-CA-1B	Carmel	121	88	N	0.11	N
SP-CA-1B	Carmel	99	86	N	0.26	N
SP-CA-1B	Carmel	118	83	N	0.17	N
SP-CA-1B	Carmel	113	81	N	0.23	Y
SP-CA-1B	Carmel	124	85	N	0.26	Y
SP-CA-1B	Carmel	138	86	N	0.09	N
SP-CA-1B	Carmel	115	88	N	0.11	N
SP-CA-1B	Carmel	129	89	N	0.23	N
SP-CA-1B	Carmel	136	84	N	0.05	N
SP-CA-1B	Carmel	142	85	N	0.11	N
SP-CA-2A	Carmel	138	89	S	0.19	Y
SP-CA-2A	Carmel	129	87	S	0.17	Y
SP-CA-2A	Carmel	133	88	S	0.04	Y
SP-CA-2A	Carmel	135	89	S	0.14	Y
SP-CA-2A	Carmel	138	87	S	0.21	Y
SP-CA-2A	Carmel	134	84	S	0.15	Y
SP-CA-2A	Carmel	135	86	S	0.12	Y
SP-CA-2A	Carmel	136	89	S	0.13	Y

SP-CA-2A	Carmel	145	87	S	0.23	Y
SP-CA-2A	Carmel	136	86	S	0.17	Y
SP-CA-2A	Carmel	148	88	S	0.26	Y
SP-CA-2A	Carmel	147	89	S	0.1	Y
SP-CA-2A	Carmel	152	84	S	0.08	Y
SP-CA-2A	Carmel	139	81	S	0.09	Y
SP-CA-2A	Carmel	144	87	S	0.12	Y
SP-CA-2A	Carmel	149	88	S	0.13	Y
SP-CA-1A	Carmel	42	58	W	0.07	Y
SP-CA-1A	Carmel	44	75	W	0.15	Y
SP-CA-1A	Carmel	29	64	W	0.09	Y
SP-CA-1A	Carmel	35	73	W	0.22	Y
SP-CA-1A	Carmel	21	74	W	0.04	Y
SP-CA-1A	Carmel	21	82	W	0.18	Y
SP-CA-1A	Carmel	28	86	W	0.19	Y
SP-CA-1A	Carmel	16	79	W	0.21	Y
SP-CA-1A	Carmel	19	73	W	0.28	Y
SP-CA-1A	Carmel	356	79	W	0.22	Y
SP-CA-1A	Carmel	39	77	W	0.25	Y
SP-CA-1A	Carmel	19	69	SW	0.03	Y
SP-CA-1A	Carmel	18	62	SW	0.16	Y
SP-CA-1A	Carmel	16	66	SW	0.1	Y
SP-CA-1A	Carmel	25	69	SW	0.24	Y
SP-CA-1A	Carmel	20	72	SW	0.09	Y
SP-CA-1A	Carmel	20	65	SW	0.11	Y
SP-CA-1A	Carmel	18	72	SW	0.21	Y
SP-CA-1A	Carmel	25	71	SW	0.19	Y
SP-CA-1A	Carmel	24	76	SW	0.15	Y
SP-CA-1A	Carmel	48	64	W	0.16	Y
SP-CA-1A	Carmel	51	72	W	0.06	Y
SP-CA-1A	Carmel	35	71	W	0.18	Y
SP-CA-1A	Carmel	39	74	W	0.19	Y
SP-CA-1A	Carmel	28	74	W	0.2	Y
SP-CA-1A	Carmel	26	81	W	0.24	Y
SP-CA-1A	Carmel	33	87	W	0.13	Y
SP-CA-1A	Carmel	23	81	W	0.23	Y
SP-CA-1A	Carmel	24	86	W	0.11	Y
SP-CA-1A	Carmel	352	81	W	0.19	Y
SP-CA-1A	Carmel	44	82	W	0.22	Y
SP-CA-1A	Carmel	26	74	SW	0.25	Y
SP-CA-1A	Carmel	23	66	SW	0.06	Y

SP-CA-1A	Carmel	28	68	SW	0.27	Y
SP-CA-1A	Carmel	29	69	SW	0.12	Y
SP-CA-1A	Carmel	31	72	SW	0.11	Y
SP-CA-1A	Carmel	30	66	SW	0.06	Y
SP-CA-1A	Carmel	24	73	SW	0.13	Y
SP-CA-1A	Carmel	29	72	SW	0.17	Y
SP-CA-1A	Carmel	26	77	SW	0.15	Y
SP-CA-1B	Carmel	138	89	S	0.24	Y
SP-CA-1B	Carmel	129	87	S	0.25	Y
SP-CA-1B	Carmel	133	88	S	0.23	Y
SP-CA-1B	Carmel	135	89	S	0.17	Y
SP-CA-1B	Carmel	138	87	S	0.29	Y
SP-CA-1B	Carmel	134	84	S	0.12	Y
SP-CA-1B	Carmel	135	86	S	0.05	Y
SP-CA-1B	Carmel	136	89	S	0.24	Y
SP-CA-1B	Carmel	146	88	S	0.16	Y
SP-CA-1B	Carmel	148	88	S	0.11	Y
SP-CA-1B	Carmel	139	87	S	0.08	Y
SP-CA-1B	Carmel	137	89	S	0.09	Y
SP-CA-1B	Carmel	142	84	S	0.01	Y
SP-CA-1B	Carmel	146	83	S	0.09	Y
SP-CA-1B	Carmel	131	85	S	0.2	Y
SP-CA-1B	Carmel	129	88	S	0.08	Y
SP-NA-3A	Navajo	115	88	N	0.14	Y
SP-NA-3A	Navajo	127	86	N	0.26	Y
SP-NA-3A	Navajo	128	87	N	0.14	Y
SP-NA-3A	Navajo	128	58	E	0.12	Y
SP-NA-3A	Navajo	188	89	N	0.17	Y
SP-NA-3A	Navajo	124	86	N	0.23	Y
SP-NA-3A	Navajo	131	83	N	0.28	Y
SP-NA-3A	Navajo	136	84	N	0.18	Y
SP-NA-3A	Navajo	135	69	E	0.31	Y
SP-NA-3A	Navajo	192	78	N	0.11	Y
SP-NA-2A	Navajo	136	89	NW	0.14	Y
SP-NA-2A	Navajo	161	88	NW	0.18	Y
SP-NA-2A	Navajo	121	88	N	0.14	Y
SP-NA-2A	Navajo	133	86	N	0.11	Y
SP-NA-2A	Navajo	136	87	N	0.13	Y
SP-NA-2A	Navajo	142	64	E	0.05	Y
SP-NA-2A	Navajo	184	89	N	0.18	Y
SP-NA-2A	Navajo	144	89	NW	0.06	Y

SP-NA-2A	Navajo	171	88	NW	0.14	Y
SP-NA-2A	Navajo	123	88	N	0.12	Y
SP-NA-2A	Navajo	129	86	N	0.12	Y
SP-NA-2A	Navajo	139	87	N	0.14	Y
SP-NA-2A	Navajo	138	58	E	0.16	Y
SP-NA-2A	Navajo	193	89	N	0.17	Y
SP-NA-1A	Navajo	320	89	W	0.11	Y
SP-NA-1A	Navajo	6	86	W	0.16	Y
SP-NA-1A	Navajo	322	88	W	0.12	Y
SP-NA-1A	Navajo	317	88	W	0.17	Y
SP-NA-1A	Navajo	9	87	W	0.21	Y
SP-NA-1A	Navajo	322	89	W	0.07	Y
SP-NA-1A	Navajo	7	85	W	0.26	Y
SP-NA-1A	Navajo	321	84	W	0.04	Y
SP-NA-1A	Navajo	317	86	W	0.24	Y
SP-NA-1A	Navajo	319	86	W	0.09	Y
SP-NA-1A	Navajo	4	89	W	0.35	Y
SP-NA-1A	Navajo	6	88	W	0.17	Y
SP-NA-1A	Navajo	326	89	W	0.15	Y
SP-NA-1A	Navajo	12	86	W	0.18	Y
SP-NA-1A	Navajo	329	88	W	0.17	Y
SP-NA-1A	Navajo	328	88	W	0.22	Y
SP-NA-1A	Navajo	15	87	W	0.23	Y
SP-NA-1A	Navajo	327	89	W	0.09	Y
SP-NA-1A	Navajo	19	85	W	0.16	Y
SP-NA-1A	Navajo	325	84	W	0.15	Y
SP-NA-1A	Navajo	219	86	W	0.22	Y
SP-NA-1A	Navajo	324	86	W	0.11	Y
SP-NA-1A	Navajo	8	89	W	0.29	Y
SP-NA-1A	Navajo	9	88	W	0.16	Y

SRS South Fracture Orientations

STATION	FORMATION	STRIKE	DIP	DIRECTION	FRACTURE SPACING (m)	ALTERATION (Y/N)
TM-EN-1A	Entrada	150	86	SW	0.28	Y
TM-EN-1A	Entrada	151	86	SW	0.48	Y
TM-EN-1A	Entrada	132	88	S	0.86	Y
TM-EN-1A	Entrada	154	87	S	0.46	Y
TM-EN-1A	Entrada	163	81	S	0.32	Y

TM-EN-1A	Entrada	175	84	S	0.17	Y
TM-CA-2A	Carmel	251	89	N	0.07	N
TM-CA-2A	Carmel	21	88	W	0.07	Y
TM-CA-2A	Carmel	72	87	NE	0.36	N
TM-CA-2A	Carmel	262	87	S	0.2	N
TM-CA-2A	Carmel	249	89	N	0.11	N
TM-CA-2A	Carmel	261	87	N	0.03	Y
TM-CA-2A	Carmel	262	88	N	0.04	Y
TM-CA-2A	Carmel	299	84	N	0.16	Y
TM-CA-2A	Carmel	263	86	N	0.25	N
TM-CA-2A	Carmel	332	87	W	0.07	N
TM-CA-2A	Carmel	276	87	N	0.24	Y
TM-CA-2A	Carmel	246	84	N	0.05	N
TM-CA-2A	Carmel	272	82	N	0.06	Y
TM-CA-2A	Carmel	288	86	NE	0.01	Y
TM-CA-2A	Carmel	264	84	N	0.14	N
TM-CA-2A	Carmel	305	87	NE	0.3	Y
TM-CA-2A	Carmel	252	89	N	0.11	N
TM-CA-2A	Carmel	264	89	N	0.13	N
TM-CA-2A	Carmel	42	88	W	0.27	Y
TM-CA-2A	Carmel	86	87	NE	0.32	N
TM-CA-2A	Carmel	278	87	S	0.14	N
TM-CA-2A	Carmel	235	89	N	0.39	N
TM-CA-2A	Carmel	251	87	N	0.38	Y
TM-CA-2A	Carmel	258	88	N	0.17	Y
TM-CA-2A	Carmel	308	84	N	0.26	Y
TM-CA-2A	Carmel	275	86	N	0.11	N
TM-CA-2A	Carmel	341	87	W	0.28	N
TM-CA-2A	Carmel	284	87	N	0.09	Y
TM-CA-2A	Carmel	266	84	N	0.11	N
TM-CA-2A	Carmel	284	82	N	0.32	Y
TM-CA-2A	Carmel	298	86	NE	0.09	Y
TM-CA-2A	Carmel	256	84	N	0.08	N
TM-CA-2A	Carmel	352	87	NE	0.11	Y
TM-CA-2A	Carmel	268	89	N	0.06	N
TM-CA-1B	Carmel	320	85	SE	0.08	Y
TM-CA-1B	Carmel	326	86	SE	0.02	Y
TM-CA-1B	Carmel	316	79	NE	0.37	Y
TM-CA-1B	Carmel	320	87	NE	0.46	Y
TM-CA-1B	Carmel	310	77	NE	0.31	Y
TM-CA-1B	Carmel	314	80	NE	0.07	Y

TM-CA-1B	Carmel	320	84	NE	0.1	Y
TM-CA-1B	Carmel	319	87	NE	0.07	Y
TM-CA-1B	Carmel	321	89	NE	0.32	Y
TM-CA-1B	Carmel	323	84	NE	0.05	Y
TM-CA-1B	Carmel	325	87	NE	0.33	Y
TM-CA-1B	Carmel	323	87	NE	0.06	Y
TM-CA-1B	Carmel	322	87	NE	0.08	Y
TM-CA-1B	Carmel	319	89	NE	0.15	Y
TM-CA-1B	Carmel	331	86	SE	0.11	Y
TM-CA-1B	Carmel	342	86	SE	0.06	Y
TM-CA-1B	Carmel	336	81	NE	0.26	Y
TM-CA-1B	Carmel	327	87	NE	0.34	Y
TM-CA-1B	Carmel	320	84	NE	0.15	Y
TM-CA-1B	Carmel	326	80	NE	0.09	Y
TM-CA-1B	Carmel	334	84	NE	0.12	Y
TM-CA-1B	Carmel	311	88	NE	0.18	Y
TM-CA-1B	Carmel	316	89	NE	0.36	Y
TM-CA-1B	Carmel	317	84	NE	0.11	Y
TM-CA-1B	Carmel	346	82	NE	0.01	Y
TM-CA-1B	Carmel	352	86	NE	0.12	Y
TM-CA-1B	Carmel	338	84	NE	0.09	Y
TM-CA-1B	Carmel	327	89	NE	0.11	Y
TM-CA-2B	Carmel	251	89	N	0.41	N
TM-CA-2B	Carmel	21	88	W	0.57	Y
TM-CA-2B	Carmel	72	87	NE	0.08	N
TM-CA-2B	Carmel	262	87	S	0.01	N
TM-CA-2B	Carmel	249	89	N	0.01	N
TM-CA-2B	Carmel	261	87	N	0.02	Y
TM-CA-2B	Carmel	262	88	N	0.04	Y
TM-CA-2B	Carmel	299	84	N	0.09	Y
TM-CA-2B	Carmel	263	86	N	0.04	N
TM-CA-2B	Carmel	332	87	W	0.06	N
TM-CA-2B	Carmel	276	87	N	0.22	Y
TM-CA-2B	Carmel	246	84	N	0.04	N
TM-CA-2B	Carmel	272	82	N	0.05	Y
TM-CA-2B	Carmel	288	86	NE	0.05	Y
TM-CA-2B	Carmel	264	84	N	0.25	N
TM-CA-2B	Carmel	305	87	NE	0.05	Y
TM-CA-2B	Carmel	252	89	N	0.33	N
TM-CA-2B	Carmel	272	89	N	0.32	N
TM-CA-2B	Carmel	33	88	W	0.07	Y

TM-CA-2B	Carmel	64	87	NE	0.02	N
TM-CA-2B	Carmel	254	86	S	0.02	N
TM-CA-2B	Carmel	233	89	N	0.01	N
TM-CA-2B	Carmel	252	87	N	0.01	Y
TM-CA-2B	Carmel	268	88	N	0.11	Y
TM-CA-2B	Carmel	306	84	N	0.02	Y
TM-CA-2B	Carmel	275	86	N	0.03	N
TM-CA-2B	Carmel	324	82	W	0.09	N
TM-CA-2B	Carmel	288	85	N	0.08	Y
TM-CA-2B	Carmel	266	84	N	0.04	N
TM-CA-2B	Carmel	284	82	N	0.02	Y
TM-CA-2B	Carmel	285	86	NE	0.21	Y
TM-CA-2B	Carmel	256	84	N	0.03	N
TM-CA-2B	Carmel	299	88	NE	0.22	Y
TM-CA-2B	Carmel	267	89	N	0.07	N
TM-CA-3B	Carmel	131	88	NE	0.02	Y
TM-CA-3B	Carmel	129	89	NE	0.06	Y
TM-CA-3B	Carmel	126	87	NE	0.31	Y
TM-CA-3B	Carmel	122	86	NE	0.22	Y
TM-CA-3B	Carmel	123	88	NE	0.07	Y
TM-CA-3B	Carmel	142	84	NE	0.03	N
TM-CA-3B	Carmel	140	86	NE	0.02	N
TM-CA-3B	Carmel	136	87	NE	0.01	N
TM-CA-3B	Carmel	143	87	NE	0.02	N
TM-CA-3B	Carmel	128	88	NE	0.06	N
TM-CA-3B	Carmel	111	86	NE	0.02	N
TM-CA-3B	Carmel	104	88	NE	0.05	N
TM-CA-3B	Carmel	101	88	NE	0.13	N
TM-CA-3B	Carmel	141	87	NE	0.03	N
TM-CA-3B	Carmel	140	89	NE	0.06	N
TM-CA-3B	Carmel	116	89	NE	0.07	N
TM-CA-3B	Carmel	114	88	NE	0.39	N
TM-CA-3B	Carmel	123	87	NE	0.03	Y
TM-CA-3B	Carmel	142	88	NE	0.25	Y
TM-CA-3B	Carmel	149	89	NE	0.21	Y
TM-CA-3B	Carmel	133	89	NE	0.04	Y
TM-CA-3B	Carmel	134	86	NE	0.01	Y
TM-CA-3B	Carmel	138	88	NE	0.06	Y
TM-CA-3B	Carmel	144	84	NE	0.04	N
TM-CA-3B	Carmel	156	86	NE	0.03	N
TM-CA-3B	Carmel	142	87	NE	0.08	N

TM-CA-3B	Carmel	149	87	NE	0.02	N
TM-CA-3B	Carmel	132	88	NE	0.02	N
TM-CA-3B	Carmel	119	86	NE	0.01	N
TM-CA-3B	Carmel	108	88	NE	0.06	N
TM-CA-3B	Carmel	106	88	NE	0.04	N
TM-CA-3B	Carmel	131	87	NE	0.02	N
TM-CA-3B	Carmel	152	87	NE	0.16	N
TM-CA-3B	Carmel	118	89	NE	0.39	N
TM-CA-3B	Carmel	117	86	NE	0.26	N
TM-CA-3B	Carmel	127	87	NE	0.08	Y
TM-CA-3A	Carmel	122	87	NW	0.13	Y
TM-CA-3A	Carmel	115	86	NW	0.15	Y
TM-CA-3A	Carmel	114	87	NW	0.38	Y
TM-CA-3A	Carmel	106	89	NW	0.15	Y
TM-CA-3A	Carmel	122	88	NW	0.02	Y
TM-CA-3A	Carmel	111	88	NW	0.08	Y
TM-CA-3A	Carmel	108	87	NW	0.33	Y
TM-CA-3A	Carmel	104	85	NW	0.44	Y
TM-CA-3A	Carmel	111	89	NW	0.05	Y
TM-CA-3A	Carmel	113	88	NW	0.07	Y
TM-CA-3A	Carmel	112	87	NW	0.01	Y
TM-CA-3A	Carmel	110	87	NW	0.42	Y
TM-CA-3A	Carmel	132	85	NW	0.03	N
TM-CA-3A	Carmel	122	89	NW	0.08	N
TM-CA-3A	Carmel	135	89	NW	0.06	N
TM-CA-3A	Carmel	111	89	NW	0.03	N
TM-CA-3A	Carmel	133	88	NW	0.08	N
TM-CA-3A	Carmel	140	87	NW	0.07	N
TM-CA-3A	Carmel	114	84	NW	0.06	N
TM-CA-3A	Carmel	144	86	NW	0.03	N
TM-CA-3A	Carmel	133	88	NW	0.41	N
TM-CA-3A	Carmel	130	87	NW	0.04	N
TM-CA-3A	Carmel	109	89	NW	0.26	N
TM-CA-3A	Carmel	120	86	NW	0.18	N
TM-CA-3A	Carmel	131	89	NW	0.09	Y
TM-CA-3A	Carmel	122	88	NW	0.04	Y
TM-CA-3A	Carmel	117	89	NW	0.02	Y
TM-CA-3A	Carmel	132	86	NW	0.08	Y
TM-CA-3A	Carmel	136	87	NW	0.01	Y
TM-CA-3A	Carmel	134	87	NW	0.15	Y
TM-CA-3A	Carmel	137	88	NW	0.02	Y

TM-CA-3A	Carmel	134	90		0.03	Y
TM-CA-3A	Carmel	129	89	NE	0.11	Y
TM-CA-3A	Carmel	122	88	NW	0.03	Y
TM-CA-3A	Carmel	131	89	NW	0.28	Y
TM-CA-3A	Carmel	94	88	NW	0.02	Y
TM-CA-3A	Carmel	91	87	NW	0.37	Y
TM-CA-3A	Carmel	92	88	NW	0.18	Y
TM-CA-3A	Carmel	132	87	NW	0.2	Y
TM-CA-3A	Carmel	127	86	NW	0.09	Y
TM-CA-3A	Carmel	118	87	NW	0.01	Y
TM-CA-3A	Carmel	102	89	NW	0.01	Y
TM-CA-3A	Carmel	136	88	NW	0.29	Y
TM-CA-3A	Carmel	128	88	NW	0.17	Y
TM-CA-3A	Carmel	119	87	NW	0.08	Y
TM-CA-3A	Carmel	105	85	NW	0.04	Y
TM-CA-3A	Carmel	120	89	NW	0.12	Y
TM-CA-3A	Carmel	128	88	NW	0.02	Y
TM-CA-3A	Carmel	136	84	NW	0.22	Y
TM-CA-3A	Carmel	114	87	NW	0.01	Y
TM-CA-3A	Carmel	146	85	NW	0.02	N
TM-CA-3A	Carmel	148	89	NW	0.06	N
TM-CA-3A	Carmel	149	89	NW	0.08	N
TM-CA-3A	Carmel	132	89	NW	0.04	N
TM-CA-3A	Carmel	138	88	NW	0.28	N
TM-CA-3A	Carmel	144	87	NW	0.09	N
TM-CA-3A	Carmel	129	84	NW	0.21	N
TM-CA-3A	Carmel	119	86	NW	0.05	N
TM-CA-3A	Carmel	139	88	NW	0.33	N
TM-CA-3A	Carmel	138	87	NW	0.38	N
TM-CA-3A	Carmel	119	89	NW	0.03	N
TM-CA-3A	Carmel	126	86	NW	0.02	N
TM-CA-3A	Carmel	139	89	NW	0.07	Y
TM-CA-3A	Carmel	127	88	NW	0.05	Y
TM-CA-3A	Carmel	119	89	NW	0.04	Y
TM-CA-3A	Carmel	143	86	NW	0.03	Y
TM-CA-3A	Carmel	152	87	NW	0.07	Y
TM-CA-3A	Carmel	139	85	NW	0.03	Y
TM-CA-3A	Carmel	134	88	NW	0.02	Y
TM-CA-3A	Carmel	145	87	NW	0.06	Y
TM-CA-3A	Carmel	139	89	NE	0.08	Y
TM-CA-3A	Carmel	118	88	NW	0.09	Y

TM-CA-3A	Carmel	117	89	NW	0.14	Y
TM-CA-3A	Carmel	106	88	NW	0.11	Y
TM-CA-3A	Carmel	111	87	NW	0.29	Y
TM-CA-3A	Carmel	117	88	NW	0.11	Y
TM-PA-2A	Page	139	88	NE	0.12	Y
TM-PA-2A	Page	123	89	NE	0.2	Y
TM-PA-2A	Page	122	87	NE	0.16	Y
TM-PA-2A	Page	61	88	NW	0.06	Y
TM-PA-2A	Page	62	89	NW	0.03	Y
TM-PA-2A	Page	52	88	NW	0.29	Y
TM-PA-2A	Page	147	88	NE	0.06	Y
TM-PA-2A	Page	156	89	NE	0.13	Y
TM-PA-2A	Page	149	87	NE	0.21	Y
TM-PA-2A	Page	84	88	NW	0.36	Y
TM-PA-2A	Page	76	89	NW	0.22	Y
TM-PA-2A	Page	69	88	NW	0.11	Y
TM-PA-1A	Page	282	89	NW	0.19	Y
TM-PA-1A	Page	238	86	NW	0.04	Y
TM-PA-1A	Page	319	85	NW	0.13	Y
TM-PA-1A	Page	309	87	NW	0.11	Y
TM-PA-1A	Page	274	89	NW	0.06	Y
TM-PA-1A	Page	304	84	NW	0.27	Y
TM-PA-1A	Page	311	86	NW	0.06	Y
TM-PA-1A	Page	285	88	NW	0.12	Y
TM-PA-1A	Page	275	89	NW	0.22	Y
TM-PA-1A	Page	236	89	NW	0.36	Y
TM-PA-1A	Page	310	87	NW	0.56	Y
TM-PA-1A	Page	226	88	NW	0.53	Y
TM-PA-1A	Page	301	88	NW	0.14	Y
TM-PA-1A	Page	217	89	NW	0.1	Y
TM-PA-1A	Page	326	89	NW	0.18	Y
TM-PA-1A	Page	272	86	NW	0.27	Y
TM-PA-1A	Page	323	85	NW	0.11	Y
TM-PA-1A	Page	222	86	NW	0.09	Y
TM-PA-1A	Page	294	89	NW	1.04	Y
TM-PA-1A	Page	257	86	NW	0.06	Y
TM-PA-1A	Page	327	85	NW	0.18	Y
TM-PA-1A	Page	298	87	NW	0.05	Y
TM-PA-1A	Page	284	89	NW	0.15	Y
TM-PA-1A	Page	315	84	NW	0.16	Y
TM-PA-1A	Page	325	86	NW	0.14	Y

TM-PA-1A	Page	274	88	NW	0.06	Y
TM-PA-1A	Page	291	89	NW	0.18	Y
TM-PA-1A	Page	246	89	NW	0.34	Y
TM-PA-1A	Page	326	87	NW	0.42	Y
TM-PA-1A	Page	229	88	NW	0.47	Y
TM-PA-1A	Page	315	88	NW	0.26	Y
TM-PA-1A	Page	221	89	NW	0.22	Y
TM-PA-1A	Page	342	89	NW	0.06	Y
TM-PA-1A	Page	299	86	NW	0.25	Y
TM-PA-1A	Page	336	85	NW	0.24	Y
TM-PA-1A	Page	226	86	NW	0.04	Y
TM-PA-1B	Page	144	87	NW	0.13	Y
TM-PA-1B	Page	123	88	NW	0.14	Y
TM-PA-1B	Page	119	88	NW	0.18	Y
TM-PA-1B	Page	145	88	NW	0.08	Y
TM-PA-1B	Page	144	86	NW	0.09	Y
TM-PA-1B	Page	133	84	NW	0.16	Y
TM-PA-1B	Page	143	87	NW	0.15	Y
TM-PA-1B	Page	134	88	NW	0.13	Y
TM-PA-1B	Page	131	89	NW	0.04	Y
TM-PA-1B	Page	136	88	NW	0.11	Y
TM-PA-1B	Page	149	90		0.08	Y
TM-PA-1B	Page	131	87	NW	0.16	Y
TM-PA-1B	Page	159	87	NW	0.05	Y
TM-PA-1B	Page	142	88	NW	0.14	Y
TM-PA-1B	Page	141	88	NW	0.22	Y
TM-PA-1B	Page	137	88	NW	0.08	Y
TM-PA-1B	Page	139	86	NW	0.13	Y
TM-PA-1B	Page	150	84	NW	0.09	Y
TM-PA-1B	Page	148	87	NW	0.11	Y
TM-PA-1B	Page	147	88	NW	0.04	Y
TM-PA-1B	Page	152	89	NW	0.08	Y
TM-PA-1B	Page	146	88	NW	0.11	Y
TM-PA-1B	Page	158	86	NW	0.14	Y
TM-PA-1B	Page	140	87	NW	0.06	Y
TM-NA-2A	Navajo	144	88	NE	0.32	Y
TM-NA-2A	Navajo	143	85	NE	0.37	Y
TM-NA-2A	Navajo	85	87	NE	0.52	Y
TM-NA-2A	Navajo	154	87	NE	0.83	Y
TM-NA-2A	Navajo	162	84	NE	0.67	Y
TM-NA-2A	Navajo	109	86	NE	0.56	Y

TM-NA-1B	Navajo	326	87	W	0.23	Y
TM-NA-1B	Navajo	323	88	W	0.38	Y
TM-NA-1B	Navajo	322	87	W	0.52	Y
TM-NA-1B	Navajo	214	85	NE	0.62	Y
TM-NA-1B	Navajo	201	89	NE	0.74	Y
TM-NA-1B	Navajo	286	89	NE	0.18	Y
TM-NA-1B	Navajo	228	88	NE	0.14	Y
TM-NA-1B	Navajo	267	84	NE	0.16	Y
TM-NA-1B	Navajo	251	86	NE	0.33	Y
TM-NA-1B	Navajo	188	87	NW	0.26	Y
TM-NA-1B	Navajo	263	89	NE	0.18	Y
TM-NA-1B	Navajo	337	87	W	0.19	Y
TM-NA-1B	Navajo	345	88	W	0.85	Y
TM-NA-1B	Navajo	344	87	W	0.65	Y
TM-NA-1B	Navajo	230	85	NE	0.62	Y
TM-NA-1B	Navajo	228	89	NE	0.32	Y
TM-NA-1B	Navajo	297	89	NE	0.14	Y
TM-NA-1B	Navajo	247	88	NE	0.19	Y
TM-NA-1B	Navajo	246	84	NE	0.16	Y
TM-NA-1B	Navajo	263	86	NE	0.44	Y
TM-NA-1B	Navajo	210	87	NW	0.18	Y
TM-NA-1B	Navajo	275	89	NE	0.39	Y
TM-NA-1A	Navajo	136	88	NW	0.15	Y
TM-NA-1A	Navajo	137	89	NW	0.93	Y
TM-NA-1A	Navajo	144	86	NW	0.72	Y
TM-NA-1A	Navajo	145	88	NW	0.55	Y
TM-NA-1A	Navajo	143	84	NW	0.49	Y
TM-NA-1A	Navajo	141	86	NW	0.04	Y
TM-NA-1A	Navajo	146	88	NW	0.08	Y
TM-NA-1A	Navajo	119	89	NE	0.07	Y
TM-NA-1A	Navajo	106	87	NE	0.49	Y
TM-NA-1A	Navajo	110	88	NW	0.1	Y
TM-NA-1A	Navajo	96	88	NW	0.34	Y
TM-NA-1A	Navajo	91	85	NE	0.28	Y
TM-NA-1A	Navajo	116	87	NE	0.36	Y
TM-NA-1A	Navajo	146	88	NW	0.48	Y
TM-NA-1A	Navajo	122	86	NW	0.86	Y
TM-NA-1A	Navajo	118	87	NE	0.78	Y
TM-NA-1A	Navajo	144	88	NW	0.16	Y
TM-NA-1A	Navajo	142	89	NW	0.18	Y
TM-NA-1A	Navajo	146	86	NW	0.14	Y

TM-NA-1A	Navajo	153	88	NW	0.34	Y
TM-NA-1A	Navajo	156	84	NW	0.18	Y
TM-NA-1A	Navajo	157	86	NW	0.16	Y
TM-NA-1A	Navajo	159	88	NW	0.14	Y
TM-NA-1A	Navajo	127	89	NE	0.85	Y
TM-NA-1A	Navajo	112	87	NE	0.42	Y
TM-NA-1A	Navajo	118	88	NW	0.22	Y
TM-NA-1A	Navajo	106	88	NW	0.24	Y
TM-NA-1A	Navajo	110	85	NE	0.12	Y
TM-NA-1A	Navajo	121	87	NE	0.11	Y
TM-NA-1A	Navajo	158	88	NW	0.08	Y
TM-NA-1A	Navajo	134	86	NW	0.52	Y
TM-NA-1A	Navajo	123	87	NE	0.13	Y

MU Central A Fracture Orientations

STATION	FORMATION	STRIKE	DIP	DIRECTION	FRACTURE SPACING (m)	ALTERATION (Y/N)
BL-EN-2B	Entrada	239	66	W	26	N
BL-EN-2B	Entrada	234	72	W	39	N
BL-EN-2B	Entrada	225	75	W	41	N
BL-EN-2B	Entrada	271	89	W	71	N
BL-EN-2B	Entrada	267	87	W	67	N
BL-EN-2B	Entrada	250	67	NE	38	N
BL-EN-2B	Entrada	246	66	W	24	N
BL-EN-2B	Entrada	244	72	W	28	N
BL-EN-2B	Entrada	232	75	W	37	N
BL-EN-2B	Entrada	283	89	W	46	N
BL-EN-2B	Entrada	274	87	W	68	N
BL-EN-2B	Entrada	266	67	NE	64	N
BL-CA-3B	Carmel	267	89	N	0.22	N
BL-CA-3B	Carmel	269	88	N	0.34	N
BL-CA-3B	Carmel	268	87	N	0.42	N
BL-CA-3B	Carmel	318	89	N	0.41	N
BL-CA-3B	Carmel	321	89	N	0.42	N
BL-CA-3B	Carmel	273	89	N	0.54	N
BL-CA-3B	Carmel	284	88	N	0.46	N
BL-CA-3B	Carmel	276	87	N	0.33	N
BL-CA-3B	Carmel	332	89	N	0.21	N
BL-CA-3B	Carmel	329	89	N	0.53	N

BL-NA-2A	Navajo	264	88	N	0.28	N
BL-NA-2A	Navajo	260	87	N	0.44	N
BL-NA-2A	Navajo	259	89	N	0.58	N
BL-NA-2A	Navajo	256	86	N	0.71	N
BL-NA-2A	Navajo	260	88	N	0.49	N
BL-NA-2A	Navajo	264	87	N	0.5	N
BL-NA-2A	Navajo	284	88	N	0.42	N
BL-NA-2A	Navajo	276	87	N	0.37	N
BL-NA-2A	Navajo	266	89	N	0.26	N
BL-NA-2A	Navajo	259	86	N	0.63	N
BL-NA-2A	Navajo	278	88	N	0.38	N
BL-NA-2A	Navajo	252	87	N	0.55	N

MU Central B Fracture Orientations

STATION	FORMATION	STRIKE	DIP	DIRECTION	FRACTURE SPACING (m)	ALTERATION (Y/N)
BL-EN-2A	Entrada	12	87	E	0.18	N
BL-EN-2A	Entrada	14	88	E	0.36	N
BL-EN-2A	Entrada	351	86	E	0.52	N
BL-EN-2A	Entrada	357	89	E	0.48	N
BL-EN-2A	Entrada	8	89	E	0.69	N
BL-EN-2A	Entrada	5	84	W	0.38	N
BL-EN-2A	Entrada	12	81	W	0.47	N
BL-EN-2A	Entrada	15	80	W	0.45	N
BL-EN-2A	Entrada	18	78	W	0.31	N
BL-EN-2A	Entrada	21	82	W	0.5	N
BL-EN-2A	Entrada	276	68	N	0.43	N
BL-EN-2A	Entrada	9	87	E	0.21	N
BL-EN-2A	Entrada	13	88	E	0.21	N
BL-EN-2A	Entrada	355	86	E	0.33	N
BL-EN-2A	Entrada	354	89	E	0.48	N
BL-EN-2A	Entrada	7	89	E	0.46	N
BL-EN-2A	Entrada	2	84	W	0.65	N
BL-EN-2A	Entrada	9	81	W	0.32	N
BL-EN-2A	Entrada	12	80	W	0.43	N
BL-EN-2A	Entrada	10	78	W	0.39	N
BL-EN-2A	Entrada	11	82	W	0.28	N
BL-EN-2A	Entrada	294	68	N	0.51	N
BL-CA-3A	Carmel	276	89	N	0.2	N

BL-CA-3A	Carmel	279	88	N	0.34	N
BL-CA-3A	Carmel	282	87	N	0.39	N
BL-CA-3A	Carmel	324	89	N	0.29	N
BL-CA-3A	Carmel	331	89	N	0.17	N
BL-CA-3A	Carmel	283	89	N	0.59	N
BL-CA-3A	Carmel	274	88	N	0.34	N
BL-CA-3A	Carmel	276	87	N	0.23	N
BL-CA-3A	Carmel	322	89	N	0.37	N
BL-CA-3A	Carmel	325	89	N	0.26	N
BL-NA-2A	Navajo	264	88	N	0.18	N
BL-NA-2A	Navajo	260	87	N	0.36	N
BL-NA-2A	Navajo	259	89	N	0.52	N
BL-NA-2A	Navajo	256	86	N	0.48	N
BL-NA-2A	Navajo	260	88	N	0.69	N
BL-NA-2A	Navajo	264	87	N	0.38	N
BL-NA-2A	Navajo	314	88	N	0.47	N
BL-NA-2A	Navajo	313	89	N	0.45	N
BL-NA-2A	Navajo	309	86	N	0.31	N
BL-NA-2A	Navajo	276	88	N	0.5	N
BL-NA-2A	Navajo	278	87	N	0.43	N
BL-NA-2A	Navajo	265	89	N	0.21	N
BL-NA-2A	Navajo	267	86	N	0.44	N
BL-NA-2A	Navajo	269	88	N	0.41	N
BL-NA-2A	Navajo	278	87	N	0.33	N
BL-NA-2A	Navajo	326	88	N	0.52	N
BL-NA-2A	Navajo	333	89	N	0.56	N
BL-NA-2A	Navajo	318	86	N	0.28	N

MU South Fracture Orientations

STATION	FORMATION	STRIKE	DIP	DIRECTION	FRACTURE SPACING (m)	ALTERATION (Y/N)
BL-EN-1A	Entrada	1	87	E	0.28	N
BL-EN-1A	Entrada	2	88	E	0.32	N
BL-EN-1A	Entrada	354	86	E	0.33	N
BL-EN-1A	Entrada	353	89	E	0.41	N
BL-EN-1A	Entrada	2	89	E	0.4	N
BL-EN-1A	Entrada	359	84	W	0.33	N
BL-EN-1A	Entrada	4	81	W	0.41	N
BL-EN-1A	Entrada	4	80	W	0.19	N

BL-EN-1A	Entrada	9	78	W	0.31	N
BL-EN-1A	Entrada	10	82	W	0.21	N
BL-EN-1A	Entrada	282	68	N	0.32	N
BL-EN-1A	Entrada	8	87	E	0.34	N
BL-EN-1A	Entrada	6	88	E	0.29	N
BL-EN-1A	Entrada	348	86	E	0.38	N
BL-EN-1A	Entrada	347	89	E	0.36	N
BL-EN-1A	Entrada	3	89	E	0.31	N
BL-EN-1A	Entrada	344	84	W	0.33	N
BL-EN-1A	Entrada	8	81	W	0.17	N
BL-EN-1A	Entrada	6	80	W	0.35	N
BL-EN-1A	Entrada	9	78	W	0.24	N
BL-EN-1A	Entrada	10	82	W	0.34	N
BL-EN-1A	Entrada	342	88	W	0.25	N
BL-CA-1A	Carmel	262	87	S	0.28	N
BL-CA-1A	Carmel	249	89	N	0.36	N
BL-CA-1A	Carmel	261	87	N	0.49	N
BL-CA-1A	Carmel	262	88	N	0.38	N
BL-CA-1A	Carmel	299	84	N	0.47	N
BL-CA-1A	Carmel	263	86	N	0.34	N
BL-CA-1A	Carmel	332	87	W	0.42	N
BL-CA-1A	Carmel	276	87	N	0.41	N
BL-CA-1A	Carmel	246	84	N	0.29	N
BL-CA-1A	Carmel	272	82	N	0.26	N
BL-CA-1A	Carmel	262	89	N	0.25	N
BL-CA-1A	Carmel	274	87	N	0.24	N
BL-CA-1A	Carmel	286	88	N	0.31	N
BL-CA-1A	Carmel	306	84	N	0.44	N
BL-CA-1A	Carmel	254	86	N	0.42	N
BL-CA-1A	Carmel	319	87	W	0.43	N
BL-CA-1A	Carmel	287	87	N	0.29	N
BL-CA-1A	Carmel	258	84	N	0.37	N
BL-CA-1A	Carmel	286	82	N	0.38	N
BL-NA-1A	Navajo	252	86	SW	0.28	N
BL-NA-1A	Navajo	294	88	SW	0.33	N
BL-NA-1A	Navajo	289	87	N	0.42	N
BL-NA-1A	Navajo	72	86	SW	0.64	N
BL-NA-1A	Navajo	294	87	SW	0.53	N
BL-NA-1A	Navajo	66	88	SW	0.51	N
BL-NA-1A	Navajo	281	86	SW	0.42	N
BL-NA-1A	Navajo	314	88	N	0.47	N

BL-NA-1A	Navajo	265	86	SW	0.39	N
BL-NA-1A	Navajo	306	88	SW	0.58	N
BL-NA-1A	Navajo	294	87	N	0.37	N
BL-NA-1A	Navajo	88	86	SW	0.36	N
BL-NA-1A	Navajo	289	87	SW	0.33	N
BL-NA-1A	Navajo	75	88	SW	0.36	N
BL-NA-1A	Navajo	274	86	SW	0.43	N
BL-NA-1A	Navajo	309	88	N	0.57	N

MU North Fracture Orientations

STATION	FORMATION	STRIKE	DIP	DIRECTION	FRACTURE SPACING (m)	ALTERATION (Y/N)
DR-EN-1A	Entrada	310	53	S	0.22	Y
DR-EN-1A	Entrada	313	76	S	0.28	Y
DR-EN-1A	Entrada	326	68	S	0.31	Y
DR-EN-1A	Entrada	304	62	S	0.11	Y
DR-EN-1A	Entrada	292	71	S	0.08	Y
DR-EN-1A	Entrada	290	73	S	0.07	Y
DR-EN-1A	Entrada	291	86	S	0.19	Y
DR-EN-1A	Entrada	297	84	N	0.12	Y
DR-EN-1A	Entrada	294	69	S	0.16	Y
DR-EN-1A	Entrada	295	66	S	0.09	Y
DR-EN-1A	Entrada	297	69	S	0.2	Y
DR-EN-1A	Entrada	294	72	S	0.17	Y
DR-EN-1A	Entrada	324	79	S	0.22	Y
DR-EN-1A	Entrada	309	71	S	0.17	Y
DR-EN-1A	Entrada	313	64	S	0.09	Y
DR-EN-1A	Entrada	318	88	S	0.08	Y
DR-EN-1A	Entrada	234	76	S	0.27	Y
DR-EN-1A	Entrada	312	73	S	0.06	Y
DR-EN-1A	Entrada	286	79	S	0.12	Y
DR-EN-1A	Entrada	272	77	S	0.13	Y
DR-EN-1A	Entrada	285	87	S	0.21	Y
DR-EN-1A	Entrada	299	84	N	0.18	Y
DR-EN-1A	Entrada	306	72	S	0.13	Y
DR-EN-1A	Entrada	312	66	S	0.1	Y
DR-EN-1A	Entrada	318	69	S	0.3	Y
DR-EN-1A	Entrada	283	72	S	0.09	Y
DR-EN-1A	Entrada	317	79	S	0.13	Y

DR-EN-1A	Entrada	311	71	S	0.15	Y
DR-EN-1B	Entrada	356	73	SW	0.27	Y
DR-EN-1B	Entrada	284	64	S	0.24	Y
DR-EN-1B	Entrada	311	82	S	0.26	Y
DR-EN-1B	Entrada	308	82	S	0.09	Y
DR-EN-1B	Entrada	300	72	S	0.13	Y
DR-EN-1B	Entrada	314	80	S	0.25	Y
DR-EN-1B	Entrada	309	78	S	0.29	Y
DR-EN-1B	Entrada	304	74	S	0.1	Y
DR-EN-1B	Entrada	308	79	S	0.15	Y
DR-EN-1B	Entrada	299	79	S	0.12	Y
DR-EN-1B	Entrada	348	73	SW	0.23	Y
DR-EN-1B	Entrada	292	64	S	0.19	Y
DR-EN-1B	Entrada	313	82	S	0.24	Y
DR-EN-1B	Entrada	317	82	S	0.17	Y
DR-EN-1B	Entrada	305	72	S	0.11	Y
DR-EN-1B	Entrada	321	80	S	0.16	Y
DR-EN-1B	Entrada	320	78	S	0.33	Y
DR-EN-1B	Entrada	307	74	S	0.08	Y
DR-EN-1B	Entrada	308	79	S	0.18	Y
DR-EN-1B	Entrada	305	79	S	0.14	Y
DR-CA-2B	Carmel	45	54	E	0.28	Y
DR-CA-2B	Carmel	50	55	E	0.24	Y
DR-CA-2B	Carmel	239	66	W	0.2	Y
DR-CA-2B	Carmel	234	72	W	0.12	Y
DR-CA-2B	Carmel	225	75	W	0.31	Y
DR-CA-2B	Carmel	46	52	E	0.03	Y
DR-CA-2B	Carmel	271	89	W	0.04	Y
DR-CA-2B	Carmel	267	87	W	0.03	Y
DR-CA-2B	Carmel	100	69	W	0.13	Y
DR-CA-2B	Carmel	250	67	NE	0.05	Y
DR-CA-2B	Carmel	62	61	E	0.07	Y
DR-CA-2B	Carmel	58	58	E	0.12	Y
DR-CA-2B	Carmel	254	67	W	0.05	Y
DR-CA-2B	Carmel	246	75	W	0.25	Y
DR-CA-2B	Carmel	249	78	W	0.13	Y
DR-CA-2B	Carmel	64	59	E	0.16	Y
DR-CA-2B	Carmel	282	88	W	0.21	Y
DR-CA-2B	Carmel	279	84	W	0.09	Y
DR-CA-2B	Carmel	110	73	W	0.24	Y
DR-CA-2B	Carmel	261	76	NE	0.05	Y

DR-NA-1A	Navajo	43	44	SW	0.2	Y
DR-NA-1A	Navajo	353	72	SW	0.28	Y
DR-NA-1A	Navajo	36	52	SW	0.16	Y
DR-NA-1A	Navajo	339	66	N	0.26	Y
DR-NA-1A	Navajo	334	60	N	0.06	Y
DR-NA-1A	Navajo	329	64	N	0.29	Y
DR-NA-1A	Navajo	45	26	SW	0.15	Y
DR-NA-1A	Navajo	332	61	N	0.07	Y
DR-NA-1A	Navajo	318	66	N	0.06	Y
DR-NA-1A	Navajo	306	51	NW	0.27	Y
DR-NA-1A	Navajo	56	58	SW	0.23	Y
DR-NA-1A	Navajo	342	65	SW	0.32	Y
DR-NA-1A	Navajo	43	57	SW	0.21	Y
DR-NA-1A	Navajo	334	69	N	0.18	Y
DR-NA-1A	Navajo	328	64	N	0.11	Y
DR-NA-1A	Navajo	326	65	N	0.33	Y
DR-NA-1A	Navajo	51	38	SW	0.18	Y
DR-NA-1A	Navajo	315	69	N	0.09	Y
DR-NA-1A	Navajo	318	64	N	0.08	Y
DR-NA-1A	Navajo	309	52	NW	0.32	Y